

The composition and mechanical properties of the stomatal cell wall: Implications for stomatal function

By: Samuel M J Amsbury

A thesis submitted to the University of Sheffield for the
degree of Doctor of Philosophy



The University of Sheffield

Faculty of Science

Department of Animal and Plant Sciences

Submitted October 2016

Acknowledgements

Firstly, I would like to thank my supervisors Professor Andrew Fleming and Professor Julie Gray, their guidance and supervision made this research possible. I have had a great time during my PhD and the advice, support and freedom offered to me by my supervisors was instrumental in making this experience enjoyable.

This research would not have been possible without the support and input of a number of colleagues. Thanks to Professor Jamie Hobbs for the use of his AFM and for his advice and support. Ross Carter's help with learning and developing the AFM technique was invaluable. I would also like to thank Alice Baillie for the huge amount of help and support during this project, her patience with teaching me cloning and her frequent advice. Thanks to Marjorie Lundgren for her willingness to give up her time to provide LI-COR training, advice and maintenance and for her help in designing gas exchange experiments. I would also like to thank Professor Paul Knox for opening up his lab at the university of Leeds to us and for providing antibodies and endless advice. Finally, I would like to thank Lee Hunt for his help and support on this project and for the donation of a number of plant lines.

My time at the University has been made enjoyable by the great friends I have made during my time here. I would especially like to thank Serina and Carla for their friendship and advice throughout my PhD. I would also like to thank Richard, Alex and Luke for their friendship, distractions from work and their willingness to listen and give advice. I would also like to thank all of the members of the Gray lab-group and the Fleming lab-group for their friendship and assistance during my project. There are also numerous other members of APS and MBB, too many to list, that have added to the enjoyment of my time here, especially the morning coffee, lunch and Friday pub group

I would like to thank my family for their support, interest and advice. I would especially like to thank my Mum and Dad for their confidence in me and for giving me the confidence to pursue a career in science. I would also like to thank Emma's parents Pete and Cath for their constant encouragement and support.

I would like to extend a special thanks to Emma for her endless support during my PhD. Your willingness to move to Sheffield with me to allow me to do my PhD and the constant support, advice and encouragement helped me push on when the work was challenging. Countless hours were spent proof-reading or listening to practice presentations.

Abstract

Stomata are crucial for gaseous exchange in plants. The ability of stomata to open and close depends on changes in turgor pressure acting within guard cells to alter cell shape. The extent of these shape changes is limited by the mechanical properties of the cells, which will be largely dependent on the structure of the cell walls. Although it has long been observed that guard cells are anisotropic due to differential thickening and the orientation of cellulose microfibrils, our understanding of the composition of the cell wall that allows them to undergo repeated swelling and deflation remains surprisingly poor.

In this thesis antibody labelling is used to study the composition of the guard cell wall. Pectin composition is shown to be crucial for guard cell structure and function and I show that disruption of pectin composition disrupts stomatal function. The development of an atomic force microscopy technique to directly measure the mechanical properties of stomata is also reported here. I show that the mechanical properties of stomata change throughout plant development and highlight the potential for this in the future study of guard cell walls. Although this thesis focuses on the role of pectins I also demonstrate a potential role for other cell wall matrix components such as xyloglucan and structural proteins in the maintenance of guard cell mechanical properties.

Altering the mechanical properties of guard cell walls has an impact on the mechanical properties of the guard cell wall which impacts on stomatal function. This has an effect on plant physiology and carbon assimilation. The targeted modulation of guard cell walls provides a novel avenue for the future manipulation of stomatal function.

Table of contents

Acknowledgements	i
Abstract.....	iii
Table of contents.....	v
Table of figures	xii
List of tables	xvi
List of equations	xvii
Chapter 1. Introduction.....	1
1.1 The role of stomata in leaf function	2
1.2 The stomatal development pathway	3
1.3 Guard cell signalling	7
1.4 Structural properties of guard cells	10
1.5 Cell walls.....	12
1.5.1 Cellulose	13
1.5.2 Hemicelluloses.....	14
1.5.3 Pectins	15
1.6 Plant mechanics	20
1.7 Aims and objectives	21
Chapter 2. Materials and Methods	23
2.1 Plant Material	23
2.1.1 Loss of function mutants: NASC lines	23
2.1.2 Gain of function mutants: Transgenic lines.....	23

2.2 Plant Growth.....	24
2.2.1 Soil grown plants	24
2.2.2 Media grown plants.....	24
2.3 RT-PCR.....	25
2.3.1 RNA extraction.....	25
2.3.2 RNA quantification and quality analysis	27
2.3.3 First strand cDNA synthesis.....	27
2.4 PCR	27
2.4.1 Isolation of genomic DNA	27
2.4.2 PCR reaction	28
2.5 Agarose gel electrophoresis	29
2.6 Immunohistochemical techniques	29
2.6.1 Fixation and embedding of plant material	29
2.6.2 Immunolabelling of tissue sections	30
2.6.3 Enzymatic removal of pectin.....	31
2.7 Histochemical localization using the GUS reporter gene.....	31
2.8 Tissue clearing using Chloral Hydrate.....	32
2.9 Plant growth analysis.....	32
2.9.1 Seed weight.....	32
2.9.2 Seed size	33
2.9.3 Germination rate	33
2.9.4 Rosette area	33
2.9.5 FW and DW and relative water content	33
2.10 Analysis of stomatal aperture.....	34
2.10.1 CO ₂ effects on stomatal aperture.....	34
2.10.2 ABA effects on stomatal aperture	34
2.10.3 Mannitol effects on stomatal aperture	35
2.11 Analysis of stomatal number	35
2.12 Gas exchange analysis	36

2.12.1 A/CI curves	36
2.12.2 Light curves	36
2.12.3 Stomatal response to CO ₂ shifts.....	36
2.12.4 Blue light induced stomatal opening	37
2.13 Thermal imaging	37
2.14 Atomic force microscopy of leaf tissue.....	38
2.14.1 Viability of AFM samples	38
2.15 Sample preparation for TEM	39
2.16 Histological analysis using toluidine blue.....	39
Chapter 3. Analysis of guard cell wall composition by immunocytochemistry.....	41
3.1 Introduction.....	41
3.1.1 Guard cell walls.....	42
3.1.2 Antibody labelling of cell wall components.....	44
3.1.3 The guard cell cuticular ledge	44
3.2 Results	45
3.2.1 Analysis of guard cell wall composition.....	45
3.2.2 Guard cell wall composition is distinct from epidermal pavement cells...	58
3.2.3 Composition of the guard cell cuticular ledge.....	65
3.2.4 Unmasking cell wall components: Enzyme deconstruction	67
3.2.5 Does the guard cell wall undergo rapid remodelling during opening and closing?	71
3.3 Discussion.....	73
3.3.1 Screening of antibodies	74
3.3.2 Revealing hidden guard cell wall epitopes	78
3.3.3 Elucidating the structure of the guard cell cuticular ledge.....	79
3.3.4 Conclusions.....	80
Chapter 4. Analysis of a pectin methylesterase mutant.....	81

4.1 Introduction.....	81
4.2 Results	86
4.2.1 <i>PME6</i> is expressed in mature guard cell.....	86
4.2.2 Characterising the <i>pme6-1</i> insertion mutant.....	88
4.2.3 <i>PME6</i> expression is restricted to mature guard cells	90
4.3 Growth data.....	93
4.3.1 Seed characteristics	93
4.3.2 Size is altered in <i>pme6-1</i> plants at ambient CO ₂	95
4.3.3 Stomatal size and density in <i>pme6-1</i> plants.	97
4.4 Assessing the functionality of <i>pme6</i> stomata	98
4.4.1 <i>pme6-1</i> stomatal aperture in response to altered CO ₂ levels.....	99
4.4.2 Stomatal responses to other guard cell stimuli	100
4.4.3 <i>pme6-1</i> stomata and whole plant drought responses	103
4.5 <i>pme6-1</i> plants have altered pectin composition	105
4.6 <i>pme6-1</i> plants have altered gas exchange.....	109
4.6.1 A/ci and Light curves	109
4.6.2 <i>pme6-1</i> responses to shifts in CO ₂ concentration.....	110
4.6.3 <i>pme6</i> stomatal response to blue light.....	112
4.7 TEM microscopy of <i>pme6-1</i> stomata	114
4.8 Discussion.....	115
4.8.1 <i>pme6-1</i> has impaired stomatal function	116
4.8.2 <i>pme6-1</i> plants have altered physiology	119
4.8.3 Conclusions.....	122

Chapter 5. Further analysis of the cell wall: selection of new genes	123
--	-----

5.1 Introduction.....	123
5.1.1 The PME/PMEI family.....	124
5.2 Results	126
5.2.1 Selection of T-DNA insertion lines	126
5.3 Analysis of insertion mutants	129
5.3.1 Confirming homozygous insertion lines	129
5.3.2 Screening for stomatal density and size.....	133
5.3.3 Growth analysis.....	137
5.3.4 Thermal imaging	141
5.3.5 Stomatal aperture responses to CO ₂	144
5.3.6 <i>focl</i> plants have covered stomata.....	149
5.3.7 Immunolabelling NASC lines with altered stomatal function	152
5.3.8 <i>focl</i> plants do not show alterations to their cell wall structure	153
5.4 Creation of PMEI overexpression lines	156
5.5 Creating and selecting mutant plants.....	159
5.6 Analysis of <i>pCA1:PMEI</i> lines	160
5.6.1 Stomatal size and patterning is unaffected in overexpression lines	160
5.6.2 Thermal imaging.....	162
5.6.3 Antibody analysis of mutants	164
5.6.4 Gas exchange analysis of transgenic lines	166
5.7 Discussion.....	171
5.7.1 Cell wall mutants and stomatal function.....	171
5.7.2 <i>FOCL</i> is required for stomatal function.	173
5.7.3 Creation of transgenic lines	176
Chapter 6. Atomic force microscopy.....	179
6.1 Introduction.....	179
6.2 Development of an AFM method for imaging live leaf samples	187
6.2.1 Plant growth	187

6.2.2 Sample preparation.....	192
6.2.3 Mounting the sample.....	193
6.2.4 Sample viability.....	195
6.3 Analysis of guard cell topography.....	196
6.3.1 Topographical analysis of <i>focl</i> plants.....	203
6.4 Analysis of stomatal elasticity.....	206
6.5 Discussion.....	216
6.5.1 Experimental validation of an AFM method.....	216
6.5.2 AFM allows high resolution imaging of live tissue.....	217
6.5.3 <i>focl</i> plants have altered stomatal coverings.....	218
6.5.4 Stomatal stiffness changes throughout development.....	219
Chapter 7. General Discussion.....	225
7.1.1 Future work.....	227
Bibliography.....	231
Appendices.....	253
Appendix 1: A selection of control samples incubated with secondary antibody in the absence of primary antibody.....	254
Appendix 2: Antibody binding summary.....	255
Appendix 3: Summary of antibodies tested for binding in leaves treated with ABA.....	256
Appendix 4: Information on plant lines used in this project.....	257
Appendix 5: Primers used during the project.....	259
Appendix 6: Antibodies tested against <i>pme6-1</i> samples which are not shown in Chapter 4.....	261

Appendix 7: Putative cell wall genes with high guard cell expression.....	262
Appendix 8: Plasmid map showing locations of key features of the TOPO 2.1 vector	264
Appendix 9: Plasmid map showing locations of key features of the PMDC32 vector.....	265
Appendix 10: DNA sequences for PME1 genes overexpressed in <i>A. thaliana</i>	266
Appendix 11. DNA sequences for tissue specific promoters.....	268
Appendix 12. Correlation analysis of AFM force data.....	272
Appendix 13: Publications arising from this thesis	273

Table of figures

Figure 1.1. Monocot vs Dicot stomata.....	2
Figure 1.2. Stomatal development.....	4
Figure 1.3. The effect of gene knockout on stomatal development.....	7
Figure 1.4. The signalling mechanisms for stomatal closing and opening.....	9
Figure 1.5. Major structural properties of guard cells.....	11
Figure 1.6. The structure of cellulose.....	13
Figure 1.7. The main structural features of xyloglucan.....	15
Figure 1.8. The structure of the four different types of pectin.....	17
Figure 3.1. Anatomy of guard cells.....	42
Figure 3.2. Arabidopsis leaf cross-section showing guard cells.....	45
Figure 3.3. Antibody binding of hemicellulose antibodies.....	49
Figure 3.4. Antibody binding of pectin antibodies.....	53
Figure 3.5. Antibody binding of other cell wall components.....	56
Figure 3.6. Pectic antibody labelling of stomatal cell walls. 1.....	61
Figure 3.7. Guard cell labelling of non-pectic cell wall components.....	64
Figure 3.8. Cell wall components of the cuticular ledge.....	66
Figure 3.9. Pectate lyase treatment reveals masked cell wall epitopes.....	70
Figure 3.10. Antibody labelling comparing opened and closed stomata.....	72
Figure 4.1. Schematic representation of homogalacturonan.....	85
Figure 4.2. EFP browser data showing expression data for <i>PME6</i>	87
Figure 4.3. The structure of the <i>PME6</i> gene.....	88
Figure 4.4. Genotyping of <i>pme6-1</i> insertion line from NASC.....	89
Figure 4.5. Semi quantitative RT-PCR of <i>pme6-1</i>	90
Figure 4.6. GUS histochemical staining showing localisation of <i>pme6-1</i>	91

Figure 4.7. EFP browser data.....	92
Figure 4.8. <i>pme6-1</i> seed characteristics are unchanged.....	94
Figure 4.9. <i>pme6-1</i> growth responses to CO ₂	96
Figure 4.10. Stomatal size or density in <i>pme6-1</i>	98
Figure 4.11. Guard cell opening/closure response to changing CO ₂ concentration in the <i>pme6-1</i> plants.....	99
Figure 4.12. Guard cell opening/closure response to changing ABA concentrations in the <i>pme6-1</i> mutant.....	100
Figure 4.13. <i>pme6-1</i> stomatal response to mannitol.....	102
Figure 4.14. <i>pme6-1</i> guard cells treated with mannitol have a reduced aspect ratio to WT plants.....	102
Figure 4.15. <i>pme6-1</i> plants are less able to adjust leaf temperature under drought conditions.....	104
Figure 4.16. Guard cell wall pectin composition is altered in <i>pme6-1</i>	107
Figure 4.17. Pectin methylation pattern in guard cells is restored to WT in complemented <i>pme6-1</i> plants	108
Figure 4.18. <i>pme6-1</i> plants have altered assimilation rates.	110
Figure 4.19. Response of <i>pme6-1</i> plants to shifts in CO ₂ concentration.....	112
Figure 4.20. Stomatal opening with blue light.....	114
Figure 4.21. TEM analysis of <i>pme6-1</i> guard cell structure.....	115
Figure 4.22. Schematic diagram of guard cell HGA distribution	121
Figure 5.1. Cell wall genes with upregulated expression in guard cells	128
Figure 5.2. Primer design for genotyping on T-DNA insert lines	130
Figure 5.3. Genotyping of NASC lines.....	132
Figure 5.4. Stomatal size is unchanged in the NASC insertion lines.....	134
Figure 5.5. Stomatal density is unchanged in the NASC insertion lines	135
Figure 5.6. Stomatal patterning is unchanged in NASC insertion lines	136
Figure 5.7. <i>focl</i> plants have altered stomatal patterning.....	137

Figure 5.8. Growth rate of NASC lines compared to Col-0.	140
Figure 5.9. Growth rate of <i>focl</i> is slower than Col-0.....	141
Figure 5.10. Whole plant transpiration is the same for NASC lines.....	142
Figure 5.11. <i>focl</i> plants are hotter than Col-0 plants.....	143
Figure 5.12. Responses of NASC lines to CO ₂	147
Figure 5.13. <i>focl</i> responses to CO ₂	148
Figure 5.14. <i>focl</i> stomata have a pore covering	150
Figure 5.15. <i>focl</i> plants have altered mesophyll structure	151
Figure 5.16. Immunolabelling of NASC mutants reveals no differences in the cell wall composition	153
Figure 5.17. Immunolabelling of <i>focl</i> revealed no major differences in cell wall composition	155
Figure 5.18. Isolation of PME1 genes.....	156
Figure 5.19. Verification of inserts in pENTR/D-TOPO vector	157
Figure 5.20. Digestion of TOPO with <i>nsiI</i> to remove kan resistance.....	157
Figure 5.21. Verification of LR reaction.	158
Figure 5.22. Isolation of promoters and addition of restriction sites.....	158
Figure 5.23. Removal of CaMV promoter by <i>pmeI</i> and <i>bamHI</i> digestion ...	158
Figure 5.24. Stomatal patterning and size is unaffected in mutant plants ...	161
Figure 5.25. Thermal imaging of transgenic lines.	163
Figure 5.26. Antibody labelling of AtPMEI2 lines.	164
Figure 5.27. Antibody labelling of AdPMEI1 lines.	165
Figure 5.28. Gas exchange analysis of transgenic lines – A/Ci curves	168
Figure 5.29. Gas exchange analysis of transgenic lines - Light curves.....	170
Figure 6.1. Setup for a typical Atomic Force Microscope	180
Figure 6.2. AFM cantilever.	181
Figure 6.3. A force curve comparing a plant sample and a glass sample.....	184

Figure 6.4. Topographical images of stomata from plants grown either on soil MS media.....	189
Figure 6.5. Length of time samples can be imaged for.....	191
Figure 6.6. Comparison of stomatal responses to CO ₂ for plants grown on soil and plants grown on MS media.....	192
Figure 6.7. Stomatal complement	193
Figure 6.8. Stomatal aperture response to ABA in adhered samples.....	194
Figure 6.9. Fluorescein diacetate staining of stomata.....	196
Figure 6.10. 3D rendering of topographical data	197
Figure 6.11. Topography of stomata from early development through to mature stomata.....	199
Figure 6.12. The response of a single stomata to ABA.	202
Figure 6.13. <i>focl</i> stomatal covering can be observed by AFM.....	204
Figure 6.14. Deflection maps of a <i>focl</i> stomata imaged sequentially	205
Figure 6.15. Absolute stiffness values show large variability.	207
Figure 6.16. Schematic diagram clarifying stomatal dimensions.....	208
Figure 6.17. Stomatal stiffness does not correlate with size or shape..	210
Figure 6.18. Schematic diagram illustrating how the guard cell area is split into inner stomata and outer stomata.	211
Figure 6.19. Inner stomatal elasticity increases as outer stomatal elasticity increases.....	212
Figure 6.20. Stomatal elasticity properties are dependent on the stage of stomatal development	215
Figure 6.21. Stomatal topography schematic.	218
Figure 6.22. Schematic of cell wall deformation and indentation.....	220

List of tables

Table 2.1 Components per 25µl PCR reaction using <i>Taq</i> DNA polymerase... 28	
Table 2.2. PCR components per 50µl PCR reaction using Q5® High-Fidelity DNA Polymerase..... 29	
Table 3.1. Cell wall antibodies which showed no binding in mature <i>Arabidopsis</i> leaves..... 57	
Table 3.2. The effect of pectate lyase treatment on antibody binding 68	
Table 4.1. Expression of <i>PME6</i> in different tissues..... 86	
Table 5.1. <i>A. thaliana</i> genes identified as upregulated in guard cells 129	
Table 5.2. List of gene constructs 159	

List of equations

Equation 2.1. Relative water content.	34
Equation 2.2. Pore area calculation	34
Equation 2.3. Stomatal index.....	35
Equation 5.1. Percentage of stomatal complex taken up by pore.....	145
Equation 6.1. Force applied	183
Equation 6.2. Distance.....	183
Equation 6.3. Aspect ratio.....	209

Chapter 1. Introduction

Plant productivity is crucial to the success of human endeavour; increasing the yield of crops remains a crucial goal in order to feed a growing global population (United Nations Department of Economic and Social Affairs/Population Division and Nationen, 2011). Despite this need for increased productivity, yield increases conferred by conventional breeding methods introduced during the green revolution are beginning plateau (Pingali, 2012).

The effects of climate change, including changing CO₂ levels and increased climatic variability (Parry et al., 2004) coupled with the rise in biofuel use competing with crops for land (Boddiger, 2007; Fargione et al., 2008) will place further pressure on finding ways to increase crop yields. In order to meet these yield demands more insights are needed into fundamental pathways and mechanisms in plants in order to be able to optimise crops for increased growth in current and future climates. Climate models predict increasing variability in environmental conditions (Long et al., 2004; Southworth et al., 2000) in the coming years. The manner in which plants are able to respond and adapt to this increased variability may be crucial in maintaining and improving crop productivity. Stomata which are present on the epidermis of plants function as valves which regulate the loss of water by evapotranspiration and the fixation of CO₂ for photosynthesis (P. Franks and Farquhar, 2007). Stomata are crucial in allowing plants to react to fluctuating environments to maximise CO₂ uptake while minimising water loss. This thesis aims to increase our understanding of stomata and their role in plant growth.

1.1 The role of stomata in leaf function

Stomata consist of a pair of specialised epidermal cells, known as guard cells, which flank a pore in the leaf surface (Figure 1.1). In monocots guard cells are 'dumbbell shaped' and have a pair of subsidiary cells, thought to provide support, which form the stomatal complex ((Srivastava and Singh, 1972) Figure 1.1.B). In dicots stomata do not have subsidiary cells and guard cells are kidney shaped ((Zhao and Sack, 1999) Figure 1.1.A). In plants with kidney shaped stomata it is unclear what role, if any, the neighbouring epidermal cells play in stomatal function.

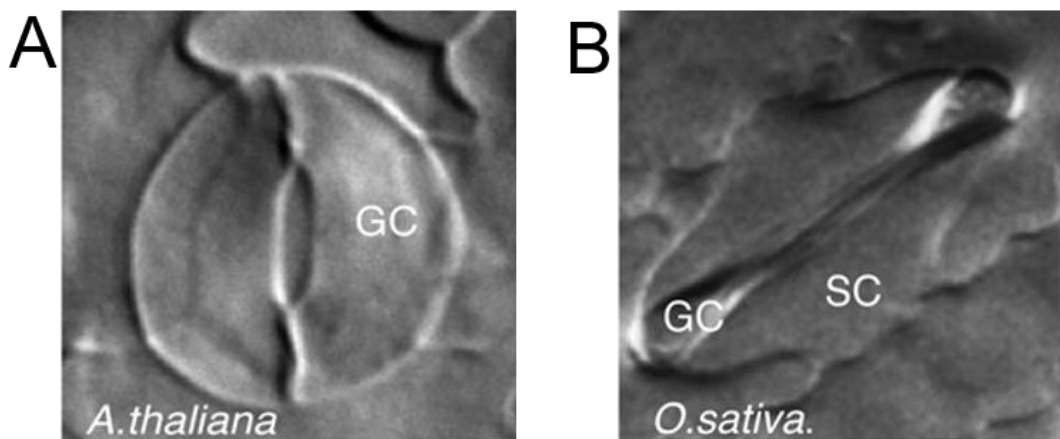


Figure 1.1. (A) Stomata from the dicot *A. thaliana*. (B) Stomata from the monocot *O. sativa*. Guard cell indicated by GC and subsidiary cell indicated by SC.

Image adapted from Liu et al., 2009.

Guard cells change in both size and shape to regulate the aperture of the pore in response to intrinsic and extrinsic signalling cues (Kim et al., 2010). The modulation of stomatal aperture is achieved by the control of guard cell turgor pressure (DeMichele and Sharpe, 1973; Mott and Franks, 2001). During stomatal opening turgor pressure increases as water is taken into the guard cell, causing the cells to expand and bend open.

CO₂ uptake for photosynthesis is only one aspect of stomatal function. Although water loss by evapotranspiration must be minimised to prevent drought stress it can play important roles in the temperature regulation of the plant (Doheny-Adams et al., 2012) as the loss of water causes an evaporative cooling effect. The flow of water out of the leaves creates a transpiration pull within the plant which can lead to greater nutrient uptake (Novák and Vidovič, 2003). Stomata are also a point of entry for pathogens such as *Pseudomonas syringae* (Melotto et al., 2006), and it has been shown that stomatal closure is part of the plants defence pathway to prevent pathogen entry (Zeng et al., 2010).

In the short term plants respond to environmental fluctuation by regulating stomatal aperture, whereas longer term environmental changes can cause changes in the number and spacing of stomata on a leaf through the stomatal development pathway.

1.2 The stomatal development pathway

Stomata have been studied extensively and many of the genes involved in regulating stomatal development and patterning have now been elucidated (Bergmann et al., 2004; Hara et al., 2007; Hunt et al., 2010; Hunt and Gray, 2009). Altering stomatal development in plants can have drastic consequences for whole plant physiology (Doheny-Adams et al., 2012), in particular water use efficiency. The stomatal lineage is initiated by a protodermal cell, which becomes committed to divide and is known as a meristemoid mother cell (MMC). This MMC divides asymmetrically, giving rise to a small meristemoid and a larger cell known as a stomatal lineage

ground cell (SLGC) (Bergmann and Sack, 2007). The meristemoid undergoes additional rounds of asymmetric divisions (amplifying divisions) which increases the number of SLGCs while maintaining the original meristemoid. After one to three rounds of amplifying divisions the meristemoid differentiates into a guard mother cell (GMC). The GMC undergoes a symmetric division to form two guard cells which make up the stomatal complex. The SLGCs differentiate into epidermal pavement cells and can also divide asymmetrically to increase the number of meristeoids, these divisions are known as spacing division (Figure 1.2). Spacing divisions are orientated such that there is always one cell between meristeoids ensuring that stomata are not placed adjacent to each other. In Figure 1.2 the major steps of stomatal development are shown and the key genes acting at each step are shown.

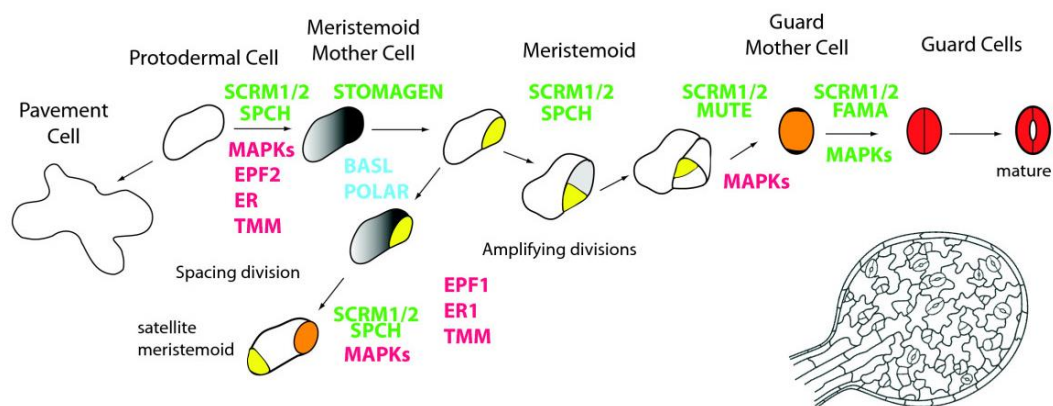


Figure 1.2 . Stomatal development. The major stages of stomatal development showing different cell division pathways and the major regulatory genes acting at each step. Positive regulators shown in green, negative regulators in red and polarity regulators in blue. Figure taken from Vatén and Bergmann, 2012.

The stomatal development pathway not only produces the stomata but is also responsible for a significant proportion of the cells in the epidermis (Dong and Bergmann, 2010). It is thought that the spacing of the epidermal cells is regulated to maximise CO₂ uptake by optimising the distances that gases have to diffuse (Rowe and Bergmann, 2010).

The discovery of multiple genes affecting stomatal differentiation highlights the advances made in our understanding of stomatal development in recent years. The function of many of these genes is still being confirmed and the characterisation of a complete stomatal development pathway will prove extremely beneficial to the field. Progress has been made on this with mutants in many of the genes in this pathway leading to an alteration in stomatal density and a breakdown of the one cell spacing pattern as shown in Figure 1.3 (Bergmann and Sack, 2007). The leucine rich-repeat containing receptor-like protein (LRR-RLP) TOO MANY MOUTHS (TMM), the subtilisin-like serine protease STOMATAL DENSITY AND DISTRIBUTION 1 (SDD1) and the ERECTA family (ER;ERL1;ERL2) of leucine rich-repeat-containing receptor-like kinases (LRR-RLK) all function upstream of a mitogen activated protein kinase (MAPK) signalling cascade (Bhave et al., 2009; Groll et al., 2002; Lampard et al., 2008; Masle et al., 2005). Loss of function mutants *tmm*, *sdd1-1* and *erecta* show increased stomatal density and stomatal clustering (Groll et al., 2002; Masle et al., 2005; Yang and Sack, 1995). These upstream signalling components are involved in the negative regulation of stomatal patterning and are important in establishing the stomatal one cell spacing pattern (Dong and Bergmann, 2010; Wang et al., 2007). They feed into a mitogen activated protein kinase (MAPK) pathway which includes the MAP kinases MPK3 and MPK6, the MAPK kinases MKK4 and MKK522 and the MAPKK kinase YODA (Bergmann et al., 2004; Lampard et al., 2008; Wang et al., 2007). Three basic helix-loop-helix (bHLH) transcription factors SPEECHLESS (SPCH), MUTE and FAMA are proposed to positively regulate stomatal development by directing entry into the stomatal lineage and regulating subsequent divisions (Lampard et al., 2008; Liu et al., 2009; Ohashi-Ito and Bergmann, 2006). SCREAM and SCREAM2 are thought to regulate the actions of SPCH, MUTE and FAMA (Ohashi-Ito and Bergmann, 2006). Importantly it has been shown that SPCH is regulated

by YODA (Bergmann et al., 2004), providing a link between positive and negative regulation of stomatal development.

The EPFs (EPIDERMAL PATTERNING FACTORS) are purportedly ligands for the receptors TMM and ERECTA discussed above. EPF1 has been shown to be important in enforcing the one-cell-spacing rule during stomatal development (Hara et al., 2007) while EPF2 has been shown to be involved in controlling the entry of cells into the stomatal lineage (Hunt and Gray, 2009). EPF1 and 2 are negative regulators of stomatal development. EPFL9 (EPIDERMAL PATTERNING FACTOR-LIKE 9) otherwise known as STOMAGEN is a positive regulator of stomatal development (Hunt et al., 2010; Sugano et al., 2010). STOMAGEN activity was shown to be dependent on the SPCH pathway and to require TMM to function. It is suggested the negative signalling peptides (EPF1 and EPF2) compete with positive signalling peptides (EPFL9/STOMAGEN) for the same receptor (TMM) (Sugano et al., 2010).

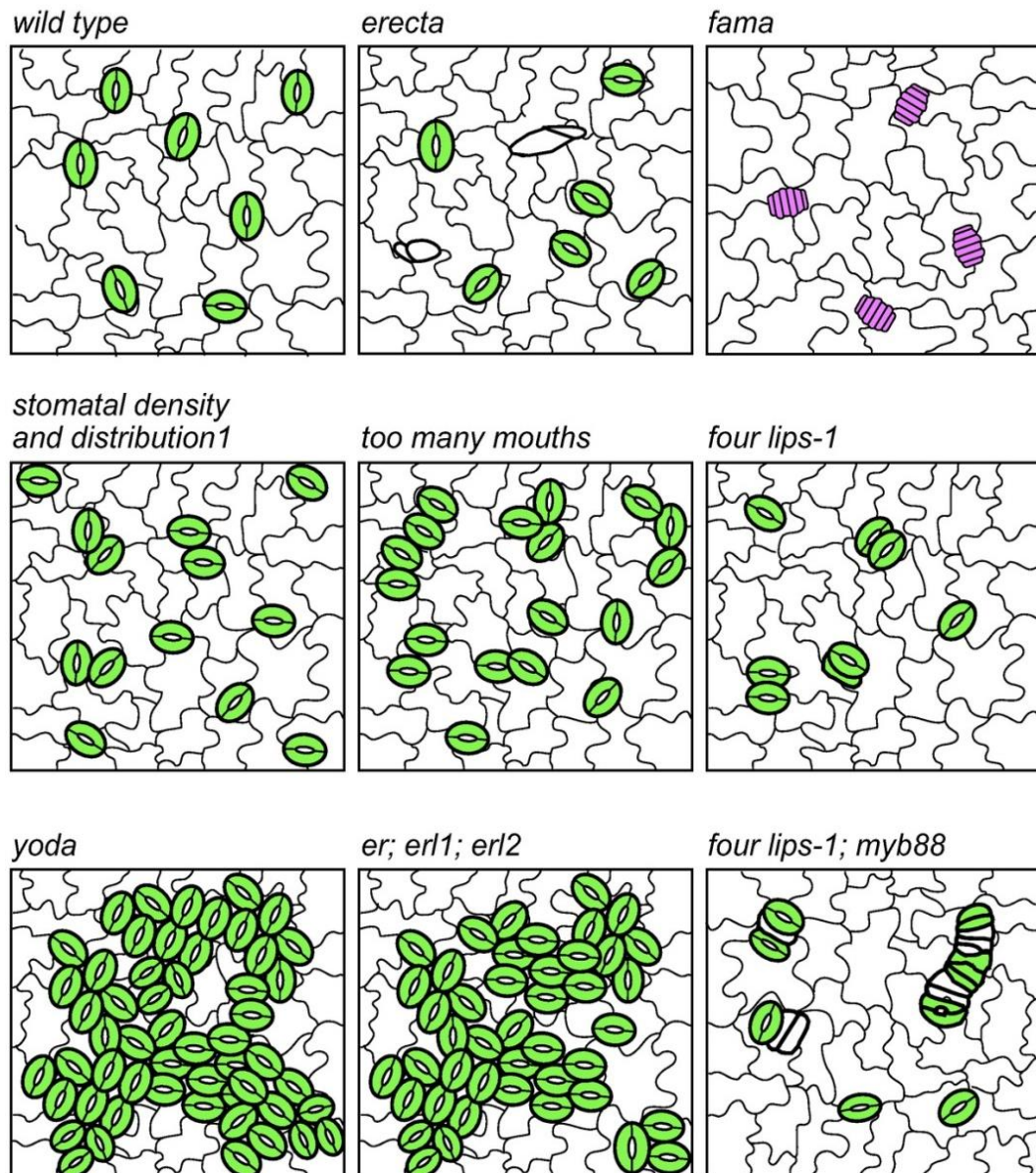


Figure 1.3. Knocking out genes in the stomatal development pathway leads to alterations in stomatal density and patterning. Epidermal schematics showing the effect of gene knockouts on stomatal patterning. Guard cells are shown in green while guard mother cells are shown in pink. Figure from (Bergmann and Sack, 2007)

1.3 Guard cell signalling

Significant advances have been made in understanding the signalling mechanisms behind stomatal opening and closing (Kim et al., 2010; Pandey et al., 2007). Multiple mutants have been identified in these pathways, some of which are due to defects in ion channels in the guard cell membranes.

Much focus has been placed on signalling mechanisms, especially the responses to CO₂ and ABA.

Stomata are extremely dynamic, being able to adjust aperture rapidly and repeatedly to suit varying environmental conditions (Chen et al., 2012; Lu et al., 1997). Stomatal closure is an early response to abiotic stresses such as drought (Davies and Zhang, 1991), high ozone and pathogen attack (Zeng et al., 2010). Stomata of most species, with the exception of CAM plants, also close in response to darkness.

It has long been known that alterations in stomatal aperture are due to changes in turgor pressure in the guard cells. During opening, internal guard cell turgor pressure changes causes the guard cells to swell in size by up to 70% (Jones et al., 2005). Stomatal opening is driven by H⁺ extrusion mediated by plasma membrane bound H⁺ ATPases. This causes hyperpolarisation of the membrane, activating K⁺ channels causing K⁺ influx. Changes to guard cell water potential due to influx of K⁺, which is balanced by the accumulation of solutes, such as Malate²⁻, Cl⁻ and NO₃⁻, cause the influx of water and this increased turgor pressure causes stomatal opening (Schroeder and Allen, 2001). Stomatal closure is caused by K⁺ outward rectifying channels causing K⁺ efflux from the guard cells. This is triggered by anion efflux from the guard cells which cause membrane depolarisation (Kim et al., 2010). Figure 1.4 shows the key components of guard cell opening and closure.

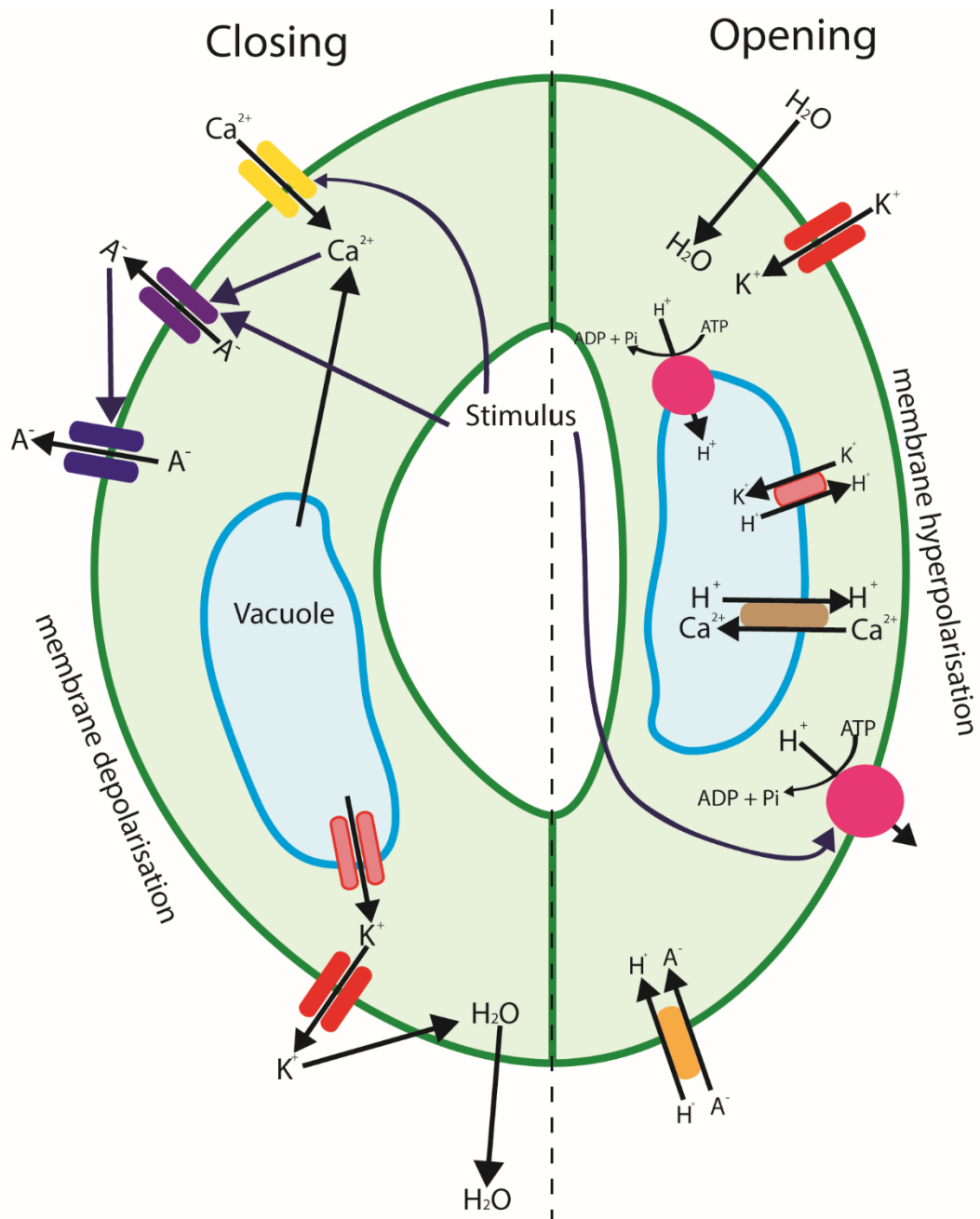


Figure 1.4. An overview of the signalling mechanisms for stomatal closing (left) and opening (right). Stomatal closure is triggered by a stimulus, often ABA. This can activate inward acting Ca^{2+} channels leading to an increase in cytosolic Ca^{2+} , release of Ca^{2+} also occurs from the vacuole. The increase in Ca^{2+} activates S-type anion channels which can also be activated by stimuli independently of Ca^{2+} . The S-type anion channels cause the influx of ions such as malate and Cl^- which activates R-type anion channels. This causes membrane depolarisation which activates outward rectifying K^+ channels, this changes the water potential of the guard cell leading to the efflux of H_2O which causes a reduction in turgor pressure and guard cell closure. In stomatal opening a stimulus activates membrane H^+ -ATPases. The extrusion of H^+ ions causes a membrane hyperpolarisation activating inward rectifying K^+ channels. The influx of K^+ is balanced by the import of anions by H^+ symporters. Hyperpolarisation of the vacuolar membrane by H^+ -ATPases causes inhibition of calcium induced stomatal closure by activating H^+ - Ca^{2+} antiporters leading to a decrease in cytosolic Ca^{2+} . A⁻ = Anions.

Disruption of ion channels, such as the potassium influx channels encoded by KAT1 and KAT2 lead to impaired stomatal function (Lebaudy et al., 2010), similarly knockout of *GORK*, encoding a potassium efflux channel, led to impaired stomatal closure (Ache et al., 2000; Hosy et al., 2003). *SLAC1* (*SLOW ANION CHANNEL-ASSOCIATED 1*) has been shown to be necessary for stomatal closure. Disruption of *SLAC1* impairs the action of slow (S-type) anion channels while rapid (R-type) anion channels are unaffected (Vahisalu et al., 2008).

1.4 Structural properties of guard cells

The signalling mechanisms discussed above cause changes in guard cell turgor pressure which ultimately lead to stomatal opening or closure. The structural characteristics of stomata are crucial in allowing turgor pressure changes to cause stomatal movement. As the major structural component in plants it is clear that the cell wall will have a key role in dictating the structural properties of guard cells. Despite this, much remains to be elucidated about the composition of the guard cell wall or how this contributes to stomatal functioning.

Guard cells are highly anisotropic. Radially orientated cellulose microfibrils in the guard cells create hoops perpendicular to the length axis of the pore (Palevitz and Heple, 1976). This guides the direction of cell expansion meaning that the guard cells expand in length more than they do in width (Figure 1.5.A). Additionally, guard cells have asymmetrically thickened cell walls with the inner cell walls (facing the pore) being thicker than the outer cell walls ((Zhao and Sack, 1999) Figure 1.5.B). This disparity in cell wall thickness means the inner cell walls extend less than the outer cell walls, causing the stomata to bend open to leave a central pore.

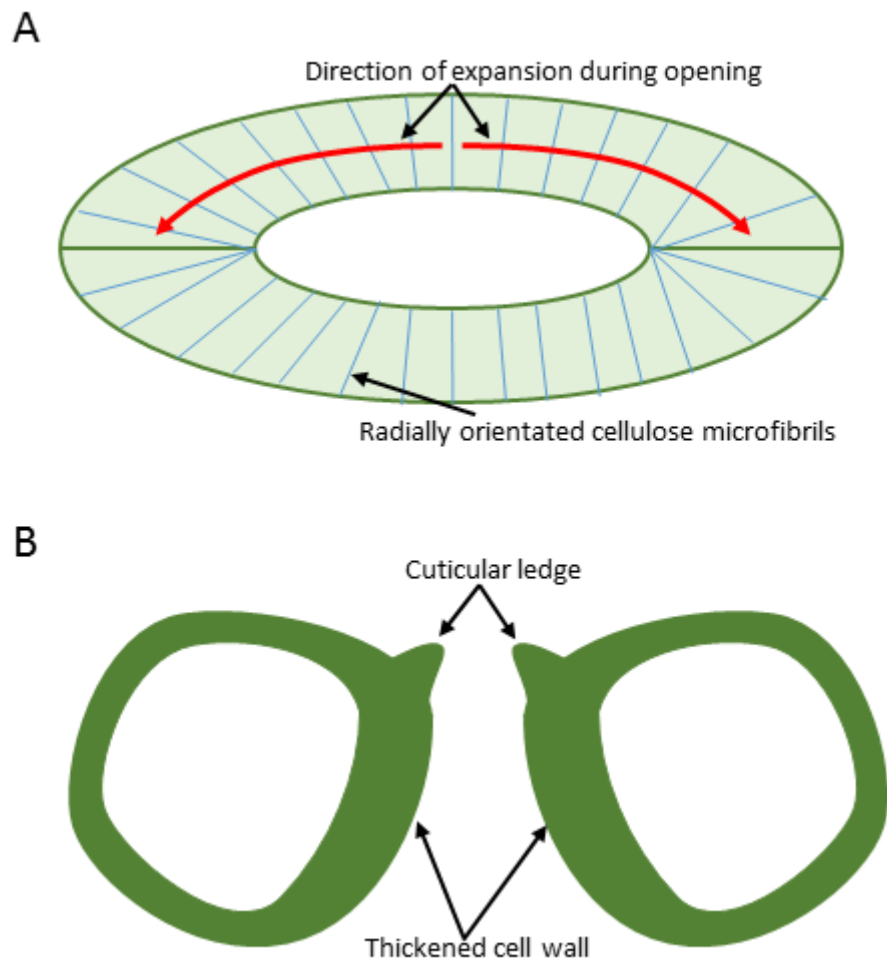


Figure 1.5. Major structural properties of guard cells. (A) Guard cells have highly ordered cellulose microfibrils radiating in hoops perpendicular to the long axis of the guard cells. These guide the direction of expansion anisotropically during high turgor pressure conditions. (B) A schematic of a stomatal cross-section showing differential cell wall thickening. The cell walls facing the pore are thicker than the outer cell wall. During turgor-induced guard cell expansion this causes the inner wall to extend less than the outer wall causing the guard cells to bend apart and open.

Very little is known about the finer structure of stomatal cell walls and to what extent this contributes to the wider mechanical properties of stomata. Stomata have been shown to be enriched in pectin (Jones et al., 2005; Majewska-Sawka et al., 2002) and pectic arabinan has been shown to be crucial to stomatal function (L. Jones et al., 2003). Recent work has shown that plants lacking xyloglucan had impaired stomatal function and showed that plants with reduced cellulose content had wider stomatal apertures (Rui

and Anderson, 2016). These findings suggest that cell wall composition is important for guard cell function. Despite these advances it is remarkable how little is known about the mechanical properties of guard cell walls or how their properties could affect stomatal function. Both the composition and the mechanical properties of cell walls are in general poorly defined although some advances have been made in recent years (Braybrook and Jönsson, 2016; Geitmann, 2010; Hamant et al., 2008; Knox, 2008).

1.5 Cell walls

Cell walls surround virtually all plant cells and are essential to provide rigidity and support (Albersheim et al., 2011; Wei et al., 2009). Changes in cell shape and size, both reversible and irreversible, are driven by the action of turgor pressure pushing outwards from a cell causing expansion (COSGROVE, 1993; Mott and Franks, 2001). The cell wall opposes turgor pressure preventing unwanted deformation of the cell. Thus the extensibility of the cell wall is a key factor in allowing cellular growth and also the reversible changes in cell size observed during stomatal opening and closing.

The cell wall is a complex matrix consisting primarily of cellulose microfibrils, hemicelluloses and pectins with a small number of structural proteins also incorporated. Some cells, which have ceased to grow, incorporate lignin to provide further strength and become known as secondary cell walls. There is very little secondary cell wall production in *Arabidopsis thaliana* most of it being limited to the vascular tissue and the floral stem. Secondary cell walls are of great interest in the production of biofuels (Pauly and Keegstra, 2010; Somerville et al., 2010) and have been the subject of numerous recent detailed reviews (Kumar et al., 2016; Miedes et al., 2014; Zhong and Ye, 2015) but are not covered further in this thesis.

1.5.1 Cellulose

Cellulose is the predominant polymer in most cell walls and is arguably the best characterised of the cell wall components. Cellulose makes up to a third of total plant biomass (Somerville, 2006). Formed from a repeating dimer of β -1,4 linked glucose monomers (Figure 1.6), linear chains of around 10000 residues in length are formed.

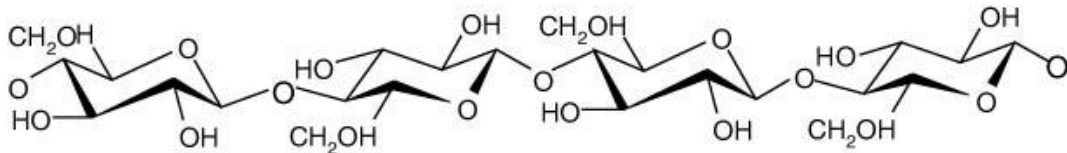


Figure 1.6. β -1,4 Linked glucose dimer which forms the repeating structure of cellulose. Thought to have a degree of polymerisation of around 10000. Figure from Somerville, 2006.

These individual glucan chains bond together via hydrogen bonding to form cellulose microfibrils. There is some debate regarding the number of glucan chains which make up a cellulose microfibril, with the historical view being that 36 glucan chains were coalesced into one microfibril (Cosgrove, 2014). Recent data has suggested that the diameter of cellulose microfibrils is more conducive to an 18 strand model (Newman et al., 2013). It is not yet clear to what extent the construction of cellulose microfibrils varies between species and tissue types but the identification of large numbers of genes involved in cellulose biosynthesis (Andersson-Gunneras et al., 2006) provides scope for variation. Cellulose is synthesised at the cell membrane and the construction of glucan chains and assembly into microfibrils is controlled by the cellulose synthase complex. Cellulose synthesis has been reviewed extensively (McFarlane et al., 2014) with a large number of involved genes having been elucidated (Zhong and Ye, 2015) and is only summarised here briefly. The cellulose synthase complex is a rosette constructed of 6 subunits each of which are thought to be aggregates of three cellulose synthase subunits. In the 18 strand model each subunit (of which there are 18 in total) is proposed

to synthesise a single glucan chain (Newman et al., 2013; Zhong and Ye, 2015). Cellulose is secreted to the cell wall and microtubules are key in modulating the deposition of cellulose (Palevitz and Heple, 1976). Cellulose is responsible for most of the load-bearing strength of the cell walls and increased cellulose deposition is observed when cell walls are placed under mechanical stress (Andersson-Gunneras et al., 2006).

1.5.2 Hemicelluloses

Hemicelluloses are highly heterogeneous and some dispute exists as to what constitutes a hemicellulose and what does not. For the purpose of this thesis hemicelluloses are classed as cell wall polysaccharides which do not fit into the classes of cellulose or pectin and having a β -(1→4)-linked backbone made of glucose, mannose, or xylose (Scheller and Ulvskov, 2010). In *A. thaliana* the main hemicellulose in primary cell walls is xyloglucan (XyG) with small amounts of glucomannan and mannan being present (Scheller and Ulvskov, 2010). Secondary cell walls have low XyG levels and instead contain large amounts of xylan. As guard cells and their surrounding cells do not contain secondary cell walls xylan is not covered here.

Xyloglucan

Xyloglucan is the most abundant hemicellulose found in primary cell walls of the majority of dicot plants. A β -1,4-linked glucan chain forms the xyloglucan backbone which is highly substituted to form a branched structure (Scheller and Ulvskov, 2010). The structure is variable but is usually classed based on its main repeating units. These repeating units are given single letter codes to denote the side groups attached to the glucose residue (Scheller and Ulvskov, 2010). Figure 1.7 shows the main side groups and the

one letter codes for different structures of xyloglucan. The highly substituted XXXG is the predominate XyG structure in dicots such as *A. thaliana*. The extent of branching has functional impacts on XyG as more branched chains are more soluble. XyG biosynthesis is becoming reasonably well understood, however insights into the roles of different xyloglucan conformations have remained elusive.

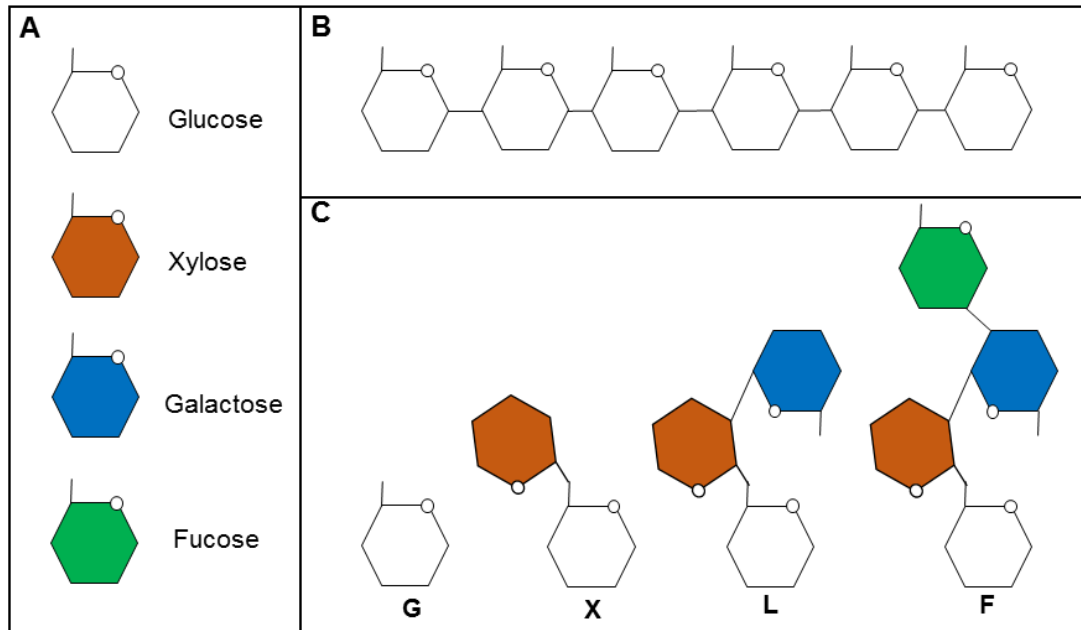


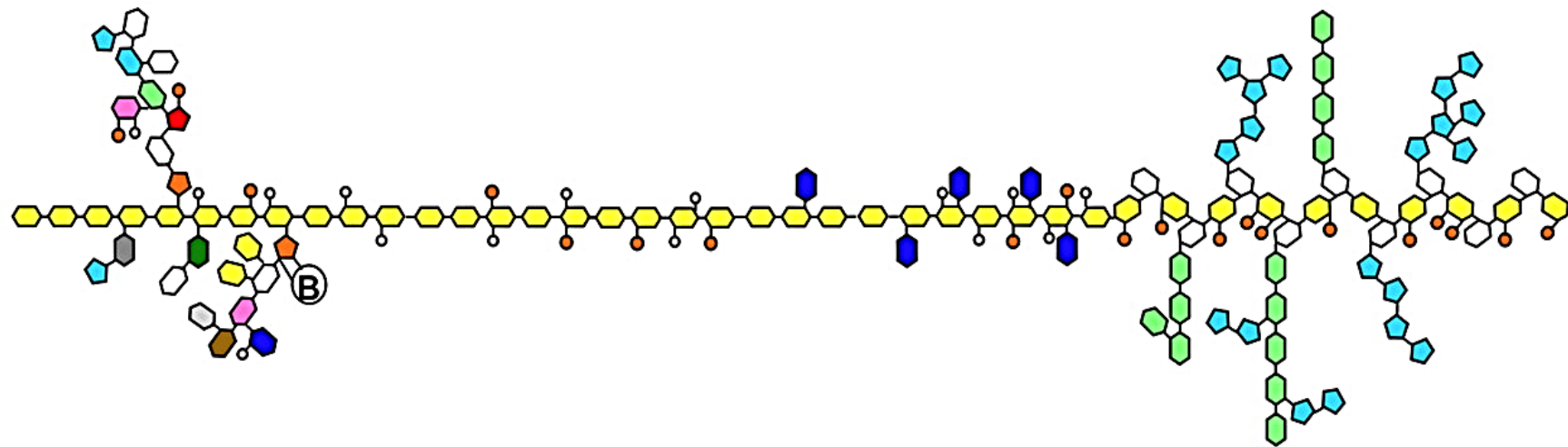
Figure 1.7. Xyloglucan: The main structural features of xyloglucan. A) Different sugar residues present in xyloglucan. B) The xyloglucan backbone of repeating glucose residues. C) The common xyloglucan side chains and their one letter codes.

1.5.3 Pectins

Pectins are one of the major non-cellulosic components of the primary cell wall, especially in dicotyledonous plants (Caffall and Mohnen, 2009). They link together to form a distinct network which connects to the cellulosic network (Jones et al., 2005). Pectins are highly complex polysaccharides (Cosgrove, 2005) and it has become apparent that their functions are key to the mechanical properties and functioning of primary cell walls (Wolf and Greiner, 2012; Yoneda et al., 2010). Pectic polysaccharides are characterised by their high galacturonic acid (GalA) content (Caffall and Mohnen, 2009)

and are traditionally categorised into 3 main classes: rhamnogalacturonan I (RGI); rhamnogalacturonan II (RGII) and homogalacturonan (HGA) (Ridley et al., 2001). HGA also makes up the backbone of xylogalacturonans (Schols et al., 1995). As shown in Figure 1.8 all of the pectins classes have a GalA backbone with the exception of RGI which has alternating GalA and Rhamnose residues. As shown in figure 1.8 HGA is relatively linear compared to RGI and RGII which are extensively branched. RGI and II side branches are particularly enriched in arabinan and galactan and are known to have an impact on cell wall mechanical properties (Pena and Carpita, 2004). The ratio between the different types of pectin varies between species but HGA is usually the most abundant form (Mohnen, 2008) and in *Arabidopsis* accounts for up to 23% of the dry weight of the cell wall (Caffall and Mohnen, 2009).

Rhamnogalacturonan II Homogalacturonan Xylogalacturonan Rhamnogalacturonan I



- | | | | |
|-------------------------|-------------------|-----------------|--------------|
| ⬡ = D-Galacturonic acid | ⬢ = L-Arabinose | ⬢ = D-Apiose | ⬢ = O-Acetyl |
| ⬡ = L-Rhamnose | ⬢ = D-Galactose | ⬢ = L-Fucose | ⬢ = O-Methyl |
| ⬢ = D-Glucuronic acid | ⬢ = L-Aceric acid | ⬢ = D-Xylose | Ⓟ = Borate |
| ⬢ = Kdo | ⬢ = D-Dha | ⬢ = L-Galactose | |

Figure 1.8. A schematic for the structure of the four different types of pectin. Kdo stands for 3-Deoxy- D-manno-2-octulosonic acid and DHA stands for 3-deoxy-D-lyxo-2-heptulosaric acid. Figure from Harholt et al., 2010

Pectin biosynthesis is a complex process and little is known about it. Pulse chase experiments determined that pectin is synthesised in the golgi and transported to the cell wall in vesicles (Harris and Northcote, 1971; Northcote and Pickett-Heaps, 1966; Pickett-Heaps, 1968). It is thought that pectin is synthesised by glycosyltransferases (GTs), enzymes which transfer sugar moieties. It is predicted that at least 67 transferases are required for the synthesis of pectin and to date very few of these have been identified (Mohnen, 2008). In addition to GTs, methyltransferases and acetyltransferases are also required for the synthesis of pectin (Harholt et al., 2010). The few pectin biosynthetic enzymes that have been identified have been Golgi localised, further suggesting the Golgi as the site of pectin synthesis (Harholt et al., 2010; Sterling et al., 2001). The first pectin biosynthesis enzyme fully identified was an α -1,4-GalA transferase known as GALACTURONOSYLTRANSFERASE1 (GAUT1 (Sterling et al., 2006)). GAUT1 has been shown to be able to synthesis polygalacturonic acid in vitro (Sterling et al., 2006). Another GT enzyme QUASIMODO1 (QUA1/GAUT8) has also been implicated in pectin biosynthesis (Bouton et al., 2002). *qua1* loss of function mutants are deficient in HGA and have severe growth defects (Bouton et al., 2002; Orfila et al., 2005). Two further GTs, GAUT13 and GAUT14 (from glycosyltransferase family 8) are putatively involved in pectin biosynthesis. *gaut13gaut14* double mutants had altered distribution of HGA epitopes (as shown by immunolabelling) and stunted pollen tube growth (L. Wang et al., 2013).

The pectin network has diverse roles in plants. The role of pectin in cell-cell adhesion is well known as it has implications for food ripening and storage (Ahmed and Labavitch, 1980). Pectin breakdown has been shown to reduce cellular adhesion which leads to fruit softening (Brummell and Harpster, 2001). A tomato mutant with reduced calcium linked HGA showed reduced fruit quality due to large intercellular air spaces, putatively due to defects in

cell-cell adhesion (Eriksson et al., 2004; Thompson et al., 1999). Pectin has also been implicated in cell-cell adhesion outside of fruit (Knox, 1992; Marry et al., 2006) and is known to be abundant in the middle lamella.

Pectin is known to impact on the mechanical properties of the cell wall. Knockout of *PME35*, a gene regulating pectin composition, leads to a reduction in the mechanical strength of *A. thaliana* inflorescence stems (Hongo et al., 2012). Cell wall expansibility has been correlated with increased pectic arabinan and galactan content (Stolle-Smits et al., 1999) and enzymatic removal of pectic arabinan has been shown to reduce stomatal movement, possibly due to increased rigidity (L. Jones et al., 2003). As well as direct impacts on cell wall mechanics it has also been posited that pectin is involved in the deposition and orientation of cellulose microfibrils (Yoneda et al., 2010) with some evidence showing binding of cellulose to pectin (Zykwinska et al., 2005), although little information exists on this.

The fact that pectin is involved in plant growth and morphogenesis is unsurprising given its role in cellular adhesion and cell wall expansibility. As discussed above, pectin synthesis mutants have severely impaired growth (Bouton et al., 2002; Orfila et al., 2005) and mutants in pectin composition have also been shown to have reduced growth (Derbyshire et al., 2007; Wen et al., 1999). It has been shown that changes to pectin composition cause localised regions of softer tissue which precedes organ outgrowth in *A. thaliana* primordia. Similarly, perturbation of pectin methylesterification leads to developmental defects in *A. thaliana* embryos (Pelloux et al., 2007).

Given these diverse functions, and the prevalence of genomic data and available mutants, it is surprising that so little is known about the finer structure of the pectin network and how this impacts on the function of the cell wall.

1.6 Plant mechanics

Cellular growth in plants is a balance of internal and external stresses. Turgor pressure within the cell pushes outwards while the cell wall surrounding the outside of the cell restricts expansion. The force of turgor pressure acts equally in all directions and so cell wall anisotropy is crucial for the generation of cells which are non-spherical. Digestion of the cell wall by enzymes results in protoplasts which are perfectly spherical (Geitmann and Ortega, 2009) demonstrating the importance of the cell wall in the generation of cell shape. The alignments of cellulose microfibrils is one factor known to cause cell wall anisotropy (Baskin, 2005) and it has been shown that cellulose can re-order in response to stresses (Williamson, 1990) to change the direction of cell wall anisotropy. Disruption of the microtubule network by oryzalin disrupts cellulose deposition and causes spherical growth (Corson et al., 2009). In shoot apical meristems it was shown that microtubule orientation is correlated with the orientation of stress, with ablation of cells causing a shift in the stress orientation and, thus, causing a realignment of microtubules (Hamant et al., 2008).

Cellular growth requires irreversible cell wall expansion and this is dictated by the cell wall extensibility. Acid promoted cell wall extensibility in cell walls under constant tension, termed cell wall creep, has been demonstrated (Cosgrove et al., 1984; Ortega et al., 1989) and expansins, which promote cell wall creep (McQueen-Mason et al., 1992) have been proposed to play a role in this process. These observations combined with the observation that xyloglucan chains bind to cellulose microfibrils (Hayashi et al., 1987; Vincken et al., 1995) led to a model of cell wall extensibility in which cellulose microfibrils, crosslinked by xyloglucan, form the main load bearing structure of the wall and that expansins control the extensibility. It was thought that pectins were important for the control of cell wall porosity, which in turn

controls the access of enzymes, such as expansin, which control cell wall extensibility (Peaucelle et al., 2012). Only a small proportion of xyloglucan seems to bind to pectin (Dick-Pérez et al., 2011) and, as discussed above, there is evidence that pectin binds to cellulose (Zykwinska et al., 2005). It has been suggested that pectin competes with xyloglucan for cellulose interactions, possibly mediated by pectic side chains such as arabinan (Peaucelle et al., 2012). This suggests that the ratio of pectin to xyloglucan may be important in determining cell wall extensibility. As discussed above, pectin is known to influence cell wall mechanical properties. In plants lacking xyloglucan cell wall creep was reduced, and treatment which perturbed the pectin network led to increased cell wall creep, demonstrating the role for pectin in modulating cell wall extensibility (Park and Cosgrove, 2012).

As previously discussed, the opening of stomata is also regulated by turgor pressure driven cell expansion. Although cellular growth requires cell expansion this expansion is irreversible, the cell expansion during stomatal opening must be reversible to allow for stomatal closure. The dynamic manner in which stomata open and close provides an interesting system in which to study reversible cell wall expansion and greater insight into the structure of the guard cell wall and that of the neighbouring epidermal cells could provide insights into the function of stomata.

1.7 Aims and objectives

The aims of this research described in this thesis were to better understand the structure and composition of the guard cell wall. I aimed to utilise an immunohistochemical technique to analyse the structural composition of guard cell walls and to apply this knowledge to identify relevant *Arabidopsis*

mutants. By understanding the genetics of guard cell wall composition, I aimed to investigate the relationship between the guard cell wall and stomatal function. Alongside the molecular genetics approach, atomic force microscopy was used to better understand the mechanical properties of guard cells.

These aims were addressed as follows:

- 1) Immunocytochemistry was used to spatially determine the location of specific cell wall epitopes in the cell wall of guard cells and their neighbouring epidermal cells in order to better understand guard cell wall composition.
- 2) A mutant in a gene encoding a guard cell localised PME was analysed for alterations to guard cell wall composition and alterations to stomatal function.
- 3) Using transcriptomic data, this approach was extended to investigate other cell wall genes that are putatively expressed in guard cells.
- 4) An atomic force microscopy technique was developed to directly measure the mechanical properties of stomata.

Chapter 2. Materials and Methods

2.1 Plant Material

2.1.1 Loss of function mutants: NASC lines

Arabidopsis thaliana of two background ecotypes were used; Columbia (*Col-0*) and *Landsberg erecta* (*L.er*). Various mutant lines in these backgrounds were obtained from the Nottingham Arabidopsis Stock Centre (NASC) and complemented mutants in these lines produced by Lee Hunt. PME lines are in the *L.er* ecotype while extensin mutants are in *Col-0*. Homozygous T-DNA insertion lines were identified by PCR while complemented mutants were identified by selecting for resistance to hygromycin and advanced to the F3 generation for further analysis.

2.1.2 Gain of function mutants: Transgenic lines

All lines were created by transforming constructs into *Col-0* plants. Seeds were harvested from T=0 plants and transformants selected by hygromycin resistance and bulked to obtain T1 seed. The T1 generation plants were analysed in batches of 100 seeds to look for segregation patterns of 1:2:1 to ensure plants with only 1 insertion were selected for further growth. T2 plants were grown on selection and grown for seed. 50 T3 seeds were placed on selection to determine homozygous lines and those lines that were homozygous were grown for experimental analysis. Further details on these lines are in chapter 5.

2.2 Plant Growth

2.2.1 Soil grown plants

For soil grown plants seeds were sown in pots containing M3 compost and perlite in the ratio 3:1 which was thoroughly mixed and wetted prior to planting. Pots were filled to level with the pot surface and soil was lightly compressed. Pots were stratified at 4°C for 72 hours in dark conditions and transferred to a controlled environment growth chamber (12 hours light, 300 μ mol PPFD⁻¹, 22°C light/16°C dark). Plants were kept in sealed clear bags until germination at which point the bags were opened and left on for a further 2 days and then removed. Following removal of the bags vented lids were placed on trays of plants until plants were 2 weeks old at which point plants were thinned out to one plant per pot. Plants for experimental analysis were grown in square 6cm diameter pots square pots and watered daily so that soil was kept moist at all times but plants were not left standing in water. In order to mitigate any position effect created by possible uneven light distribution the entire trays were rotated daily while pots were rotated between trays on a Monday, Wednesday and Friday with pots being assigned random locations. Plants grown for seed were grown in plastic trays of 6x4 plants. Each plant was in 4 cm square pots. Trays were rotated on a Monday and Thursday.

2.2.2 Media grown plants

Seeds were surface sterilised in a bleach solution (1:5 economy bleach in water) containing 0.05% Tween-20 for 10 minutes. Seeds were then rinsed 5 times in sterile water and stratified at 4°C for 5 days. Stratified seeds were grown on 1/2 strength Murashige and Skoog basal medium containing 0.8% (w/v) plant agar and 1% (w/v) sucrose. 70ml of medium was poured into

square Petri dishes (120x120x17mm) and allowed to cool fully before seeds were added to the surface.

2.3 RT-PCR

2.3.1 RNA extraction

RNA extractions were used to assess the expression of genes of interest during this project. Two methods were used, the TRIzol® extraction method was used when only small amounts of tissue were available or gene expression was supposed to be low due to its greater potential yield. All other extractions were conducted using 'Spectrum Plant Total RNA Kit' from Sigma Aldrich.

TRIzol® method

Plant material was harvested, placed in a 1.5ml Eppendorf tube and immediately plunged into liquid nitrogen. After all samples are in collected they are removed from liquid nitrogen and ground up using a micropestle. The samples are then homogenised over ice in 500µm TRIzol®. Once the sample is fully homogenised TRIzol® is topped up to 1000µl and heated for 2 minutes at 37°C and 5 minutes at room temperature. Cellular debris is pelleted by centrifugation of samples at 4°C and 12000RPM for 10 minutes. 500µl of supernatant is removed and transferred to an ice cold 1.5ml Eppendorf tube, 200µl of chloroform is added and sample mixed by inversion. Samples are centrifuged at 4°C and 12000RPM for 20 minutes until the mixture separates into 3 phases; a lower red phase, an interphase and a colourless upper phase. The upper phase is collected, transferred to a new ice cold Eppendorf tube and the RNA is precipitated by the addition of 0.5ml of 100% isopropanol. Samples are incubated for 10 minutes at room temperature and then overnight at -20°C. The sample is centrifuged for 15 minutes at 4°C and 12000RPM until a pellet forms and the supernatant

discarded. 1000µl of 80% (v/v) ethanol in H₂O is added to the pellet, and centrifuged for 5 minutes at 4°C and 12000RPM. The supernatant is removed and pellet air-dried. RNA is re-suspended in 20µl of nuclease-free water and used for quantification and first strand cDNA synthesis (as described in 2.3.2 and 2.3.3).

Spectrum Plant Total RNA Kit method

RNA was extracted according to the instructions from sigma. Plant tissue was harvested (approximately 100mg per extraction), frozen in liquid nitrogen and ground to a fine powder. 500µl of lysis solution mixed with 5µl of 2-mercaptoethanol was added to the sample and thoroughly homogenised. Samples were then vortexed for 30 seconds and incubated at 56°C for 5 minutes. Cellular debris was collected into a pellet by centrifuging at 14000nRPM for 4 minutes. The supernatant was transferred to a filtration column seated in a 2ml collection tube and centrifuged at 14000 RPM for 1 minute. 500µl of binding solution was added to the flow-through from the filtration column and vortexed for 5 seconds. The mixture was pipetted onto a binding column seated in a 2ml Eppendorf tube and centrifuged at 14000 RPM for 1 minute. The flow-through was discarded and collection tube turned upside down and tapped onto clean absorbent paper. 500µl of wash solution 1 was pipetted onto the column and centrifuged at 14000 RPM for 1 minute, the flow-through was discarded. 500µl of wash solution 2 was added to the column and centrifuged at 14000 RPM for 30 seconds, the flow-through was discarded, this wash step was repeated once. The column was centrifuged at 14000 RPM to dry and then transferred to a new collection tube. 50µl of elution solution was pipetted onto the centre of the column and incubated at room temperature for 1 minute. The column was centrifuged at 14000 RPM to elute. The eluate contained RNA and was used for RNA quantification and first strand synthesis (as described below)

2.3.2 RNA quantification and quality analysis

5µl of RNA was analysed by agarose gel electrophoresis (as described in 2.5) to check that the RNA was not degraded. 1.5µl of each sample was analysed using a NanoDrop8000 according to the machines instructions. The RNA concentrations were recorded.

2.3.3 First strand cDNA synthesis

RNA samples were firstly subjected to a DNase treatment to remove trace amounts of genomic DNA. A DNA-free kit from Ambion was used, the reaction was set up to contain 5µg of RNA and this was added to 5µl of 10x DNase I buffer and 1 µl of DNase, the mixture was then made up to 50µl using nuclease-free water. The samples were incubated at 37°C for 20-30 minutes and 5µl of DNase Inactivation Reagent added. The samples were then incubated at room temperature for 2 minutes and centrifuged at 13200 RPM for 90 seconds. The clear precipitate containing the RNA was removed and used for first strand synthesis.

For first-strand cDNA synthesis a reaction was set up containing 1µg of RNA, 2µl of a poly-T primer (18 Ts) and made up to 15µl with RNase-free water. This mixture was heated to 70°C for 5 minutes and transferred immediately to ice. The 15µl mixture was added to 5µl of 5x M-MLV reaction buffer (from Promega, UK), 1.25µl 10mM dNTP-mix. 1µl of M-MLV reverse transcriptase (from Promega, UK) and 2.75µl of RNase-free water to form a 25µl mixture. This mixture was incubated at 42°C for 80 minutes and then used for the PCR reaction (see below).

2.4 PCR

2.4.1 Isolation of genomic DNA

All centrifugation steps were carried out at room temperature in an Eppendorf 5418 centrifuge at 13000 RPM. Leaf tissue was excised and flash

frozen in liquid nitrogen. Sample was ground to a powder then homogenised in 500µl of extraction buffer (0.2M Tris/HCl pH9, 0.4M LiCl, 25mM EDTA pH8 and 1%SDS). Samples were then centrifuged for 10 minutes. 350µl of supernatant was added to 350µl of isopropanol and centrifuged for 10 minutes to pellet DNA and the resulting supernatant discarded. 350µl of 70% (v/v) EtOH in water was added to the pellet, samples were then centrifuged for 10 minutes and the liquid discarded. The pellet was dried and then re-suspended in 200µl of TE buffer (10mM Tris/HCL pH7.5, 1mM EDTA).

2.4.2 PCR reaction

Standard PCR was conducted using *Taq* DNA polymerase from NEB Biosciences. For any applications where the PCR product was used for downstream applications such as cloning Q5® High-Fidelity DNA Polymerase was used from NEB biosciences. Standard PCR reactions (25µl) were assembled, as detailed in Table 2.1, was conducted with a 95°C initial denaturation and 68°C extension. Extension time was 1 minute per KB of DNA.

Cloning PCR using a proofreading polymerase was assembled as 50µl reactions as detailed in Table 2.2. PCR was carried out with a 98°C initial extension and a 72°C extension. Extension time was 20 seconds per KB DNA.

Table 2.1 Components per 25µl PCR reaction using *Taq* DNA polymerase.

Component	Volume (µl)	Final concentration
10X Standard Taq Buffer	2.5	1X
10 mM dNTPs	0.5	200µM
10 µM Forward Primer	0.5	0.2µM
10 µM Reverse Primer	0.5	0.2µM
DNA template	2	Variable
Taq DNA Polymerase	0.125	0.625 units/25 µl PCR
Nuclease-free water	18.875	

Table 2.2. PCR components per 50 μ l PCR reaction using Q5[®] High-Fidelity DNA Polymerase.

Component	Volume (μ l)	Final concentration
5X Q5 Reaction Buffer	10	1X
10 mM dNTPs	1	200 μ M
10 μ M Forward Primer	2.5	0.5 μ M
10 μ M Reverse Primer	2.5	0.5 μ M
DNA template	2	Variable
Q5 High-Fidelity DNA Polymerase	0.5	0.2 units/ μ l
Nuclease-free water	31.5	

2.5 Agarose gel electrophoresis

Agarose gels were prepared by dissolving 1% Agarose (w/v) in TAE buffer (40mM Tris, 20mM acetic acid, and 1mM EDTA). Ethidium bromide was added to a final concentration of 0.5 μ g/ml. DNA samples were mixed with 6x loading dye (0.25% (w/v) bromophenol blue, 0.25% (w/v) xylene cyanol, 30% (v/v) glycerol) in a 5:1 ratio and ran at 90V.

2.6 Immunohistochemical techniques

2.6.1 Fixation and embedding of plant material

Leaf tissue was harvested from soil grown plants in short day environment at 4 weeks post germination. 3 leaves per plant were harvested, excluding the 2 youngest and 2 oldest. Leaf squares of 2x2mm were excised from harvested leaves and immediately and plunged into a fixative solution of 4% v/v

formaldehyde in 0.05 PEM buffer (50mM Pipes, 5mM EGTA, 5mM MgSO₄, pH 7.0) for 3 hours at slight vacuum and a further 16 hours at 4°C. Samples were washed with 3x10 minute changes of PEM buffer and dehydrated in an ascending ethanol series (10, 20, 30, 50, 70, 90 and 100% v/v ethanol in H₂O). Samples were then infiltrated with resin (LR White hard grade resin) at 4°C using an increasing concentration of resin in ethanol (10%, 20%, 30%, 50%, 70%, 90% v/v) for one hour per change and then 100% resin overnight followed by 100% for 8 hours and a final 100% overnight change. Samples were then transferred to gelatine capsules filled with resin, sealed to exclude air and left to polymerise at 37°C for 5-9 days until capsules were completely solidified and clear. Gelatine capsules were removed from the samples

2.6.2 Immunolabelling of tissue sections

Embedded samples were sectioned using a Reichert-Jung Ultracut Ultra-microtome to a thickness of 2µm using glass knives. Sections were floated onto water and transferred to 8-well glass microscope slides coated with Vectabond (Vector labs, UK) to promote tissue adherence. Samples were then incubated in phosphate buffered saline (PBS, pH 7.2) containing 3% w/v milk protein (Marvel, Premier Beverages, UK) (PBS/MP) for 30 minutes to prevent non-specific binding. Samples were washed by incubation in PBS for 5 minutes. Slides were then incubated in a tenfold dilution of primary monoclonal antibody diluted in 3% w/v milk protein in PBS for 1 hour at room temperature. Primary antibodies were provided by Paul Knox (Plant Probes UK) and a full list of antibodies used is in Appendix 2. Primary antibody was washed off with 3x5 minute changes of PBS. Secondary antibody diluted 100-fold in PBS/MP was applied for 1 hour at room temperature, from this step onwards samples are kept covered as the secondary antibody is not stable in light. For the JIM and LM series of antibodies Anti-rat-IgG (whole molecule) coupled to fluorescein isothiocyanate (FITC) was used, for the 2F4 antibody Anti-mouse-IgG (whole

molecule) coupled to FITC was used. Samples were washed with 3x5 minute changes of PBS and incubated with a 0.25% w/v calcofluor white solution (in water) which was diluted 10-fold in PBS for 5 minutes. Samples were then washed with 3 changes of PBS and mounted with citifluor AF1 anti-fade solution (Agar Scientific, UK) and visualized by a microscope with epifluorescence optics. Microscopes used were an Olympus BX52 and Olympus BX51.

2.6.3 Enzymatic removal of pectin

Sections were prepared as described above (2.6.1). Sections were then incubated with a solution of 0.1M NaCO₃ (pH 11.4) for 2 hours followed by 2 10 minute washes in PBS. Samples were then incubated with for 2 hours in pectate lyase (from *Cellvibrio japonicus*, Megazyme, Bray, Ireland) at a concentration of 10µg/mL in CAPS buffer (50mM CAPS, 2mM CaCl₂, pH10) and washed with 3 changes of PBS. Sections were then labelled and imaged as described above (2.6.2)

2.7 Histochemical localization using the GUS reporter gene

The β-glucuronidase (GUS) reporter system is used to analyse the expression patterns of genes of interest. The promoter for the gene of interest is fused to GUS gene from *Escherichia coli* and expressed in plants. GUS encodes a hydrolase that breaks down the substrate 5-bromo-4-chloro-3-indolyl β-D-glucuronide cyclohexamine salt (X-gluc) producing a blue coloured precipitate. For this project GUS expressing lines were provided by Lee Hunt and Najat Ali.

Tissue was harvested and placed in cold 90% (v/v) Acetone on ice. Samples were then placed under vacuum for 10 minutes at room temperature followed by a wash with water. 2mM of X-gluc (dissolved in di-methyl formamide) was added to GUS staining buffer (50mM PO₄ buffer; 0.2% Triton-X) and added to samples until samples were fully submerged. Samples were incubated at 37°C for 24 hours and then rinsed in water. An ascending ethanol series was used to dehydrate the samples (20, 30, 50 and 70% v/v in water) for 30 minutes per change. Samples were fixed in FAA (50% ethanol, 3.7% formaldehyde, 5% acetic acid, water to volume) for 30 minutes. Samples were then cleared using chloral hydrate (see 2.8) and observed using an Olympus BX51 microscope with a DP71 camera.

2.8 Tissue clearing using Chloral Hydrate

Samples were washed with 90% Ethanol (v/v in H₂O) for 30 minutes per wash. Samples were then immersed in Chloral Hydrate (2.5g/mL in 30% glycerol (v/v) and left to clear at room temperature for 24 hours. Samples were then washed in 2 changes of 50% (v/v) ethanol for 10 minutes per changed and 2 changes of water.

2.9 Plant growth analysis

2.9.1 Seed weight

Seed weight was measured by counting out 100 seeds and weighing on a fine balance. An average weight per seed was calculated which was counted as a single replicate. This was repeated 10 times per line.

2.9.2 Seed size

Seeds were surface sterilised as described in 2.2.2 to ensure nothing was coating the seed. Seeds were mounted on glass slides in batches of 5 per slide in 60% (v/v) glycerol solution to prevent seed movement. Samples were viewed on an Olympus BX51 microscope and illuminated from below. Images were captured using a 40x objective with an DP71 Olympus digital camera.

Images were analysed on Image-J using the wand tracing tool to select an entire seed and measure the area. 75 seeds from each line were imaged.

2.9.3 Germination rate

To analyse germination rate seeds were planted on media as described in 2.2.2. 5 plates for each plant line was plated with 100 seeds per plate.

2.9.4 Rosette area

Rosette area was calculated by photographing plants from above using an Olympus pen 3 digital camera mounted on a tripod. Rosette area was calculated using Easy Leaf Area software (Easlon and Bloom, 2014). Accuracy of easy leaf area was validated by comparing results to areas calculated by manually using the colour threshold tool in Image-J. Results were found to be within 2% of each other.

2.9.5 FW and DW and relative water content

Fresh weight (FW) analysis of above ground biomass was carried out on well-watered plants which still had water in the tray. Entire rosettes were excised at soil level and any soil was brushed off the plants. Rosettes were then immediately weighed. Rosettes were then transferred to paper envelopes which were dried at 70°C for a 48 hours. Rosettes were then weighed again.

Relative water content was calculated using the following equation:

Equation 2.1. Relative water content.

$$RWC (\%) = \frac{(FW - DW)}{FW} \times 100$$

2.10 Analysis of stomatal aperture

2.10.1 CO₂ effects on stomatal aperture

Abaxial epidermal peels were taken from mature leaves of five to six week old plants with 4 peels taken per treatment using fine forceps. Peels were placed in petri dishes opening buffers (10mM MES, 50mM KCl pH 6.2), petri dishes were placed in a glass tank containing water and incubated in light from below at a light intensity of 300 μ mol m⁻² s⁻¹. An air pump was used to bubble air into the opening buffer at a rate of 100ml min⁻¹ to ensure the epidermal peels were not excessively disturbed. The air was controlled to contain varying concentrations of CO₂, for CO₂-free treatment air was forced through self-indicating soda lime in order to remove the CO₂. For high CO₂ treatments a 1000ppm canister was used. Samples were treated for 3 hours and then imaged with an Olympus BX51 microscope with an Olympus DP71 camera attached. Images were analysed using ImageJ. For pore area values the area of an ellipse was calculated using the following equation where A= pore area, W=pore width and H=pore height

Equation 2.2. Pore area calculation

$$A = \pi \times \left(\frac{W}{2}\right) \times \left(\frac{H}{2}\right)$$

2.10.2 ABA effects on stomatal aperture

Samples were gathered as in 2.10.1 and treated in the same manner. Ambient air was bubbled through the petri dishes which were supplemented with varying concentrations of ABA (0, 10, 20, 30 μ M)

2.10.3 Mannitol effects on stomatal aperture

Samples were prepared as described in 34. Ambient air was bubbled into the petri dishes which were supplemented with either 0M mannitol or 0.5M mannitol.

2.11 Analysis of stomatal number

Stomatal index and density was measured from excised leaves. The three largest leaves were excised from mature rosettes (35-40 days old) and underwent tissue clearing to improve visibility of stomata.

Tissue was plunged into fixative solution (9:1 Ethanol: Acetic acid) and vacuum was applied for 15 minutes. Tissue was fixed for 2hr at room temperature and then washed with 90% (v/v) ethanol in water twice for 30 minutes. Tissue was transferred to 15M chloral hydrate solution in 30% (v/v) glycerol for 24 hours to clear tissue before observation.

Cleared leaves were imaged using a 40x objective on an Olympus BX51 microscope using DIC settings. 4 fields of view were imaged per leaf. Images were analysed using Image-J cell counter and epidermal cells and stomata were counted.

Stomatal size was measured by using stomatal length as a proxy and density calculated as number of stomata per mm².

Stomatal index was calculated using the following equation where I =stomatal index, S =number of stomata and E =number of epidermal cells

Equation 2.3. Stomatal index.

$$I = \frac{S}{(E + S)} \times 100$$

2.12 Gas exchange analysis

For gas exchange data analysis was started 2 hours into the photoperiod of the growth chamber and did not continue into the last 3 hours of the photoperiod. Measurements were taken using a LI-6400 infrared gas exchange analyser system using a leaf fluorometer chamber (LI-COR Inc.) with a 2cm² circular area for measurement.

2.12.1 CO₂ response curves

CO₂ response curves, otherwise known as A/Ci curves, were measured on young fully expanded leaves at 21°C leaf temperature, 1200 $\mu\text{mol m}^{-2} \text{s}^{-1}$ PPFD light, and approximately 60% relative humidity. Once leaves were acclimated to chamber conditions, measurements were taken at 400, 250, 150, 100, 80, 60, and 40ppm CO₂ every 2-3 minutes at 200 $\mu\text{mol s}^{-1}$ flow rate, then at 400, 500, 600, 800, 900, 1000, 1200, 1400, and 1600ppm CO₂ every 3-5 minutes at 300 $\mu\text{mol s}^{-1}$ flow rate.

2.12.2 Light response curves

Light response curves were measured on young fully expanded leaves at 21°C leaf temperature, 400ppm CO₂ and approximately 60% relative humidity. Once leaves were acclimated to chamber conditions measurements were taken at 1500, 1200, 1000, 800, 600, 500, 400, 200, 150, 100, 80, 60, 40, 20, 10, 0 $\mu\text{mol m}^{-2} \text{s}^{-1}$ PPFD of light with 10% blue light.

2.12.3 Stomatal response to CO₂ shifts.

CO₂ shifts were conducted on 28-day old plants using mature non-senescent leaves. Temperature was held at 21°C and humidity was kept above 58% and below 65%. Photon flux density was held at 300 $\mu\text{mol m}^{-2} \text{s}^{-1}$ with 10% blue light. In cases where the leaf did not fill the chamber, leaf area was measured and a correction made in subsequent analysis. To assess stomatal response to

CO₂ conductance was stabilised at 500 ppm for 40 minutes, CO₂ was then shifted to 1000 ppm for 50 minutes to stimulate stomatal closing, and then to 100ppm for 50 minutes to stimulate stomatal opening.

2.12.4 Blue light induced stomatal opening

Fully expanded leaves were acclimatised at 400 PPM CO₂, 60% humidity and 21°C in the presence of 300 $\mu\text{mol m}^{-2} \text{s}^{-1}$ PPFD containing 0% blue light for 40 minutes. At this point the light regime was changed to contain 30% blue light for 30 minutes and then changed back to 0% blue light for a further 25 minutes.

2.13 Thermal imaging

Thermal imaging was conducted using a FLIR thermal imaging camera. For thermal images in (Chapter 4) a FLIR SC660 camera was used and for all other thermal images a FLIR T650SC camera was used. Plants were imaged in the growth chamber to minimize alterations to plant temperature by changes to the environment. The background was imaged for 20 minutes before placement of plants to ensure that the background temperature was stable. The camera was positioned 1 m above the leaf rosettes and emissivity was set to 0.965 as previously described (H. G. Jones et al., 2003). Images were analysed using researchIR software and the average temperature of the 8 largest leaves was taken, for cases where there are less than 8 leaves every leaf was measured.

The analysis was verified by comparing the average temperature of the 8 largest leaves to the average temperature of the entire rosette when traced around and results were within 0.2°C of each other.

2.14 Atomic force microscopy of leaf tissue

Plants were grown on media or soil as described in section 2.2.2 and allowed to reach 21 days old before sampling. Tissue was excised from the plant and fixed onto microscope slides using a variety of fixation techniques. Samples were then imaged under liquid using an Asylum MFP-3D atomic force microscope mounted on an inverted optical microscope. Silicon nitride cantilevers (SNL, Bruker, UK) were used with a 2 nm diameter sharp tip. A nominal stiffness of 0.35 Nm^{-1} and nominal resonant frequency 65 kHz, although this was measured every time to account for variation in the tip construction. Prior to scanning biological samples, a reference force curve was acquired by using a glass microscope slide. This is an incompressible surface meaning the deflection purely reflects the properties of the cantilever and allows the software to calculate the sample deflection in (nm/V).

Samples were scanned using contact mode and topographical images were captured using a set point of 1V at a speed of 1 Hz. Once an area of interest has been identified a force map was captured (50x50 points) with a deflection trigger point set at 150 nm at a speed of 1 Hz.

2.14.1 Viability of AFM samples

It is important that samples imaged using the AFM are still alive. To test this, we used fluorescein diacetate (FDA) staining. FDA is taken up by cells and converted into fluorescein which fluoresces green. This conversion is esterase dependant so can be used to indicate viable cells. Leaf samples were harvested and imaged by AFM prior to staining to ensure that leaves were still viable after the AFM treatment.

2.15 Sample preparation for TEM

Samples were harvested, fixed and dehydrated as in 2.6.1 except that instead of fixing in 4% formaldehyde fixative samples were fixed in 2.5% glutaraldehyde in 0.1M sodium cacodylate (pH 7.0). TEM was carried out by Chris Hill at the Sheffield Electron Microscopy unit.

2.16 Histological analysis using toluidine blue

Samples were harvested, fixed and dehydrated as in 2.6.1. Samples were sectioned as in 2.6.2 and stained by incubation in 0.5% (w/v) toluidine blue in water for 1 minute. Samples were then rinsed with water and imaged using an Olympus BX51 microscope.

Chapter 3. Analysis of guard cell wall composition by immunocytochemistry

3.1 Introduction

Guard cells are highly specialised cells and have distinct properties which enable them to carry out their function. During stomatal opening the guard cells undergo substantial changes in size, shape and intercellular pressure. Crucially these changes must be reversible in order to allow the stomata to close again. The internal turgor pressure can reach as high as 5 MPa during stomatal opening (Franks et al., 2001) and this internal pressure is crucial for driving the shape change required for stomatal opening (Raschke, 1975). The guard cell wall must fulfil two key, and seemingly opposed, functions; firstly, it needs to remain flexible enough to allow the requisite changes in cell size and to accommodate the large change in shape without tearing. Secondly it must be strong enough to withstand the huge pressure which builds up without the cell bursting. As the major structural component of the cell it is logical that the cell wall must dictate the mechanical properties of the cell. These mechanical properties will be key to guard cells being able to carry out their function (Franks et al., 1998). Despite the clear importance of guard cell walls to the correct functioning of stomata very little is known about the composition of guard cell walls. It is an interesting proposition to manipulate the guard cell walls but before we do this it is crucial to understand what “normal” guard cell walls look like.

3.1.1 Guard cell walls

Guard cell walls are known to be anisotropic, with radially oriented cellulose microfibrils radiating from the ventral side adjacent to the pore purportedly acting to guide the direction of cellular expansion perpendicular to the cellulose orientation during stomatal opening (Aylor et al., 1973). In addition to cellulose it has been noted that there are asymmetric cell wall thickenings on the ventral (see Figure 3.1 for definition of stomatal anatomy) side of stomata (Zhao and Sack, 1999). This anisotropy is reported to be the cause of cell bending during stomatal opening; the anticlinal cell walls on the dorsal side can stretch more than the anticlinal ventral walls and this causes the stomata to bend open as opposed to simply elongating.

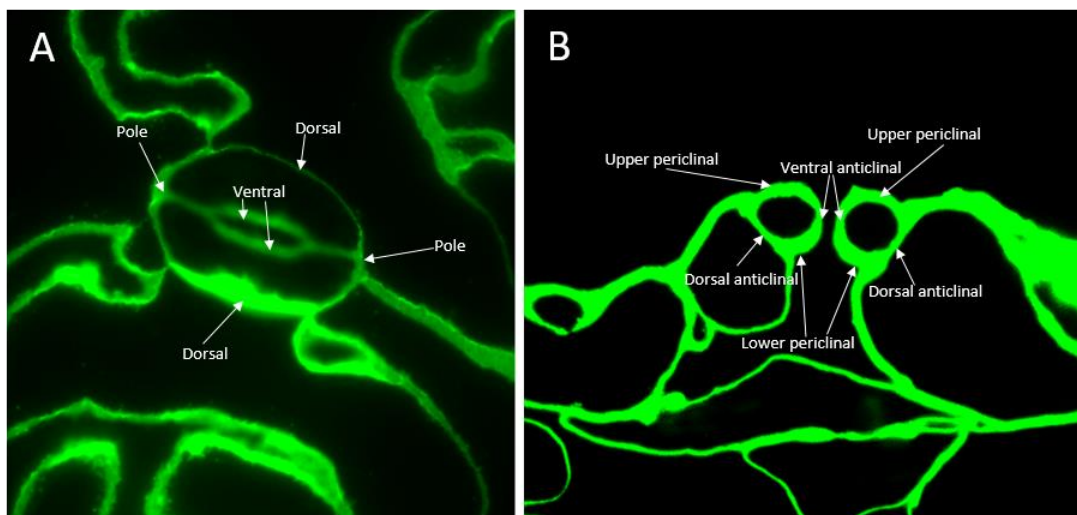


Figure 3.1. Anatomy of guard cells. A) View looking down on a stomata showing the dorsal and ventral cell walls and the poles. B) Transverse section of a stomata showing the upper and lower periclinal walls

Classical modelling of stomatal mechanics has tended to focus on asymmetric thickening and its role in stomatal shape change or on radially orientated cellulose. Rubber balloon models (Aylor et al., 1973) and rectangular beam models (DeMichele and Sharpe, 1973) have shown that asymmetric thickening, where the ventral walls are thicker than the dorsal walls, coupled with changes to internal turgor pressure is sufficient to cause

opening and closing of the guard cells. These models tend to rely on a number of key assumptions which do not generally hold true. The key assumptions made are that the cell wall material is uniform and that individual cellulose strands act independently of each other, meaning that there are no lateral pressures acting between them (DeMichele and Sharpe, 1973). It is clear that cell walls are not uniform materials and it is known that hemicelluloses and pectins interact with the cellulose network causing crosslinking (Wang et al., 2012; Zykwiniska et al., 2005). It is not known to what extent the heterogeneity of the guard cell wall and its composition impact on stomatal movement.

Very little is known about the finer structure of stomatal cell walls. It has been shown that pectins are abundant in the guard cell wall (Jones et al., 2005; L. Jones et al., 2003) especially unesterified pectins (Majewska-Sawka et al., 2002). It was also shown that guard cell wall arabinan is essential for guard cell function, removal of arabinans leading to the locking of stomata so that they did not change shape in response to normal triggers (L. Jones et al., 2003). It has been hypothesised that the presence of arabinan side chains on the pectin prevents close association between the pectin chains and thus contributes to the maintenance of cell wall flexibility required for shape change. Callose is also known to be present in guard cells (Peterson et al., 1975) and it has been suggested that rapid removal and deposition of callose can occur during stomatal opening and closure, at least in ferns (Apostolakos et al., 2010). This suggests that during guard cell wall opening and closing rapid cell wall remodelling could occur to accommodate the stresses placed upon the cell wall.

Lignin has been identified in the guard cells of some species such as corn and ferns (Srivastava and Singh, 1972). The lignin network is extremely complex and has been the subject of several extensive reviews (Boerjan et al., 2003; Bonawitz and Chapple, 2010; Vanholme et al., 2010). Elliptical stomata, such

as those in *A. thaliana*, do not test positive for lignin (Peterson et al., 1975; Sack and Paolillo, 1983), indicating that this component is not a feature of these stomatal cell walls. For this reason, lignin is not covered further in this work.

3.1.2 Antibody labelling of cell wall components

Antibodies have long been used for the detection of cell wall epitopes. Libraries of monoclonal antibodies have been raised against numerous specific epitopes of cell wall components.

To date very few studies have used antibodies against cell walls of guard cells. As discussed above, Majewska-Sawka et al used immunolabelling to demonstrate the presence of pectin-related polymers in the guard cells (Majewska-Sawka et al., 2002) and Jones et al showed that pectic polymers and also side chains, such as arabinans were abundant in the guard cells (L. Jones et al., 2003). Biochemical analysis of guard cell pectin carried out in the same group showed that enzymatic modification of the pectin network has implications for guard cell function (Jones et al., 2005). This chapter aims to utilise a wide range of monoclonal antibodies to determine the composition of guard cell walls and to investigate if the stomatal cell wall changes to facilitate guard cell movement

3.1.3 The guard cell cuticular ledge

Guard cells have defined cuticular ledges which are located on the joint between the upper periclinal walls and the ventral walls (see Figure 3.2). It has been shown that cuticle is hydrophobic and it is thought that the main role of the cuticular ledge is to prevent water ingress through open stomata (Li et al., 2007; Macgregor et al., 2008). When stomata close the cuticular ledges press together, which is thought to aid in the sealing of the stoma to

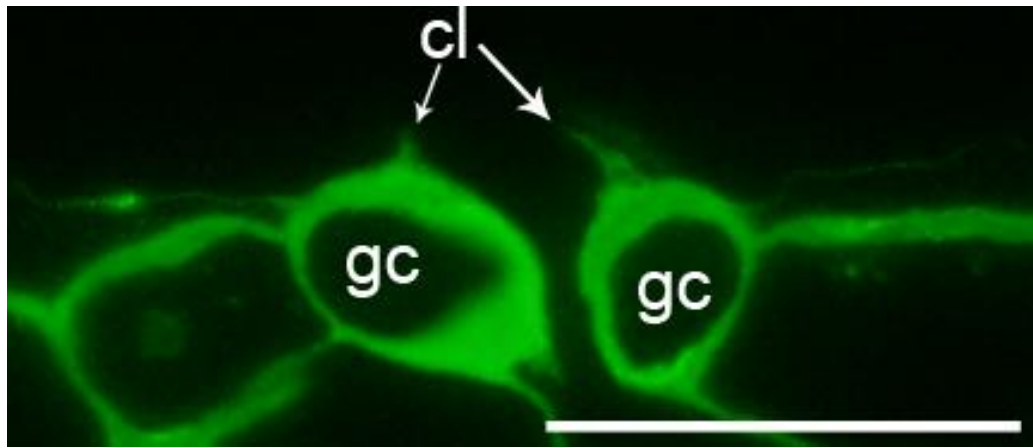


Figure 3.2. Arabidopsis leaf cross-section with guard cells labelled (gc) indicating the cuticular ledges (cl) which protrude outwards from the stomata. Scale bars=20 μ m.

minimize leakage of water, both in and out, through closed stomata. It is unclear whether the cuticle plays a role in prevention of pathogen entry through the stomata but some evidence exists to support this (Li et al., 2007). Very little is known about the structure of the cuticular ledges and greater knowledge could help inform studies into their function. The cuticle has been shown to be enriched in pectin (L. Jones et al., 2003) and it is suggested that the presence of unesterified pectin on the outer layer of the guard cell facing the environment could function to adhere the cuticle to the epidermis (Majewska-Sawka et al., 2002).

Understanding guard cell wall structure may provide insights into stomatal function and make manipulation of the guard cell wall possible. In this chapter a library of monoclonal antibodies to a wide range of cell wall epitopes is utilised to study guard cell wall composition.

3.2 Results

3.2.1 Analysis of guard cell wall composition

A broad screen was carried out using wild type plants to determine the suitability of immunolabelling as a technique to detect fine differences in cell

wall components of *A. thaliana* leaves. We looked at the binding of a wide range of antibodies to assess their binding in *A. thaliana* leaves.

Hemicelluloses

Binding of antibodies against hemicellulose epitopes reveals a range of patterns. Several antibodies tested showed no binding in sections from mature leaves of *A. thaliana* plants. Figure 3.3 shows representative images for the hemicellulose antibodies which showed binding in 4 week old, untreated Arabidopsis leaf cross sections.

LM10 (Figure 3.3.A) recognises relatively unsubstituted xylan (McCartney et al., 2005) and shows binding only in the developing xylem tissue. LM11 (Figure 3.3.B) shows the same binding pattern as LM10 and recognises unsubstituted xylan, arabinoxylan and more extensively substituted xylan (McCartney et al., 2005). Neither antibody showed binding to the guard cells or epidermal cells.

LM15 (Figure 3.3.C), LM24 (Figure 3.3.E) and LM25 (Figure 3.3.F) all recognise xyloglucan and show differing binding patterns. LM15 recognises the XXXG motif of xyloglucan (Marcus et al., 2008) and this antibody was found to bind exclusively to the epidermis. Much stronger binding was observed in the guard cells than in epidermal pavement cells and binding was stronger on the periclinal and ventral anticlinal walls, while little or no binding was observed on the dorsal anticlinal walls. No binding was observed elsewhere in the leaf. In contrast LM24, which recognises the XLLG motif of xyloglucan (Pedersen et al., 2012), shows no binding at all to leaf tissue. LM25 recognises a broader range of xyloglucan epitopes than LM24 (Pedersen et al., 2012) and this showed strong guard cell and epidermal binding, with a weak signal observed in the mesophyll.

LM21 (Figure 3.3.D) recognises β -linked mannans and provides recognition of mannan, glucomannan and galactomannans (Marcus et al., 2010). Broad

binding was observed in the leaf with signal present in the vasculature, mesophyll and the epidermis, including guard cells. Binding in the mesophyll is extensive, even more so than the calcofluor. In the epidermis the converse is true, with binding being limited to narrow strips within the calcofluor signal.

Very limited signal was observed in any of the controls hybridisations lacking the primary antibody (Figure 3.3.G), with the exception of occasional chloroplast autofluorescence (see Appendix 1: A selection of control samples incubated with secondary antibody in the absence of primary antibody..

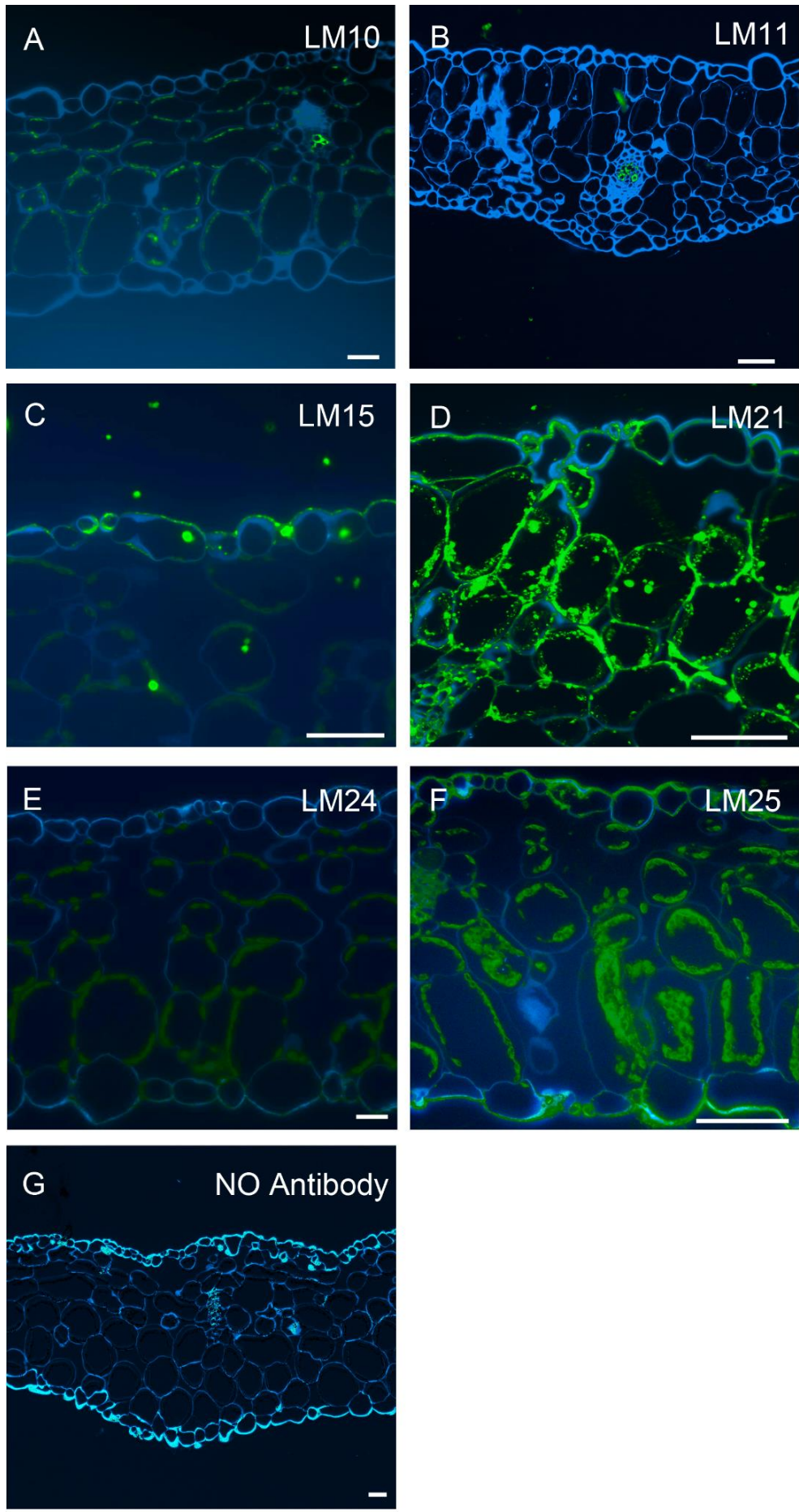


Figure 3.3. Binding of hemicellulose antibodies. Green channel is antibody signal and blue channel is calcofluor counterstain. (A) LM10 recognises unsubstituted xylan and is shown to bind only in the xylem. B) LM11 recognises xylan and arabinoxylan and is only observed in the xylem. C) LM15 recognises the XXXG motif of xyloglucan. Binding was observed weakly in the epidermis and strongly in the ventral anticlinal guard cell walls. D) LM21 recognises heteromannan, glucomannan and galactomannan. Broad binding is observed in the mesophyll with patchy binding shown in the epidermis. Binding is relatively uniform throughout the guard cells. E) LM24 recognises xyloglucan, specifically the XLLG motif. Fluorescence was very faint and it is hard to determine if binding is substantially different from autofluorescence. F) LM25 recognises a range of xyloglucan motifs. Binding was strong in the guard cells and the epidermis. No binding was observed in the mesophyll but abundant chloroplast fluorescence may have obscured binding. G) Samples with no primary antibody show a low level of autofluorescence in the green channel. Images are representative from n=6 (2 technical replicates). Exposure times for calcofluor imaging was 100ms, exposure times for antibody fluorescence ranged from 500ms to 1s with the NO antibody control being 1s.

Pectins

Pectins are known to be abundant in *A. thaliana* but little is known about the distribution of specific pectin epitopes, especially within the guard cell walls. A range of monoclonal antibodies against pectin epitopes was tested against *Arabidopsis thaliana* leaves. The results show that homogalacturonan, as indicated by JIM7 which recognises a range of esterification states (Verhertbruggen et al., 2009a), is highly abundant in the leaves of *A. thaliana* (Figure 3.4.A). Broad binding is observed throughout the leaf and binding intensity appears to be even in all tissue types. LM19 recognises pectin which is relatively unesterified. In particular, it does not bind pectin in the presence of calcium and as such is used to indicate unesterified pectin which is not crosslinked (Verhertbruggen et al., 2009a). LM19 shows a similar binding pattern to JIM7 with signal throughout the leaf, including the stomata (Figure 3.4.E). LM18 was used to indicate partially esterified and unesterified HGA (Verhertbruggen et al., 2009a). Binding was absent from the guard cells despite being present in the rest of the leaf (Figure 3.4.D). Methyl-esterified pectin is indicated by LM20 (Verhertbruggen et al., 2009a). Weak binding was observed in the mesophyll with signal being limited to cellular junctions. Strong binding was observed in the epidermis, with signal being excluded from the guard cells (Figure 3.4.F). Calcium crosslinked pectin is recognised by the 2F4 antibody (Moller et al., 2008). Very little binding was observed in the leaf with this antibody (Figure 3.4.G) with signal being limited to the mesophyll and junctions between epidermal cells. LM5 recognises a linear epitope of (1-4)- β -D-galactan (Jones et al., 1997). No signal was observed in the guard cells or mesophyll cells with binding being limited to the epidermis and vasculature (Figure 3.4.B). LM13 recognises linear (1-5)- α -L-arabinan (Verhertbruggen et al., 2009b) and overall showed very low levels of binding, including guard cell (Figure 3.4.C). High levels of chloroplast

signal were observed with this antibody whereas very low fluorescence was seen in control samples incubated with only secondary antibody (Figure 3.4.H).

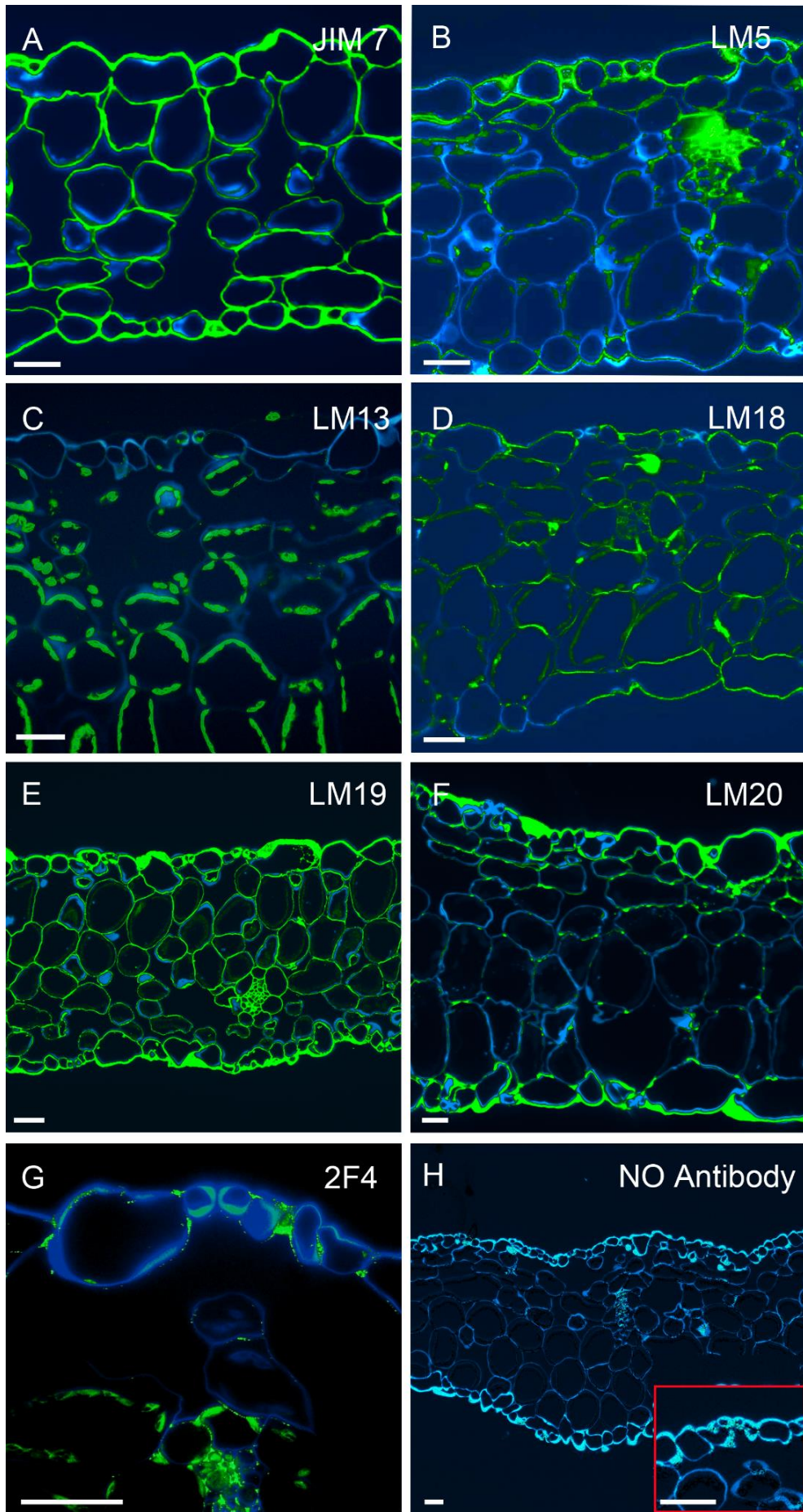


Figure 3.4. Binding of pectin antibodies. Green channel is antibody signal and blue channel is calcofluor counterstain. A) J1M7 recognises a broad range of HGA epitopes and is used as a general probe for pectic HGA. Strong binding was observed throughout all tissues in the leaf. B) LM5 recognises a linear epitope (1-4)- β -D-galactan. Binding was observed in the epidermis and vasculature but appears to be absent from the guard cells. C) LM13 recognises linear (1-5)- α -L-arabinan. Binding was absent from the majority of the leaf. Small amounts of binding was observed in the guard cells. D) LM18 recognises partially esterified and low-level esterified HGA. Binding was observed in the epidermis and in the mesophyll but was absent from the guard cells. E) LM19 recognises unesterified HGA. Binding was observed throughout the leaf being especially strong in the epidermis. F) LM20 recognises to methylesterified HGA. Bind was observed strongly in the epidermis but was absent from the guard cells. Mesophyll binding appears to be restricted to cellular junctions. G) 2F4 indicates calcium crosslinked HGA. Weak binding was observed in epidermal cellular junctions. Binding was also observed in the vasculature but was almost entirely absent from the mesophyll. H) Samples with no primary antibody show a low level of autofluorescence in the green channel Scale bars=30 μ m. Images are representative from n=6 (3 technical replicates per biological replicate) except for 2F4 which is n=3 (2 technical replicates per biological replicate) 4 separate viewpoints were imaged per technical replicate and representative images displayed. Calcofluor images were all taken at 100ms exposure time and Antibody channel images were taken at 1s exposure time.

Other cell wall components

While hemicelluloses and pectins are the main non-cellulose classes of cell wall components there are numerous other glycoproteins that are known to form part of cell walls. These components are less extensively studied than pectic and hemicellulose components. Monoclonal antibodies against a range of epitopes were tested for binding.

JIM16 is known to recognise arabinogalactan proteins which form part of the cell wall (Yates and Knox, 1994). Broad binding was observed in the vascular tissue and specific binding was observed in the outer epidermal cell walls (Figure 3.5.A). Interestingly, no binding was observed in guard cell walls and the epidermal cells flanking the guard cells sometimes showed less strong binding. LM2 also recognises arabinogalactan proteins but shows no binding outside of the vascular tissue (Figure 3.5.B). In contrast LM14, which also recognises arabinogalactan (Moller et al., 2008), was highly abundant throughout the section. Guard cells appeared to have increased intensity of binding of LM14 than neighbouring epidermal cells. Binding in the mesophyll was hard to identify due to high levels of chloroplast fluorescence. Vascular tissue showed especially strong binding of LM14 (Figure 3.5.D).

LM12 recognises feruloylated polymers which are known to be a component of the pectin and heteroxylan networks (Pedersen et al., 2012). This antibody showed strong binding in the vasculature and weak binding to the outer epidermal cell walls (Figure 3.5.C). Strong binding was observed in the guard cells on the ventral anticlinal walls and on the lower periclinal walls. No binding was observed in the anticlinal dorsal walls or in the upper periclinal walls. Interestingly, although this pattern was consistently

observed between replicates, a small number of stomata within each replicate showed no binding of LM12.

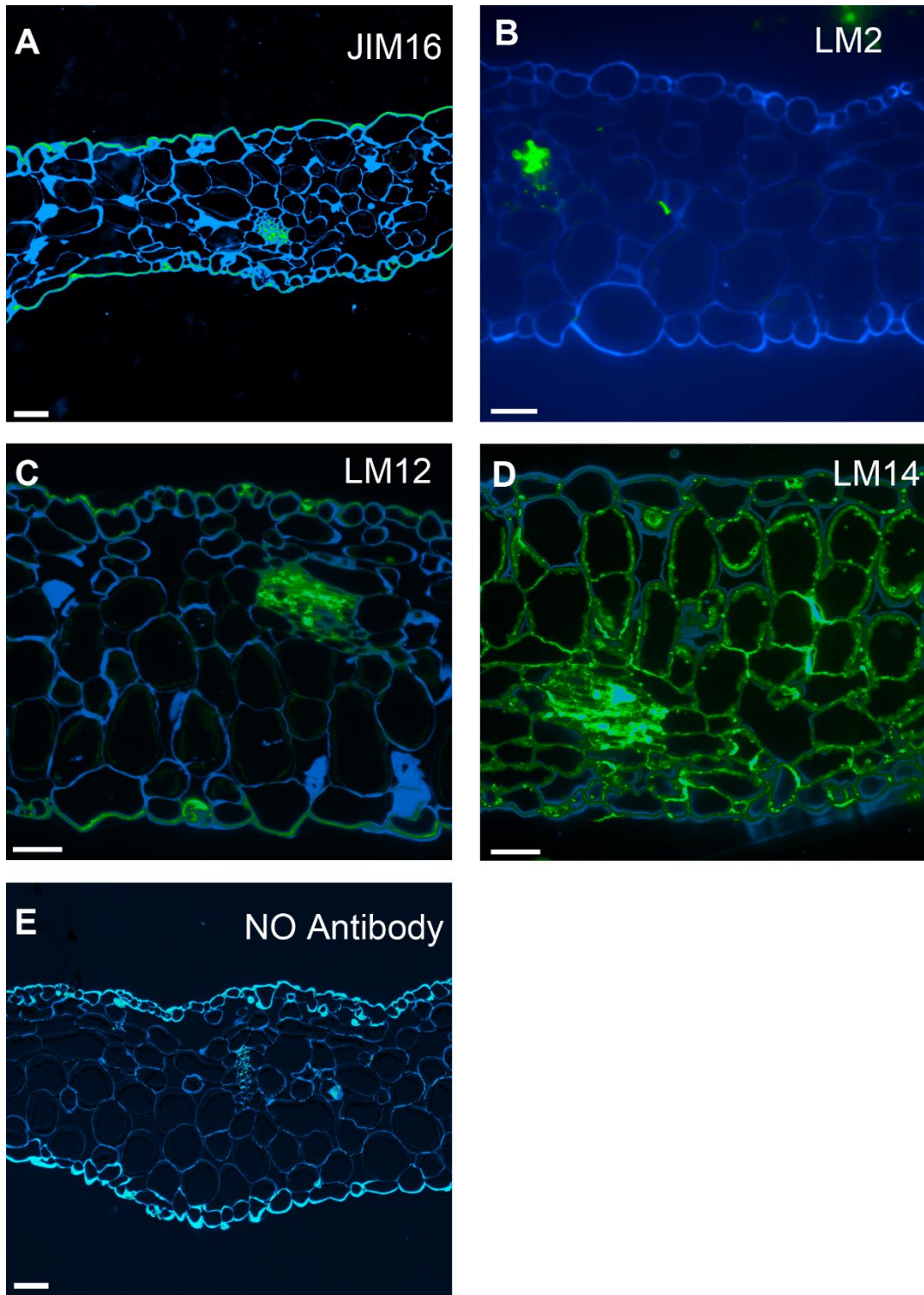


Figure 3.5. Binding of other cell wall components. Green channel is antibody binding and blue channel is calcofluor counterstain. A) JIM16 recognises AGP and is observed in the vasculature and outer epidermal walls B) LM2 recognises AGP and is observed only in the vasculature C) LM12 recognises feruloylated polymers. Binding is limited to the epidermis. It appears to bind more strongly in the guard cells than neighbouring epidermal cells D) LM14 recognises AGPs and labels broadly, signal is stronger in guard cells than neighbouring epidermal cells E) No primary antibody showing low autofluorescence in the green channel. Scale bars are 20 μ m. Images are representative from n=6 (2 technical replicates). Exposure times were 100ms for calcofluor imaging and 1s for antibody imaging.

As the results above demonstrate a large number of antibodies showed binding to *A. thaliana* leaves, revealing a diversity of binding patterns. Not all of the antibodies tested showed binding and Table 3.1 lists these antibodies.

Table 3.1. Cell wall antibodies which showed no binding in mature *Arabidopsis* leaves

Antibody	Epitope
LM1	Extensin
LM6	(1-5)- α -L-galactan
LM7	Partially-esterified HGA
LM8	Xylogalacturonan
LM9	Feruloylated-(1-4)- β -D-galactan
LM16	RG-I associated processed arabinan
LM22	β -(1-4)-manno-oligosaccharides
LM23	Non-acetylated xylosyl
JIM4	Arabinogalactan protein
JIM5	Arabinogalactan protein
JIM8	Arabinogalactan protein
JIM11	Extensin
JIM12	Extensin
JIM13	Arabinogalactan protein
JIM14	Arabinogalactan protein
JIM15	Arabinogalactan protein
JIM19	Extensin
JIM20	Extensin
MAC205	Arabinogalactan protein
PTD5	Heteroxylan
PAM1	Long stretches of unesterified HGA

Overall, it is clear from the images that pectic compounds are abundant throughout the leaf and guard cells appear to have distinct cell wall profiles.

3.2.2 Guard cell wall composition is distinct from epidermal pavement cells

The above data identified a number of antibodies which bind to sections of *Arabidopsis* leaves. A number of these appeared to show distinct guard cell wall profiles while other components are clearly present in the guard cell wall but at a similar level to the neighbouring epidermal cells. A number of antibodies were studied in greater detail to elucidate guard cell wall structure.

Pectin in the guard cell wall

Antibodies against homogalacturonan (HGA) were looked at in greater detail (Figure 3.6). The JIM7 antibody against HGA recognises a wide range of esterification states and as such this antibody is used as a general HGA indicator. Strong guard cell binding is observed with JIM7 (Figure 3.6.A) and this binding is of a similar intensity to surrounding epidermal cells. 2F4 recognises blockwise de-methylesterified HGA which has been calcium crosslinked. Calcium crosslinked pectin is known to have a role in cell-cell adhesion and strengthening of the cell wall (Marry et al., 2006). 2F4 binding was only observed in the junctions between the guard cells and neighbouring epidermal cells in mature leaves (Figure 3.6.B) and binding did not extend into the guard cell wall.

LM19 recognises HGA with low levels of methylesterification (around 20% (Verhertbruggen et al., 2009a)) and is present throughout the leaf. It appears to extend beyond the calcofluor signal, especially in the epidermal cells, suggesting that unesterified HGA may protrude outside the main body of the cell wall, possibly forming the middle lamella (Figure 3.6.C). LM19 binding mirrors the distribution of JIM7 and appears to be even more extensive. Although LM20, which recognises only highly esterified HGA, was observed throughout the epidermis and mesophyll, signal was relatively

weak. Binding was strongest at cell-cell junctions, especially in the epidermal cells adjacent to guard cells. LM20 was completely absent from guard cell walls (Figure 3.6.D) except for the cuticular ledges. LM5 (indicating (1-4)- β -D-galactan) showed no binding to guard cell walls (Figure 3.6.E).

These data show that guard cell wall has a distinct pectin composition to that of the surrounding epidermal cells. The methylesterification status of HGA is clearly differentially regulated. It appears that only partially methylesterified HGA is present in the guard cell while neighbouring epidermal also have highly esterified HGA.

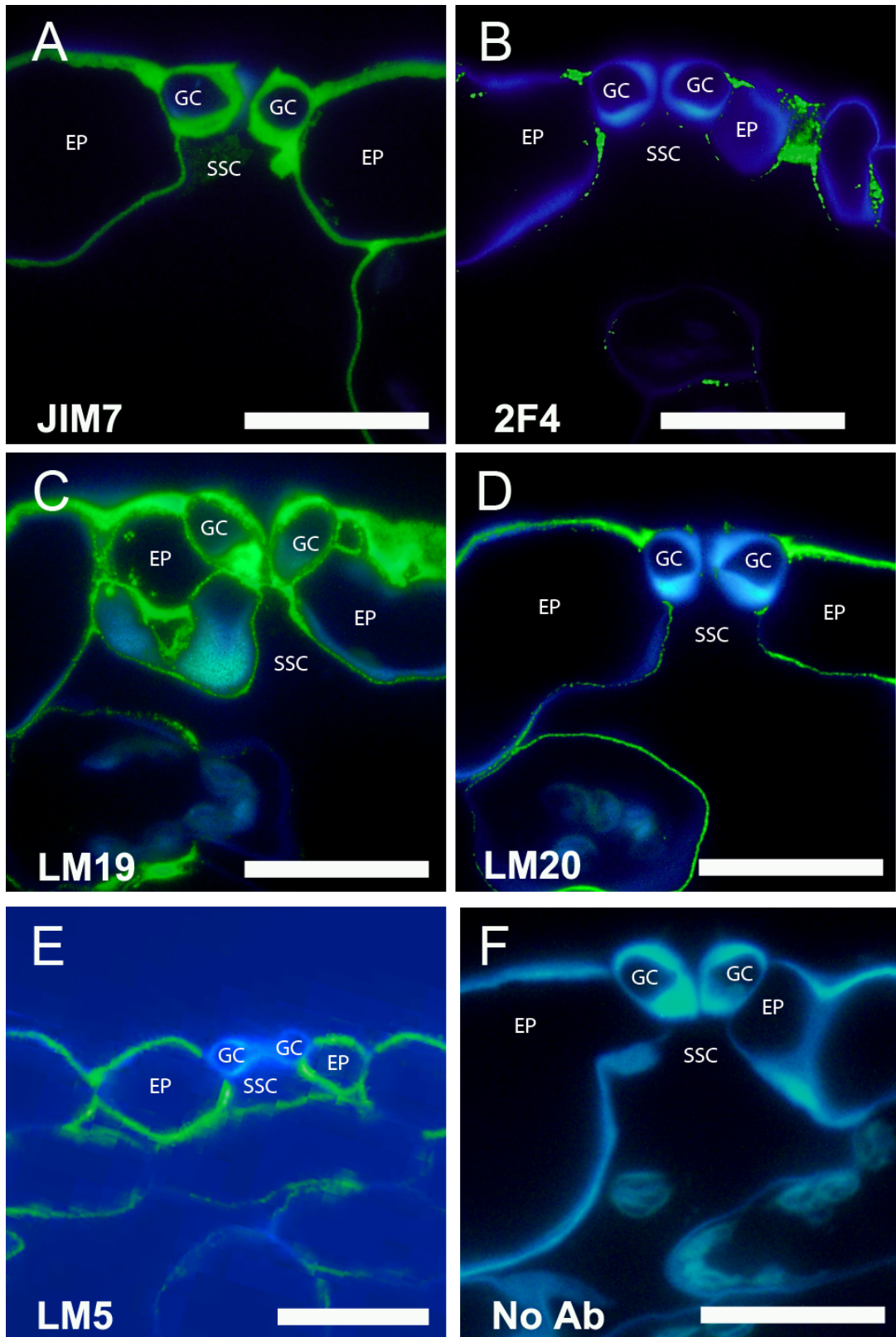


Figure 3.6. Antibody labelling of stomatal cell walls. Guard cells indicated by GC, epidermal pavement cells indicated by EP, substomatal cavity indicated by SSC. Green channel indicates antibody signal for binding of primary antibody, blue channel indicates calcofluor fluorescence (A) JIM7 recognises a broad range of HGA methylesterification and is present throughout the guard cell and epidermal cells (B) 2F4 indicates calcium crosslinked HGA characterised by long stretches of unesterified HGA residues and is only present in the junctions between guard cells and epidermal cells and between epidermal cells (C) LM19 indicates relatively unesterified HGA and is present throughout the guard cell (D) LM20 indicates highly methylesterified pectin and is excluded from the guard cells (E) LM5 indicates (1-4)- β -D-galactan and is present in the epidermal cells but absent from the guard cells (F) Control sample with no primary antibody demonstrating low levels of autofluorescence. Scale bars represent 20 μ m. Images are representative from n=6 (2 technical replicates). Exposure times were 100ms for calcofluor imaging and 1s for antibody imaging.

Other guard cell specific components

A small number of antibodies against non-pectic cell wall components also appeared to show guard cell specific patterns of binding. These were looked at in greater detail and the results described below.

JIM16 recognises AGPs which protrude into the cell wall. A low level of guard cell binding was observed but signal was weaker than in the neighbouring epidermal cells (Figure 3.7.A). Guard cell chloroplast fluorescence also leaked into the green channel meaning visualisation of the guard cell binding was challenging. LM14 also recognises AGPs but demonstrates a markedly different binding pattern. Strong binding was observed in the guard cells compared to very weak binding observed in the neighbouring epidermal cells (Figure 3.7.C).

LM12 recognises feruloylated polymers, a structural component linked to the pectic network (Jones et al., 2005). Guard cell binding was localised to the ventral periclinal walls and the ventral edge of the lower anticlinal wall. No binding was observed in the rest of the guard cell. Epidermal binding was observed but was significantly weaker than the guard cell binding (Figure 3.7.B).

Xyloglucan was also present in the guard cell walls. LM25 (indicating XXLG and XLLG motifs) showed strong binding in the guard cells and the epidermis (Figure 3.7.E). LM15, which indicates the XXXG motif of xyloglucan is only present in the stomata and appears to show asymmetric guard cell distribution (Figure 3.7.D). Binding is present on the ventral anticlinal and lower periclinal guard cell walls only.

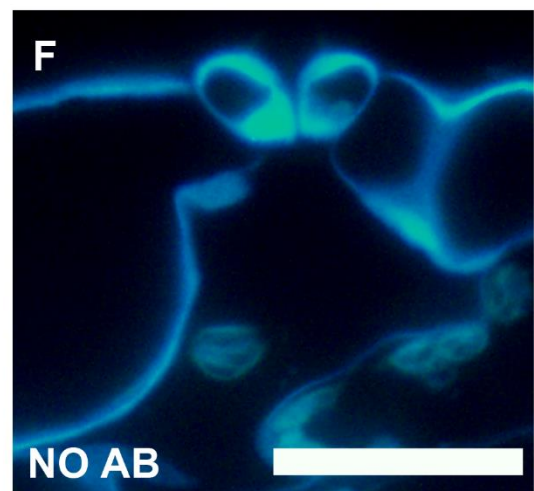
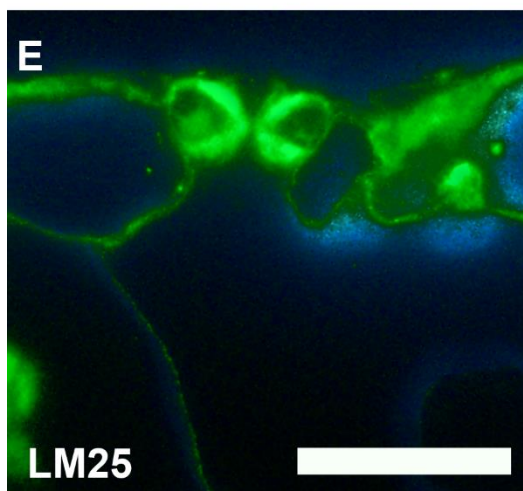
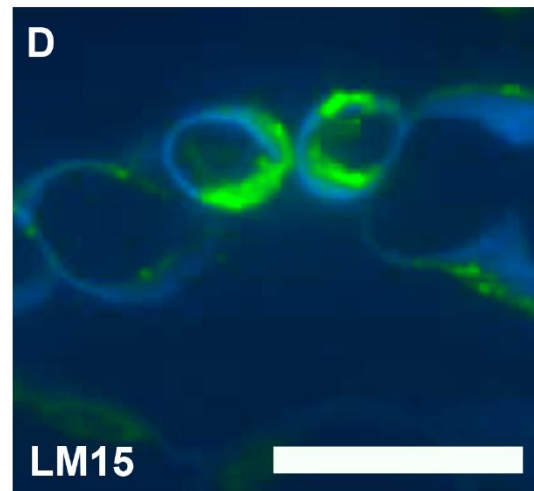
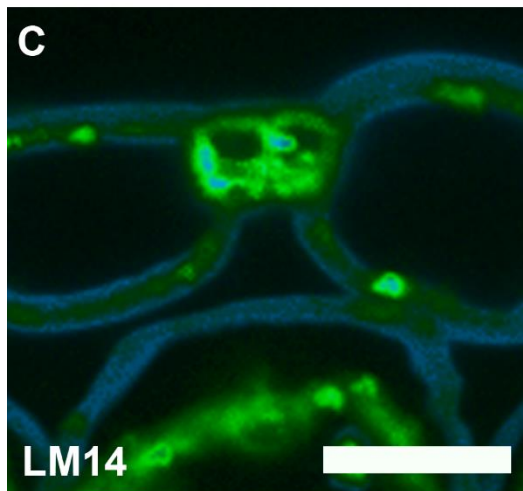
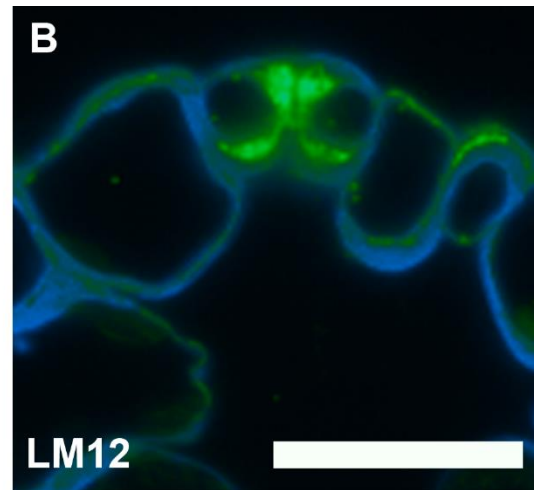
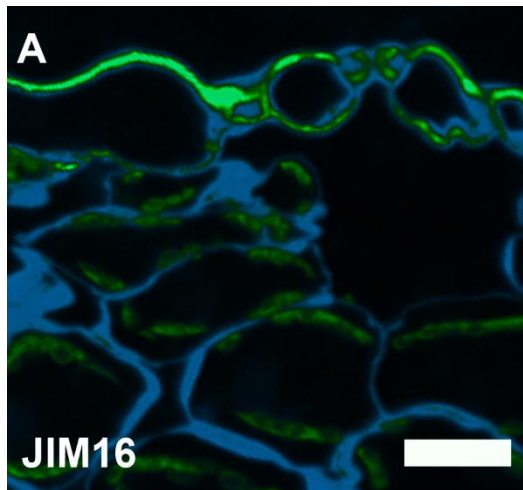


Figure 3.7. Non-pectic cell wall components show distinct guard cell binding profiles. Green channel is antibody binding and blue channel is calcofluor counterstain. A) JIM16 recognises AGP and is present only in the outer epidermis. Binding is weaker in the guard cells than in neighbouring epidermal cells B) LM12 recognises feruloylated polymers. Binding is weakly observed in the epidermal cells but is strongly present in the ventral anticlinal walls. C) LM14 recognises AGP and demonstrates strong binding in the guard cells. D) LM15 recognises the XXXG motif of xyloglucan. Strong binding was observed in the ventral anticlinal cell walls and lower periclinal walls. No binding was observed on the dorsal or upper guard cell walls. E) LM25 recognises xyloglucan and showed strong epidermal binding including guard cells and cuticular ledges. F) Control sample with no primary antibody demonstrating low levels of autofluorescence. Scale bars are 30µm. Images are representative from n=6 (2 technical replicates). Exposure times were 100ms for calcofluor imaging and 1s for antibody imaging.

3.2.3 Composition of the guard cell cuticular ledge

The guard cell cuticular ledge was investigated using high magnification images of antibody labelled sections. Only a subsection of antibodies are shown here (see Appendix 2 for all antibodies which show no cuticular binding). For clarity, the antibody channel is separated from the calcofluor channel. JIM7 binding is seen in the cuticular ledges demonstrating that HGA is abundant in this region (Figure 3.8.A). LM20 binding indicates that highly methyl-esterified HGA is present in the cuticular ledge (Figure 3.8.C) whereas there is no binding of LM19 (which recognises unesterified pectin (data not shown)). JIM5, which also recognises unesterified HGA, showed no cuticular binding (Figure 3.8.G) which is contrary to previous work (L. Jones et al., 2003; Majewska-Sawka et al., 2002). Arabinan is also present in the cuticular ledge, as indicated by LM13 binding (Figure 3.8.E). The cellulose network, as indicated by calcofluor binding, does not extend into the cuticular ledge (Figure 3.8.B, D, F, H, J).

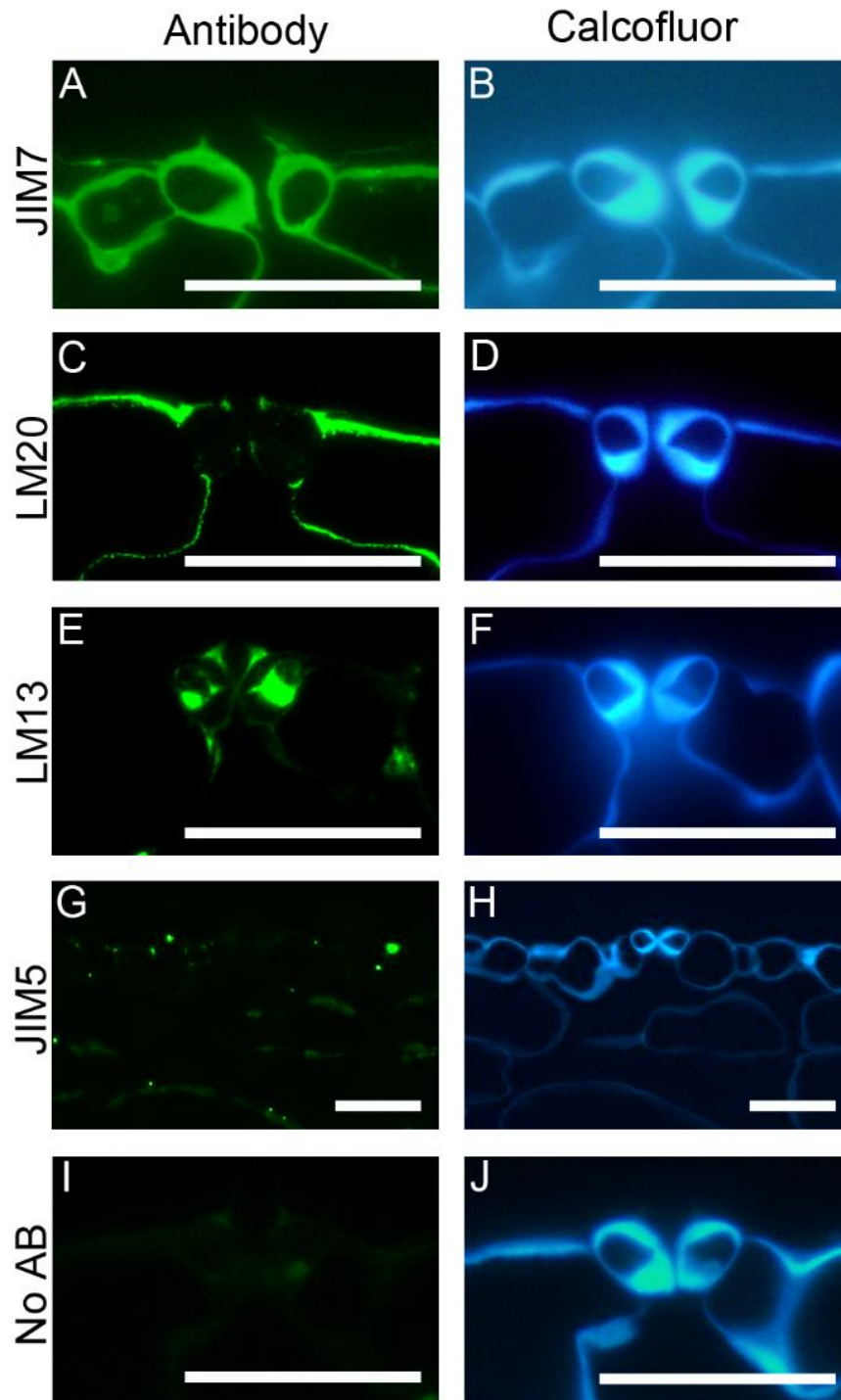


Figure 3.8. Cell wall components of the cuticular ledge are identified by antibody labelling. A) JIM7, indicating HGA, binding is present in the cuticular ledges B) Calcofluor binding indicating cellulose. C) LM20, indicating unesterified pectin, is present in the cuticular ledges despite not being present in the guard cells. D) Calcofluor binding indicating cellulose. E) LM13 recognises linear arabinan and is found in the cuticular ledge of the guard cells. F) Calcofluor binding indicating cellulose. G) JIM5 recognises unesterified homogalacturonan and no binding was observed in the cuticular ledges of the guard cells. H) Calcofluor binding indicating cellulose. I) Sample labelled with no primary antibody shows low levels of autofluorescence in the cuticular ledges. J) Calcofluor binding indicating cellulose. Antibody images all taken with 1 second exposure. Images are representative from at least n=4 Scale bars= 20µm.

3.2.4 Unmasking cell wall components: Enzyme deconstruction

Pectin, and in particular HGA, is highly abundant in the leaves of *Arabidopsis* (Zablackis et al., 1995). It has previously been shown that some cell wall components can be masked in immunocytochemical due to overlying pectins prevent antigen access, especially to xyloglucans (Marcus et al., 2008) and mannans (Marcus et al., 2010). Many of the antibodies tested here showed no binding in the initial screen, others showed punctate binding, while others showed limited binding (e.g. Figure 3.5.B) and it is possible that this is due to pectic masking of the underlying epitopes. To test this idea pectin was enzymatically removed and the primary antibody labelling repeated to see if the observed patterns changed. Due to time limitations, enzymatic pre-treatment was only carried out for a subset of antibodies. Table 3.1 lists the antibodies which showed no binding.

Table 3.2 shows the effect of pectate lyase treatment on the subset of antibodies tested while Figure 3.9 shows representative images for the antibodies which showed changed binding patterns. A number of antibodies showed no change to their binding pattern at all and these images are not shown. LM19 and LM20 both demonstrated complete absence of binding following enzymatic removal of pectin (data not shown).

Table 3.2. The effect of pectate lyase treatment on antibody binding

No change to binding	Increased binding	Reduced binding
JIM16	LM6	JIM7
LM1	LM8	LM19
LM5	LM13	LM20
LM11	LM14	
LM16	LM25	
LM24		
PAM1		
LM21		

JIM7 changes from strong binding prior without enzymatic treatment (Figure 3.9.A) to very weak binding following pectate lyase treatment (Figure 3.9.B). Some weak binding was observed still in 1 of the 4 replicates but this overall very weak signal indicates that pectin has been successfully removed. LM6 binding is very faint without enzymatic pre-treatment and it is hard to determine if this is substantially greater than autofluorescence (Figure 3.9.C). Following enzymatic treatment LM6 binds to the epidermis with an increased signal intensity being seen in guard cells (Figure 3.9.D). LM8 shows no binding under normal conditions (Figure 3.9.E) but following removal of pectin binding is observed uniformly across the epidermis, including the guard cells (Figure 3.9.F).

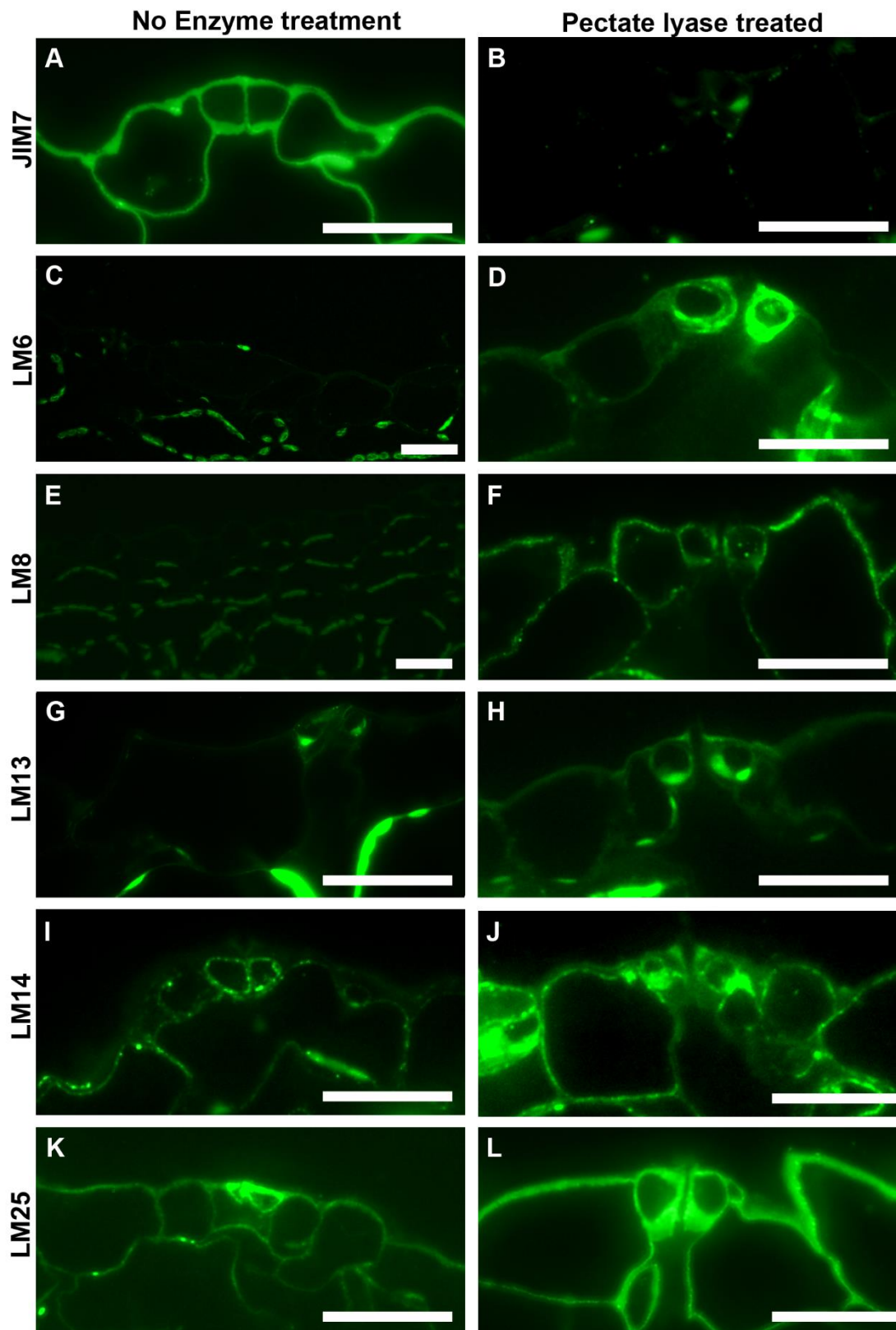


Figure 3.9. Pectate lyase treatment reveals masked cell wall epitopes. Left column shows samples incubated directly with antibody. Right column shows samples incubated with pectate lyase to remove pectin prior to antibody labelling. A) JIM7 labelling shows broad antibody labelling. B) Pectate lyase treatment causes loss of JIM7 binding. C) No LM6 binding is observed only chloroplast fluorescence is seen. D) LM6 binding is observed in pectate lyase treated samples. Binding is weak in the epidermis but strong binding is observed in the guard cells. E) No LM8 binding is observed. F) Pectate lyase treatment reveals LM8 binding in both the epidermis and the mesophyll. G) LM13 is observed weakly in the stomata and in the cuticular ledges. H) Pectate lyase treatment leads to stronger guard cell binding of LM13. Asymmetric guard cell binding is observed with much stronger binding on the lower periclinal and ventral anticlinal cell wall. Binding is also observed in the cuticular ledge and weak binding in the epidermis. I) LM14 shows weak punctate binding in the guard cells and epidermal cells. J) Pectate lyase treatment reveals strong LM14 binding in the epidermal and in the guard cells. Strong binding is also observed in the cuticular ledges. K) LM25 weakly in the epidermis and shows stronger binding in the guard cells. L) Pectate lyase treatment doesn't change the LM25 binding distribution but binding is much stronger in the epidermal cells meaning that guard cell binding and epidermal cell binding are equivalent. Images are representative of n=4 replicates (2 technical replicates). Image exposure times are all 1s. Scale bars= 20 μ m.

3.2.5 Does the guard cell wall undergo rapid remodelling during opening and closing?

A previous study has indicated rapid changes to callose deposition is possible and it was suggested that this was happening within the timeframe of stomatal opening and closing (Apostolakos et al., 2010). This suggests that there is a possibility that structural components within the cell wall could be remodelled in a rapid and dynamic manner in order to accommodate changes to guard cell shape and size.

To test this idea, tissue was harvested from *Col-0* plants and incubated in either opening buffer (2.10) or resting buffer containing 20 μ M ABA in order to stimulate opening or closing of the stomata respectively. The tissue was then embedded and sections prepared as described in 2.6. A selection of monoclonal antibodies were applied to determine if any cell wall epitopes had changed between the treatments to indicate rapid remodelling of the guard cell wall during opening and closing. Figure 3.10 shows representative images for JIM7 (A-B), LM19 (C-D), LM20 (E-F) and LM25 (G-H). These data show no major changes to binding pattern or intensity between opening buffer (Figure 3.10-Left hand column) and resting buffer with ABA (Figure 3.10-Right hand column). The control lacking primary antibody (Figure 3.10.I-J) shows that there is no substantial autofluorescence caused by either treatment. This technique was repeated for a number of other antibodies, Appendix 3 summarises this data but no obvious change in pattern or signal intensity was observed. These data indicate that no large scale cell wall remodelling is occurring during stomatal opening and closure.

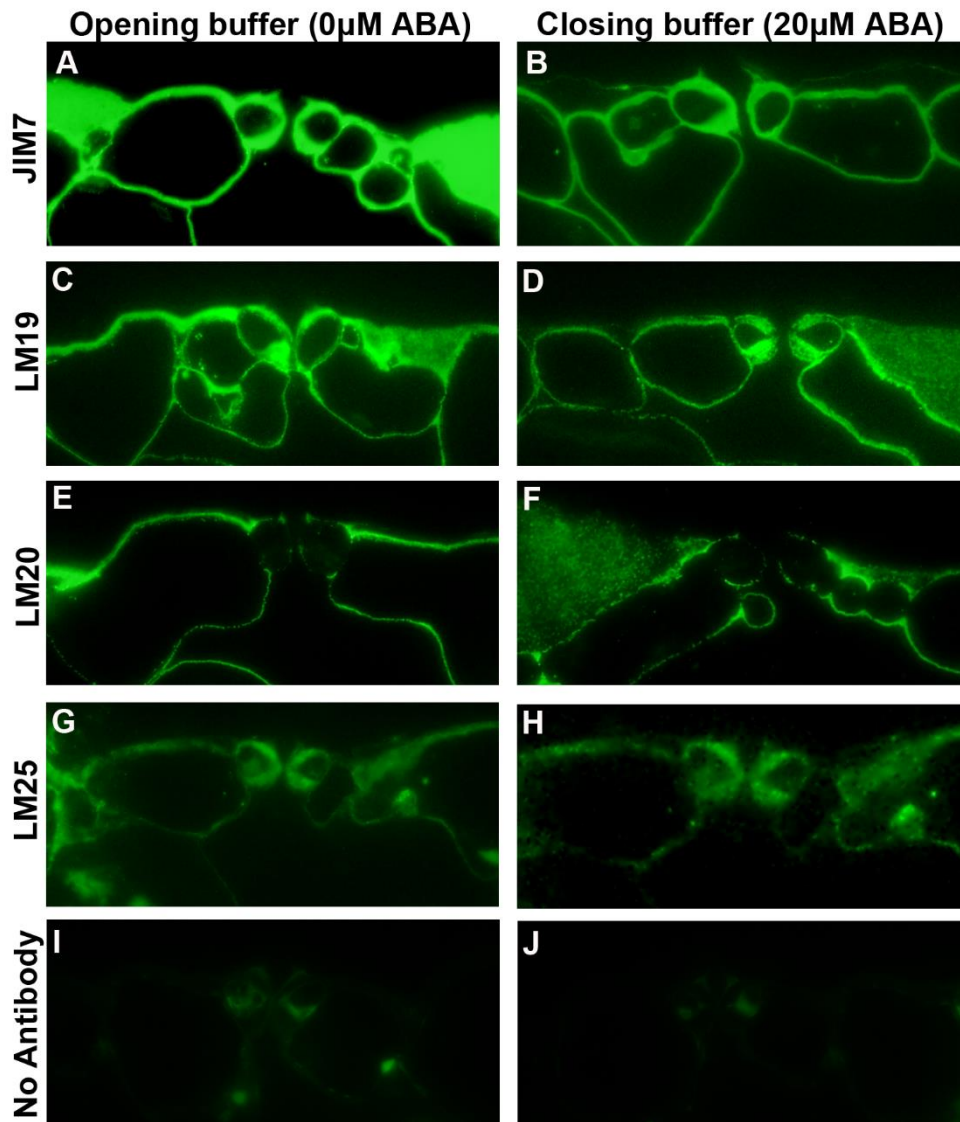


Figure 3.10. Antibody labelling comparing opened and closed stomata. Left column shows samples incubated in opening buffer while right column indicates samples incubated in closing buffer containing 20 μ M ABA. No differences are observed between the treatments for any of the antibodies A) JIM7 and opening buffer. B) JIM7 with closing buffer. C) LM19 with opening buffer. D) LM19 with closing buffer. E) LM20 with opening buffer. F) LM20 with closing buffer. G) Lm25 with opening buffer. H) LM25 with closing buffer. I) No antibody control with opening buffer. J) No antibody control with closing buffer. Samples are representative images from n=4. Exposure time for all images is 1s. Scale bars=20 μ m.

3.3 Discussion

In this chapter guard cell walls are characterised using an immunolabelling technique. This has enabled the visualisation of cell wall components within the guard cells and allowed comparisons with other cell types.

The general antibody screen showed that a wide range of cell wall components can be detected by antibody binding in *Arabidopsis* leaves. It is important to understand the limitations of such a technique to avoid over interpretation of data. Some antibodies tested did not bind, or showed sporadic binding. Some of the antibodies were not designed for use with *A. thaliana*, often being raised against rice or cotton epitopes, which may explain why some antibodies did not show a signal. It is also possible that the soluble cell wall components, such as some glycoproteins, are lost during the fixation and embedding process. There is also the issue of abundant cell wall components masking less abundant components by restricting antigen access and this issue is discussed in more detail later. Due to these limitations it is impossible to conclude that the components associated with the antibodies which showed no binding (see Appendix 2) are absent from the *Arabidopsis* guard cell wall.

The antibody labelling technique does not allow for quantification of cell wall components, but rather relies on relative intensities within a single image. We can infer whether a guard cell has more or less pectin than the surrounding epidermal cells by the relative fluorescence intensities, however we cannot infer whether there is more pectin than, for example, xyloglucan. Some studies have utilised careful control of image capture settings to allow comparison of binding between samples by measuring pixel intensity, however this technique is fraught with difficulties. It still does not allow comparison between antibodies as it does not take into account relative

binding affinities or antigen access, as dictated by the cell wall structure and embedding technique. Additionally, many epifluorescence systems use mercury or xenon arc lamps and the intensity of excitation decays over the lifetime of the bulb. Similarly, secondary antibody binding can become less intense over the lifetime of the aliquot, impacting on results acquired at different times. For these reasons any quantification of signal intensity was avoided in this project.

Some cell wall studies have attempted to quantify cell wall components using mass spectrometry (Alonso et al., 2010). This approach can be highly informative but to utilise this with stomata would require the separation of guard cells from the rest of the epidermis, which is technically challenging. To separate guard cells and epidermal cells without interference from mesophyll cells would require laser dissection microscopy, which is beyond the scope of this project.

Despite these limitations antibody labelling can be a very informative technique. A key advantage of this method is that the cell wall remains intact. Extraction of cell wall components for mass spectrometry or ELISA analysis can cause changes to the structure of cell wall components, for example methyl groups linked to acid residues in the pectin network are extremely sensitive to pH. Leaving the cell wall intact also provides spatial information about the distribution of cell wall components between and within cells. This spatial information within a single cell is especially relevant to guard cells which are known to have asymmetric cell walls (Zhao and Sack, 1999).

3.3.1 Screening of antibodies

Our results show that guard cell composition is clearly distinct from neighbouring epidermal cells. In particular, the pectin network showed

numerous differences. In addition to these whole cell differences there were also differences within individual guard cells. The most striking difference observed was the exclusion of highly esterified homogalacturonan (LM20 labelling) from the guard cells, which implies that guard cell pectin is on the whole less esterified than epidermal cells. This pattern corroborates previous findings in *Commelina* (L. Jones et al., 2003) and *Beta vulgaris* (Majewska-Sawka et al., 2002) but was important to confirm for *A. thaliana*. A definitive statement on the mechanical impact of this on the cell wall is hard to provide due to the technical challenges of directly measuring mechanical properties of guard cells (see Chapter 6 for more information). In the guard cell there is no detection of blockwise unesterified pectin, with calcium crosslinks (2F4). It seems reasonable to assume that this means that guard cell pectin is demethylesterified in a random rather than blockwise manner. Classical views of pectin demethylesterification tend to suggest that less esterification leads to a stiffening of the cell wall as unesterified pectin can cause calcium cross-links, forming the classical “egg box” structure. However, calcium crosslinks only form on blockwise demethylesterified pectin. Non-blockwise demethylesterified pectin can have a number of impacts on the cell wall. In pectin that is randomly de-methylesterified increased rigidity of the cell wall seems unlikely, however it is still possible. Theoretically, exposed galacturonic acid residues are able to incorporate side chains, such as arabinans (Wolf et al., 2009), which may allow for greater crosslinking with the hemicellulose network. It has also been shown that the action of polygalacturonases on de-methylesterified pectin can produce short fragments of pectin (OGAs) which are involved in cellular signalling (Ridley et al., 2001). It has been shown that OGAs can induce cell wall stiffening by the induction of peroxidase enzymes which induce crosslinking in both the pectin and hemicellulose networks (Bruce and West, 1989). In contrast, a reduction in rigidity in de-methylesterified pectin could occur as

polygalacturonase has greater access to pectin that is demethylesterified. It is important to note that it is not simply access to the pectin which modulates the activity of PGA but also pH (Denès et al., 2000), Demethylesterification of pectin leads to the release of protons into the apoplast which could alter the pH and thus change the action of cell wall remodelling enzymes (Catoire et al., 1998a). Alternatively, exposed carboxyl groups as a result of demethylesterification could incorporate water, causing hydration of the pectin network and increasing its flexibility. LM5 antibody binding, which indicates linear galactans, was excluded from the stomata but present in the epidermis. The implications of this are unclear but linear galactans are thought to be a component of the RGI network, the HGA network is known to predominate in *Arabidopsis* (Zablackis et al., 1995), so it is possible that there is little or no RGI in the guard cells, although it is also possible that it is simply the linear galactan side-chains that are lacking.

Guard cell walls have long been known to be anisotropic. For example, it was shown as far back as 1891 that guard cell walls are asymmetrically thickened, with ventral guard cell walls (pore facing) being thicker than the dorsal cell walls (Jennings and Hall, 1891). More recently it was shown that cellulose microfibrils have a distinct radial orientation (Palevitz and Heple, 1976). The rings of cellulose cause anisotropy across the whole cell, guiding the direction of cell expansion to maintain the cylindrical shape of guard cells, while the thickenings cause the cell to bend to create a pore (Marcus et al., 2001). This chapter demonstrates that other cell wall components also have asymmetric distributions, suggesting that the shape changes observed in the guard cells are not simply a function of uneven cell wall thickenings. For example, feruloylated polymers, as indicated by antibody LM12 binding, were found to be present only in the ventral walls of guard cells. Ferulic acid is known to have a role in cross-linking of pectin, especially the arabinan side chains which are prevalent on RG-I but also to a lesser extent in the HGA

network. It is possible that guard cell pectin on the ventral side is cross linked to a greater extent than the dorsal side, which would contribute to the rigidity of the ventral cell walls which is necessary to cause the guard cells to bend during opening. Interestingly it was observed that occasionally the LM12 antibody showed no binding in the stomata. It is not clear why this is the case but it could be due to the developmental stage of the stomata. Following on from this, it is not clear how the pattern of guard cell epitopes changes during development. Stomata are functional from very early in development so it is likely that the main cell wall profile is established early on, however there is scope for some epitopes to change throughout development. Staging stomatal development based on cross-section is not possible. making it challenging to track guard cell wall structure throughout development. In the future this could be achieved by paradermal sections which makes estimating stomatal age easier and also allows identification of precursor cells.

Xyloglucan distribution varied depending upon the epitope investigated. LM15, which recognises the XXXG motif of xyloglucan, showed a similar pattern to LM12, with no binding on the dorsal or periclinal walls of the guard cell. LM25, on the other hand, which recognises the XLLG or XXLG motifs showed broad binding, indicating an even guard cell distribution. Xyloglucan has been shown to interact with cellulose microfibrils and is thought to function to tether microfibrils together. It has been shown that an increase in the number of xyloglucan tethers causes the cell wall to increase in rigidity (Burgert, 2006). Xyloglucan has previously been implicated in stomatal function where it was proposed that they function as tethers between radially orientated cellulose microfibrils in the guard cells in order to limit cell elongation during opening and closing (Rui and Anderson, 2016). It is possible that the asymmetric binding distribution of xyloglucan epitopes contributes to the asymmetric cell wall stiffness across the stomata which

leads to the bending of guard cells during opening. It is not known what the structural function of each motif of xyloglucan is in the cell wall. However, XXXG is a less branched xyloglucan structure than XXLG or XLLG, so it is possible that unbranched xyloglucan has greater cross-linking attributes than its more branched counterparts.

The distinct cell wall profile of guard cells appears to corroborate previously held ideas regarding stomatal opening. It is possible that the pectin network and the cellulose network linked to xyloglucans is more rigid on the ventral side of the stomata than the dorsal, which might act to make the guard cells bend during cell expansion, leading to opening of the central pore.

3.3.2 Revealing hidden guard cell wall epitopes

Enzymatic removal of pectin caused a change in the binding pattern of some epitopes. The fact that the pectin antibodies (JIM7, LM19 and LM20) completely disappeared indicated that pectin has been successfully removed. LM6 and LM8 antibodies went from no binding to widespread binding, indicating that these epitopes were completely masked by the pectin. LM6, which recognises linear arabinan, shows much stronger binding in the stomata than in the epidermis after pectate lyase treatment. Previous work has shown arabinans to be crucial to the correct functioning of stomata (L. Jones et al., 2003), and that arabinan is present in the guard cells of *Commelina*. Interestingly enzymatic pre-treatment of *Commelina* was not required to observe LM6 binding suggesting that in this species there is greater antigen access.

3.3.3 Elucidating the structure of the guard cell cuticular ledge.

The structure of the cuticular ledge has remained ambiguous. It has been shown to be rich in lipids and phenolics (Karabourniotis, 2001), which is consistent with it being cuticle rather than an extension of the cell wall.

However, a previous study (L. Jones et al., 2003) has shown that there are also some cell wall components present in the ledges, particularly pectins.

In this chapter we confirm the result shown in *Beta vulgaris* (Majewska-Sawka et al., 2002) and *Commelina* (L. Jones et al., 2003) indicating the presence of pectin in the guard cell cuticular ledges (

Figure 3.8) My results contrast to those previously shown using the JIM5 antibody (which recognises unesterified HGA) that there was no binding in the cuticular ledge. JIM5 appears to show no consistent binding in *A. thaliana* so it is possible that this antibody is non-functional in this species. Our data is corroborated by the fact that LM19, which binds abundantly in *A. thaliana* and also recognises unesterified pectin, does not show any binding either. LM20 shows strong binding in the cuticular ledges, indicating the presence of highly esterified pectin. This is the opposite to previous finding that unesterified pectin was a component of the cuticular ledge (Jones et al., 2005). It is unclear whether this disparity in results is due to innate differences between *A. thaliana* and *Vicia fabia* or due to the advent of more specific pectin antibodies in the time between the studies. LM19 and LM20 are now recommended in the place of JIM5 and JIM7 due to their greater preference for unesterified and highly esterified pectin, respectively (Verhertbruggen et al., 2009a).

3.3.4 Conclusions

The data in this chapter has shown that guard cell wall composition is distinct from surrounding epidermal cells and suggest that cell wall composition does not change during stomatal opening and closing. To investigate the potential function of these patterns of cell wall epitopes I took a molecular genetic approach, described in the next chapter.

Chapter 4. Analysis of a pectin methylesterase mutant

4.1 Introduction

In the previous chapter, guard cell walls were shown to have distinct pectin profiles in comparison to neighbouring epidermal cells. A lack of highly esterified pectin in the guard cells compared to neighbouring epidermal cells suggests a role for guard cell pectin in stomatal function. As already discussed, arabinan has previously been implicated in stomatal opening and closing (L. Jones et al., 2003) and it is hypothesised that this arabinan is part of the pectic network. Pectin is known to have roles in plant mechanics but it is unclear how this functions in the guard cell.

Pectin in plant mechanics

The role of pectin in the mechanical properties of plants has been widely discussed (Braybrook et al., 2012; Palin and Geitmann, 2012; Peaucelle et al., 2011). It is known that composition of pectin has an important role in fruit ripening (Brummell and Harpster, 2001) plant defence (Lionetti et al., 2012), morphogenesis (Palin and Geitmann, 2012) and organ formation (Braybrook et al., 2012; Peaucelle et al., 2011). Early research focused on the cleavage and degradation of pectin (Ahmed and Labavitch, 1980; Gross and Wallner, 1979) and it is known that breakdown of the pectin network leads to a softening of plant tissues (Brummell and Harpster, 2001). It is becoming increasingly clear that fine alterations to the microstructure of the pectin has crucial roles in the regulation of cell wall mechanical properties.

Homogalacturonan (HGA) is the predominant form of pectin in *A. thaliana* and is synthesised at the Golgi apparatus and secreted to the cell wall in a predominantly methylesterified state (Figure 4.1.A (Sterling et al., 2001; Zhang and Staehelin, 1992)) as discussed in Chapter 1. At the cell wall homogalacturonan is progressively demethylesterified (Hongo et al., 2012) by the pectin methylesterase family of enzymes (PMEs) which are in turn regulated by the pectin methylesterase inhibitor family of enzymes (PMEIs). Demethylesterification of HGA alters the way in which the pectin network functions and how it interacts with other cell wall components. The many ways in which pectin can be affected by demethylesterification make it hard to predict the outcome of altering a PME/PMEI gene.

The PME/PMEI family of genes: Regulation of homogalacturonan demethylesterification

PME genes are shown to have diverse, and often contrasting functions in plants. Early studies on pectin esterification were often carried out in fruits, such as tomatoes due to the role of pectin in fruit ripening. Pectin esterase enzymes in tomato are known to be highly expressed in green fruit but increase by 2-3 fold during fruit ripening (Ray et al., 1988) and it has long been shown that pectin esterases are associated with cellular integrity in fruit possibly by the regulation of cation availability in the fruit (Tieman and Handa, 1994). Demethylesterification of pectin by PME genes has been associated with increased mechanical strength and cell wall rigidity. Knockout of *PME35* in *A. thaliana* led to reduced mechanical strength in the stems indicating that *PME35* mediated demethylesterification regulates the stem mechanical properties (Hongo et al., 2012). A reduction in PME activity in kiwi due to exogenous PMEI treatment caused an increase in root elongation and induced pollen tubes to burst suggesting that kiwi PME was responsible for mechanical integrity of cell walls in roots and pollen tubes

(Paynel et al., 2014), additionally a reduction in pectin esterification in *Arabidopsis* had the opposite effect leading to reduction in cell growth and hypocotyl extension in *Arabidopsis* (Derbyshire et al., 2007) suggesting that demethylesterification of pectin can also lead to decreased extensibility of the cell wall and increased mechanical strength. In addition demethylesterification of pectins has been shown to be associated with a decrease in the rigidity of cell walls which preceded organ outgrowth in *Arabidopsis* primordia (Peaucelle et al., 2011) and disruption of demethylesterification by PME1 overexpression has been shown to restrict organ formation leading to altered phyllotaxy (Peaucelle et al., 2008). This softening was shown to be mediated by auxin but inducible overexpression of *PMEI3* was shown to disrupt auxin transport proteins leading to disrupted organ formation (Braybrook and Peaucelle, 2013). It is likely that the mode of demethylesterification is important in determining if cell wall softening or stiffening occurs. Blockwise demethylesterification has been shown to lead to formation of calcium cross-linked gels leading to increased rigidity (W. G. Willats et al., 2001) whereas random demethylesterification makes HGA more susceptible to enzymatic degradation (Kars et al., 2005). This explains why fungal PME genes have a random (multiple attack) mode of demethylesterification (Duvetter et al., 2006; Limberg et al., 2000).

The PME/PMEI family are a large gene family containing at least 137 genes in *Arabidopsis thaliana* (M. Wang et al., 2013) and several other putative gene candidates. PMEs remove the methyl side group from galacturonic acid residues leading to an exposed carboxylic acid group, the release of methanol and a proton (W. G. T. Willats et al., 2001 Figure 4.1B)). This release of protons causes a change in the apoplastic pH which in turn can modulate the activity of the PME family and other cell wall modifying enzymes which are known to be pH sensitive (Denès et al., 2000).

PME's can act progressively, where large stretches of galacturonic acid residues are sequentially demethylesterified, or randomly where individual galacturonic acid residues in sporadic locations are demethylesterified. It was initially thought that only fungal PME's carried out random demethylesterification (Markovič and Kohn, 1984) to allow polygalacturonases to gain access to the pectin backbone during plant infection and that all plant PME's demethylesterified linearly to allow calcium crosslinking as a mechanism for strengthening cell walls (Marry et al., 2006). More recent studies have revealed that some plant PMEs act randomly while some act linearly (Denès et al., 2000; Micheli, 2001), and it has been shown that some can act both linearly and randomly depending on apoplastic pH (Denès et al., 2000). Regulation of PME activity by pH is also dependent on the level of methylesterification (Catoire et al., 1998b).

PME/PMEI genes can be classified, based upon the presence of highly conserved domains (Markovič and Janeček, 2004; M. Wang et al., 2013) into 3 distinct classes: PME's, containing the PME domain; proPME's and PMEI's. The proPME's contain a PME domain and an additional pro domain which has similarities to the PMEI domain suggesting an auto-regulatory role. There are 23 PME's, 43 proPME's and 71 PMEI's identified in *A. thaliana* (Markovič and Janeček, 2004; M. Wang et al., 2013).

The extensive and complex nature of the pectin network combined with the size of the PME/PMEI gene family and their contrasting roles in plant processes makes the study of pectin methylesterification challenging. In addition, access to pectin is limited as chemical extraction can cause changes to cell wall components altering cell wall conformation.

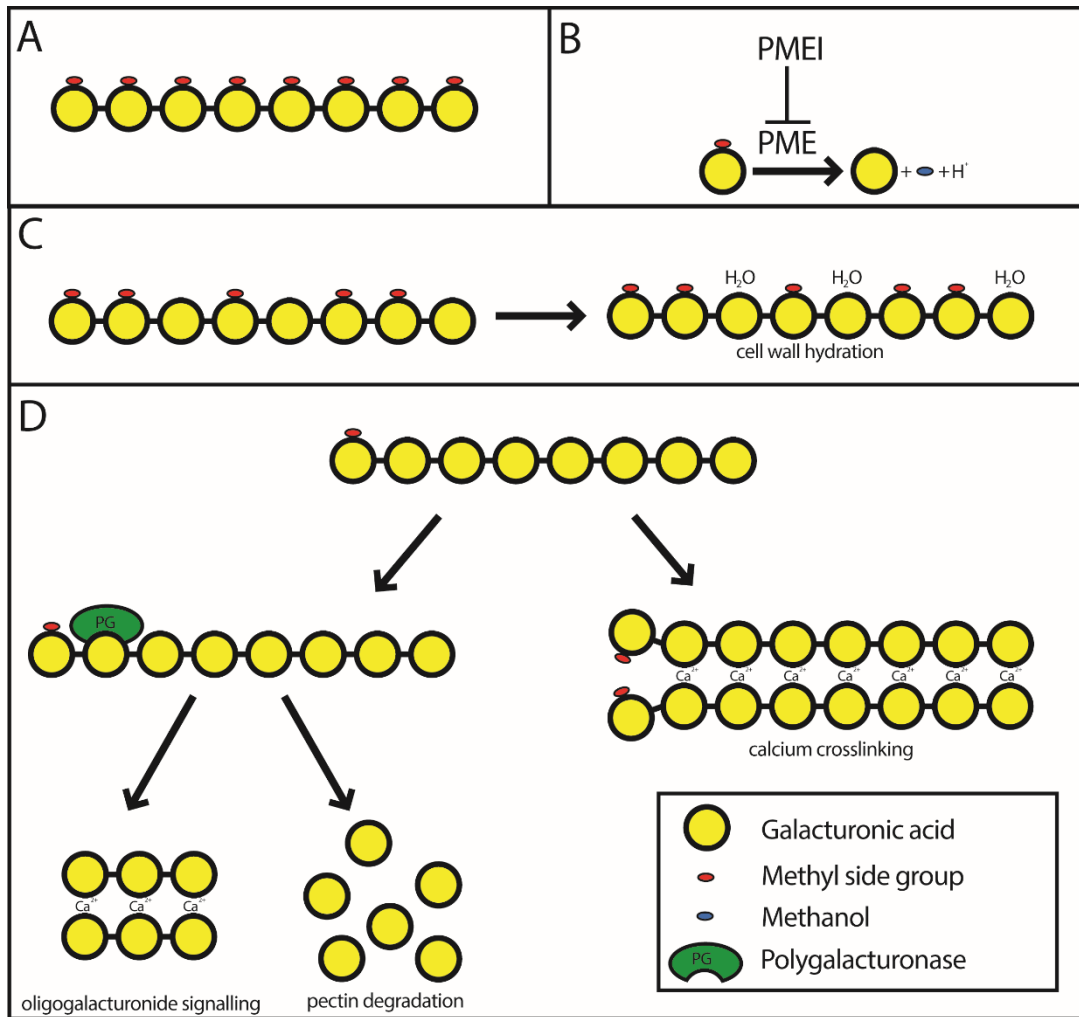


Figure 4.1. Schematic representation of homogalacturonan and the possible activities of PMEs. A) Homogalacturonan is highly methylesterified when synthesised. B) PME catalyses the removal of a methyl side group leading to the release of methanol and a proton. C) Random demethylesterification allows pectin hydration reducing the rigidity of the cell wall. D) Blockwise demethylesterification can allow access to pectin degrading enzymes such as polygalacturonase which can lead to either pectin degradation and cell wall softening or the production of small crosslinked pectin fragments used in defence response signalling causing downstream cell wall changes. Alternatively, blockwise demethylesterification can allow extensive calcium crosslinking of intact pectin leading to increased cell wall stiffness.

In this chapter an *A. thaliana* loss of function mutant in a PME gene is characterised. It is hypothesised that disruption of the guard cell pectin network will alter the function of guard cells due to changes in cell wall mechanics.

4.2 Results

4.2.1 *PME6* is expressed in mature guard cell

To identify genes encoding cell wall proteins potentially expressed specifically in guard cells a microarray analysis (NASCARRAYS 29) was conducted by Lee Hunt to look at the expression of genes in whole *A. thaliana* leaves compared to epidermal fragments enriched in guard cells. A gene, AT1G23200, hereafter referred to as *PME6*, was identified as highly expressed in guard cells fragments compared to whole leaf samples.

Table 4.1. Expression of *PME6* in different tissues.

	Mean Guard cell signal	Mean whole leaf signal
AT1G23200	106.9	35.13333333

Additional transcriptomic data analysis was carried out using the Arabidopsis EFP browser (Winter et al., 2007) as shown in Figure 4.2. Expression of *PME6* was shown to be 80 times higher in the guard cells than whole leaves (Pandey et al., 2010) and 30 times higher than in mesophyll cells ((Yang et al., 2008) Figure 4.2.C). Expression was also shown to increase following treatment with the drought stress hormone abscisic acid (ABA, (Figure 4.2.A-B)).

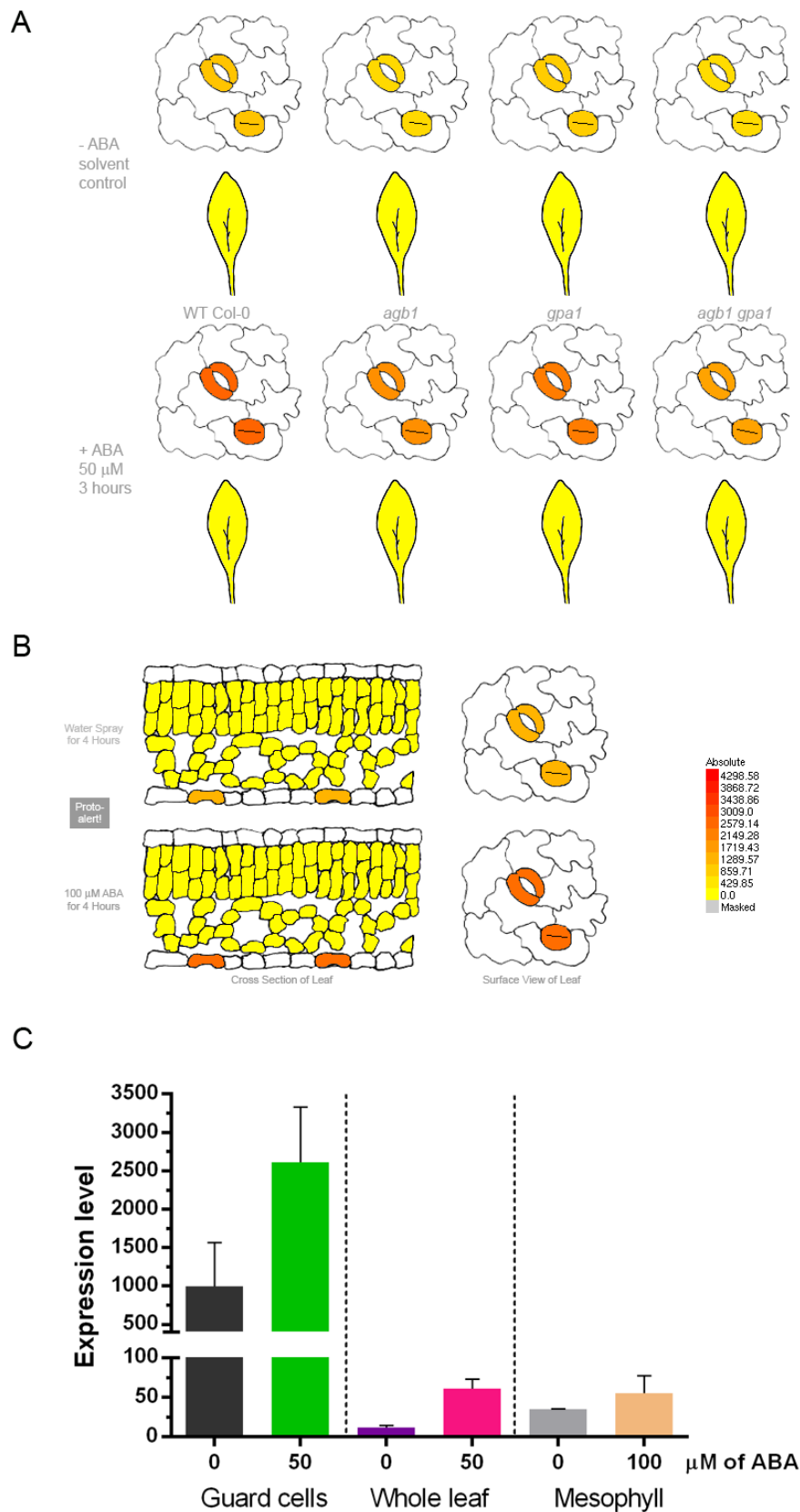


Figure 4.2. EFP browser data showing expression data for *PME6*. Darker colours represent higher gene expression level A) Expression in guard cells compared to whole leaves with and without 50 μ M ABA, (Pandey et al., 2010) B) Expression in guard cell protoplasts and mesophyll protoplasts with and without 100 μ M ABA, (Yang et al., 2008). C) Quantitative analysis of data from A and B, means=S.D, n=3.

4.2.2 Characterising a *pme6-1* insertion mutant

A T-DNA insertion mutant *pme6-1* containing a transposon insertion in *PME6* was identified from the Nottingham Arabidopsis Stock Centre (NASC) (details of all plant lines used are in Appendix 4). The transposon insertion is located to an intron between the PME and proPME domains (Figure 4.3). As only one T-DNA insertion line was available from NASC, complemented lines in which *PME6* was expressed under the control of the *PME6* promoter in the *pme6-1* mutant background, (hereafter referred to as *proPME6::PME6*) were created by Lee Hunt. These lines were used as controls in the experiments described below to confirm that the phenotypes observed reflected loss of PME6 function.

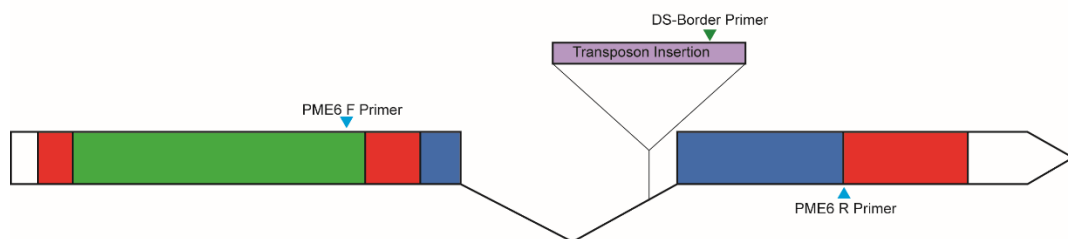


Figure 4.3. The structure of the *PME6* gene. White boxes represent UTR regions, Red boxes represent exon, green box shows putative PME domain, Blue box shows putative proPME domain (M. Wang et al., 2013), black lines represent intron. Location of transposon insertion is indicated by purple box. Primers used are marked.

Figure 4.3 shows a gene model for the *PME6* gene using data from TAIR (Arabidopsis.org). *PME6* has a single PME domain (Figure 4.3, marked in green) and a proPME domain sharing significant sequence similarity to PME1 domains (M. Wang et al., 2013). The location of the transposon insertion is shown to map within the intron in the *PME6* gene.

The location of primers used to genotype *pme6-1* plants are marked in Figure 4.3 (see Appendix 5 for a list of all primers used). The analysis revealed that *pme6-1* is a homozygous line for the insertion (Figure 4.4).

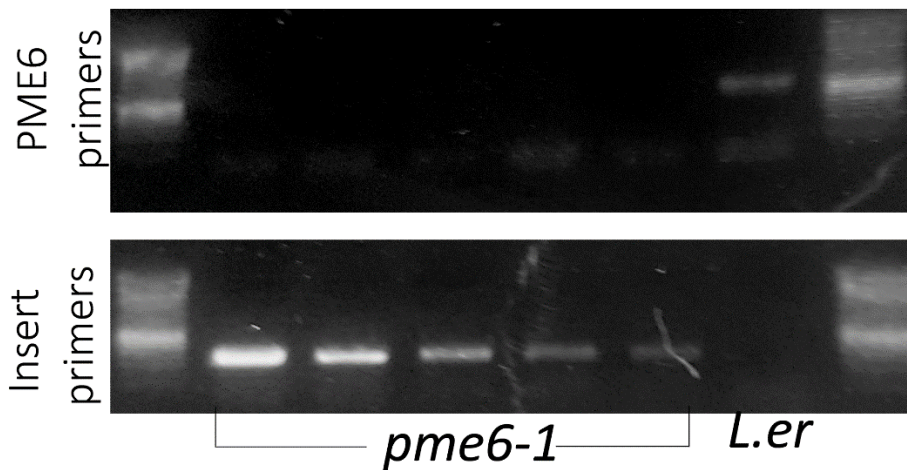


Figure 4.4. Genotyping of *pme6-1* insertion line from NASC. The top gel has gene specific primers (*PME6* Fwd – *PME6* Rev) and a single band is seen for WT *L.er*. The bottom gel has a forward primer for the insertion (DS5-1) and the *PME6* Rev primer. All 5 *pme6* plants tested were homozygous for the insert.

***pme6-1* transcript expression was restored in complemented lines**

RT-PCR analysis performed on from leaf discs of 28 day old plants showed a total loss of *PME6* transcript in *pme6-1* mutants, indicating that the transposon insertion had caused a successful gene knockout. The complemented line (*pPME6::pme6*) showed a restoration of the transcript level to approximately WT level. *RUB1* (RELATE TO UBIQUITIN 1 CONJUGATING ENZYME 1 (Rao-Naik et al., 1998)) was used as a control gene and showed similar transcript level in all lines apart from the second *proPME6::PME6* line.

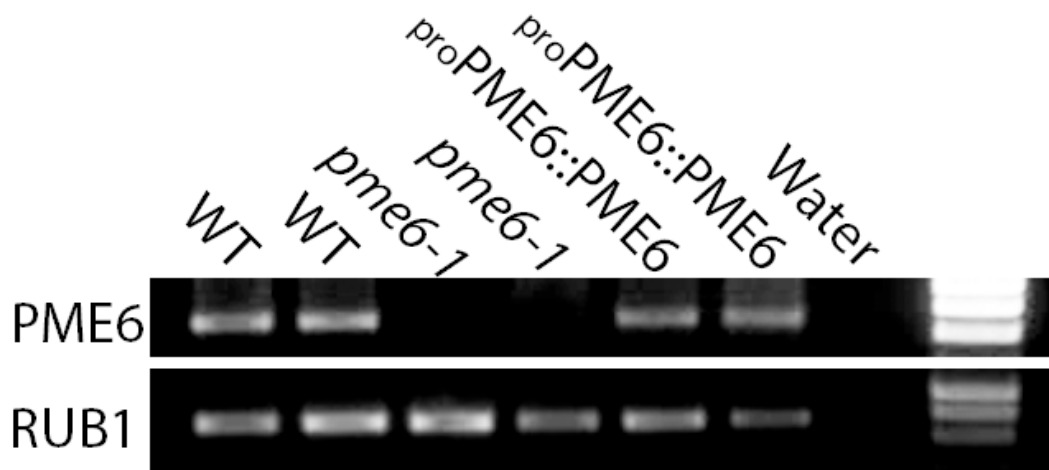


Figure 4.5. Semi quantitative RT-PCR from leaf discs of *Col-0*, *pme6-1* and *pPME6::pme6* lines. Transcript levels are not detectable in *pme6-1* plants but are restored to *Col-0* like levels in complemented lines. RUB1 was used as a loading control.

4.2.3 PME6 expression is restricted to mature guard cells

To confirm that *PME6* expression was localised to the guard cells in leaves plants expressing the *pPME6::GUS* fusion construct were created by Lee Hunt and Nagat Ali and kindly donated for use in this project. Histochemical localisation of *GUS* expression was carried out in plants aged 21 days (Figure 4.6). *PME6::GUS* expression was limited to the guard cells and to the hydathodes, which contain a high density of stomata (Figure 4.6.C), as shown in Figure 4.6. These data indicate that *PME6* is expressed predominantly in the guard cells of *A. thaliana* leaves, consistent with a possible role in stomatal functioning.

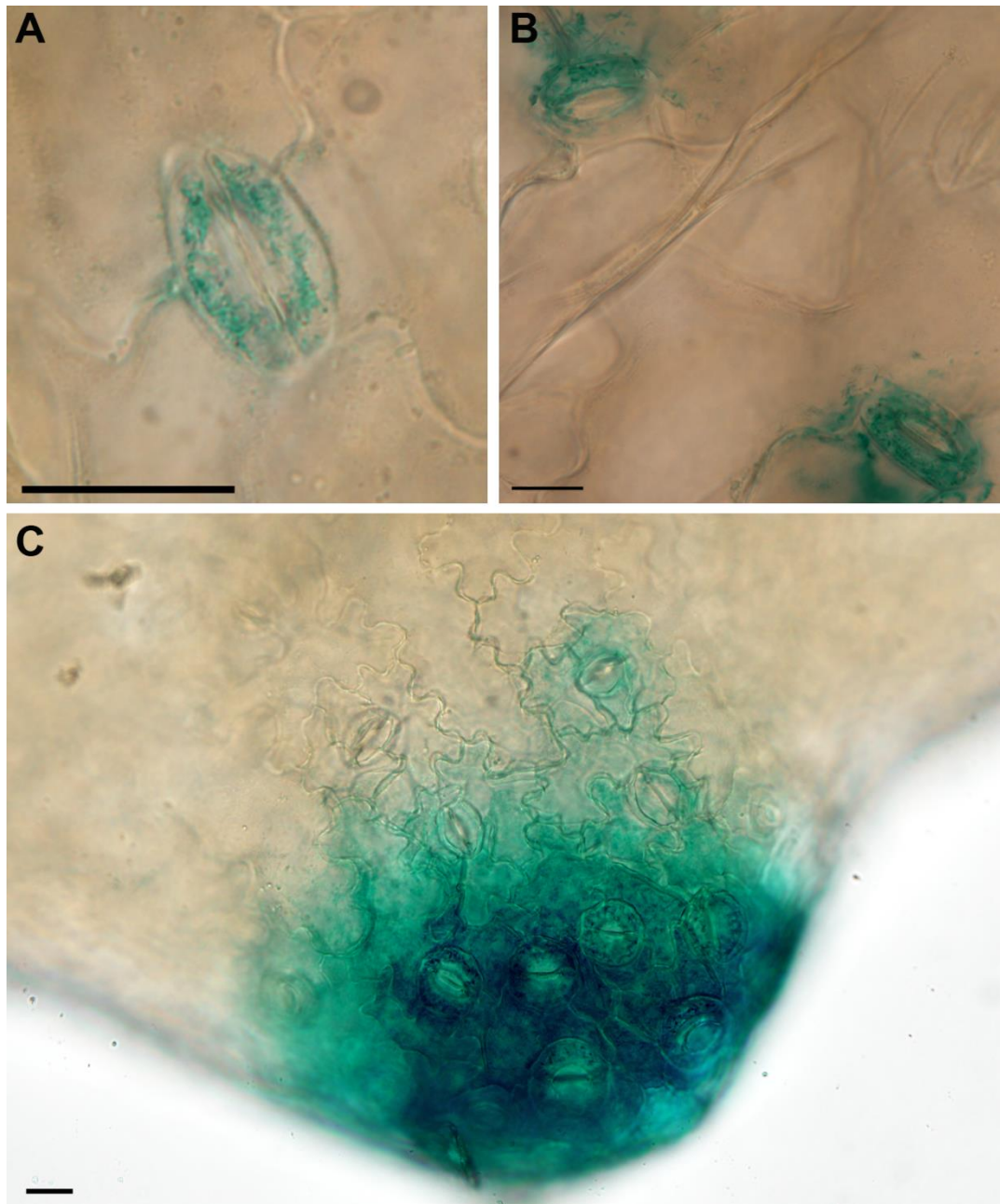


Figure 4.6. GUS histochemical staining showing localisation of *pme6-1*. A and B show GUS localisation of the *pme6-1* gene to the stomata in mature leaves (28day old plants). C) Shows GUS localisation to hydathodes in a developing Arabidopsis leaf. Scale bars represent 30μm

The GUS data show that *PME6* is specifically expressed in guard cells of mature leaves and that no localisation occurs in stomatal precursor cells. This suggests that *PME6* is unlikely to be involved in the initial formation of the guard cell wall, rather it is more likely to act after cell wall development, once the guard mother cell has undergone division. This was corroborated by EFP browser data analysis of *PME6* expression in mutants with altered

epidermal patterning (Figure 4.7). These data show that *PME6* expression is relatively low in *Col-0*, which have normal epidermal patterning, and is even lower in *spch* and *scrm-D* mutants (which only have epidermal pavement cells and meristemoids respectively (Pillitteri et al., 2011)). In contrast *scrm-D mute* mutants (which are enriched for guard cells (Pillitteri et al., 2011)) show almost a fivefold increase in *PME6* expression level compared to *Col-0* seedlings.

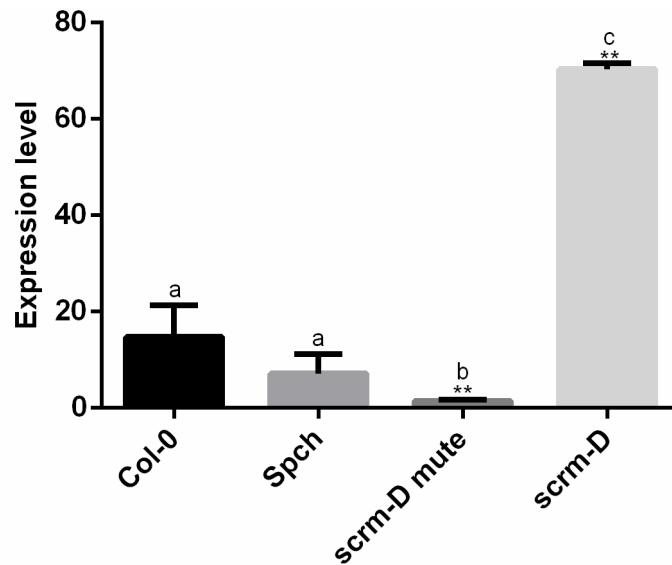


Figure 4.7. EFP browser data showing expression level in whole 5 day old seedlings for a range of stomatal development mutants and *col-0*. Different mutants have different epidermal cell patterns, *spch* mutants only have pavement cells in the epidermis, *scrm-D mute* only have meristemoids and *scrm-D* has only have guard cells in the epidermis. (Pillitteri et al., 2011)

The above transcriptomic and GUS data suggest that *PME6* is specifically expressed in mature guard cells after they have undergone the final symmetric division from a guard mother cell. This implies that *PME6* acts only after the cell wall is complete.

4.3 Growth data

4.3.1 Seed characteristics

pme6-1 plants appeared to grow normally; no leaf architecture or distinct morphological changes were noticed. Seed size and weight was analysed and no difference was found between the lines (Figure 4.8.A-C). Seed viability was also not changed as judged by germination rate (Figure 4.8.B), showing no difference between *pme6-1* and WT *L.er* (Figure 4.8.A ANOVA $p=0.8236$ $n=5$). These results imply that any differences that may be observed in plant growth or development are not due to differences in seed quality.

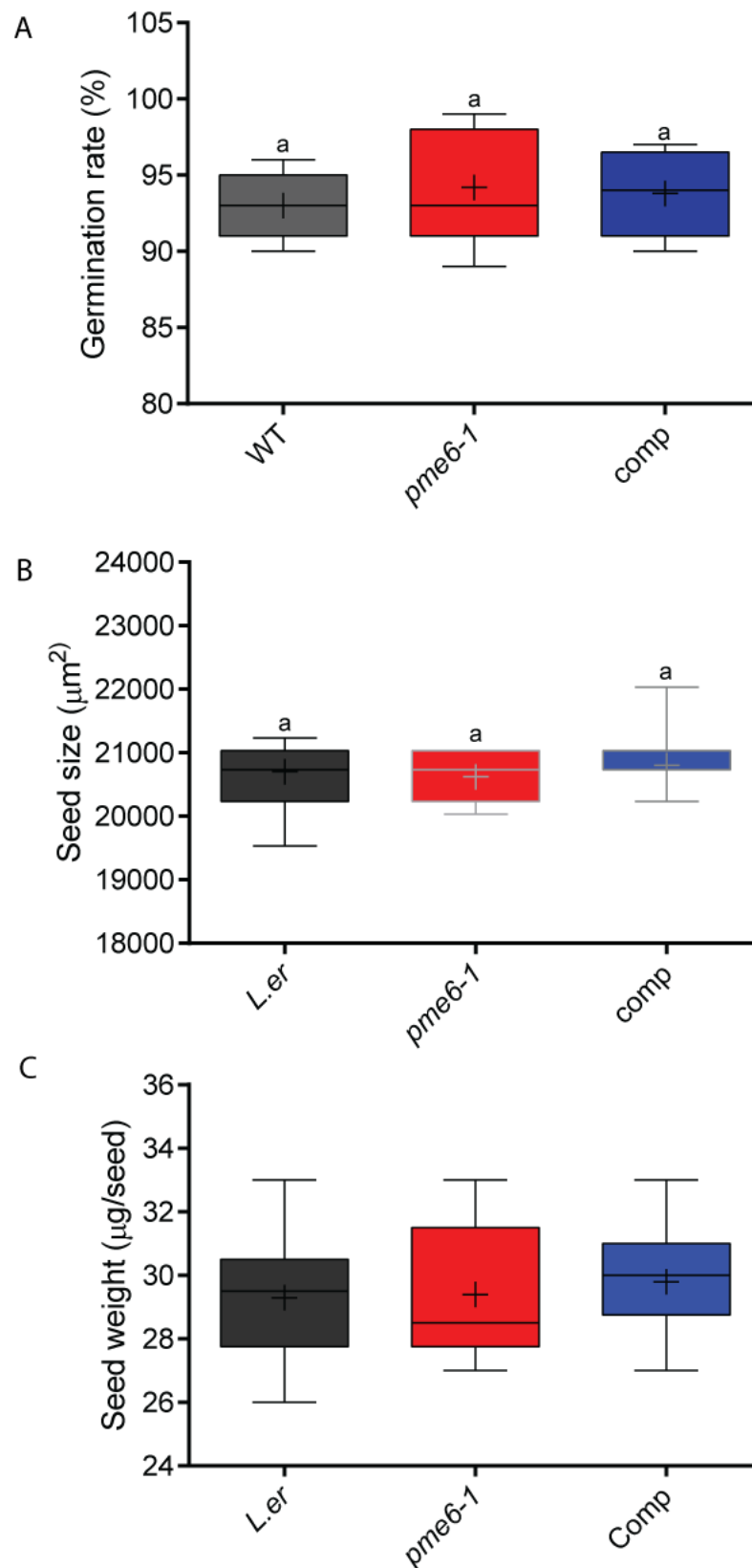


Figure 4.8. *pme6-1* seed characteristics are unchanged. A) Germination rate (as a percentage of 100 seeds) is unchanged between the lines, ANOVA $p=0.8236$ $n=5$. B) Seed size is unchanged between the lines, ANOVA, $p=0.5169$ $n=75$. C) Seed weight, each replicate point is based on an average of 100 seeds. No difference was observed between any of the lines. ANOVA $p=0.8482$ $n=10$. Error bars on all treatments represent min to max values, means indicated by +.

4.3.2 Size is altered in *pme6-1* plants at ambient CO₂

No obvious aberrant growth was observed in *pme6-1* plants by eye. Rosette size was measured to check growth under different carbon dioxide regimes. Plants grown at ambient CO₂ (400ppm) and elevated CO₂ (1000ppm) were measured to determine if the *pme6-1* mutant had any changes to overall size. Plants were measured at 32 days old when (under our growth conditions) the inflorescence stem was just becoming visible at the centre of the rosette. The same measurement was repeated at 40 days and there were no significant differences between the readings (data not shown), suggesting that the rosettes had stopped expanding and were fully mature.

pme6-1 plants were significantly smaller than WT plants at ambient CO₂ concentrations (Figure 4.9.B). The complemented *pPME6::pme6* plants showed a rosette size not significantly different to WT plants. When the WT, *pme6* and *pPME6::pme6* plants were grown under conditions of elevated CO₂ there were no differences in rosette size between any of the lines with *pme6-1* tending to be the largest (Figure 4.9.C). Increasing CO₂ concentration had the greatest effect on *pme6-1* plants, causing an increase in size of 144% compared growth of *pme6* plants grown under ambient CO₂ (Figure 4.9.B), whereas WT plants showed only an increase in rosette size of 86% when grown under elevated CO₂ (Figure 4.9.C).

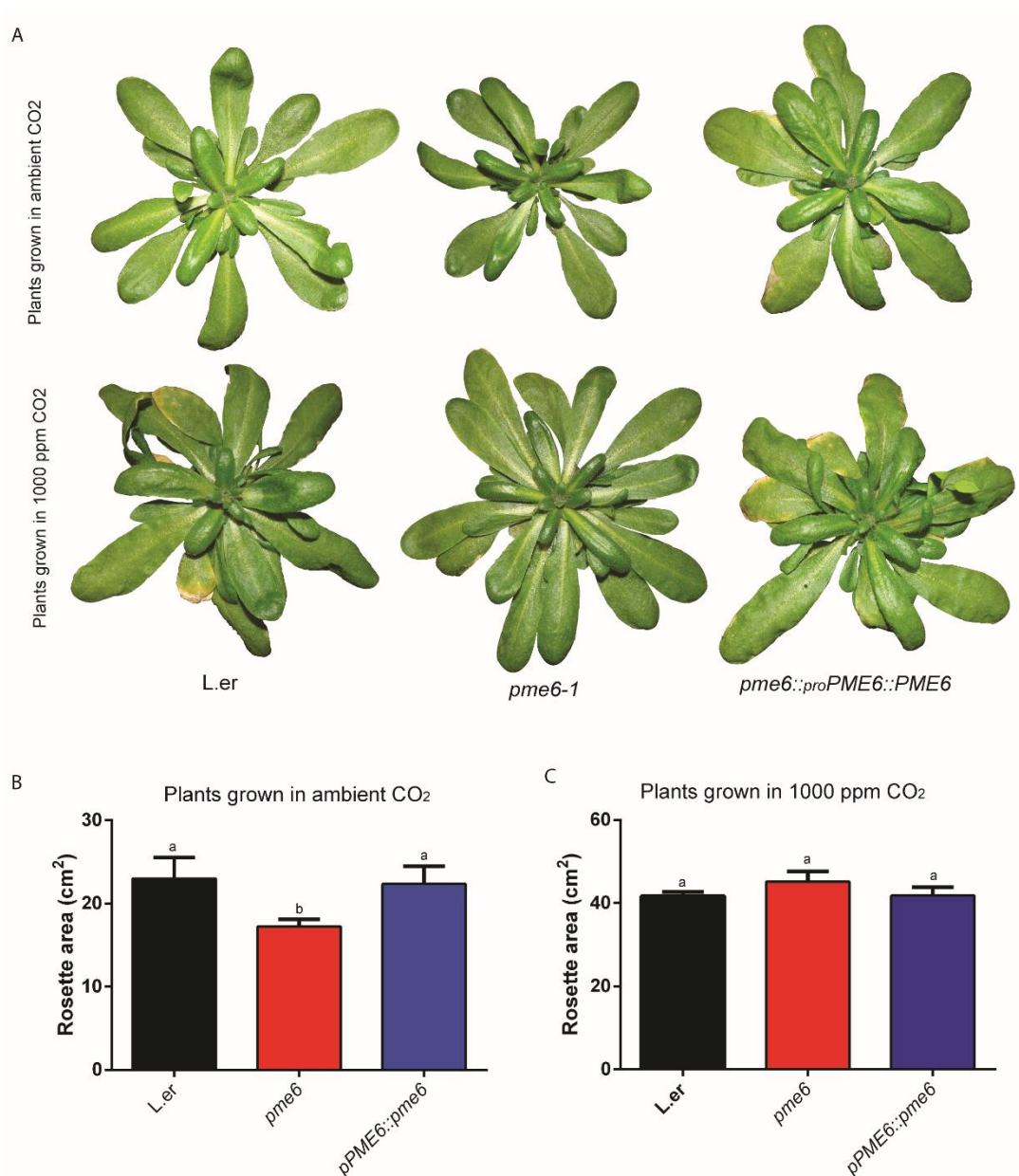


Figure 4.9. *pme6-1* plants are smaller than WT under ambient CO₂ but growth at elevated CO₂ leads to plants attaining a similar size. Images of plants (genotypes as indicated) under ambient CO₂ are shown in A (top row) and under elevated (1000 ppm) CO₂ in A (bottom row). Quantitation of total rosette area of plants grown under ambient CO₂ (B) shows that *pme6-1* plants achieve a smaller final size, whereas growth in elevated CO₂ (C) leads to all plants reaching a similar mean size. In B, C error bars = s.e.m, n= 8 statistical differences determined by ANOVA, p<0.05.

4.3.3 Stomatal size and density in *pme6-1* plants.

It has long been known that alterations in stomatal density lead to changes in transpiration, plant size and development (Doheny-Adams et al., 2012).

Similarly stomatal size has been shown to have an impact on plant growth (Drake et al., 2013). To investigate whether this could be having an impact on the *pme6-1*, plants size and density measurements were conducted on fully expanded leaves from 28 day old plants. No difference was observed in stomatal density in *pme6-1* plants or *proPME6:pme6* plants compared to WT plants at ambient CO₂ or 1000ppm CO₂ (Figure 4.10.A-B). Using stomatal complex length as a proxy for stomatal size, no differences were observed between any of the lines at either CO₂ concentration (Figure 4.10.C-D).

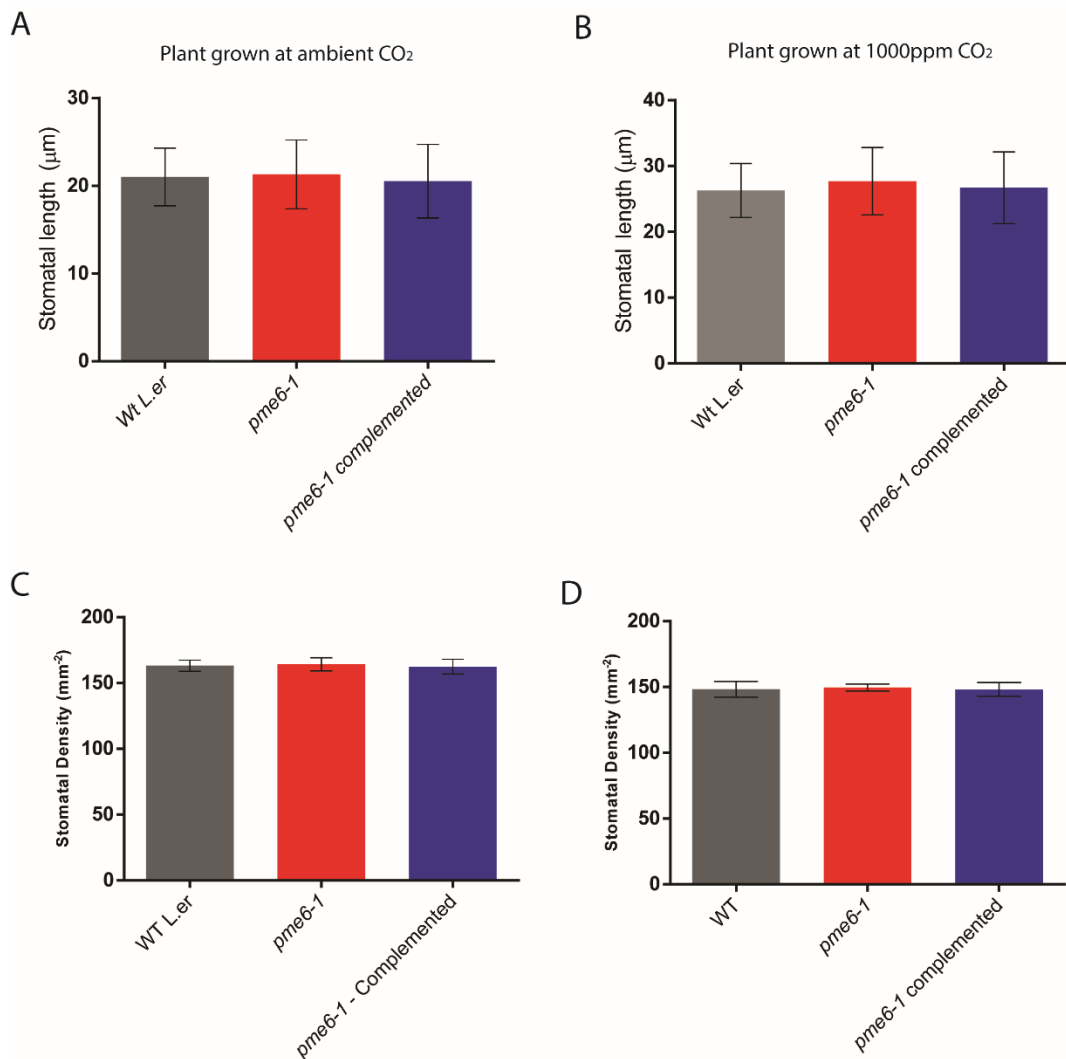


Figure 4.10. There are no differences in stomatal size or density in *pme6-1*. (A) Stomatal length in leaves from WT, *pme6-1* and *pme6-1* complemented plants grown under ambient CO₂ or (B) elevated (1000 ppm) CO₂. (C) Stomatal density in leaves from WT, *pme6-1* and *pme6-1* complemented plants grown under ambient CO₂ or (D) elevated (1000 ppm) CO₂. Columns indicate mean values, error bars = s.e.m. (n=5).

4.4 Assessing the functionality of *pme6* stomata

The specific expression of *PME6* in the guard cells suggests a potential role in stomatal function. As seen above, no differences in stomatal density or size were observed. To assess whether *PME6* has a role in the regulation of opening and closing of stomata a number of aperture bioassays were

conducted to assess stomatal response to a variety of stimuli such as CO₂, ABA and light.

4.4.1 *pme6-1* stomatal aperture in response to altered CO₂ levels

It has been shown that low CO₂ induces stomatal opening and CO₂ induces stomatal closure (Kim et al., 2010). Figure 4.11 shows the stomatal aperture response in isolated abaxial epidermal strips of *pme6-1* and WT leaves exposed to buffers supplied with elevated (1000ppm), ambient or decreased (0ppm) levels of CO₂. WT stomata showed increased aperture when exposed to low CO₂ and decreased aperture when exposed to elevated CO₂ relative to ambient CO₂, as has been previously reported. In contrast *pme6-1* stomata showed a limited capacity to respond to CO₂. There was no significant difference in aperture between the CO₂ treatments for the *pme6-1* stomata, with apertures remaining similar to those observed at ambient CO₂. The WT

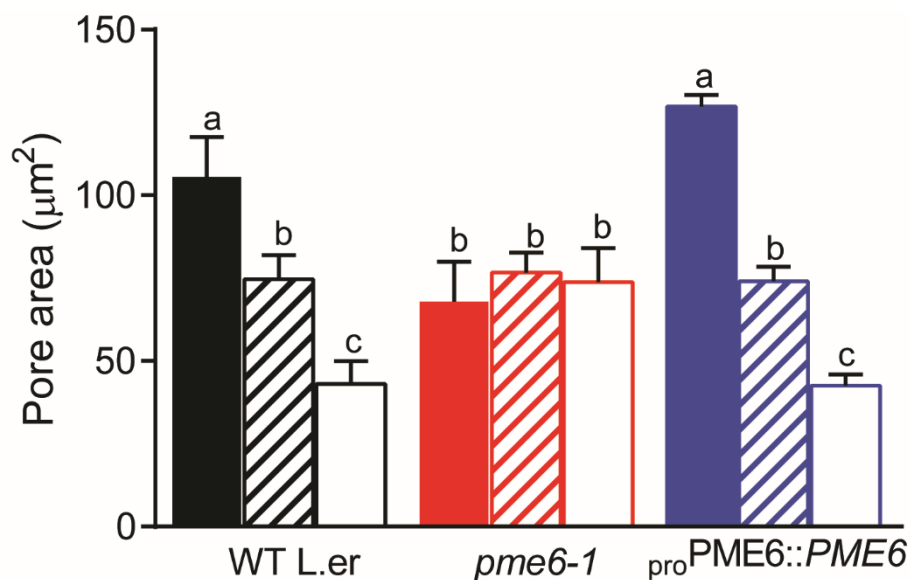


Figure 4.11. Guard cell opening/closure response to changing CO₂ concentration is lost in the *pme6-1* mutant. Pore area was measured from stomata in epidermal peels taken from the genotypes indicated (WT, *pme6-1* and *pme6-1* complemented with a *proPME6::PME6* construct) after incubation of the peels with either CO₂-free air (0 ppm CO₂) (solid bars), ambient CO₂ (hatched bars) or high (1000 ppm) CO₂ (open bars). Each column shows the mean and s.e.m. (n=6), with statistical differences determined by ANOVA with post-hoc Tukey test. Columns indicated with identical letters cannot be distinguished from each other (p < 0.01).

stomatal aperture response to CO₂ was restored in *pme6-1* complemented plants. These data show that the stomata of the *pme6-1* mutants do not respond in a normal manner to altered CO₂ level.

4.4.2 Stomatal responses to other guard cell stimuli

ABA

It has long been known that ABA promotes stomatal closure. In our assays WT stomata closed in response to increasing ABA concentration while *pme6-1* stomata showed no movement (Figure 4.12). *pme6-1* stomata showed a smaller aperture in the absence of ABA, indicating a lack of ability to open in addition to an inability to close. Complemented *pme6-1* plants showed a wild type-like phenotype in response to ABA.

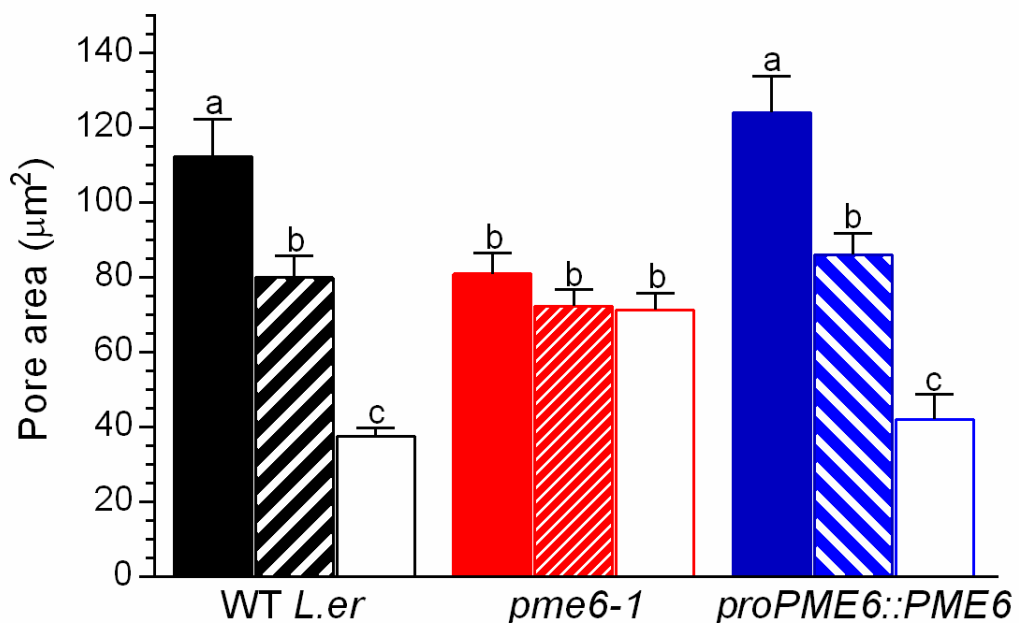


Figure 4.12. Guard cell opening/closure response to changing ABA concentrations is lost in the *pme6-1* mutant. Pore area was measured from stomata in epidermal peels taken from the genotypes indicated (WT, *pme6-1* and *pme6-1* complemented with a *proPME6::PME6* construct) after incubation of the peels in opening buffer with either 0 µM ABA (solid bars), 1 µM ABA (hatched bars) or 10 µM ABA (open bars). Each column shows the mean and s.e.m. (n=6), with statistical differences determined by ANOVA with post-hoc Tukey test. Columns indicated with identical letters cannot be distinguished from each other (p < 0.05).

Response to mannitol

Stomatal responses to CO₂, ABA and light are mediated via complex signal transduction networks which change the activity of membrane localised ion channels in the guard cell membranes. It is hard to tell from the response to these stimuli if changes in stomatal aperture are due to impaired signalling or due to underlying mechanical changes structurally limiting stomatal movement. Immersion in an osmoticum, such as mannitol, decreases the turgor pressure of the cells by altering the osmotic potential of the leaf, thus bypassing the signal transduction elements involved in stomatal closure.

Figure 4.13 shows the stomatal response of abaxial epidermal peels in resting buffer with and without 0.5 M mannitol. Mannitol caused both WT and *pme6-1* stomata to close but *pme6-1* stomata remain significantly more open than WT stomata. These data support the hypothesis that stomatal closure response is altered due to structural limitations on stomatal movement rather than a defect in stomatal signalling.

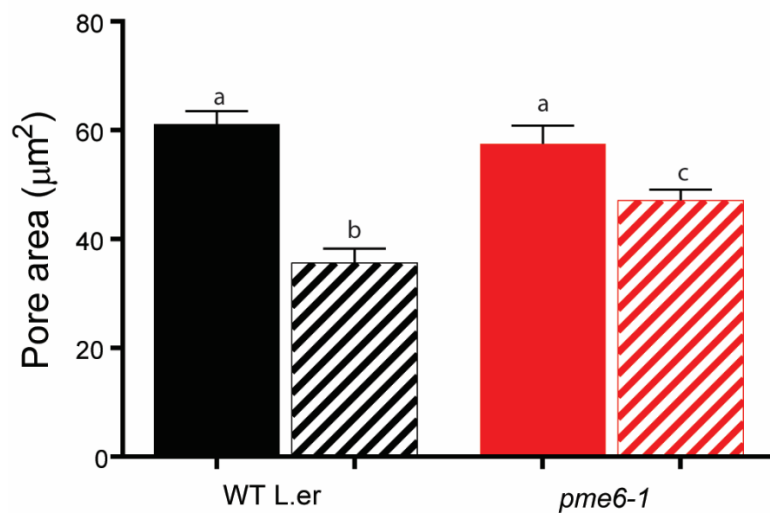


Figure 4.13. *pme6-1* stomata show a differential pore size response after incubation in high osmoticum. Stomatal pore areas were measured in epidermal peels from either WT or *pme6-1* leaves incubated either in resting buffer (solid bars) or resting buffer with addition of mannitol to 0.5M (hatched bars). Statistical differences were determined by ANOVA and a post-hoc Tukey test. Columns indicated with identical letters cannot be distinguished from each other ($p < 0.01$, $n=3$, with 40 stomata counted from a total of 4 plants, repeated on 3 consecutive days). stomatal apertures in epidermal peels in resting buffer or in the presence of 0.5M mannitol. Pore area decreases in the presence of mannitol in both lines. The *pme6-1* line is impaired in its ability to close in response to mannitol. $n=12$, statistical significance determined by ANOVA.

When exposed to mannitol the aspect ratio (length/width) of guard cells showed a small but highly significant reduction in *pme6-1* epidermal peels (Figure 4.14). This means that *pme6-1* guard cells are more circular than WT.

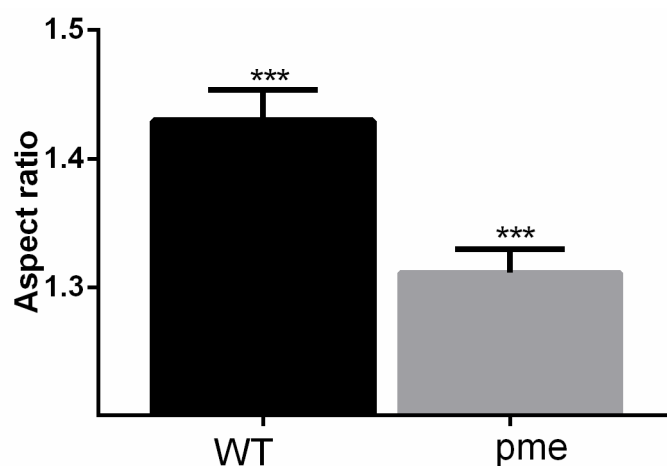


Figure 4.14. *pme6-1* guard cells treated with mannitol have a reduced aspect ratio to WT plants. Statistical differences determined by Student's T-test, $p < 0.005$, $n=15$. Error bars represent S.E.M

4.4.3 *pme6-1* stomata and whole plant drought responses

As previously discussed stomata play an important role in controlling the water relations of the plant and the data above show that *pme6-1* stomata are defective in their ability to open and close. In order to assess whether this change at the level of individual stomata had an impact at the whole plant level, thermal imaging was used. Plants were grown as described in 2.2.1 until 30 days. At this point (Day 0) plants were imaged before water was withheld for 5 days (Day 5) and then plants were imaged again at the end of the experiment. Figure 4.15.A-B shows representative thermal images from Day 0 and Day 5 and Figure 4.15.C shows this graphically. At day 0 the rosettes of all three lines (WT, *pme6-1*, complemented *pme6-1*) were approximately the same temperature, indicating similar levels of transpiration. Following 5 days of drought treatment *pme6-1* rosettes were the same temperature as at day 0 but WT and complemented plants had significantly increased in temperature. These results show that *pme6-1* plants are less able to regulate their transpiration in response to drought leading to a change at a whole plant level in terms of mean rosette temperature.

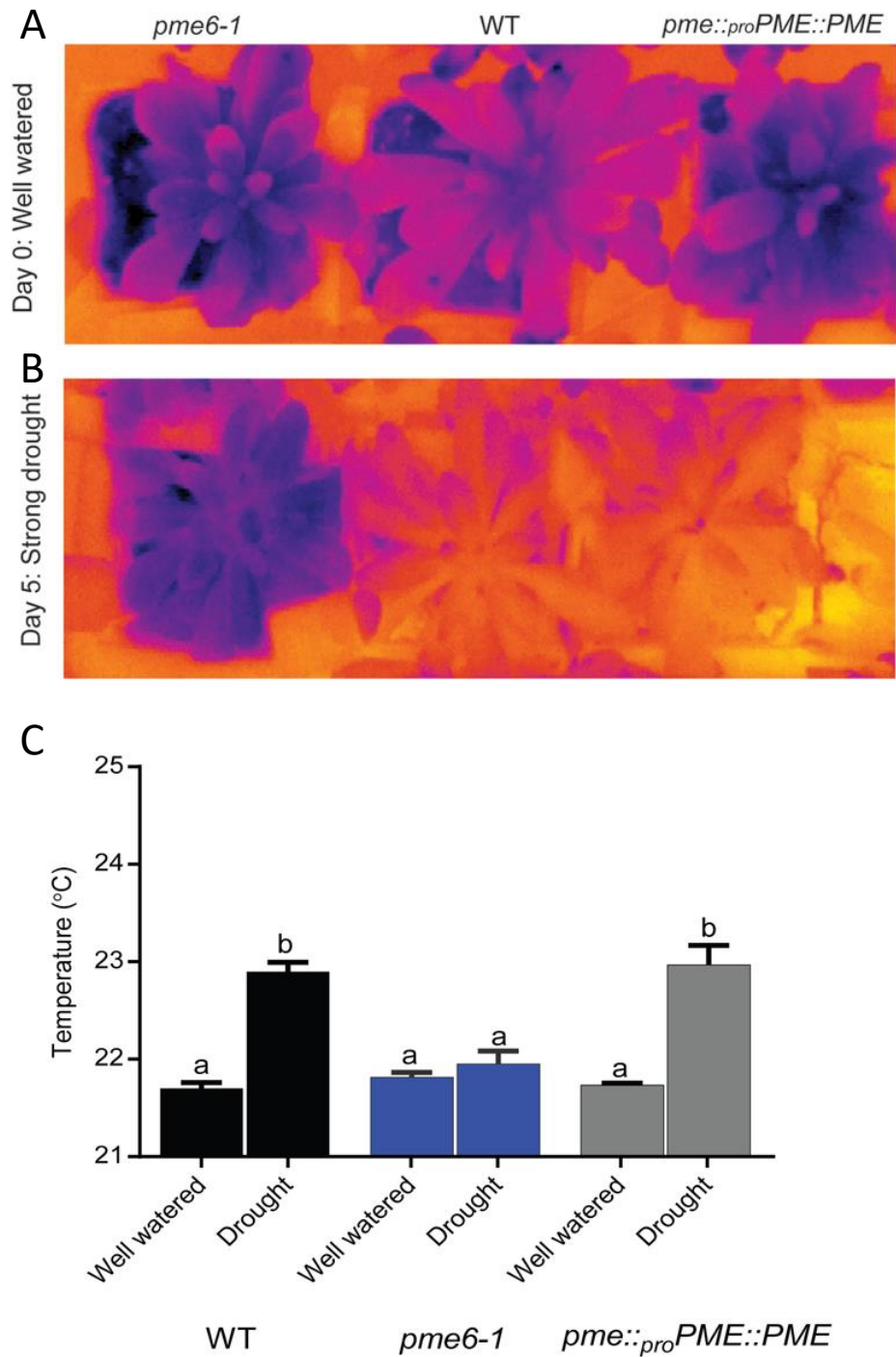


Figure 4.15. *pme6-1* plants are less able to adjust leaf temperature under drought conditions. (A) Thermal images are shown of well-watered plants of the genotypes indicated (top images) taken at day 0 post-drought. Images of equivalent plants at day 5 post-drought (lower panel) show that the *pme6-1* plants have a lower leaf temperature than WT or complemented *pme6-1* mutant. (B) Quantification of thermal image data shows that *pme6-1* leaf temperature does not change significantly under drought conditions while WT and the complemented mutant leaf temperature increases. Each bar represents the mean temperature for the rosette with error bars indicating s.e.m (n=6). Statistical differences were determined by ANOVA with a post-hoc Tukey test ($p < 0.05$). Columns indicated with identical letters cannot be distinguished from each other ($p > 0.05$).

4.5 *pme6-1* plants have altered pectin composition

The results in Chapter 3 clearly demonstrate that the pectin methylesterification status of the guard cell wall is distinct to that of other epidermal cells. To investigate whether the *pme6-1* guard cells showed any change in pectin composition I performed a series of immunohistochemical assays. Since the *pme6-1* mutation was present in the *Landsberg erecta* (*L.er*) background, I first confirmed that the patterns of pectin methylation observed in *Col-0* were also present in this genetic background.

As was shown for *Col-0* (3.2.2) *L.er* plants have a broad distribution of low level methylesterified HGA (recognised by LM19, Figure 4.16.A-B) which mirrors the distribution of JIM7 (Figure 4.16.I-J). Highly esterified pectin (indicated by LM20) was excluded from *L.er* guard cells (Figure 4.16.E-F), as was also seen in the *Col-0* background. In contrast, *pme6-1* plants show patchy LM19 labelling in the guard cells, indicating a reduction in the amount of unesterified pectin (Figure 4.16.C-D). However, there was an abundance of LM20 binding in the *pme6-1* guard cells (Figure 4.16.G.H). JIM7 labelling was unchanged between *L.er* and *pme6-1*, indicating that the overall distribution of HGA was not different between the lines (Figure 4.16.I-L). A quantitative analysis of the observed binding patterns was performed (Figure 4.16.Q-S). Guard cell binding observed with LM19, 20 and JIM7 antibodies was manually scored and their binding patterns scored as either 'Fully', 'Partial' or 'Junctions only'. 'Fully' indicates ubiquitous cell wall binding in the guard cells (exemplified in Figure 4.16.I), 'partial' indicates signal was present in the guard cell but not ubiquitous, (exemplified in Figure 4.16.D) and 'junctions only' indicates where binding was limited to the guard cell junctions or neighbouring cells only (exemplified in Figure

4.16.E). Scoring was carried out for 10 stomata each from 5 individual plants. Overall, the data in Figure 4.16 indicate that *PME6* is crucial for the demethylesterification of guard cell wall HGA.

proPME6::PME6 complemented plants showed recovery of a WT-like immunolabelling pattern, with guard cells having abundant unesterified pectin as indicated by LM19 (Figure 4.17.B) and highly esterified pectin, revealed by LM20, being restricted to the guard cell borders (Figure 4.17.C).

To investigate whether the binding patterns of PM19 and LM20 observed in *pme6-1* guard cells reflected a general shift in cell wall composition, numerous other antibodies for cell wall components were used to label *pme6-1* stomata. The individual data are summarised in Appendix 6, but no differences were observed in any non-pectin epitopes between *L.er* and *pme6-1*, suggesting that there had been no major changes to the cell wall outside of the pectin network.

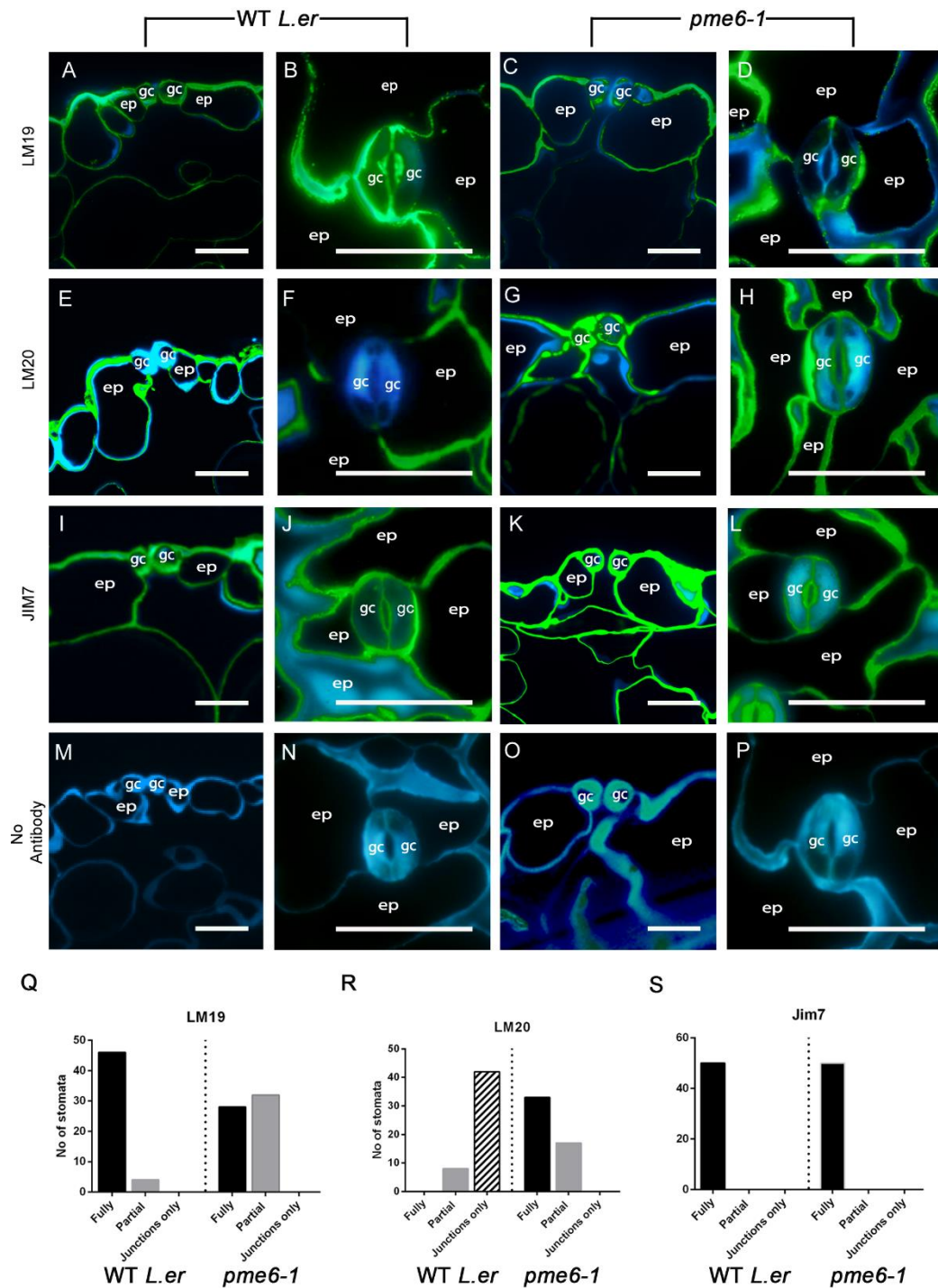


Figure 4.16 Guard cell wall pectin composition is altered in *pm6-1* plants. (A-D) The high level of unesterified HGA in WT guard cells indicated by LM19 antibody binding in both cross-sections (A) and paradermal sections (B) is greatly diminished in *pm6-1* (C, D). (E-H) Highly methylesterified HGA is absent in WT guard cell walls (E, F) but accumulates in the guard cell walls of the *pm6-1* mutant, as revealed by binding of the LM20 antibody (G, H). (I-J) The general distribution of HGA (indicated by the Jim7 antibody) is similar in WT (I, J) and the *pm6-1* mutant (K, L). (M-P) Control sections not hybridised with primary antibody but stained with Calcofluor White indicate the signal specificity of the immunolabelling experiments in A-L and the general distribution of the cell wall material. (Q-S) Counting of stomata showing the patterns of labelling with each antibody indicate the switch in LM20/LM19 labelling pattern between WT and the *pm6-1* mutant guard cells. Localisation of fluorescence in transverse sections after antibody binding was scored as either fully covering stomata (similar to guard cells in panel I), partially covering guard cells (as in panel C) or limited to cell junctions (as in panel E). Data are shown for (Q) LM19 (R) LM20 (S) Jim7 immunolabelling. Quantification was based on scoring patterns from 50 stomata, with 5 stomata scored from each of 10 plants. Scale bars = 20 μ m.

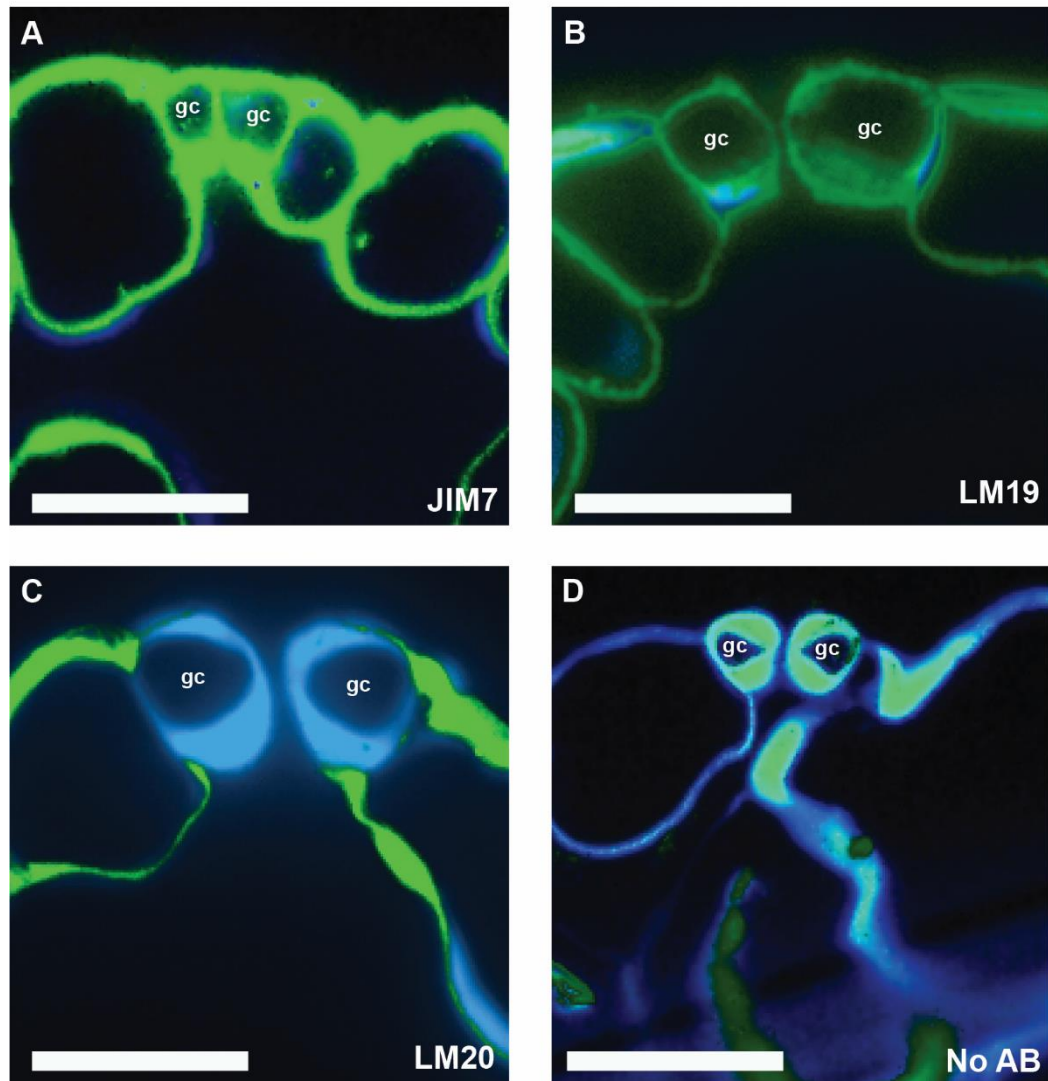


Figure 4.17. Pectin methylation pattern in guard cells is restored to WT in complemented *pme6-1* plants. (A) JIM7 antibody labelling of the epidermis of the *pme6-1* mutant complemented with the *proPME6::PME6* construct reveals that HGA is present in all cell walls. (B) Un-esterified HGA, revealed using the LM19 antibody, is present in all cell walls of the complemented mutant, including those of the guard cells (C) Methyl esterified HGA, revealed using the LM20 antibody, is excluded from the guard cell wall of the complemented line in a pattern similar to that observed in WT plants (compare Fig 2E). (D) Controls with no primary antibody reveal a low level of autofluorescence. Antibody binding is indicated by green signal whereas blue signal indicates Calcofluor staining of the cell wall. Observed patterns were consistent when replicated ($n=8$). Guard cells indicated by gc. Scale bars represent 20 μm .

4.6 *pme6-1* plants have altered gas exchange

Stomata are the gateway for the vast majority of gaseous flux between plants and the external environment. Altering this has consequences for photosynthesis and water use efficiency. To investigate whether the altered stomatal opening/closure observed in *pme6-1* leaves had an effect on these parameters a series of gas exchange experiments were carried out using a LI-6400 gas exchange analyser.

4.6.1 A/C_i and Light curves

Carbon assimilation is a function of stomatal aperture which allows CO_2 into the leaf and of internal leaf architecture which impacts on CO_2 diffusion into the cells. A/C_i curves and light curves were taken to assess changes in assimilation in response to light and carbon dioxide. As shown in Figure 4.18.A, at low CO_2 conditions the curves were very similar for all both lines analysed (WT *L.er*, *pme6-1*). This suggests that rubisco activity is similar for all three lines and that the different lines are not distinguished by fundamental differences in underlying photosynthetic biochemistry. The value of A_{max} is significantly higher in *pme6-1* than *L.er*. These data show that at ambient and sub-ambient CO_2 levels instantaneous C assimilation is comparable between *pme6-1* and *L.er* which suggests that biochemical aspects of carbon fixation, as limited by rubisco availability, remain the same. At CO_2 concentrations above ambient *pme6-1* has a substantially higher C assimilation rate CO_2 . No differences in assimilation in response to light was observed (Figure 4.18.B)

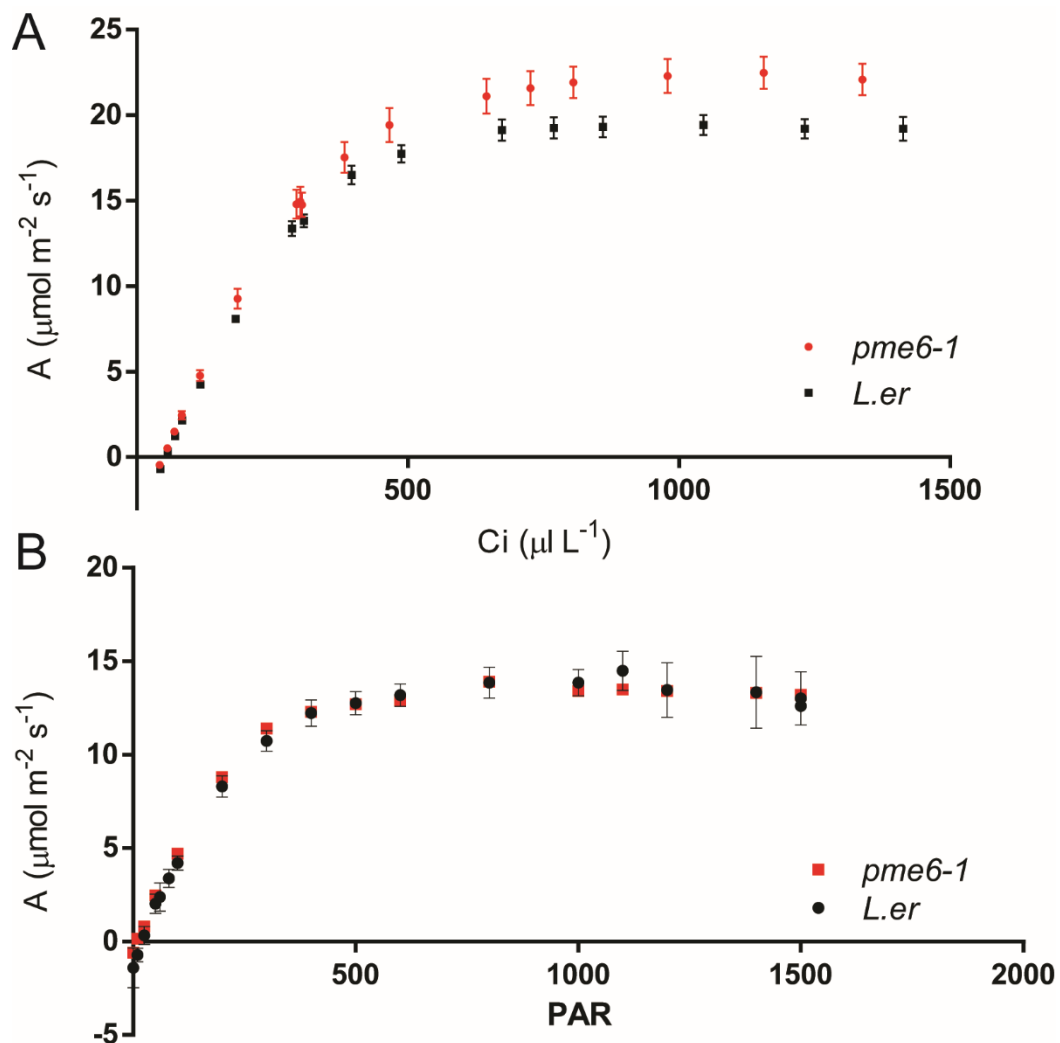


Figure 4.18 *pme6-1* plants have altered assimilation rates. A) At elevated CO₂ levels the *pme6-1* leaves have a greater potential to assimilate CO₂ than WT leaves. A/Ci curve analysis of WT and *pme6-1* leaves indicates that instantaneous C assimilation rate at ambient CO₂ levels is comparable but that as C_i increases the *pme6-1* leaves show a greater maximum potential assimilation rate (n=5 for WT; n=6 for *pme6-1*; error bars =s.e.m). B) The maximal assimilation of *pme6-1* in response to light is equivalent to WT assimilation. Error bars represent SEM, n=8.

4.6.2 *pme6-1* responses to shifts in CO₂ concentration

The A/Ci curves described above were performed rapidly to minimise perturbations to the activation status of rubisco and the rubisco binding coefficient. This means that the leaves are not given enough time in between measurement points for the stomata to adjust their aperture fully to the new CO₂ or light regime. To assess stomatal response to the different CO₂ parameters stomatal conductance (G_s) was measured. Plants were left to

acclimatise at 500ppm CO₂ for 30 minutes and then shifted to 1000ppm to induce stomatal closure for 40 minutes and then shifted to 100ppm CO₂ to induce stomatal opening and left until measured Gs plateaued (minimum 35 minutes). Measurements were made on plants which had been grown in ambient CO₂ conditions and also at elevated CO₂ conditions (1000ppm) to investigate the influence of CO₂ level on stomatal performance.

At 500ppm *pme6-1* leaves had a higher stomatal conductance than WT *L.er* leaves in plants grown, both at ambient and high CO₂ levels (Figure 4.19). Following a shift to 1000ppm both lines of plants decreased their Gs by a similar amount, meaning that WT *L.er* plants had a lower stomatal conductance than *pme6-1*. After shifting to 100ppm CO₂ both WT and *pme6-1* leaves showed an increase in Gs and this increase occurred at a similar rate. However, *pme6-1* leaves attained a lower maximum value of Gs than WT *L.er* leaves Figure 4.19. These patterns were the same for ambient and high CO₂ grown plants. These data show that *pme6-1* plants have a reduced range of Gs than WT, i.e. *pme6-1* leaves display a higher minimum and a lower maximum Gs.

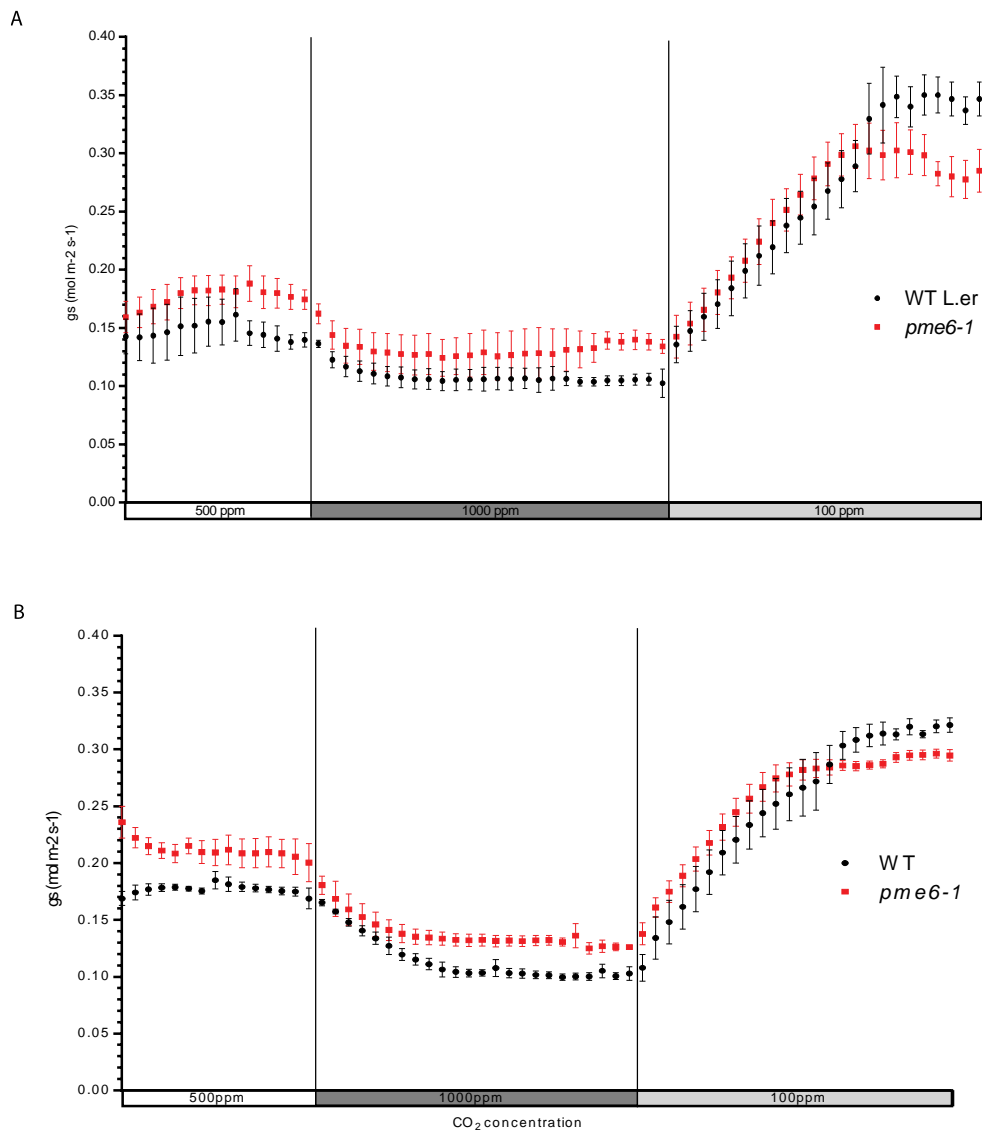


Figure 4.19. Response of *pme6-1* and *L.er* plants to shifts in CO_2 concentration. A) *pme6-1* leaves show a limited dynamic range in stomatal conductance (G_s) in response to changing CO_2 level. Gas exchange data for WT and *pme6-1* leaves show that under ambient CO_2 conditions the *pme6-1* leaves have higher G_s than WT. Following exposure to elevated (1000 ppm) CO_2 G_s in both mutant and WT fall. Exposure to a low (100 ppm) CO_2 regime induces increased G_s , but the *pme6-1* G_s trace plateaus to a lower value than for WT leaves. Error bars= s.e.m, (n=8). B) The more limited dynamic range in G_s exhibited by *pme6-1* leaves is maintained after growth of plants at elevated CO_2 . Gas exchange data for WT and *pme6-1* leaves taken from plants grown continually under elevated CO_2 . The traces for WT and *pme6-1* as CO_2 level is altered during gas exchange analysis are comparable to those shown in (A), with the *pme6-1* trace again reaching a lower plateau after exposure to sub-ambient CO_2 level (n=8).

4.6.3 *pme6* stomatal response to blue light

Bioassay data showed *pme6-1* plants displayed a small stomatal opening and closure response to light (data not shown) whereas responses to CO_2 and ABA were non-significant, in contrast to the data for WT stomata. To further

investigate the response of stomata to light, G_s was examined in response to blue light, which is known to induce stomatal opening (Assmann and Shimazaki, 1999), using gas exchange measurements. The largest leaf of 34-36 day old plants was placed in the LI-COR head (2cm² area) and plants were acclimatised at 400ppm CO₂, 60% humidity and 21°C temperature in the presence of 300µmols of light with 0% blue light. *pme6-1* plants had substantially lower G_s under these conditions (Figure 4.20. Left hand portion of graph). After acclimatisation the light conditions were changed such that the total photosynthetic active radiation (PAR) remained at 300µmols but now consisted of 30% blue light. This induced an increase in stomatal conductance in all the lines (WT, *pme6-1*, *proPME6::PME6-1*) and the increases were of a similar rate and magnitude. The *pme6-1* plants started with a lower G_s and did not reach as high a value as *L.er* or complemented plants (Figure 4.20. Centre portion of graph). After 30 minutes the blue light enriched conditions were reverted to 100% red light to induce stomatal closure. All the lines showed a decreased G_s and *pme6-1* had lower final G_s than *L.er* and complemented *pme6-1* plants (Figure 4.20. Right portion of graph).

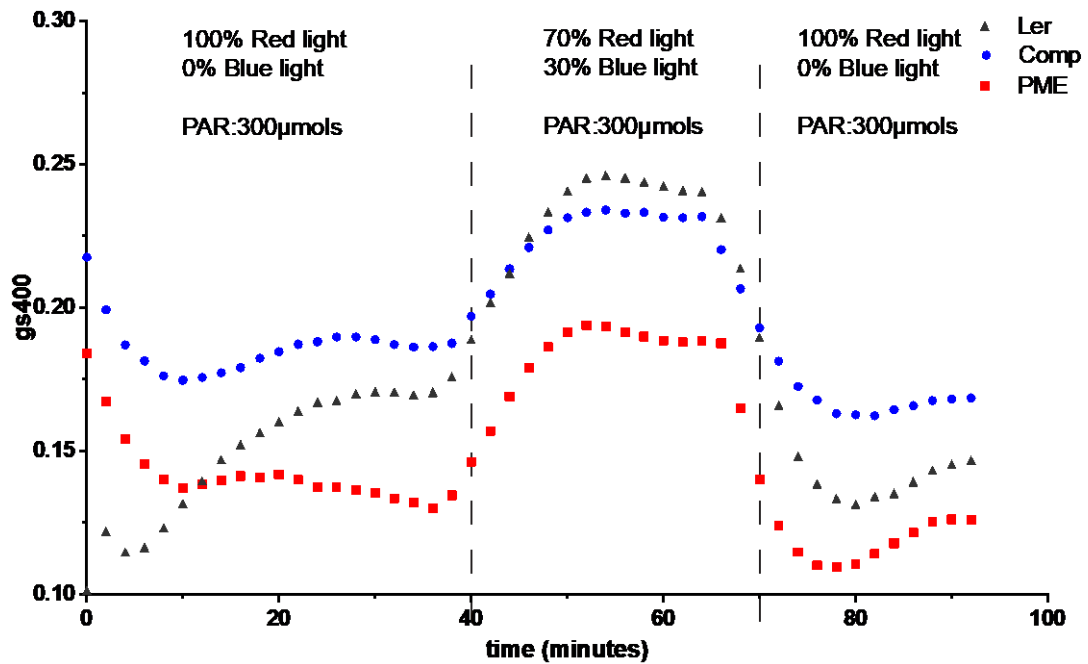


Figure 4.20. Stomatal opening with blue light. *L.er*, *pme6-1* and complemented plants are acclimatised in 300µmol PAR in the absence of blue light for 40 minutes before being exposed to 30% blue light for 30 minutes before switching back to the original conditions. *Pme6-1* plants had a substantially lower conductance at all conditions. Data are means from n=8 and error bars=S.E.M.

4.7 TEM microscopy of *pme6-1* stomata

The above data suggest that changes to the structure of the guard cell wall pectin composition have large impacts on stomatal function and whole plant physiology. To ensure that stomatal cell wall structure was not altered at a more fundamental level light and electron microscopy were used to analyse guard cell ultrastructure (Figure 4.21). Transmission electron microscopy revealed a diversity of cell wall thicknesses within the genotypes, likely based on the exact location of the section within the pore. It appears that overall stomatal cell wall structure is not observably different between Col-0 plants (Figure 4.21.A-B) and *pme6-1* plants (Figure 4.21.C-D) at the TEM level.

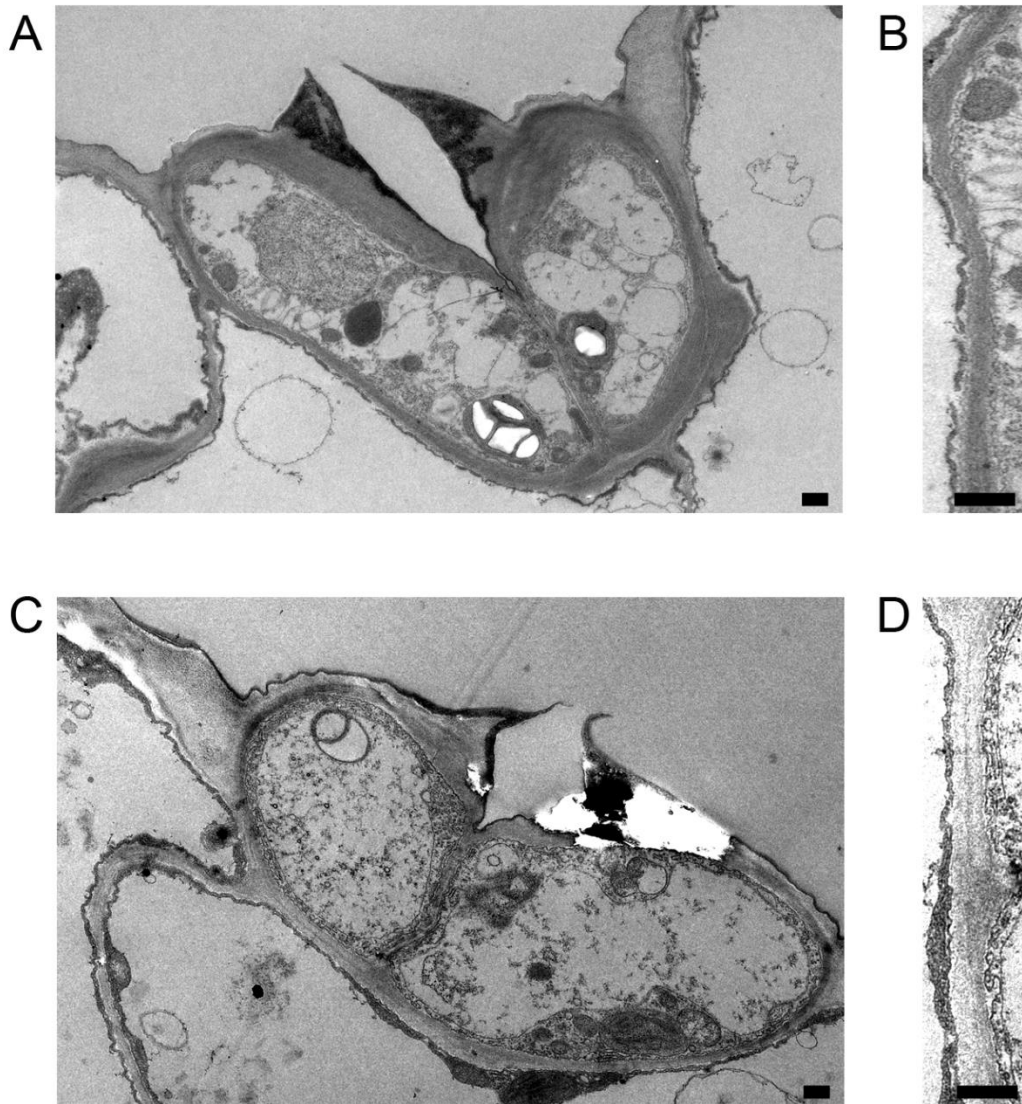


Figure 4.21. Overall guard cell wall structure does not appear markedly different in *pme6-1*. (A-B) TEM micrograph images showing cell wall guard cell structure in WT *A. thaliana* plants (C, D) TEM micrograph images showing cell wall guard cell structure in *pme6-1* plants. No Major architectural differences were observed. Scale bars=2 μ m.

4.8 Discussion

In this chapter *PME6* is shown to be important for the control of guard cell wall pectin status. *pme6-1* stomata have an abundance of highly esterified pectin which is not seen in WT stomata. It is postulated that the majority of *PMEs* act on pectin which is already incorporated into the guard cell wall

(Micheli, 2001). Our observations on PME6 transcriptomic and GUS data suggest that *PME6* is only expressed in mature guard cells, supporting this hypothesis.

It was unexpected to observe such a strong phenotype from a single knockout as the *PME* gene family is a large one and genetic redundancy was anticipated. Transcriptomic data (which is discussed in more detail in Chapter 5) showed that 11 *PME* genes are expressed highly in the guard cell (Appendix 7) and it is reasonable to expect some degree of genetic redundancy. In *pme6-1* plant there is still some LM19 binding which suggests that some degree of de-methylesterification is still occurring which suggests a slight redundancy. It has been shown that different PMEs are differentially active at different temperatures and pH (Denès et al., 2000; W. G. T. Willats et al., 2001) and the possibility that some PMEs may only be active under certain conditions may explain why there is less redundancy than expected.

4.8.1 *pme6-1* plants have impaired stomatal function

Changes to the guard cell wall have previously been shown to impact stomatal function. Enzymatic removal of pectic arabinan inhibits guard cell function by causing stomata to become 'locked in position' (L. Jones et al., 2003). It is thought that the presence of arabinan side chains in the pectin network prevents pectin chains from forming close associations and therefore they retain flexibility. Removal of pectin restored function in 'locked' stomata. Our data shows that alteration of pectin methyl-esterification status in the guard cell wall has a strong impact on stomatal function with stomata similarly being 'locked' in an intermediate position. It is not clear if the changes to the esterification status of pectin in the *pme6-1* line is having a similar effect on arabinan. Highly methyl-esterified pectin reduces the possibility of pectin interacting with other cell wall components, such as arabinan. Arabinan is more commonly thought of as a feature of RG-I but it may also be incorporated into HGA networks. It was suggested that

small RG-I regions with arabinan side chains function to separate HGA to maintain flexibility in the cell wall (L. Jones et al., 2003). It would be interesting to repeat the arabinase and pectinase treatments previously described (L. Jones et al., 2003) on *pme6-1* plants to see if this restored stomatal function.

There are a number of other possibilities as to how the change in the pectin composition observed in *pme6-1* guard cells could impact on stomatal function which must be considered. Increasing the prevalence of methylesterified galacturonic acid residues can influence how pectin interacts with other HGA components of the cell wall. It is possible that a reduction in cell wall hydration has occurred as there are fewer free galacturonic acid residues which can incorporate H₂O into the pectin network. This could increase the rigidity of the guard cell as the formation of hydrated gels may function to separate cellulose microfibrils by pushing them apart to maintain cell wall flexibility (Wolf et al., 2012). It is also possible that the way in which pectin interacts with other cell wall components, such as hemicelluloses is changed. This may be directly due to the presence of methyl esters preventing interactions with other cell wall polymers or it may be due to changes in apoplastic pH in *pme6-1* as the protons usually released during demethylesterification are no longer present.

The above discussion assume that guard cell function is impaired in *pme6-1* plants due to an increase in cell wall rigidity so that the guard cells are no longer flexible enough to undergo the required shape change for stomatal opening/closure. It is however widely accepted that higher levels of pectin methylesterification is correlated with a reduction in cell wall rigidity (Pelloux et al., 2007) and it is worth considering an alternate hypothesis. Higher levels of methylesterification can prevent calcium crosslinking, thus conceivably decreasing the strength of the pectin matrix. It has been shown that PME1 activity can lead to altered root growth and enhanced bursting of

pollen tubes (Paynel et al., 2014), both of which are consistent with an increase in methylesterification leading to a reduction in cell wall strength. A reduction in cell wall strength in the guard cells could increase the mechanical advantage that neighbouring epidermal cells have over the guard cells (P. J. P. Franks and Farquhar, 2007). In this scenario the guard cells would not be strong enough to withstand the required turgor needed to deform the neighbouring epidermal cells during stomatal opening and could explain the locked, partially open phenotype. As discussed in Chapter 3 there were very low levels of calcium cross-linked pectin within the guard cells, so a reduction in rigidity in *pme6-1* plants seems unlikely, nevertheless this possibility must be considered.

Our results indicate that *pme6-1* plants are mechanically unable to move stomata in response to a range of stimuli. A number of genes have been identified which, when disrupted, cause loss of sensitivity to some stimuli but not others (Assmann et al., 2000; Mustilli et al., 2002) and CO₂, ABA and light are all involved in complex signalling networks to control stomatal aperture (Assmann and Shimazaki, 1999; Kim et al., 2010). In contrast, the closure of stomata by mannitol is a purely physical event as a result of the osmoticum removing turgor pressure from the cells (L. Jones et al., 2003). It is thus independent of the signal transduction processes acting during stomatal closure by other stimuli. The fact that *pme6-1* stomata remained significantly more open after mannitol treatment than WT fits the hypothesis that the observed alterations in stomatal movement are not due to perturbations of guard cell signalling networks but rather due to a more fundamental change in underlying cell wall mechanics. It would be interesting to directly measure stomatal turgor change in *pme6-1* plant in response to opening and closing stimuli using a technique such as a pressure probe. It is possible that turgor pressure is still being altered in a normal manner in *pme6-1* but the changes in turgor pressure are no longer sufficient to cause stomatal movement. This

would confirm that the signalling networks in the guard cell were functional, but unfortunately this was beyond the scope of this project.

The changes to guard cell pectin discussed above represent only one aspect of the entire cell wall and it is important to determine that greater changes to overall cell wall architecture are not occurring which might also contribute to the phenotype observed. TEM images allowed us to confirm that cell wall structure and thickness were broadly similar between the different lines analysed with no major structural defects noted. There was some variation between samples in the TEM work which probably reflected technical challenges in getting equivalent sections from different locations within a stomate. These data allow us to conclude that guard cell walls of *pme6-1* plants are normal in terms of their overall architecture and it seems that only pectin status has been altered.

4.8.2 *pme6-1* plants have altered physiology

pme6-1 plants grew at the same rate as WT plants under conditions of ambient CO₂ but did not reach the same size as WT. The decrease in size was small, but significant. The stomatal aperture in *pme6* was the same as WT at ambient CO₂ conditions in the bioassay, but this bioassay provides a snapshot of aperture and does not take into account diurnal cycles of stomatal opening and closing (Tallman, 2004). Gas exchange data showed that the range of stomatal conductance is reduced in *pme6*, meaning that they are unable to maximise their carbon uptake in the same dynamic way as WT plants. Thus it is possible that for much of the day WT plants have wider stomatal apertures than *pme6-1* plants can achieve. As the *pme6-1* plants did not alter their stomatal density to compensate for this reduction in maximal aperture it is likely that the *pme6* plants will have been slightly carbon limited. Being slightly carbon limited can lead to an increase in

photorespiration further reducing the efficiency of carbon capture and photosynthesis (Buapet et al., 2013). This would explain why there was no difference in size between the lines when grown at high CO₂ as this carbon limitation would be ameliorated. In addition, Figure 4.18 showed that maximal rate of carbon assimilation is higher in *pme6-1* plants than in WT plants suggesting that the plant size difference observed at low CO₂ is due to limitations on CO₂ entering the leaf rather than post entry barriers. It is important to note that the bioassays showed no stomatal aperture response to CO₂ whereas gas exchange data showed only a reduction in range. This probably reflects the fact that stomatal conductance is not merely affected by aperture but is a function of whole leaf architecture and biochemistry and we would expect these components of the leaf to still respond to CO₂ in *pme6-1*. The fact that *pme6-1* plants start at a higher conductance than WT under ambient conditions, despite the fact that their apertures should be the same, coupled with a higher maximum assimilation value, suggests that there may have been some compensation to the plants being CO₂ limited. Lundgren et al (unpublished) found that *pme6* mesophyll channels were less circular, which would be predicted to give a greater surface area for CO₂ to diffuse over and may be an indirect response to being carbon limited.

It has previously been reported that a *pme6* mutant in the *NOS* ecotype background has a seed defect (Levesque-tremblay et al., 2015), with seeds being malformed, smaller and lighter than WT seeds. To confirm that the growth defects we observed in the *pme6-1* plants were not due to changes in seed quality we checked seed size and weight. There were no significant differences in the size or weight of seeds suggesting that the effects on growth were not due to a seed quality issue. No visual defects in the structure of the seed coat such as those previously reported (Levesque-tremblay et al., 2015) were observed and germination rate was the same for all three lines used in these experiments (WT, *pme6-1*, complemented *pme6*).

The information from Chapter 3 and this chapter give us a picture of 'normal' guard cell HGA distribution which is represented schematically in Figure 4.22.A while the distribution of HGA in *pme6-1* mutants is shown in

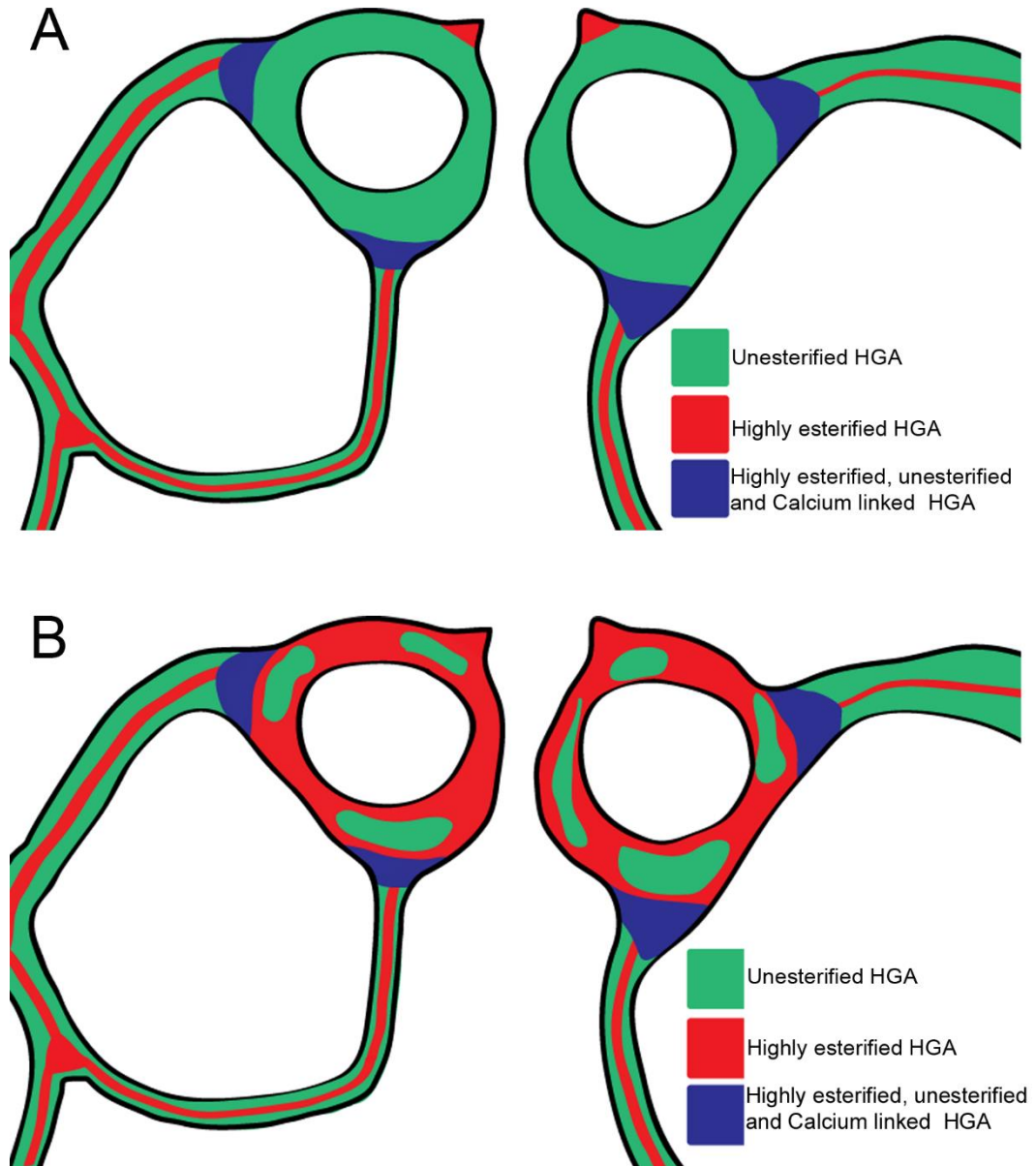


Figure 4.22. Schematic diagram of guard cell HGA distribution in WT and *pme6-1* plants. (A) In WT plants guard cells have abundant unesterified HGA in the guard cells and epidermal cell walls. Highly esterified HGA is present in the epidermal cell walls but to a lesser extent than unesterified HGA. The junctions between guard cells and epidermal cells are particularly rich in HGA having both highly esterified and unesterified HGA as well, additionally they have calcium cross-linked pectin. Only highly esterified HGA is present in the guard cell cuticular ledges (B) *pme6-1* stomata have substantially altered HGA composition. Unesterified HGA is present in much smaller amounts showing patchy distribution. Highly esterified HGA is abundant within the stomata and the cuticular ledge. The epidermal cells and the junctions between the guard cells and epidermal cells are unchanged in their HGA composition.

Figure 4.22.B. Further work is needed to determine the significance of the calcium cross-linked pectin at the cell-cell junctions, it is possible that extra strength is needed to anchor the cells together to prevent rupture of the epidermis during stomatal movement. The exclusion of highly esterified HGA from the guard cells is seemingly crucial to allow the stomata to move, likely by maintaining cell wall flexibility to accommodate guard cell swelling and shape change.

4.8.3 Conclusions

The study of guard cell walls is challenging, as separating them from other plant tissues is technically difficult. The abundance of genetic resources available for use with *A. thaliana* allows for identification and manipulation of guard cell wall genes. We have identified a guard cell wall expressed gene from the PME gene family which appears to function to de-methyl-esterify pectin in the guard cell wall. This gene is essential for correct guard cell function and disruption of it leads to an inability to modulate stomatal aperture. Further study is needed to determine unambiguously what mechanical impact this change in pectin is having but it is clear that the mechanical properties of guard cell walls are crucial to their correct function.

Manipulation of pectin targeted just to the guard cells could provide a novel avenue for the manipulation of guard cell function for crop breeding. The finding that *pme6-1* plants are reduced in size at ambient CO₂ but are not at elevated CO₂ highlights the fact that what is optimum for guard cell walls now may not be optimal in a future environment where CO₂ levels are significantly higher than today.

Chapter 5. Further analysis of the cell wall: selection of new genes

5.1 Introduction

One of the key advantages to using *A. thaliana* as a study organism is the wealth of genetic resources available. The genome has been fully sequenced and the Nottingham Arabidopsis Stock Centre (NASC) is one of several organisations possessing large collections of commercially available transgenic lines. The majority of these lines are random T-DNA insertions which are designed to knockout the genes that the T-DNA integrates into. *A. thaliana* can easily be transformed by a simple floral dip procedure (Clough and Bent, 1998) which, coupled with its short generation time, makes the acquisition of homozygous transgenic plants relatively simple.

Numerous transcriptomic resources are available to aid in the selection of genes. Microarray data is prevalent in online depositories (<http://www.ebi.ac.uk/arrayexpress>), and applications such as the EFP browser (Winter et al., 2007) or Genevestigator (Zimmermann et al., 2005) collate this information to make it easier to search.

A number of PME genes are known to be expressed highly in stomata. As discussed earlier (Chapter 4) there are numerous PME genes in *A. thaliana*. It is possible that different PME genes are responsible for distinct patterns of demethylesterification (Wolf et al., 2009) or act differently under different conditions (Denès et al., 2000) but it is also very likely that there is a degree of redundancy between these genes. This makes studying PMEs challenging

as even with a complete knockout, such as in *pme6-1*, discussed in Chapter 4, some PME activity may remain.

5.1.1 The PME/PMEI family

As touched upon in Chapter 4 there are 67 known PME family genes and 71 PMEI genes in *Arabidopsis*, which are split into 3 broad groups: PME; proPME and PMEI based on the presence of a number of domains.

Additionally, there are 2 PME-like genes which are unclassified but share significant sequence similarity with the PME/PMEI family of genes.

The PME class of proteins have between 1 and 3 PME domains which are characterised by a conserved active site containing two aspartic acid, one glutamine and one arginine residues (Pelloux et al., 2007). There are at least 24 PME's in *A. thaliana* with an average gene length of 1900bp (M. Wang et al., 2013) and 2 putative PMEs based on sequence homology. PME proteins have N-terminus secretion signals, and the proteins are secreted to the apoplastic space where they act on the formed cell wall. PMEs purified from cell wall extracts are often lacking the secretion signal suggesting that this is cleaved, possibly at the plasma membrane. PMEs have been shown to be involved in diverse functions such as fruit ripening (Brummell and Harpster, 2001), root elongation (Wen et al., 1999), mechanical support (Hongo et al., 2012) and pathogen resistance (Lionetti et al., 2012) and are able to act randomly and linearly on the HGA substrate (Denès et al., 2000; Markovič and Kohn, 1984). It has also been shown that PME activity is sensitive to changes in pH (Denès et al., 2000).

The PMEI genes tend to be significantly shorter than PMEs. They are α -helical proteins characterised by a conserved PMEI domain which is notable for the presence of a plant domain containing four conserved cysteine residues forming disulphide bonds (Juge, 2006). It is thought that PMEI

proteins act to inhibit PME activity by forming a complex with plant PME genes and covering the PME binding cleft (Hothorn et al., 2004). Their action is also highly pH dependant.

The proPMEs contain at least one PME domain and it is thought that they demethylesterify pectin in the same manner as the PMEs do. They also contain an additional N terminal pro domain which shares significant sequence homology with the PMEI domain. This raises the interesting possibility of an auto-inhibitory role, which would most likely be pH dependent. It has been shown that PME and HGA are transported together in the same secretory vesicles (Bosch et al 2005). It is possible that the pro domain may inhibit the PME activity in this situation to prevent demethylesterification of the HGA prior to incorporation in the cell wall. The removal of methyl groups by PMEs leads to the release of protons into the apoplast, which in turn could have an impact on the pH, allowing the pro domain to function in inhibiting PME activity. Some studies have suggested that the pro domain is cleaved from the mature protein and that only the PME domain reaches the cell wall. Furthermore, it has been shown that the pro domain of PMEs can regulate the release of PMEs from the Golgi (Wolf et al., 2009).

The fact that PMEI proteins inhibit PMEs provides an alternative way to investigate PME function other than via conventional gene knock-out approaches (which suffer from the potential problem of gene redundancy). Overexpression of PMEI genes in guard cells could inhibit the action of multiple PME genes creating a much broader knockdown of PME activity. In this chapter we utilise the genetic resources associated with *A. thaliana* to screen and phenotype a range of insertion mutants in cell wall associated genes and create a number of transgenic overexpression lines under the control of the tissue specific promoters pATML1, pCA1, pGC1-D1 (guard cell specific) to assess the effect of manipulating the guard cell wall.

5.2 Results

5.2.1 Selection of T-DNA insertion lines

To identify potential cell wall genes of interest we utilised widely available microarray data. Hunt and Gray (NASC_ARRAYS_29) conducted a microarray analysis of gene expression in epidermal fragments enriched for guard cells compared to whole leaves. Using available resources on TAIR and genbank (ncbi.nlm.nih.gov/genbank) the microarray was annotated to show all known PME/PMEI genes and as many pectin-related genes as possible. The ratio of expression values in the guard cell enriched fragments compared to the whole leaf was calculated and the data filtered to only include samples with a ratio of greater than 1.5. This list was then cross-referenced with another microarray (Pillitteri et al., 2011). This microarray used epidermal tissue from a series of stomatal development mutants to compare differences in gene expression between stomata-enriched tissue, meristemoid-enriched tissue or pavement cell-enriched tissue. Genes being shown as upregulated in stomata in both microarrays were then filtered to include only cell wall related genes.

This initial list was large (49 genes) and in order to streamline the selection a combination of Genevestigator (Zimmermann et al., 2005) and the EFP browser (Winter et al., 2007) was used to identify genes that were strongly regulated in guard cells but appeared to be expressed at a low level in the epidermis and the mesophyll (Pandey et al., 2010). Figure 5.1 shows the expression ratio and the absolute EFP browser values for this list of genes.

46 cell wall genes were identified as being strongly upregulated in guard cells and 39 of these were pectin related, with 21 of these being in the PME/PMEI family. A selection of T-DNA insertion knockout mutants in these lines were ordered from NASC (Scholl et al., 2000) for analysis (Table

5.1). An additional line with an insertion in At2g16630 was donated by Lee Hunt for further investigation. This line is hereafter known as *focl*.

FOCL is annotated as an extensin-family protein (TAIR) and is predicted to be secreted (Hunt et al, Unpublished). The amino acid sequence of *FOCL* lacks the conserved serine polyproline (SP4 or SP5) repeats characteristic of classical extensins (Kieliszewski and Lamport, 1994). The *FOCL* protein has a proline rich region which is characteristic of cell wall proteins (Kieliszewski and Lamport, 1994) and may be best classed as a hydroxyproline rich glycoprotein (HRGP) rather than a classical extensin. *FOCL* shows expression in the guard cells which is almost double that of the whole leaf (NASC arrays-29).

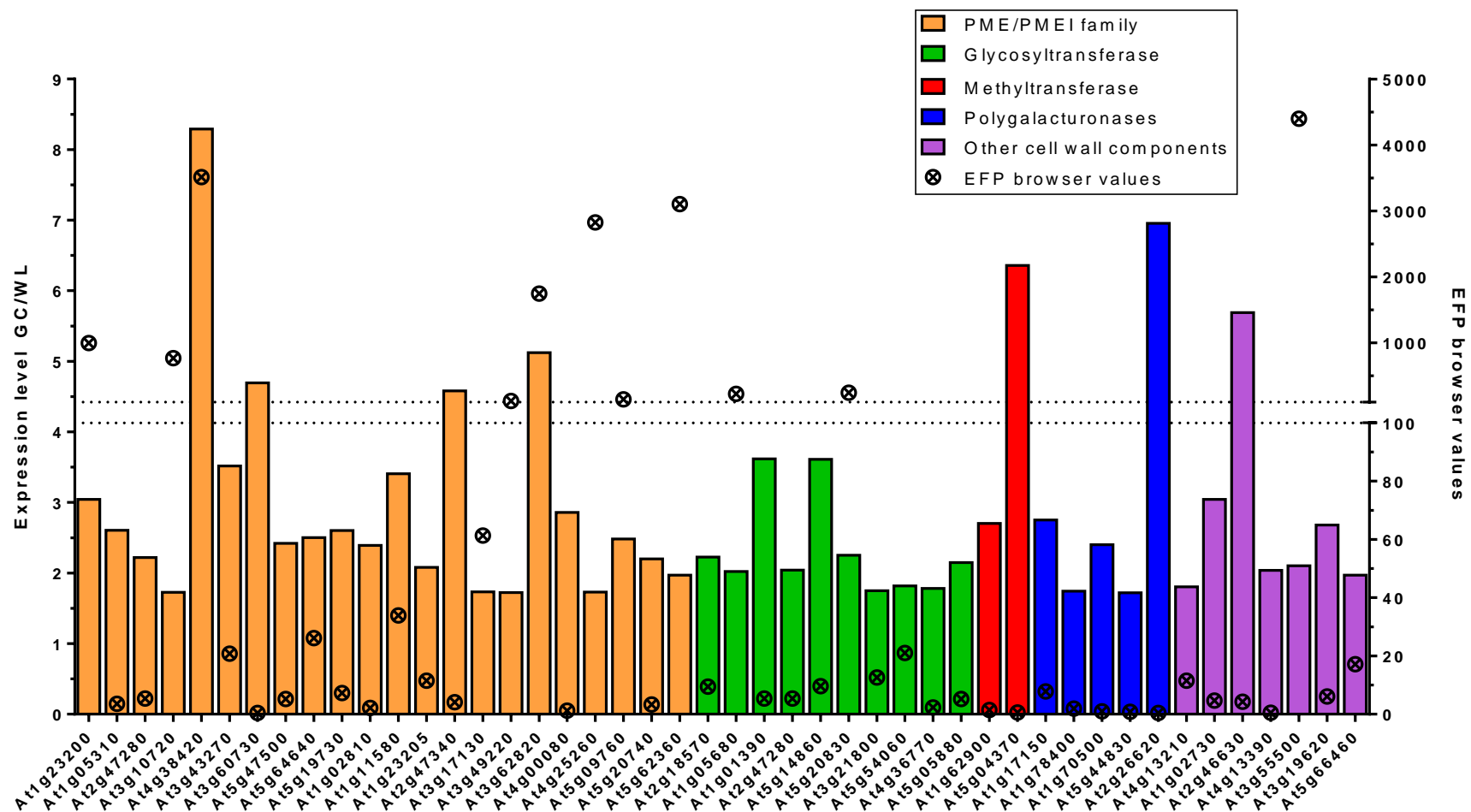


Figure 5.1. Cell wall genes with upregulated expression in guard cells compared to whole leaves. Bars show the expression level in the guard cells divided by the expression level in the whole leaf (left axis). Crosses show the expression level in the guard cells from the EFP browser (right axis).

Table 5.1. *A. thaliana* genes identified as being upregulated in guard cells. T-DNA insertion mutants in these lines were obtained from NASC.

Gene	Putative function	NASC ID
AT3G24670	Pectate lyase	SALK_109494
AT4G25260	Plant invertase/Pectin methylesterase (PME)	SALK_033203
AT3G62820	Plant invertase/Pectin methylesterase inhibitor (PMEI)	SALK_027168
AT5G19730	Pectin methylesterase (PME)	SALK_136556
AT2G26440	Plant invertase/Pectin methylesterase (PME)	SALK_117817
AT4G25260	Pectin methylesterase inhibitor (PMEI)	SALK_036325
AT2G47340	Pectin methylesterase (PME)	SALK_079711
AT3G62820	Pectin methylesterase (PME)	SALK_027168
AT1G11580	Pectin methylesterase (PME)	SALK_076974
AT1G01390	Putative Glycosyltransferase	SALK_083984
AT3G60730	Pectin methylesterase (PME)	SALK_074653
AT3G43270	Pectin methylesterase (PME)	SALK_013629
AT4G38420	Pectin methylesterase (PME)	SALK_011162
AT5G19730	Pectin methylesterase (PME)	SALK_117724

5.3 Analysis of insertion mutants

5.3.1 Confirming homozygous insertion lines

All mutant lines were genotyped to ensure that they were homozygous for the T-DNA insert. Three primers per line were designed to determine if plants were homozygous negative, homozygous positive or heterozygous for the T-DNA insert.

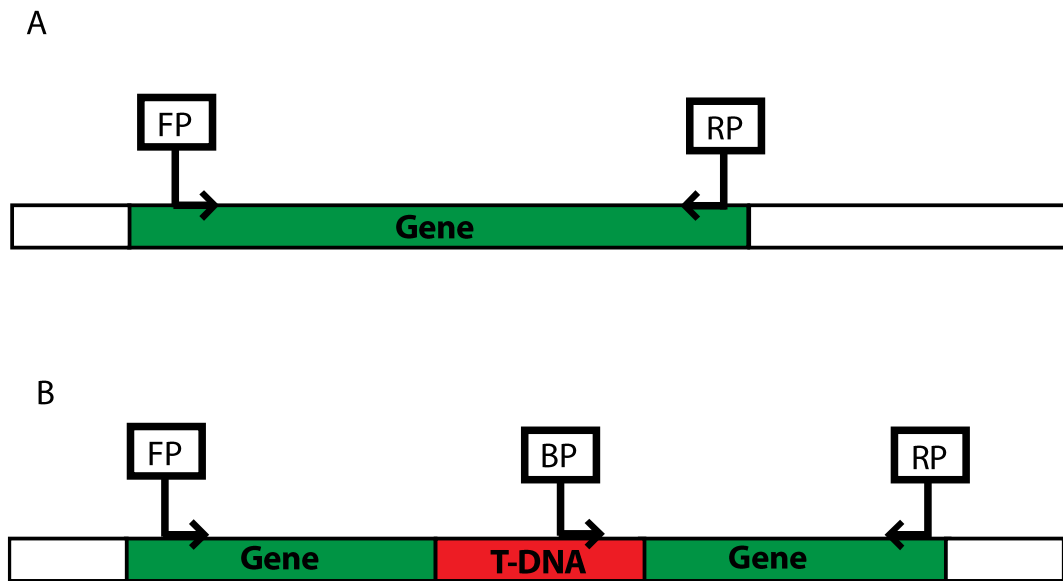


Figure 5.2 Primer design for genotyping on T-DNA insert lines. A) Primer binding if no T-DNA insert is present. B) Primer binding when a large T-DNA insert is inserted into the gene. FP: Forward primer, RP: Reverse primer, BP: T-DNA border primer.

PCR was carried out on extracted genomic DNA from individual plants and set up as paired reactions, one with FP and RP and the other with BP and RP. Homozygous negative plants would only have a band in the FP and RP lane and there is no T-DNA for the BP to bind to. Homozygous positive plants would only have a band in the BP and RP lane as the length of the T-DNA is sufficient that TAQ polymerase has insufficient time to work from FP to RP. Heterozygous plants would have a band in each lane.

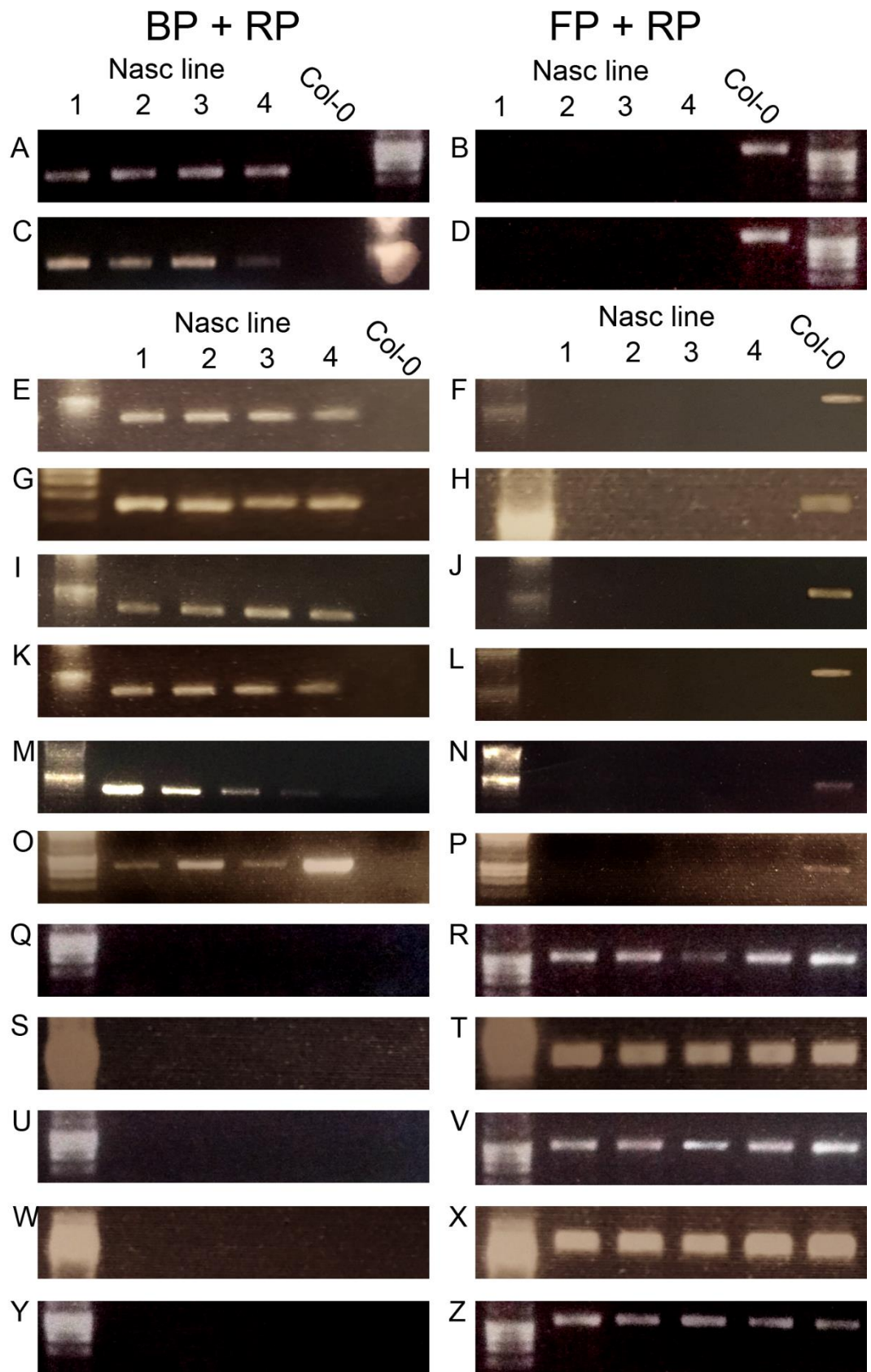


Figure 5.3. Gel images showing genotyping of NASC lines. The left column shows genomic DNA amplified with the forward primer (FP) and reverse primer (RP) for the gene with the expected T-DNA insertion. The right column shows genomic DNA amplified with the insertion border primer (BP) and the RP for the gene expected to have the insertion. In panels A-D the first 4 lanes indicate separate plants from the respective NASC line. Lane 5 is DNA from Col-0 and lane 6 indicates the 1kb DNA ladder (Bioline, UK). In all other panels lane 1 is the DNA ladder, lanes 2-5 indicates the NASC line and lane 6 is Col-0. (A-P) Identification of homozygous insertion lines. BP and RP primers give bands for all samples of the NASC line indicating the insertion is present. No band is observed for Col-0 with these primers FP and RP give no bands for the NASC samples indicating that the lines are homozygous for the insertion. A band is observed in the Col-0 lane. (A-B) Salk 117817 is homozygous for an insertion into At2G26440 (C-D) Salk 079711 is homozygous for an insertion into At2G47340 (E-F) Salk 109494 is homozygous for an insertion into At3G24670 (G-H) Salk 013629 is homozygous for an insertion into At3G43270 (I-J) Salk 027168 is homozygous for an insertion into At3G62820 (K-L) Salk 036325 is homozygous for an insertion into At4G25260 (M-N) Salk 136556 is homozygous for an insertion into At5G19730. (O-P) Salk 117724 is also homozygous for an insertion into At5G19730. (Q-Z) Identification of homozygous lines without lacking the insertion. BP and RP primers give no bands for any of the NASC lines or the Col-0 samples. FP and RP give bands for the NASC samples indicating that the lines are homozygous for the absence of an insertion. A band is observed in the Col-0 lane. (Q-R) Salk 033203 has no insertion into At4G25260. (S-T) Salk 076974 has no insertion into At1G11580. (U-V) Salk 083984 has no insertion into At1G01390. (W-X) Salk 074653 has no insertion into At3G60730. (Y-Z) Salk 011162 has no insertion into At4G38420.

These results show that several of the lines were not homozygous for the insertion. The lines which were homozygous for the insertion (SALK 117817, SALK 079711, SALK 109494, SALK 013629, SALK 027168, SALK 036325, SALK 136556) were taken forward for further experimentation and are hereafter referred to by their accession number. SALK 117724 and SALK 136556 are both homozygous for an insertion in At5G19730, but due to time constraints only SALK 136556 was carried forward for this study. The lines which did not contain the insertion were not re-ordered due to time constraints.

5.3.2 Screening for stomatal density and size

The remaining lines were screened for stomatal density and size in order to ensure there was no alterations to stomatal development. Stomatal index was also measured to ensure that no alterations to overall epidermal patterning had happened either. Figure 5.4 shows stomatal complex length, which is used as a proxy for stomatal size. Stomatal size is unchanged in all of the knockout lines. Stomatal density (as shown by Figure 5.5) was also unchanged in all of the lines tested.

In order to determine if epidermal patterning was altered stomatal index was used to determine the percentage of stomata to total cells. Figure 5.6 shows that stomatal index is unchanged in all of the lines tested. These results demonstrate that stomatal development and patterning is unaltered in these knockout lines.

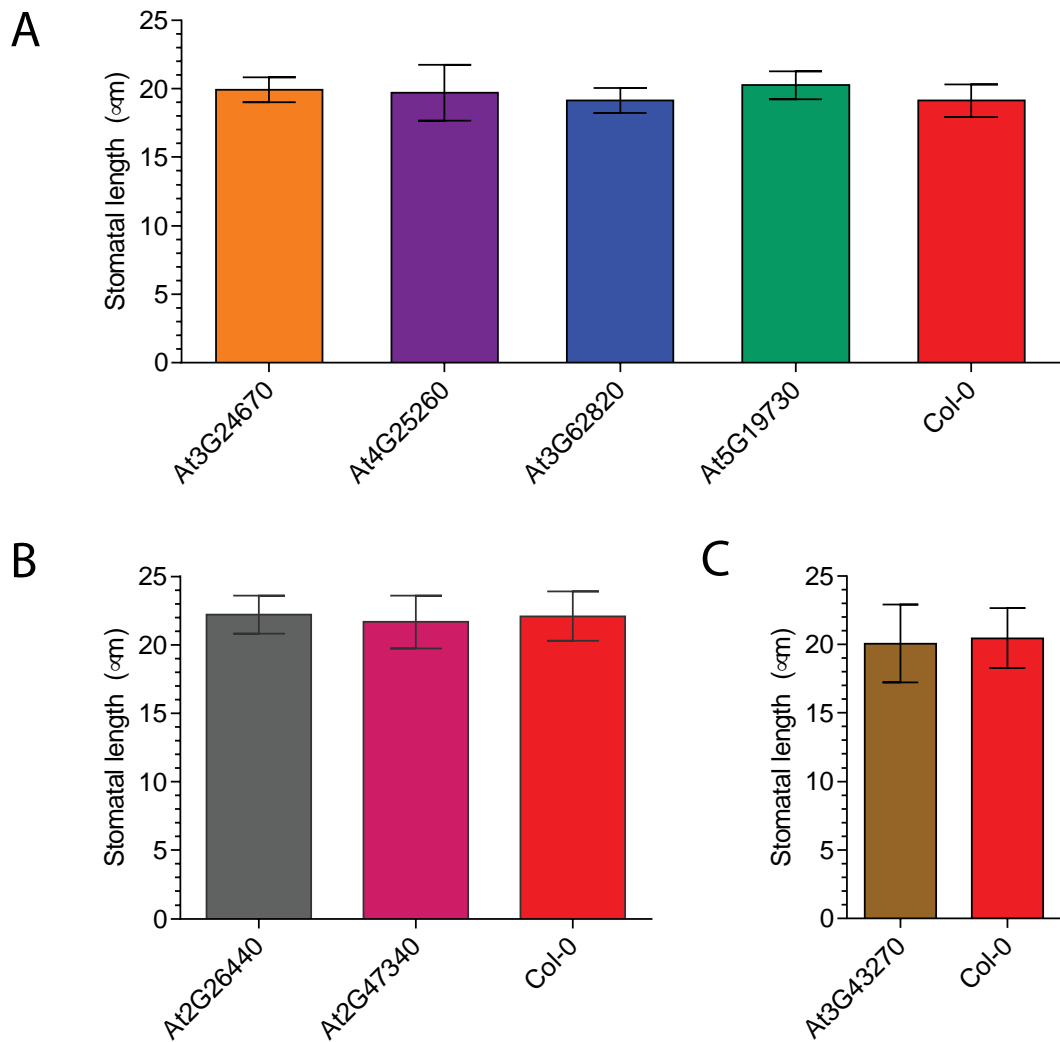


Figure 5.4. Stomatal size is unchanged in the NASC insertion lines. Stomatal complex length was used as a proxy for stomatal size. (A) Insertion mutants in At3G24670 (SALK_109494), At4G25260 (SALK_033203), At3G62820 (SALK_027168) and At5G19730 (SALK_136556) could not be statistically distinguished from Col-0. (B) Insertion mutants in At2G26440 (SALK_117817) and At2G47340 (SALK_079711) could not be statistically distinguished from Col-0. (C) The insertion mutant At3G43270 (SALK_013629) could not be statistically distinguished from Col-0. Lack of statistical significance was determined by multiple comparison ANOVA at $P > 0.05$ with each column compared to Col-0. $n=10$, error bars=SEM.

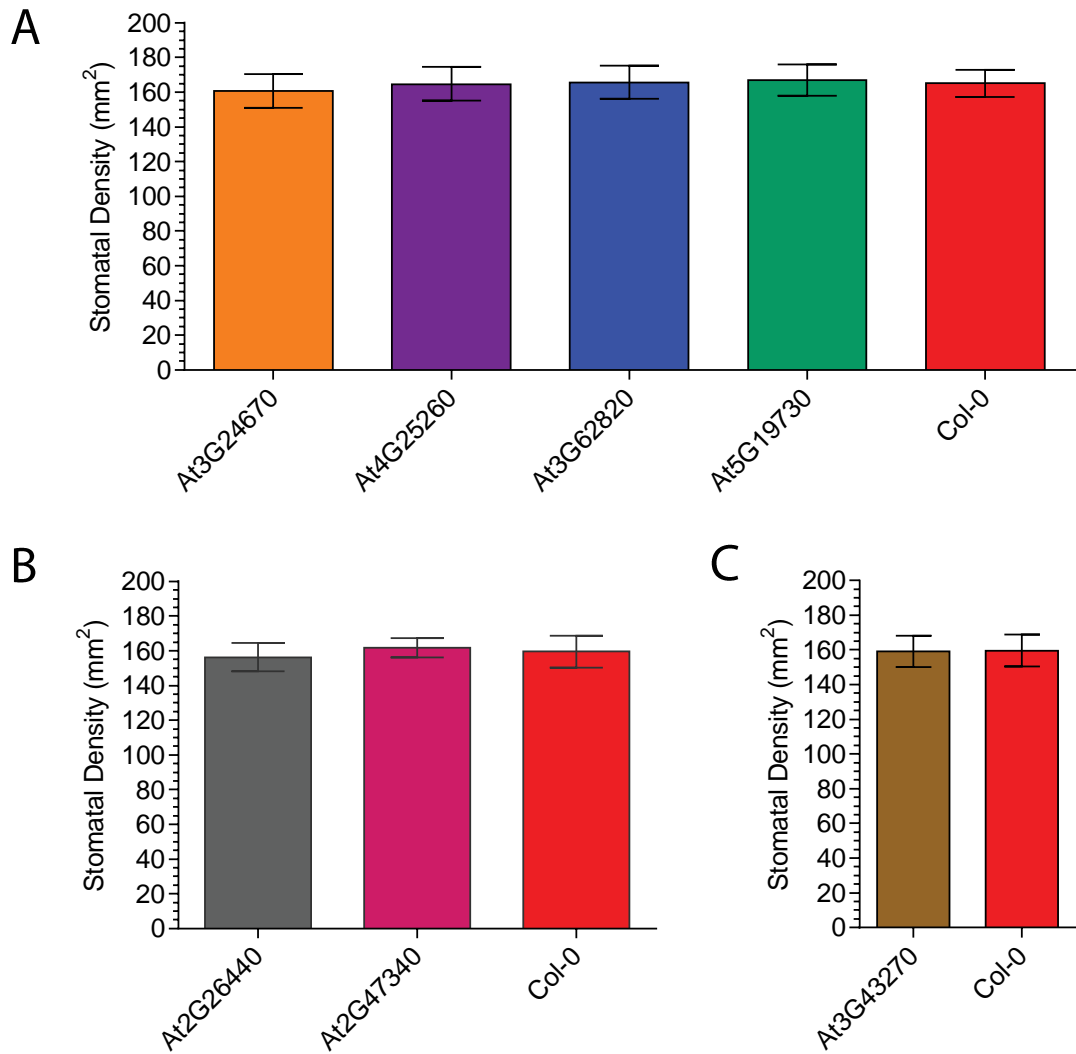


Figure 5.5. Stomatal density is unchanged in the NASC insertion lines. (A) Insertion mutants in At3G24670 (SALK_109494), At4G25260 (SALK_033203), At3G62820 (SALK_027168) and At5G19730 (SALK_136556) could not be statistically distinguished from Col-0. (B) Insertion mutants in At2G26440 (SALK_117817) and At2G47340 (SALK_079711) could not be statistically distinguished from Col-0. (C) The insertion mutant At3G43270 (SALK_013629) could not be statistically distinguished from Col-0. Lack of statistical significance was determined by multiple comparison ANOVA at $P > 0.05$ with each column compared to Col-0. $n=10$, error bars=SEM.

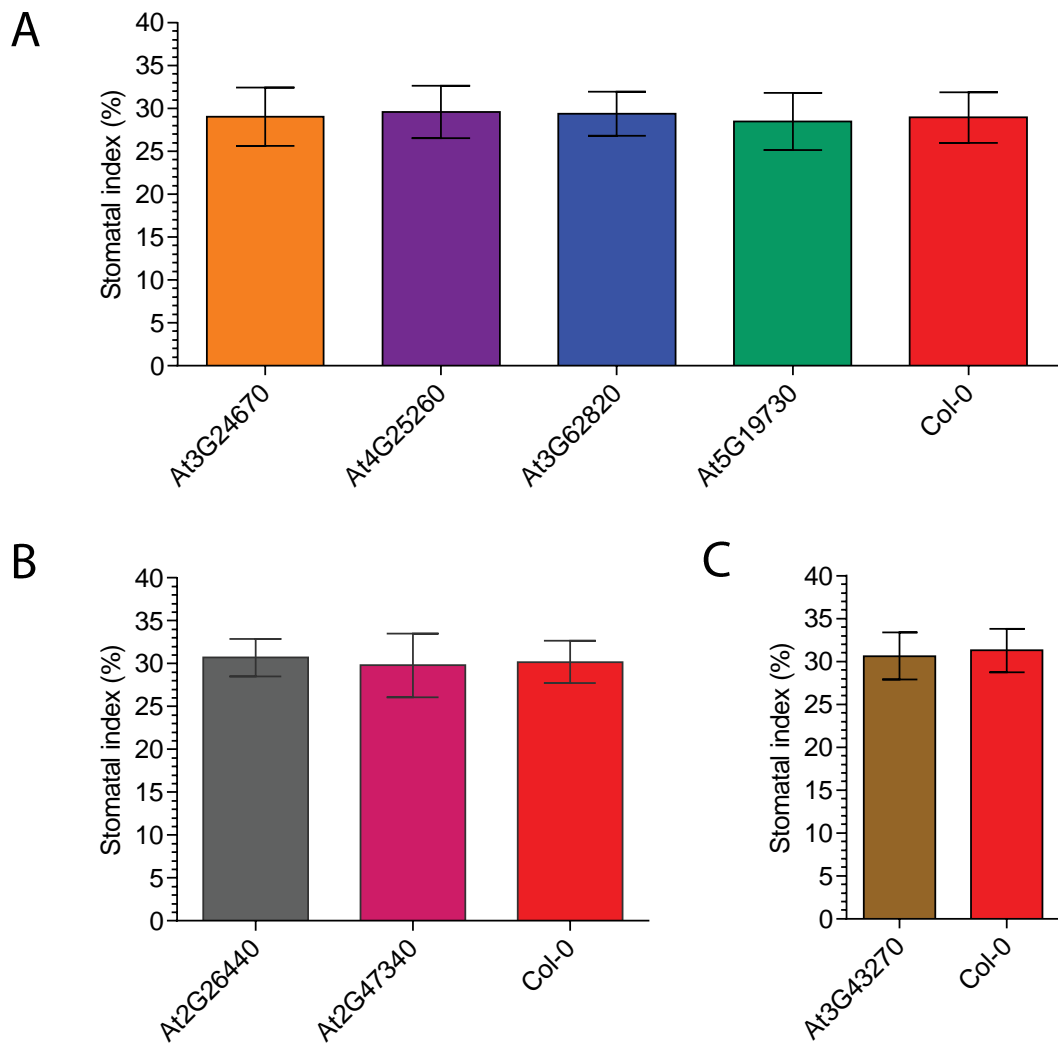


Figure 5.6. Stomatal patterning is unchanged in the NASC insertion lines. Stomatal index (the percentage of stomatal to whole cells) was unchanged in all the NASC lines. (A) Insertion mutants in At3G24670 (SALK_109494), At4G25260 (SALK_033203), At3G62820 (SALK_027168) and At5G19730 (SALK_136556) could not be statistically distinguished from Col-0. (B) Insertion mutants in At2G26440 (SALK_117817) and At2G47340 (SALK_079711) could not be statistically distinguished from Col-0. (C) The insertion mutant At3G43270 (SALK_013629) could not be statistically distinguished from Col-0. Lack of statistical significance was determined by multiple comparison ANOVA at $P > 0.05$ with each column compared to Col-0. $n=10$ error bars= SEM.

Preliminary testing suggested that *focl* plants had altered stomatal size (data not shown) and so *focl* was investigated separately in greater detail. Stomatal length was significantly increased in *focl* plants indicating that *focl* stomata were larger than Col-0 (Figure 5.7.A). Stomatal density was unchanged between *focl* and Col-0 plants (Figure 5.7.B) but pavement cell density was

significantly lower in *focl* plants than in Col-0 (Figure 5.7.C) meaning that stomatal index was significantly higher in *focl* plants (Figure 5.7.D).

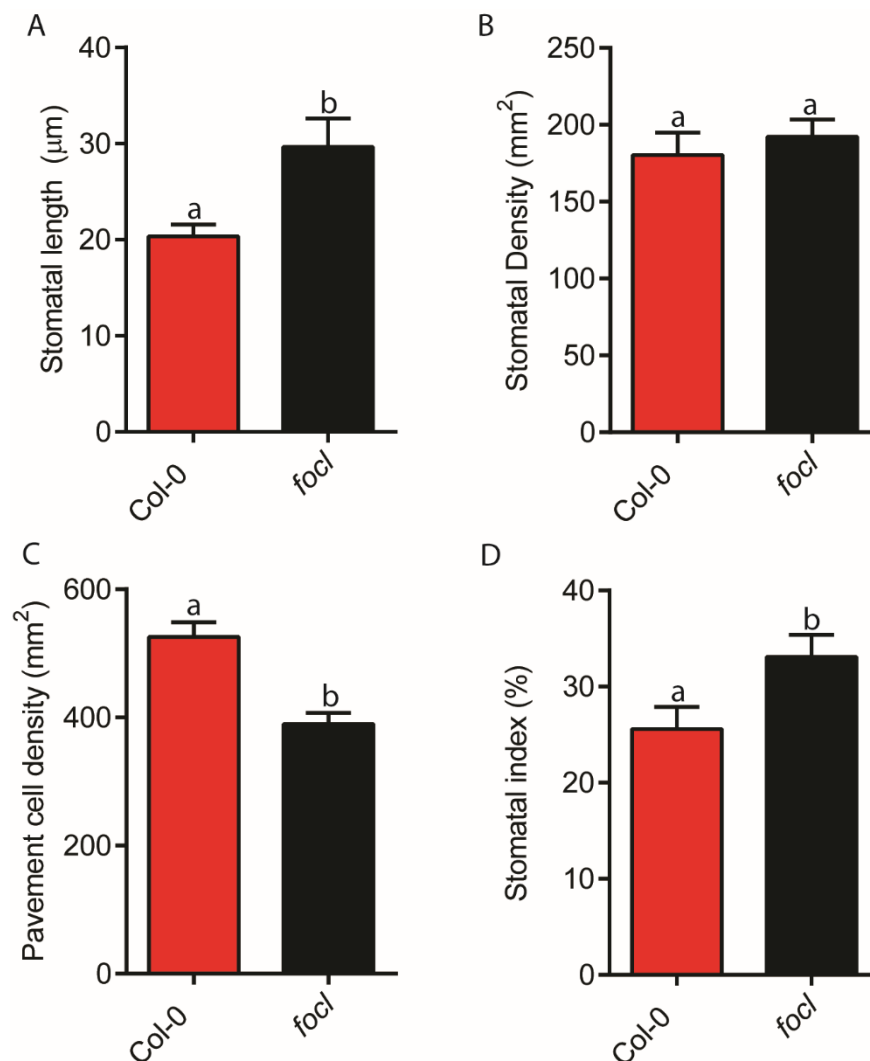


Figure 5.7. *focl* plants have altered stomatal patterning. (A) Stomatal size, as indicated by length of stomatal complex, is significantly larger in *focl* plants ($p < 0.0001$). (B) *focl* plants have the same stomatal density as Col-0 plants ($p = 0.0566$). (C) Pavement cell density is significantly lower in *focl* plants ($p < 0.0001$). (D) Stomatal index is significantly higher in *focl* plants ($p < 0.0001$). Data are means from $n = 10$, error bars are SEM. Statistical significance is determined by student's t-test.

5.3.3 Growth analysis

In Chapter 4 it was shown that a NASC cell wall insertion mutant (*pme6-1*) had altered growth at ambient CO₂. Growth of NASC insertion lines was screened throughout development using rosette area as an indicator.

The majority of the NASC lines grew at a similar rate to *Col-0* (WT) (Figure 5.8) with growth rates being indistinguishable from *Col-0* in most cases (A-F). The line with an insertion in *At5G19730* appeared to be slower getting established than *Col-0* and showed significantly reduced growth from 5 days to 35 days (with the exception of the 10-day time-point). From 40 days onwards no significant difference in growth was observed (Figure 5.8.G). This data shows that although *At5G19730* is slower than *Col-0* at getting established it ultimately reaches the same size as *Col-0*.

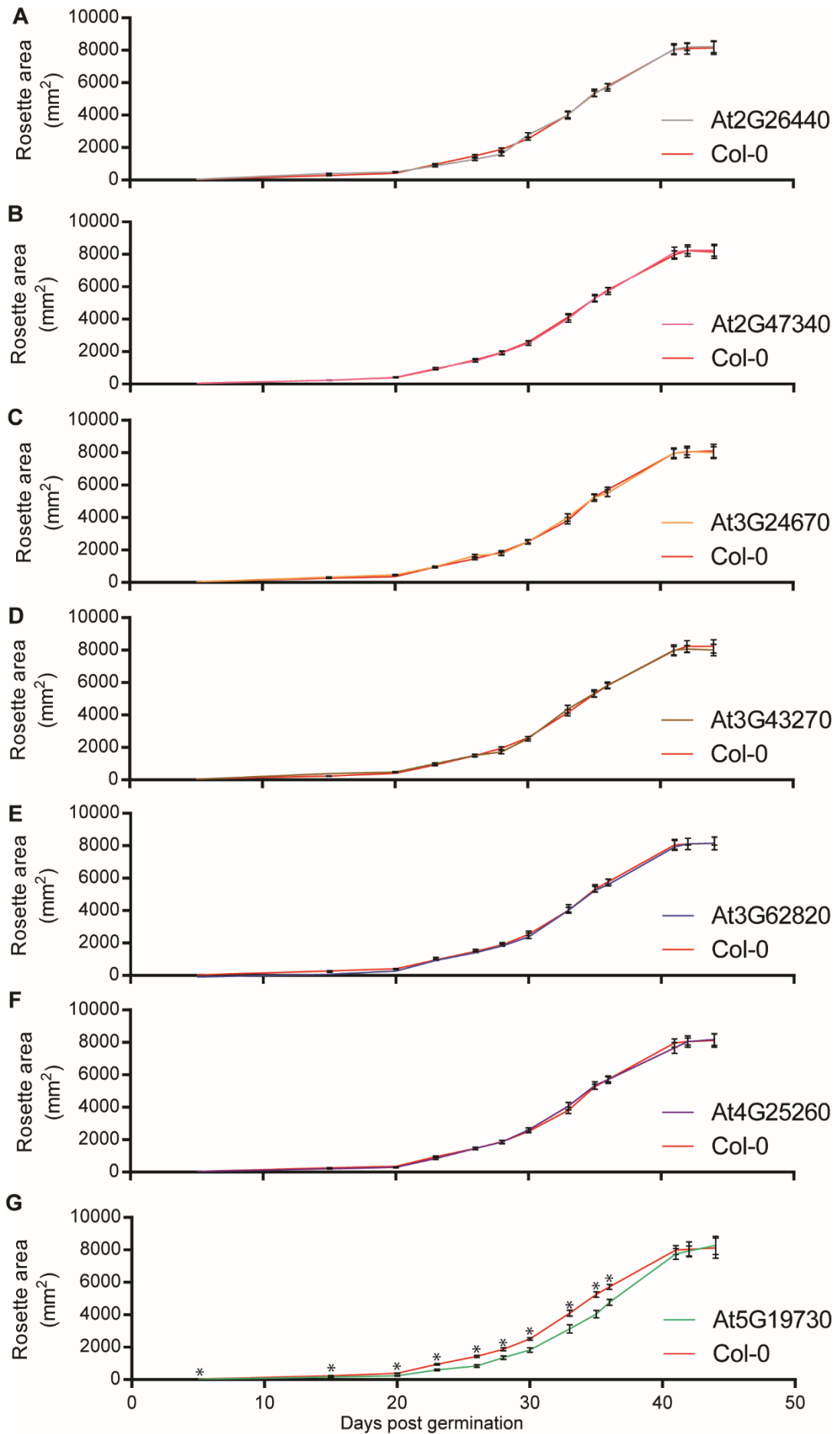


Figure 5.8. Growth rate of NASC lines compared to Col-0. Rosette area was measured throughout development to determine the growth rate of plants. (A) At2G26440 (SALK_117817) has the same growth rate as Col-0 (B) At2G47340 (SALK_079711) has the same growth rate as Col-0. (C) At3G24670 (SALK_109494) has the same growth rate as Col-0. (D) At3G43270 (SALK_013629) has the same growth rate as Col-0. (E) At3G62820 (SALK_027168) has the same growth rate as Col-0. (F) At4G25260 (SALK_033203) has the same growth rate as Col-0. (G) At5G19730 (SALK_136556) germinates at the same time as Col-0 and appears to be slower getting established. Growth is significantly different at day 5 and days 15-37. By day 40 growth has caught up with Col-0 and there is no longer a significant difference between the lines. Data are mean values from n=12, error bars are SEM. Statistical significance (indicated by *) is determined by multiple comparison t-test using the Holm-Sidak method to correct for multiple comparisons.

focl grew at a slower rate than WT, being much smaller throughout development (Figure 5.9) and transition to flowering appeared delayed in *focl* plants (data not shown). Although this experiment was extended to 55 days, *focl* plant growth had not plateaued but had reached almost the same size at WT plants, which suggests that growth rate has been slowed in *focl* rather than halted early and it is possible that if a longer experiment were conducted that *focl* growth would catch up with Col-0.

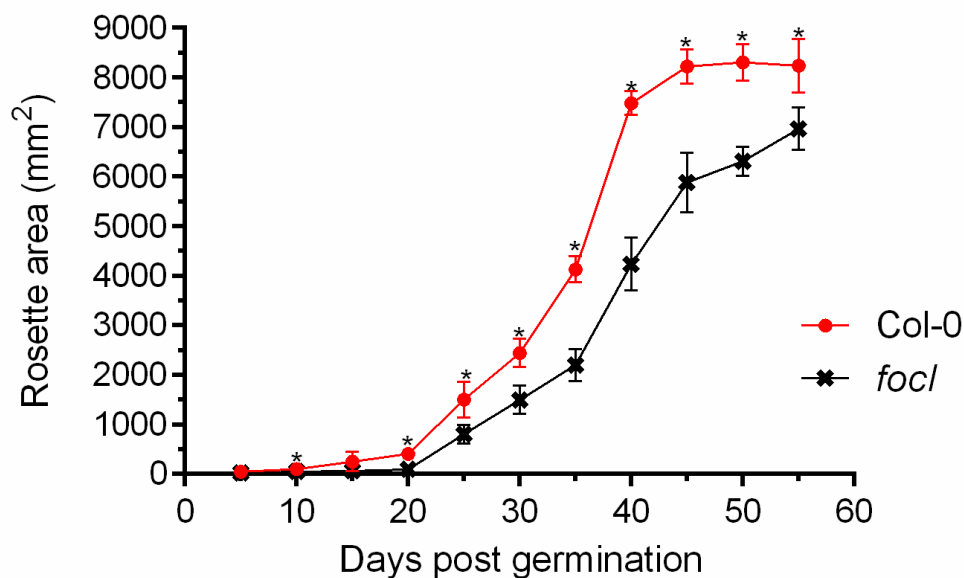


Figure 5.9. Growth rate of *focl* is slower than Col-0. Rosette areas of *focl* plants are significantly smaller than those for Col-0 at all stages of development apart from days 5 and 15. Data are mean values from n=10, error bars are SEM. Statistical significance (indicated by *) is determined by multiple comparison t-test using the Holm-Sidak method to correct for multiple comparisons.

5.3.4 Thermal imaging

To assess the water relations of the plant under normal conditions thermal imaging was conducted as a proxy for looking at whole plant transpiration. Emissivity was set at 0.96, as per the literature (H. G. Jones et al., 2003). Figure 5.10.A shows average rosette temperature for the NASC insertion mutants. Rosette temperature was indistinguishable from Col-0. Figure

5.10.B shows a representative thermal image of a 35-day old Col-0 plant. Figure 5.10.C-I shows representative images for the NASC insertion lines which are indistinguishable from Col-0.

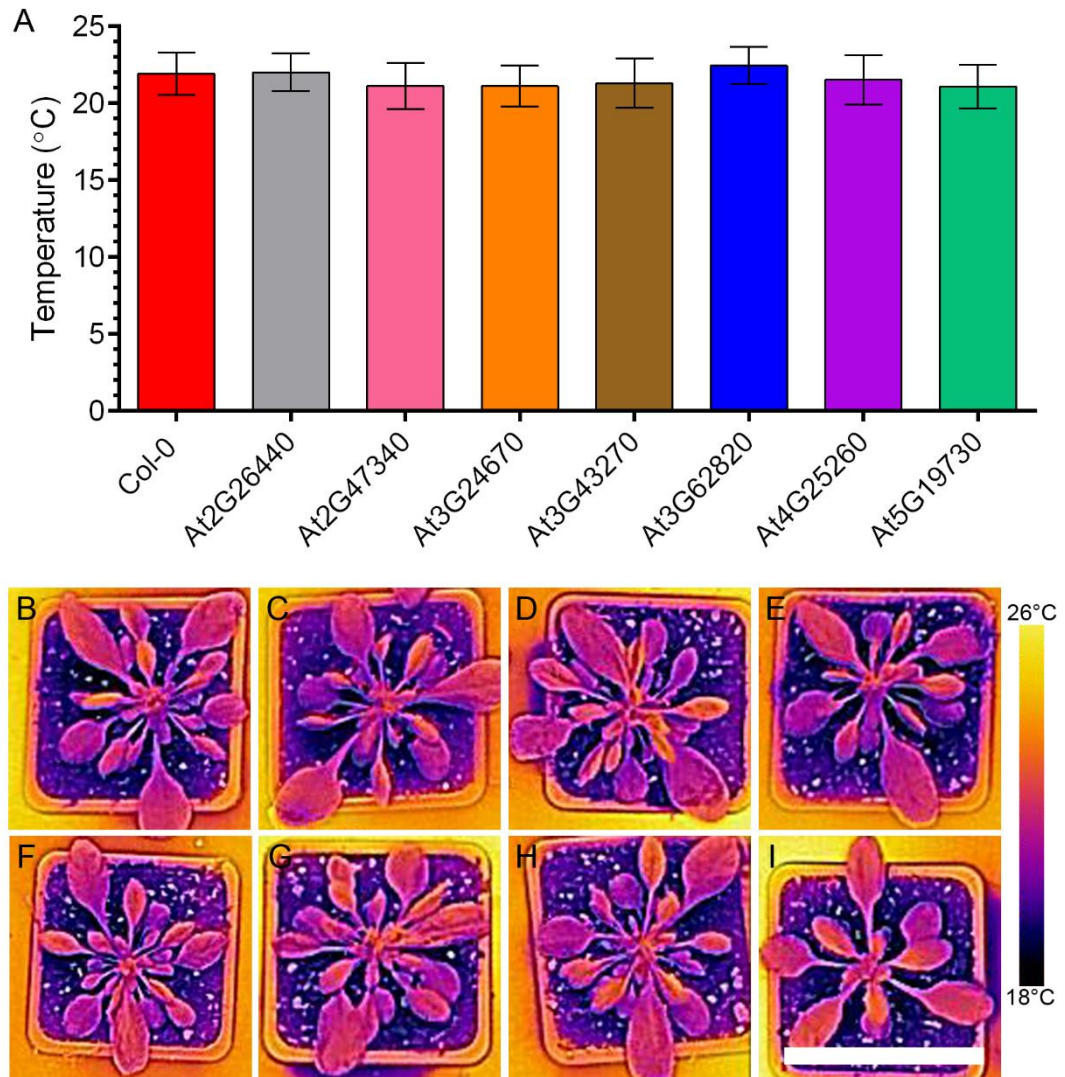


Figure 5.10. Whole plant transpiration is the same for NASC lines and Col-0. Using thermal imaging as a proxy for whole plant transpiration average rosette temperature was measured. (A) Average rosette temperature at 35 days for each line. No significant differences were detected by multiple comparison anova where each line was compared to col-0, $p > 0.05$, $n = 8$. (B-I) Representative thermal images from 35 day old plants. (B) Col-0 (C) At2G26440 (Salk 117817) (D) At2G47340 (Salk 079711) (E) At3G24670 (Salk 109494) (F) At3G43270 (Salk 013629) (G) At3G62820 (Salk 027168) (H) At4G25260 (Salk 036325) (I) At5G19730 (Salk 136556). Scale bars represent 5 cm.

focl plants were imaged at 45 days and average rosette temperature measured. *focl* plants showed a small but significant increase in temperature compared to Col-0 plants (Figure 5.11.A). *focl* plants were visibly warmer (Figure 5.11.C) than Col-0 (Figure 5.11.B). The rosette size of the plants in Col-0 is however substantially larger than *focl* plants. An increase in temperature is indicative of a reduction in transpiration in *focl* plants.

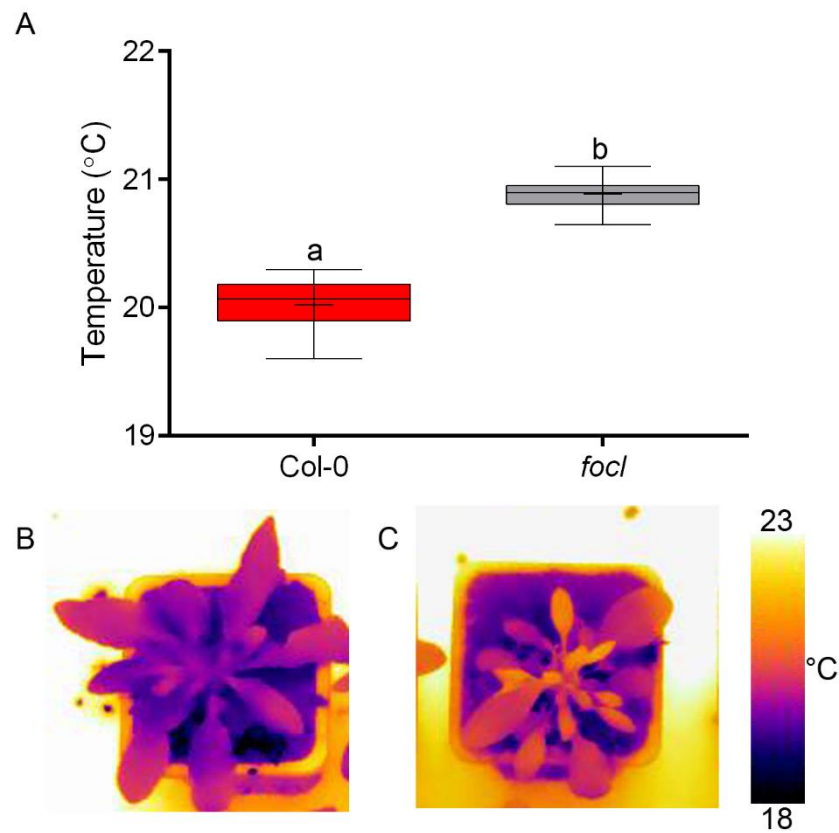


Figure 5.11. *focl* plants are hotter than Col-0 plants. (A) Average rosette temperature showed a small but significant increase in *focl* plants compared to Col-0. Means indicated by +, error bars show min and max values from n=10. Statistical significance determined by students t-test ($p < 0.0001$). (B) Representative image of a Col-0 plant. (C) Representative image of a *focl* plant. Scale bars represent 2 cm.

5.3.5 Stomatal aperture responses to CO₂

NASC insertion lines were assessed for their stomatal responses to CO₂. It has been shown that low CO₂ induces stomatal opening while high CO₂ induces stomatal closure (Kim et al., 2010). Figure 5.12 shows the stomatal aperture response in isolated abaxial epidermal strips of NASC insertion lines and Col-0 leaves exposed to buffers supplied with elevated (1000ppm), ambient (400ppm) or decreased (0ppm) levels of CO₂. Col-0 stomata showed increased aperture when exposed to low CO₂ and decreased aperture when exposed to elevated CO₂ relative to ambient CO₂, as has been previously reported (Amsbury et al., 2016). In contrast, an At2G6440 insertion mutant showed a limited capacity to respond to CO₂ (Figure 5.12.A). There was no significant difference in aperture between any of the CO₂ treatments for At2G6440 stomata, with apertures remaining similar to those observed at ambient CO₂. None of the treatments were significantly different to Col-0 ambient CO₂ treated plants.

At2G47340, At3G24670 and At3G43270 (Figure 5.12.B-D) all show the same response to CO₂ as Col-0 indicating that stomata are functioning normally in these lines. At3G62820 stomata respond in a similar manner to Col-0, closing in response to elevated CO₂ and opening in response to reduced CO₂. The stomata had significantly larger pore area's than Col-0 at 0ppm CO₂ suggesting an ability to open further.

At4G25260 (Figure 5.12.F) has the same aperture as Col-0 at ambient and 0ppm CO₂ levels. At elevated CO₂ the stomata are unable to close remaining at an ambient-like aperture. At5G19730 (Figure 5.12.G) has a similar pattern of response as Col-0 with stomata being able to open and close in response to changing CO₂. At5G19730 stomata have a larger pore area at ambient CO₂ and a slightly larger pore area at high CO₂, responses to CO₂ free air are the same as Col-0.

These data show that the stomata of the At2G6440 mutants do not respond in a normal manner to altered CO₂ level and appear to be completely unresponsive. The stomata of At3G62820 mutants respond in a normal manner but the extent of opening is enhanced while At5G19730 stomata appear to have more open stomata at ambient conditions.

As discussed in section 5.3.2 *focl* plants have an alteration to their stomatal size and as such presenting the data just as pore area could be misleading. For this reason, *focl* was separated from the main analysis and analysed separately. *focl* stomata have an increased aperture compared to Col-0 at all treatments (Figure 5.13.A). The magnitude of change in aperture appears similar between the lines. Pore length can be used as a proxy for stomatal size as it is largely unaffected by changes in pore width. *focl* stomata are significantly longer than Col-0 stomata (Figure 5.13.B) because, as has previously been discussed (Figure 5.7.A), the stomata are larger in *focl* plants than Col-0. As the stomatal size differs between the lines, the percentage of the stomatal complex which is taken up by the pore was calculated using the following equation.

Equation 5.1 Percentage of stomatal complex taken up by pore

$$\frac{\text{Stomatal pore area}}{\text{Total stomatal complex area}} \times 100$$

As a function of stomatal size, *focl* stomata are significantly more closed at all CO₂ treatments. This suggests a reduction in functionality which is masked by the increased size.

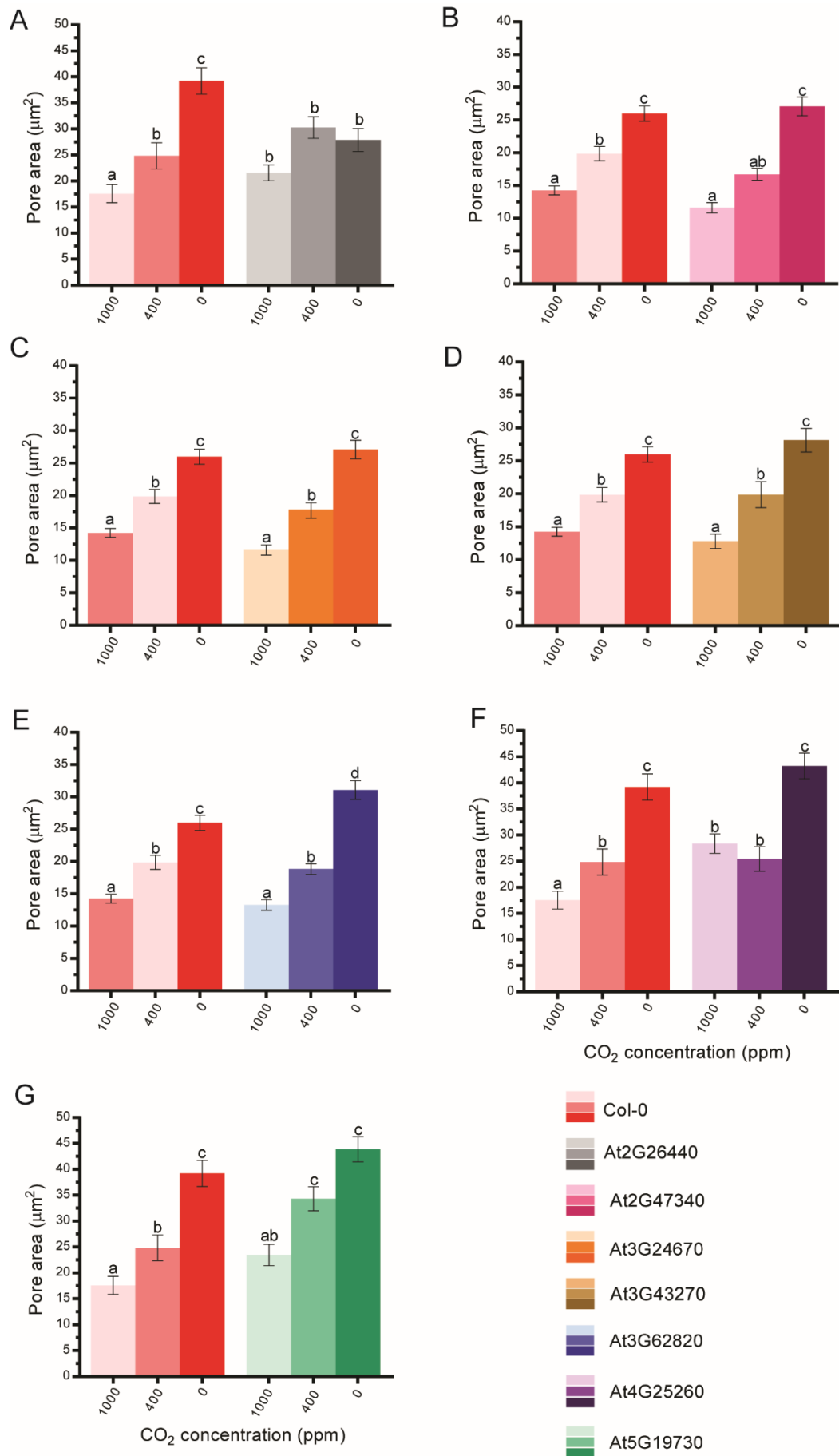


Figure 5.12. Responses of NASC lines to CO₂. Epidermal peels were exposed to differing levels of CO₂ in resting buffer and pore area calculated. (A) Col-0 increases pore area as the CO₂ level decreases. At2G26440 (Salk 117817, PME) was unable to adjust its stomata in response to CO₂ with all treatments having apertures the same as ambient (400ppm) in Col-0 plants. (B) At2G47340 (Salk 079711, PME) showed the same stomatal aperture responses to CO₂ as Col-0. (C) At3G24670 (Salk 109494, pectate lyase) showed the same stomatal aperture responses to CO₂ as Col-0. (D) At3G43270 (Salk 013629, PME) showed the same stomatal aperture responses to CO₂ as Col-0. (E) At3G62820 (Salk 027168, PMEI) showed the same stomatal aperture responses to CO₂ as Col-0. (F) At4G25260 (Salk 036325, PMEI) showed the same stomatal aperture responses to CO₂ free air as Col-0 however stomatal aperture did not decrease in response to high CO₂. (G) At5G19730 (Salk 136556, PME) showed a similar response to CO₂ as Col-0. The stomata appear to open slightly more and close slightly less than Col-0 stomata. Each column shows the mean and s.e.m. (n=6), with statistical differences determined by ANOVA with post-hoc Tukey test. Columns indicated with identical letters cannot be distinguished from each other (p< 0.05).

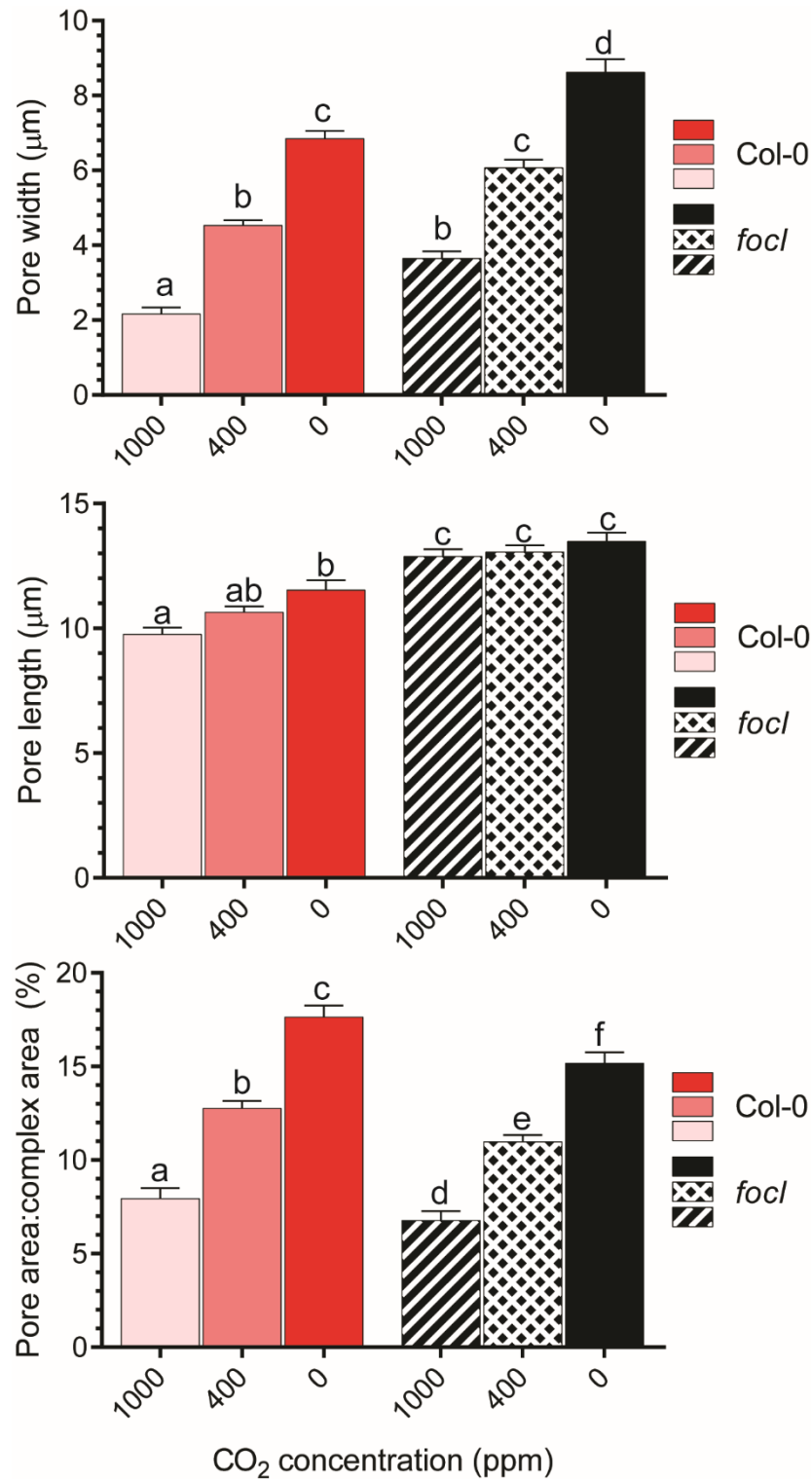


Figure 5.13. *focl* responses to CO₂. (A) *focl* stomata open in response to CO₂ free air and close in response to high CO₂. The stomatal aperture is consistently larger than the corresponding pore Col-0 treatment. (B) Pore length is significantly larger in *focl* stomata than in Col-0 plants at all treatments indicating that *focl* stomata area larger. (C) As a percentage of their size *focl* stomata have reduced mobility. At all CO₂ treatments then proportion of the stomatal complex which is pore is reduced in *focl* plants compared to Col-0. Each column shows the mean and s.e.m. (n=6), with statistical differences determined by ANOVA with post-hoc Tukey test. Columns indicated with identical letters cannot be distinguished from each other (p < 0.05).

5.3.6 *focl* plants have covered stomata

It was noted when observing epidermal peels that *focl* plants had abnormal looking stomata. To further assess this, transverse sections from mature leaf tissue were stained with toluidine blue to investigate the histology of *focl* stomata

The data, shown in Figure 5.14, show that *focl* plants have a covering over their stomata which appears to block the pore (black arrows, Figure 5.14.A and C). This covering appears to extend from the cuticular ledges on the guard cells. A small number of stomata appeared to be uncovered in *focl* plants (Figure 5.14.B) but these also seem to have extended cuticular ledges (red arrows) compared to Col-0 stomata (Figure 5.14.D) which have defined cuticular ledges (green arrows).

The majority of *focl* stomata are covered with only 10% of *focl* stomata observed being uncovered compared to 75% covered (Figure 5.14.E). In contrast no Col-0 stomata were observed to be covered with 80% being confirmed as uncovered (Figure 5.14.F). In a small number of stomata in each line it was unclear whether or not the stomata was covered due to poor section quality. This meant that in each line 15-20% of stomata were defined as unclear meaning that it was impossible to determine if they were covered or not.

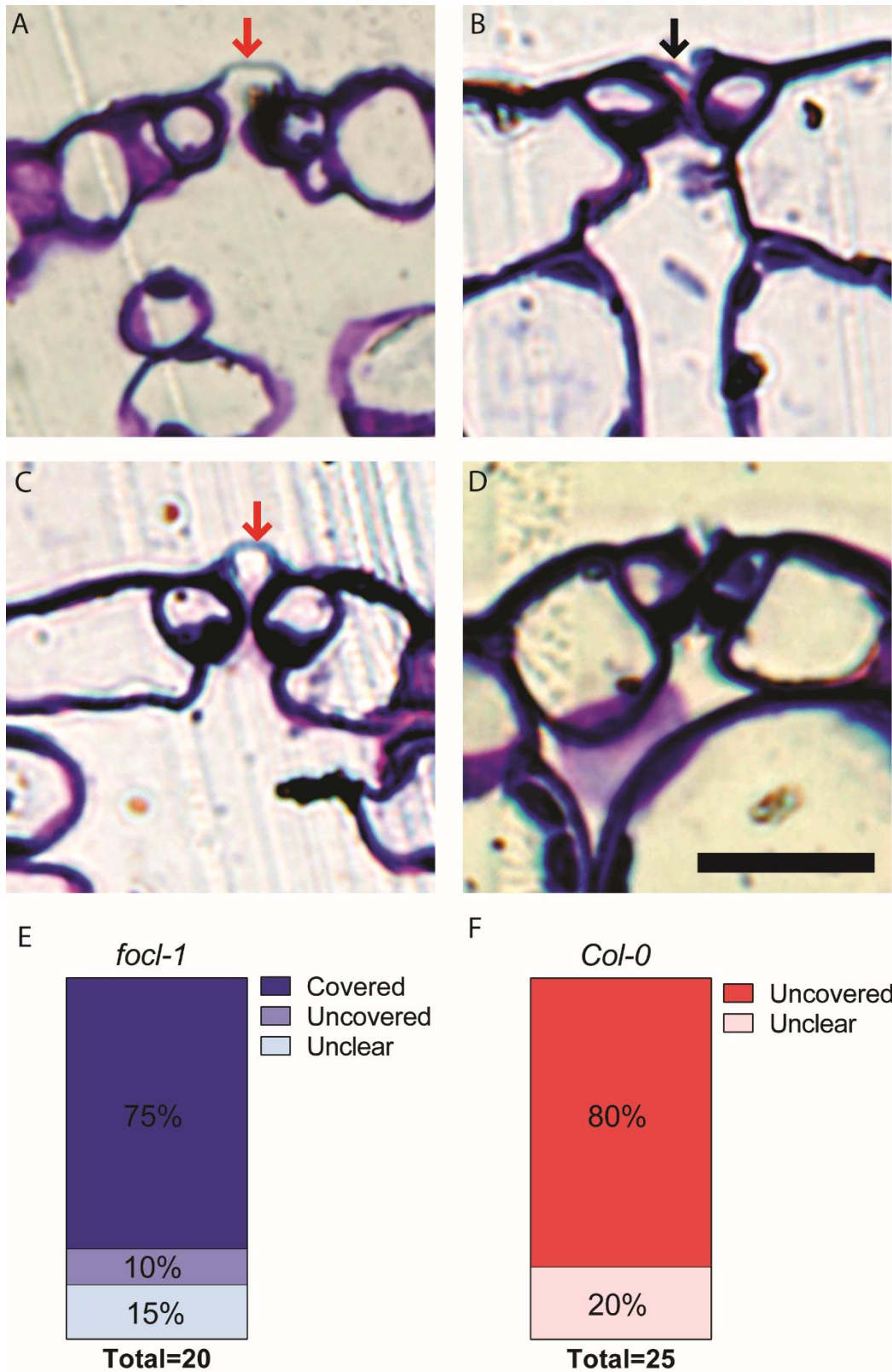


Figure 5.14. *focl* stomata have a covering. (A-C) are example *focl* stomata. (A) and (C) have a stomatal covering (indicated by red arrows). (B) some *focl* stomata have uncovered stomata but appear to have an extended cuticular ledge (black arrows). (D) *Col-0* stomata are uncovered and have defined cuticular ledges. (E) the majority of *focl* stomata are covered with a small number (10%) uncovered. A small number of stomata are unclear due to image quality. (F) No *Col-0* stomata are observed as covered. Scale bars represent 20 μ m.

Obscuring the stomata may alter carbon flux into the leaf, which could have a number of secondary effects on plant development. Further toluidine blue staining revealed altered leaf structure. Col-0 plants have small air-spaces under the guard cells (sub-stomatal cavities), as seen in Figure 5.15.A.

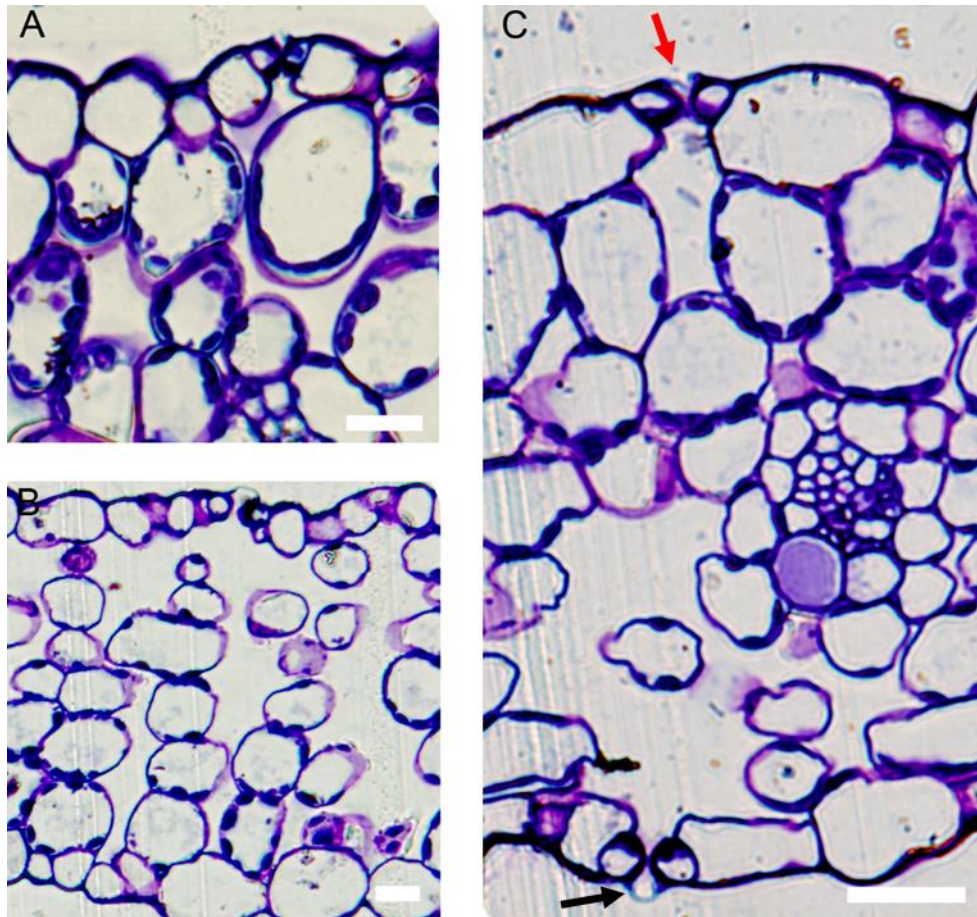


Figure 5.15. *focl* plants have altered mesophyll structure under covered stomata compared to Col-0. (A) Col-0 plants have small but defined substomatal cavities below their stomata. (B) *focl* plants appear to have much bigger air spaces under covered stomata. (C) *focl* plants seem to have WT-like air spaces under stomata which are not covered. A section containing two stomata shows one uncovered (red arrow) and one covered stomata (black arrow) with two very different sized air spaces under each. Scale bars represent 20µm

These sections show that covered stomata in the *focl* line have substantially larger substomatal cavities than in Col-0 plants (Figure 5.15.B). Interestingly in the rare cases where *focl* stomata are not covered, smaller substomatal

cavities were observed which were more analogous to WT plants (Figure 5.15.C). In Figure 5.15.C both extremes can be observed in one section: one stomata is covered and has a large sub-stomatal cavity while one stomata is uncovered and has a small sub-stomatal cavity. This raises interesting questions about the relationship between the stomata and the formation of mesophyll airspace.

5.3.7 Immunolabelling NASC lines with altered stomatal function

As discussed earlier, several mutant lines showed an alteration in stomatal opening and closing. These lines were analysed for cell wall alterations using the immunolabelling technique previously described (2.6). Due to time constraints only a small subset of antibodies were used with a focus being placed on antibodies for pectin epitopes. None of the antibodies tested showed any differences between the lines indicating that the knockouts had not caused a perceivable change in cell wall composition.

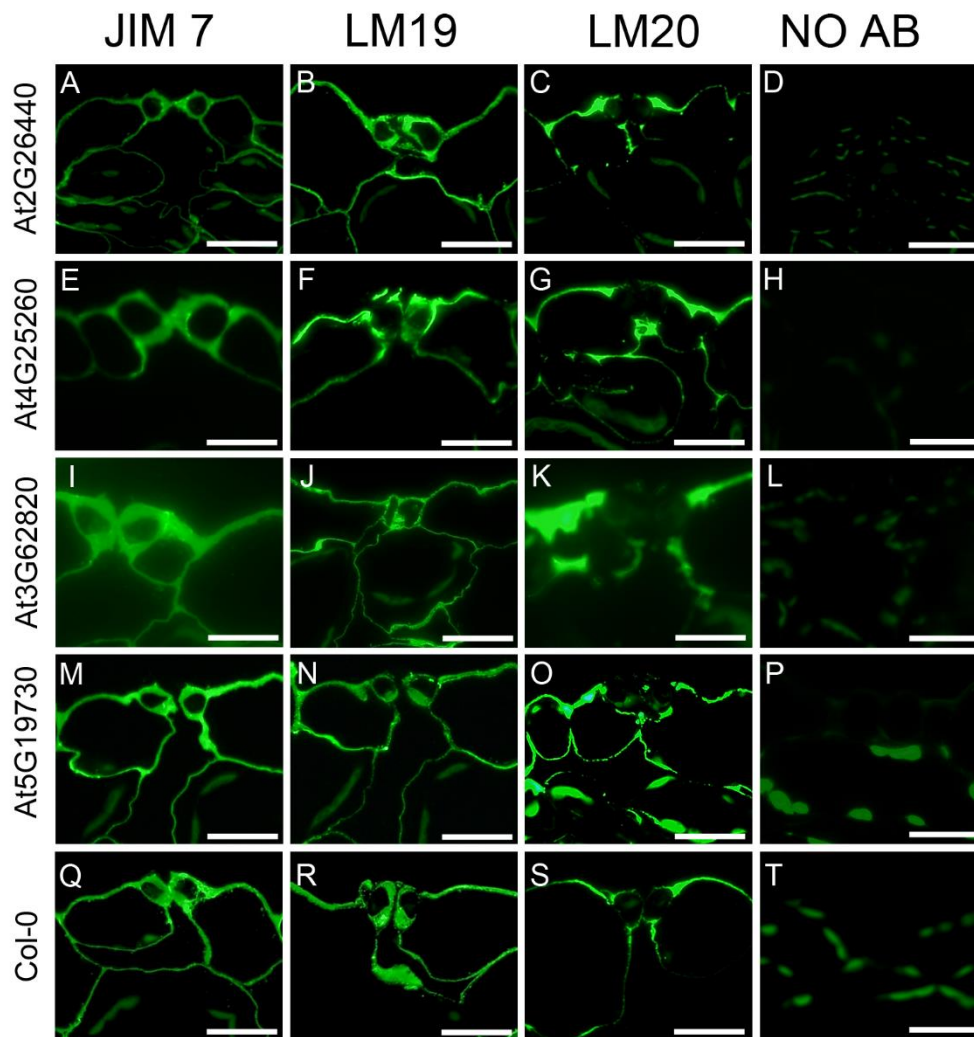


Figure 5.16. Immunolabelling of NASC mutants reveals no differences in the cell wall composition compared to WT. (A-D) Immunolabeling of At2G6440 plants (A) JIM7 (B) LM19 (C) LM20 (D) No antibody control. (E-H) Immunolabeling of At4G25260 plants (E) JIM7 (F) LM19 (G) LM20 (H) No antibody control. (I-L) Immunolabeling of At3G62820 plants (I) JIM7 (J) LM19 (K) LM20 (L) No antibody control. (M-P) Immunolabeling of At5G19730 plants (M) JIM7 (N) LM19 (O) LM20 (P) No antibody control. (Q-T) Immunolabeling of Col-0 plants (Q) JIM7 (R) LM19 (S) LM20 (T) No antibody control. Images are representative of n=3. Scale bars represent 20µm. At5G19730 and Col-0 labelling was carried by Sarah Carroll.

5.3.8 *focl* plants do not show alterations to their cell wall structure

It has been suggested that extensins function as a scaffold to guide the formation of the cell wall. Immunolabelling of *focl* plant revealed that no alterations to the stomatal cell wall could be detected. No antibodies tested bound to the stomatal covering.

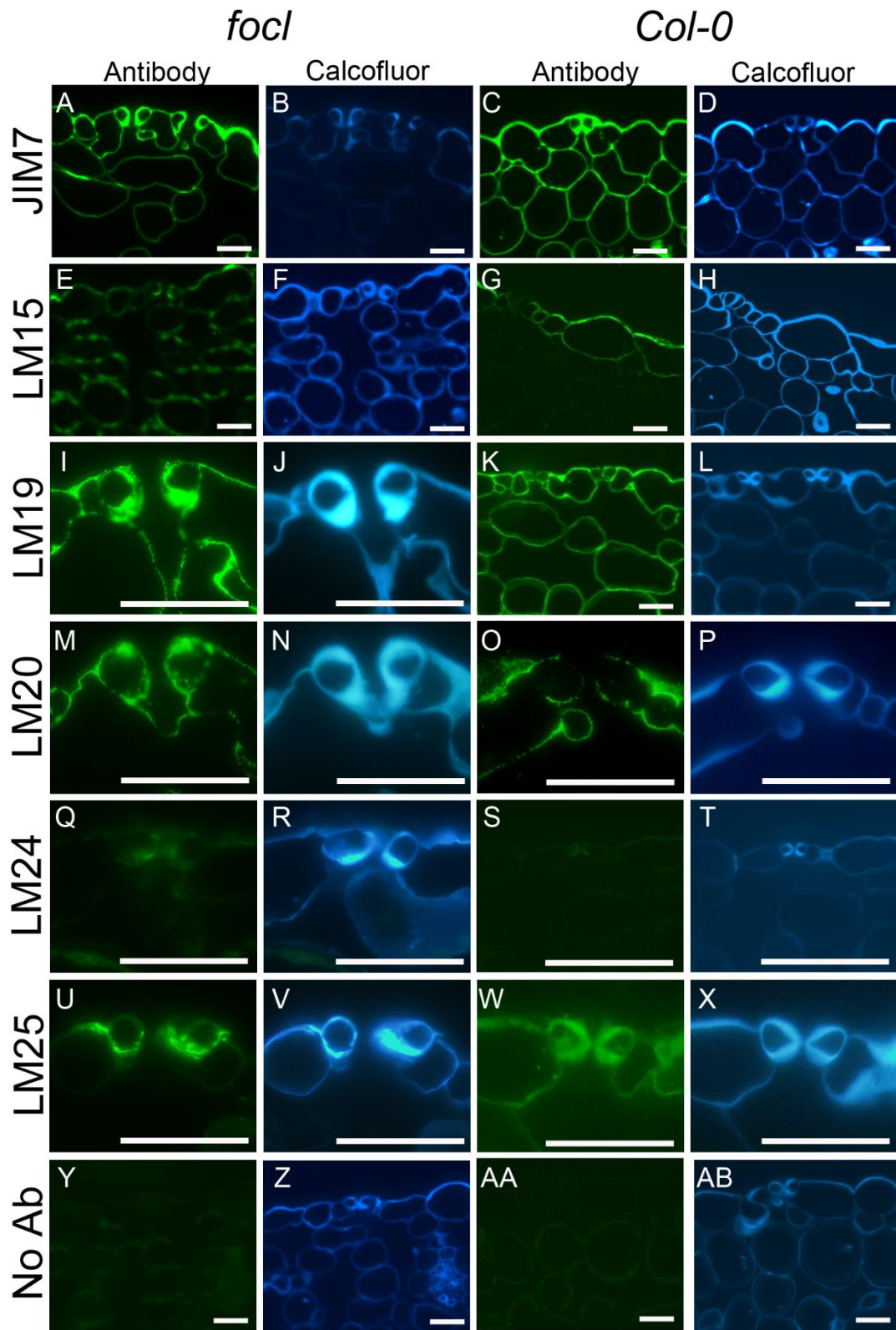


Figure 5.17. Immunolabelling of foci revealed no major differences in cell wall composition. (A-D) JIM 7 labelling indicating HGA and calcofluor binding indicating cellulose. (A-B) foci (C-D) Col-0. JIM7 binding is extensive in both lines. (E-H) LM15 labelling indicating the XXXG motif of xyloglucan and calcofluor binding indicating cellulose. (E-F) foci (G-H) Col-0. LM15 binding is faint in both lines with greater intensity in the mesophyll. (I-L) LM 19 labelling indicating unesterified HGA and calcofluor binding indicating cellulose. (I-J) foci (K-L) Col-0. LM19 labelling is abundant in both lines. (M-P) LM 20 labelling indicating highly esterified HGA and calcofluor binding indicating cellulose. (M-N) foci (O-P) Col-0. LM20 binding in foci plants (M) was greater than in Col-0 plants (O) suggesting a potential increase in highly esterified HGA. (Q-T) LM 24 labelling indicating the XLLG motif of xyloglucan and calcofluor binding indicating cellulose. (Q-R) foci (S-T) Col-0. LM24 binding was faint in both lines with a slight increase in intensity in the guard cells. (U-X) LM 25 labelling indicating a range of xyloglucan conformations and calcofluor binding indicating cellulose. (U-V) foci (W-X) Col-0. LM24 binding was present in both lines. (Y-AB) Samples incubated with secondary antibody but no primary antibody and calcofluor binding indicating cellulose. (Y-Z) foci (AA-AB) Col-0. Very low levels of cell wall autofluorescence were seen, some slight chloroplast autofluorescence was observed.

Images are representative from n=2. Scale bars represent 20µm.

5.4 Creation of PMEI overexpression lines

Using T-DNA insertion lines from NASC allows the study of loss of function mutants, as previously discussed there is a strong chance of redundancy, especially in genes from the PME/PMEI family. By capitalising on the fact that *A. thaliana* can be transformed by agrobacterium by using a floral dip method a transgenic approach was taken to overexpress PMEI genes.

For the creation of PMEI overexpression lines AtPMEI1 and AtPMEI2, target DNA was isolated from genomic DNA by PCR using primers designed to add the sequence “CACC” onto the 5’ end of the forward strand to make the sequences suitable for cloning (Appendix 5). The *Actinidia deliciosa* genome is not as thoroughly annotated as the *A. thaliana* genome thus it is possible that introns exist within the AdPMEI1 sequence. To avoid this problem AdPMEI1 was isolated from cDNA which was synthesised following the extraction of RNA (Figure 5.18).

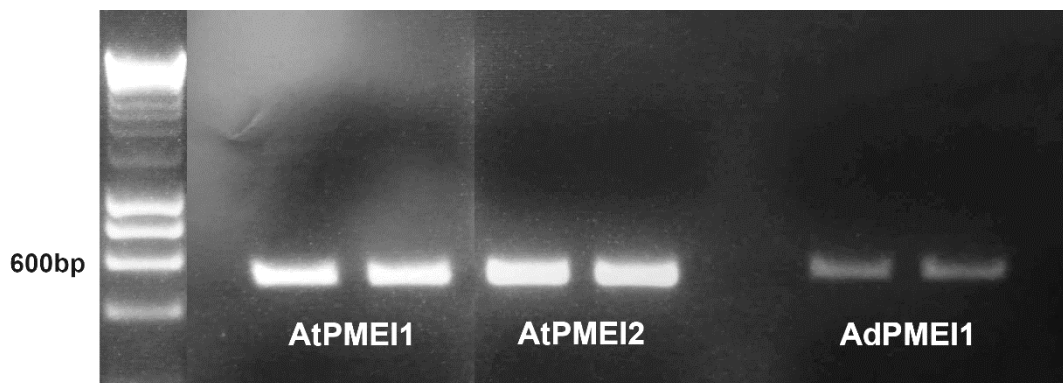


Figure 5.18. Isolation of PMEI genes. AtPMEI1 and 2 are isolated from gDNA while AdPMEI1 is isolated from cDNA. A band is seen which is slightly below the 600bp marker on the DNA ladder.

The three genes were transferred into the Gateway compatible vector pENTR/D-TOPO and transformed into *E. coli* by heat shock. Colonies were checked by PCR for the presence of the insert (Figure 5.19). Gateway cloning

has a low likelihood of inserts being incorporated in the incorrect orientation but positive colonies were sequenced to confirm this.

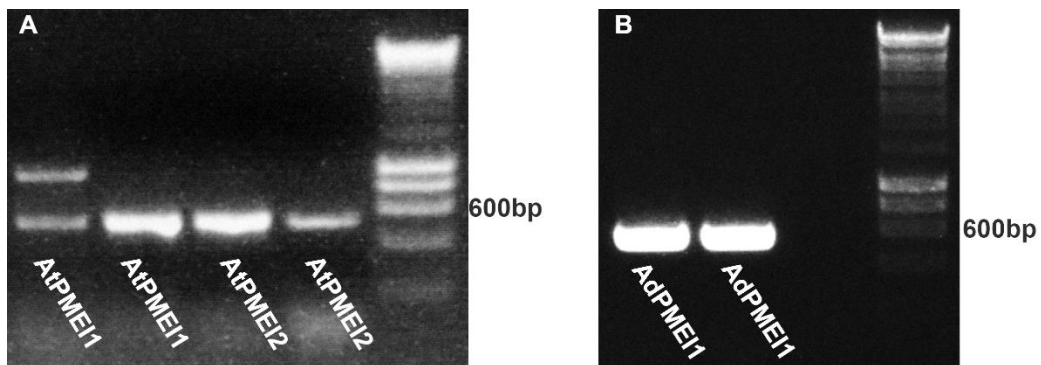


Figure 5.19. Verification of inserts in pENTR/D-TOPO vector by colony PCR using gene specific primers.

Both the pENTR/D-TOPO vector and the PMDC32 vector used as a destination vector contained kanamycin resistance (Appendix 8 and 9) Before transference into PMDC32 the TOPO vector was digested with *nsiI* to disrupt the kanamycin resistance gene to allow detection of *E.Coli* transformed with PMDC32 (Figure 5.20).

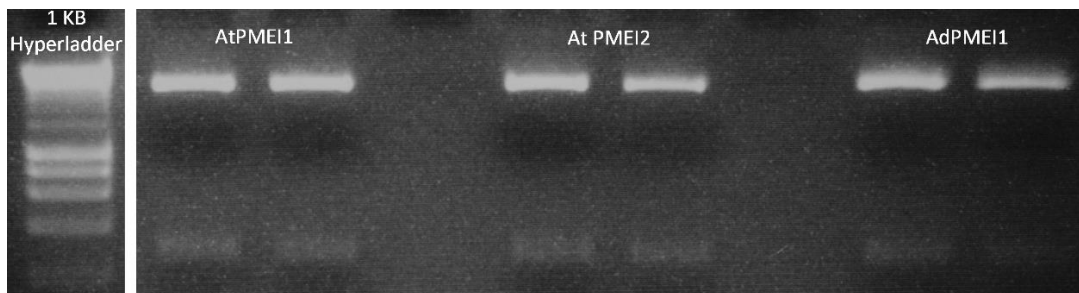


Figure 5.20. Digestion of TOPO with *nsiI* to remove kan resistance. A small excised band can be seen in each lane.

The genes were transferred from the TOPO vector to PMDC32 by the LR reaction. Colonies were selected by antibiotic resistance (Kanamycin) and tested by colony PCR (Figure 5.21).

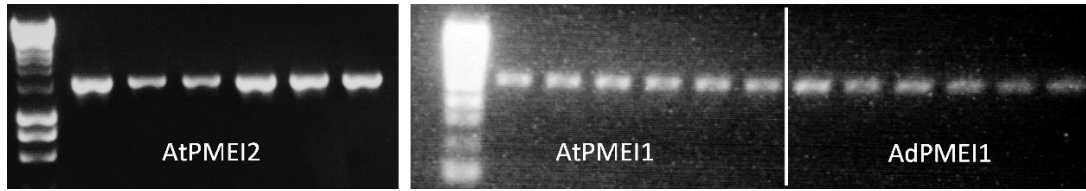


Figure 5.21. Verification of LR reaction. AtPMEI1, 2 and AdPMEI1 are observed in PMDC32 using a vector specific forward primer and a gene specific reverse primer.

The promoters were isolated from genomic DNA. Primers were used that were designed to add the required restriction sites, BamHI and SBF1 at the 5' and 3' ends respectively (Figure 5.22).

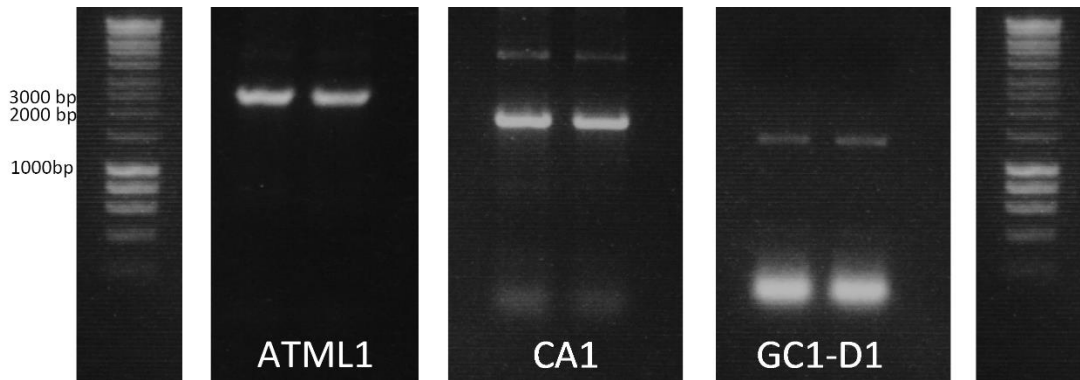


Figure 5.22. Promoters with restriction sites. BamHI +SBF1, expected sizes: ATML1 3287 GC1-D1 1219, CA1-2171

The PMDC32 vector containing the constructs was digested using BamHI and SBF1, which excised the 35S promoter from the vector backbone so that it could be replaced by the promoters of interest (Figure 5.23)



Figure 5.23. Removal of CaMV promoter by pmeI and bamHI digestion. Expected excised band 989, plasmid length post digestion 966. An excised band can be seen in each lane.

The promoters, CA1, ATML1 and GC1-D1 were annealed into the pmdc32 vector containing each construct to provide 9 complete constructs, as detailed in Table 5.2.

Table 5.2. List of gene constructs

Line Name	Gene of interest	Promoter
pGC1:AtPMEI1		
pGC1:AtPMEI2	AtPMEI1	pGC1-D1
pGC1:AdPMEI1		
pCA1:AtPMEI1		
pCA1:AtPMEI2	AtPMEI2	pCA1
pCA1:AdPMEI1		
pATML:AtPMEI1		
pATML:AtPMEI2	AtPMEI2	pATML
pATML:AdPMEI1		

The 9 gene constructs were electroporated into agrobacterium and successful transformation was confirmed by sequencing. The constructs were then transformed into *A. thaliana* by floral dip.

5.5 Creating and selecting mutant plants

Seeds were harvested from dipped plants (T_0 seed) and T_1 transformants selected by hygromycin resistance. Transformants were selfed and T_2 plants were grown on hygromycin and lines showing 3:1 survival ratio (from 50 plants) were grown to seed to ensure only one insert was present. Sister lines, where the insert had segregated out, were selected at this point by growing T_2 plants without selection and genotyping plants to select ones with no insert. T_3 plants were grown on selection to ensure they were homozygous: transformed lines all showed 100% survival on hygromycin while sister lines all showed 100% susceptibility to hygromycin. Once T_3 lines had been

confirmed as homozygous they were grown in the absence of selection for experimental analysis. Due to staggered timings for obtaining homozygous plants along with time constraints on the project, only constructs with the CA1 promoter were analysed in this chapter (Table 5.2).

5.6 Analysis of *pCA1:PMEI* lines

All experiments apart from immunocytochemistry were conducted in a blind manner where the identity of the line was not known, so preventing confirmation bias. Two independent lines for each construct were analysed along with 2 corresponding sister lines.

5.6.1 Stomatal size and patterning is unaffected in overexpression lines

Plants were assessed to find out if epidermal patterning had been altered in any of the lines. No significant difference in stomatal density (Figure 5.24.A), stomatal index (Figure 5.24.B) or in stomatal length (Figure 5.24) was observed between any of the lines and Col-0 (Anova, $p > 0.05$) indicating that stomatal patterning was unaffected in the transgenic lines.

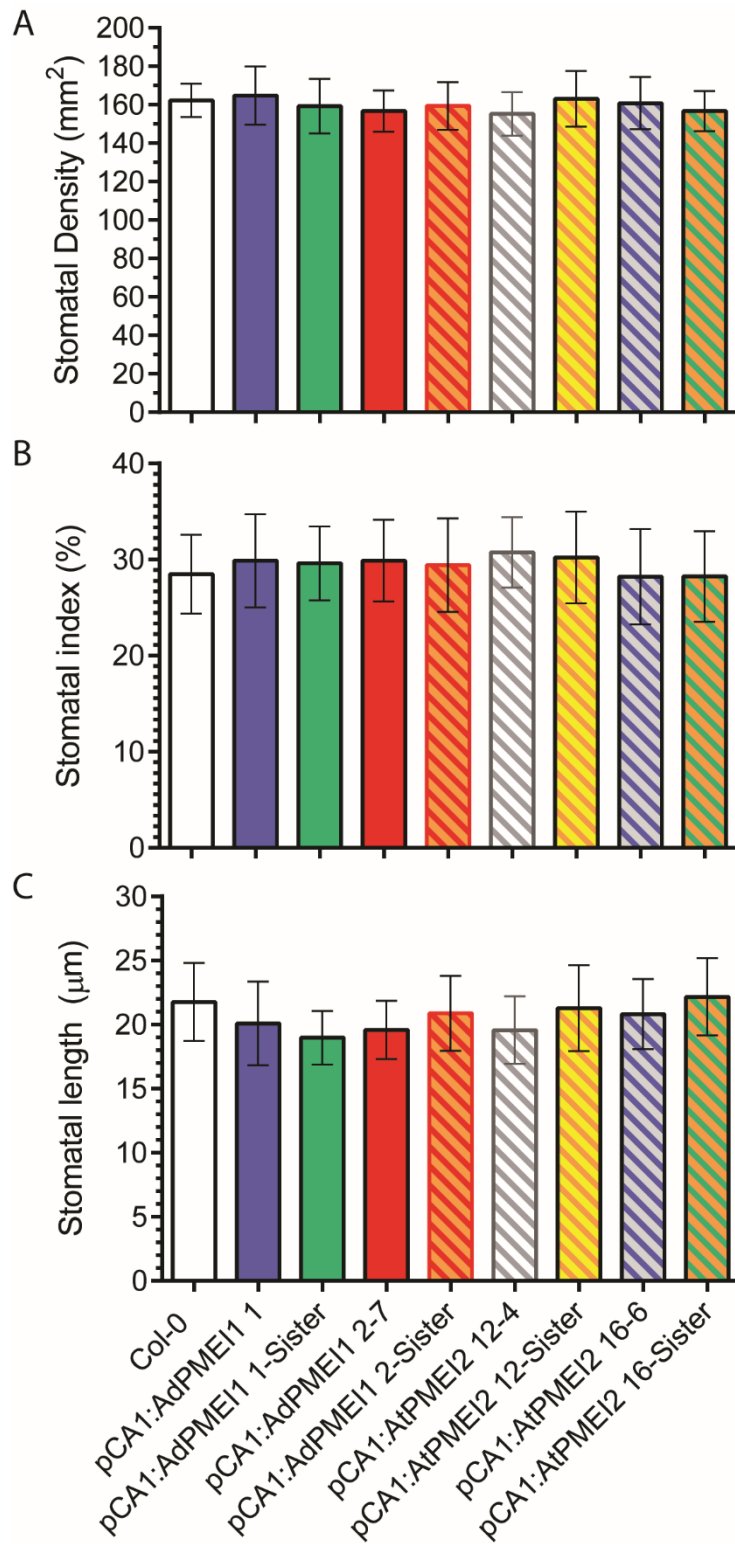


Figure 5.24. Stomatal Patterning and size is unaffected in transgenic lines. (A) Stomatal density of Col-0 and pCA1:AtPMEI2 and pCA1:AdPMEI1 overexpression lines. No statistically significant differences were observed. (B) (A) Stomatal index of Col-0 and pCA1:AtPMEI2 and pCA1:AdPMEI1 overexpression lines. No statistically significant differences were observed. (C) (A) Stomatal length of Col-0 and pCA1:AtPMEI2 and pCA1:AdPMEI1 overexpression lines. No statistically significant differences were observed. Error bars= SEM, n=10, lack of statistical significance determined by ANOVA multiple comparisons p>0.05.

5.6.2 Thermal imaging

Thermal imaging was carried out to assess plant temperature as a proxy for transpiration. Plants were imaged at 35 days in the growth chamber with the door shut to minimise external perturbations. Emissivity was set at 0.96 and average rosette temperature was measured.

No significant differences in rosette temperature were observed between any of the transgenic lines, sister lines or Col-0 plants (Figure 5.25.A). The thermal images appear to show that there is some variation in rosette size and fullness between Col-0 (Figure 5.25.B) and the transgenic and sister line (Figure 5.25.C-J) although further work is needed to confirm this.

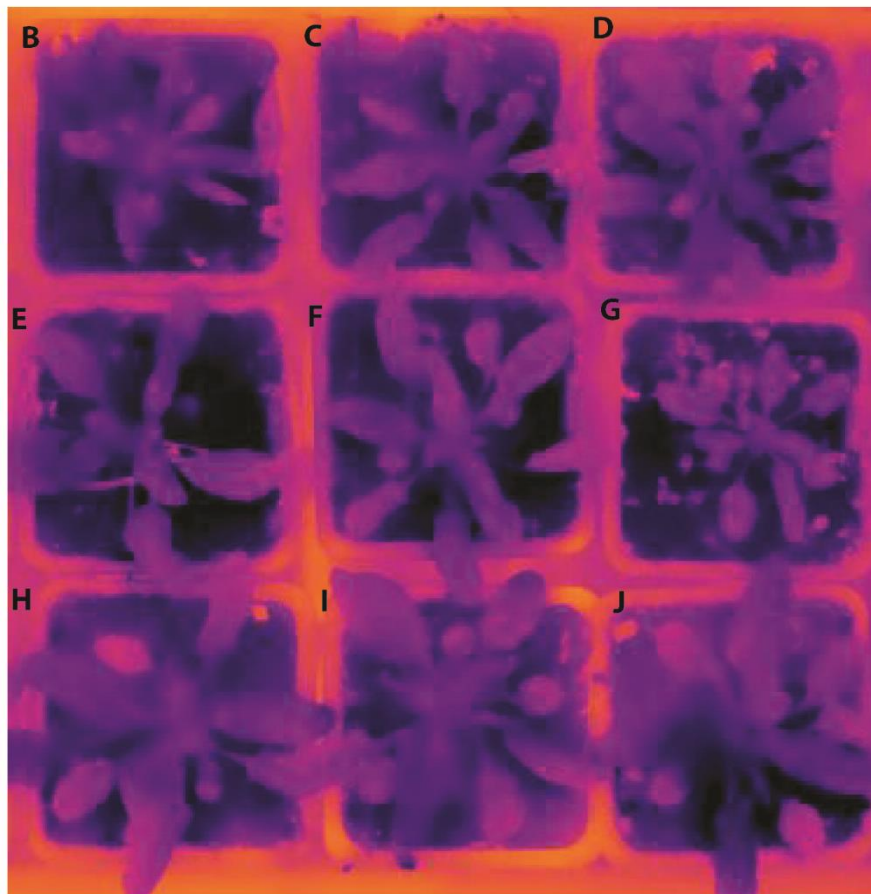
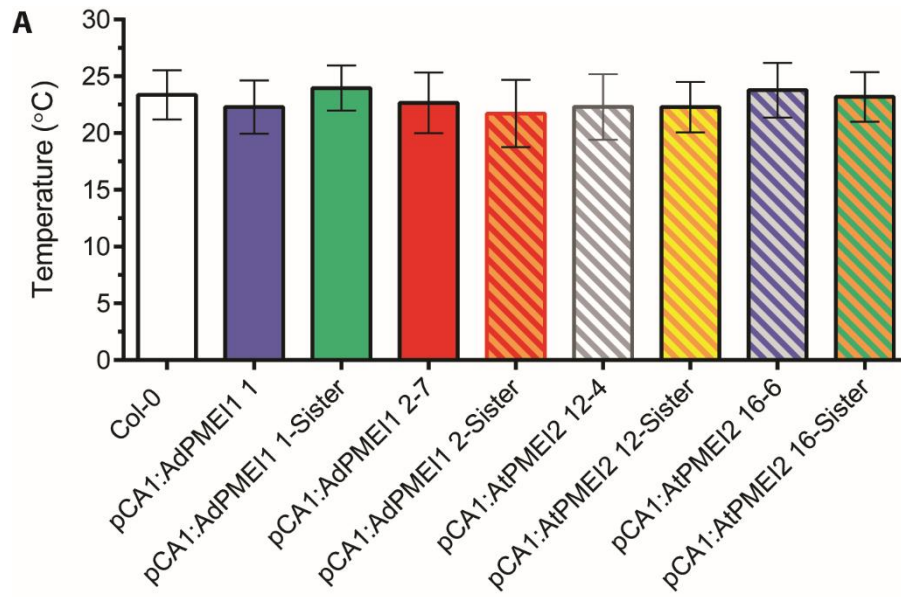


Figure 5.25. Thermal imaging of transgenic lines. (A) Average rosette temperature for 30 day old plants. Error bars represent SEM. No significant differences were observed, ANOVA $p > 0.05$, $n = 8$ (B-J) Representative thermal image of 35 day old plants. (B) Col-0 (C) pCA1:AdPMEI1 1 (D) pCA1:AdPMEI1 1-sister (E) pCA1:AdPMEI1 2-7 (F) pCA1:AdPMEI1 2-sister (G) pCA1:AtPMEI2 12-4 (H) pCA1:AtPMEI2 12-sister (I) pCA1:AtPMEI2 16-6 (J) pCA1:AtPMEI2 16-sister.

5.6.3 Antibody analysis of mutants

To assess the impact of the transgenic lines on cell wall composition immunolabelling was carried out. Jim7, LM19 and LM20 antibodies were used to detect homogalacturonan, unesterified homogalacturonan and highly esterified homogalacturonan, respectively.

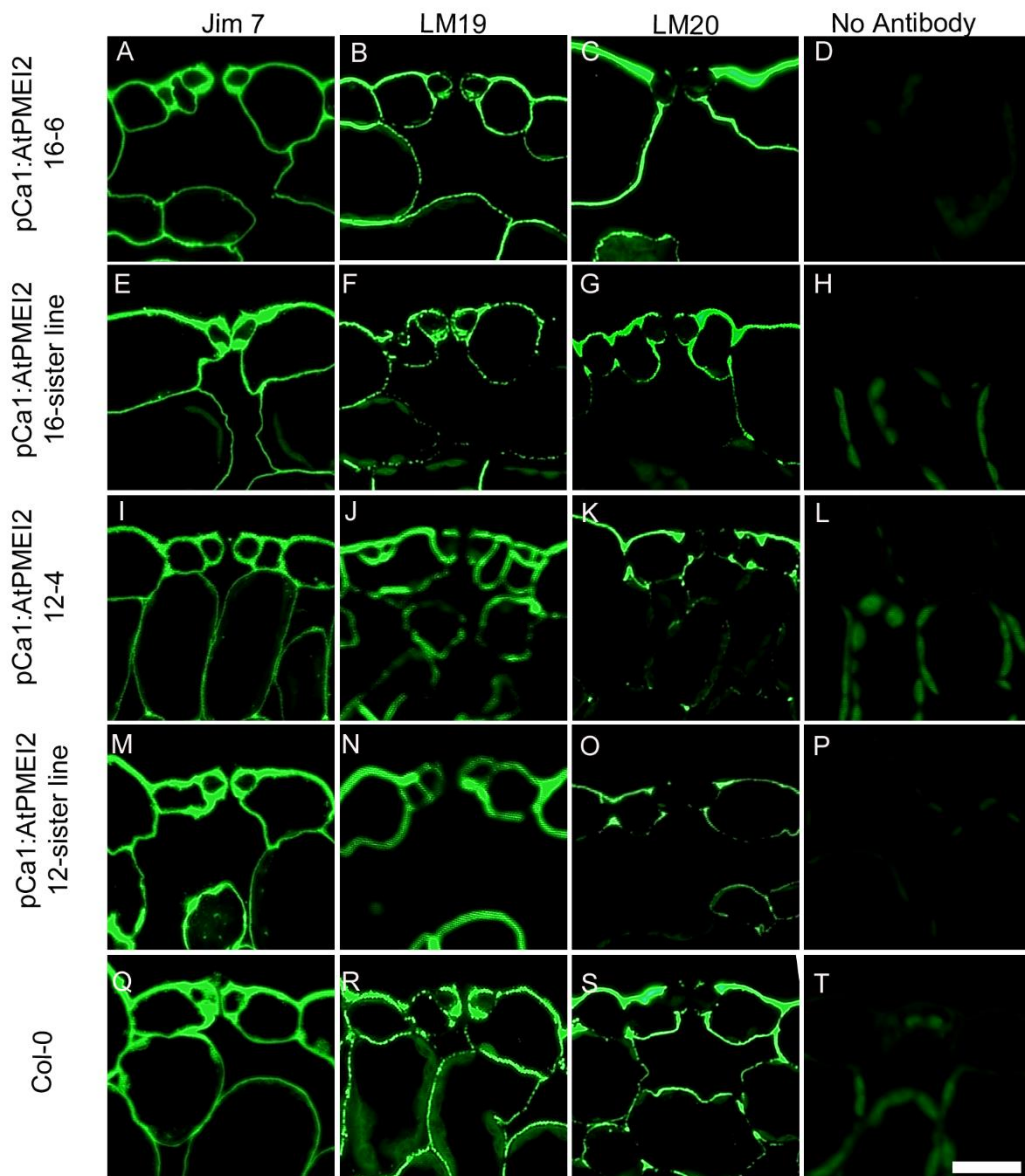


Figure 5.26. Antibody labelling of AtPMEI2 lines. (A-D) pCA1:AtPMEI2 16-6 labelling (A) JIM7 (B) LM19 (C) LM20 (D) No antibody control (E-H) pCA1:AtPMEI2 16-sister labelling (E) JIM7 (F) LM19 (G) LM20 (H) No antibody control (I-L) pCA1:AtPMEI2 12-4 labelling (I) JIM7 (J) LM19 (K) LM20 (L) No antibody control. (M-P) pCA1:AtPMEI2 12-sister labelling (M) JIM7 (N) LM19 (O) LM20 (P) No antibody control. (Q-T) Col-0 labelling (Q) JIM7 (R) LM19 (S) LM20 (T) No antibody control. Images are representative of n=3, scale bar=20µm

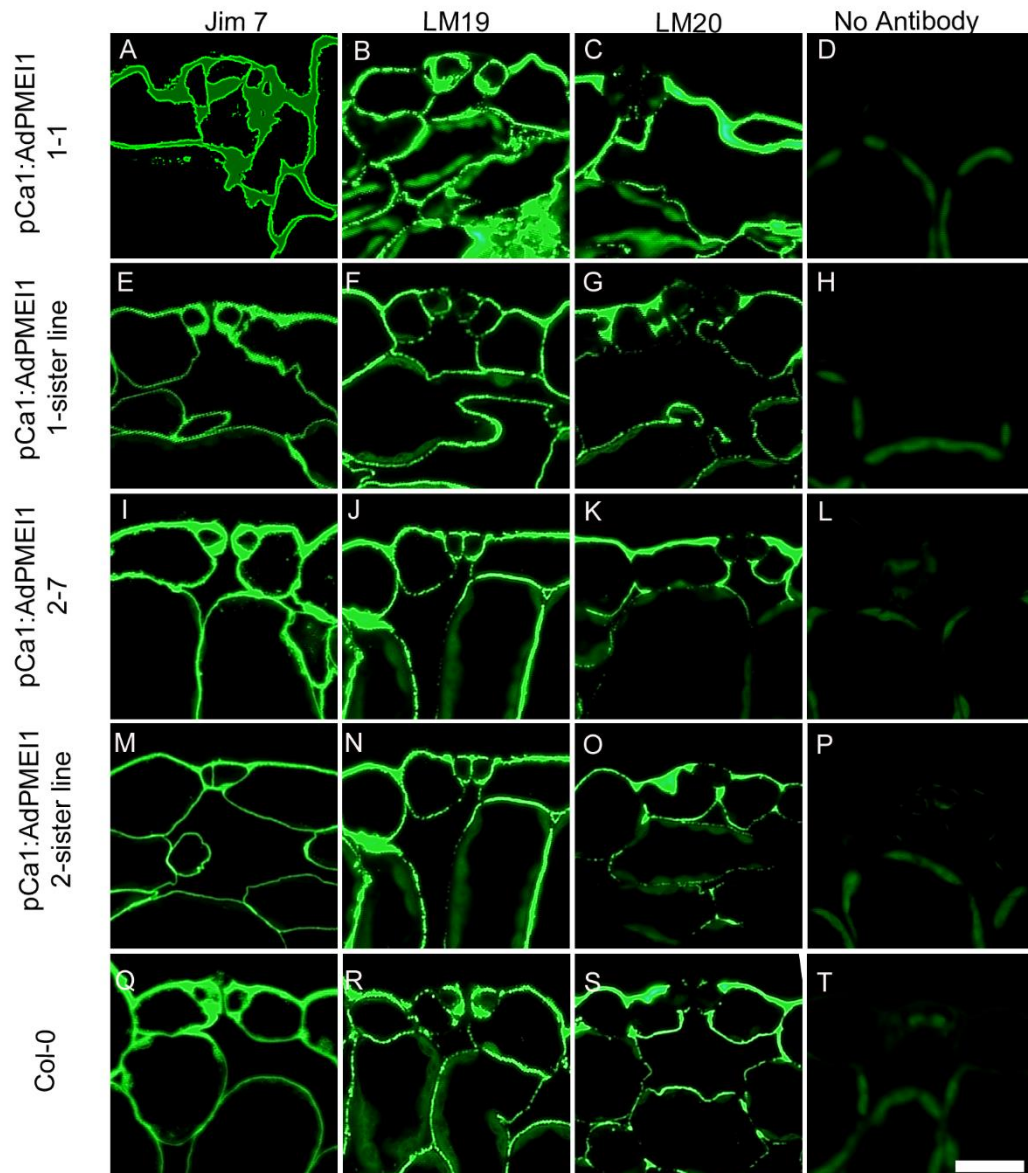


Figure 5.27 Antibody labelling of AdPMEI1 lines. (A-D) pCA1:AdPMEI1 1-1 labelling (A) JIM7 (B) LM19 (C) LM20 (D) No antibody control (E-H) pCA1:AdPMEI1 1-sister labelling (E) JIM7 (F) LM19 (G) LM20 (H) No antibody control (I-L) pCA1:AdPMEI1 2-7 labelling (I) JIM7 (J) LM19 (K) LM20 (L) No antibody control. (M-P) pCA1:AdPMEI1 2-sister labelling (M) JIM7 (N) LM19 (O) LM20 (P) No antibody control. (Q-T) Col-0 labelling (Q) JIM7 (R) LM19 (S) LM20 (T) No antibody control. Images are representative of n=3, scale bar=20µm.

No clear differences were observed in any of the transgenic lines compared to sister lines or Col-0 in either pCA1:AtPMEI2 lines (Figure 5.26) or pCA1:AdPMEI1 lines (Figure 5.27). Labelling of mesophyll and vasculature was also carried out by Alice Baillie (data not shown) and no differences were observed in these data either. pCA1:AdPMEI1 1-1 appeared to have a difference in the shape of the mesophyll cells, with the structure appearing

less ordered (Figure 5.27.B) but further work is needed to confirm and define this observation. Immunolabelling was carried out by Alice Baillie

5.6.4 Gas exchange analysis of transgenic lines

Gas exchange analysis was conducted on the transgenic lines to determine if there are any changes to carbon assimilation. A-Ci curves were conducted to determine carbon assimilation in response to differing CO₂ concentrations and light curves were conducted to determine the assimilation response to changing PAR.

Assimilation was significantly reduced at CO₂ concentrations about 400ppm in the pCA1:AtPMEI2 12-4 compared to both Col-0 and the sister line, where the insert had been segregated out (Figure 5.28.A) while pCA1:AtPMEI2 16-6 showed no difference (Figure 5.28.B). pCA1:AdPMEI1 1-1 showed no difference to Col-0 but surprisingly the sister line had significantly increased assimilation at the higher CO₂ concentration (Figure 5.28.C). pCA1:AdPMEI1 2-7 had significantly reduced assimilation compared to Col-0 while the sister line had significantly increased assimilation (Figure 5.28.D).

Similar patterns were observed from light curve measurements. Assimilation was significantly reduced in the pCA1:AtPMEI2 12-4 compared to both Col-0 and the sister line, although the sister line showed a slight reduction compared to Col-0 (Figure 5.29.A) while pCA1:AtPMEI2 16-6 showed no difference to the sister line however both lines were slightly reduced compared to Col-0 (Figure 5.29.B). pCA1:AdPMEI1 1-1 showed no difference to either Col-0 or the sister line (Figure 5.29.C). pCA1:AdPMEI1 2-7 had significantly reduced assimilation compared to both Col-0 and the sister line (Figure 5.28.D).

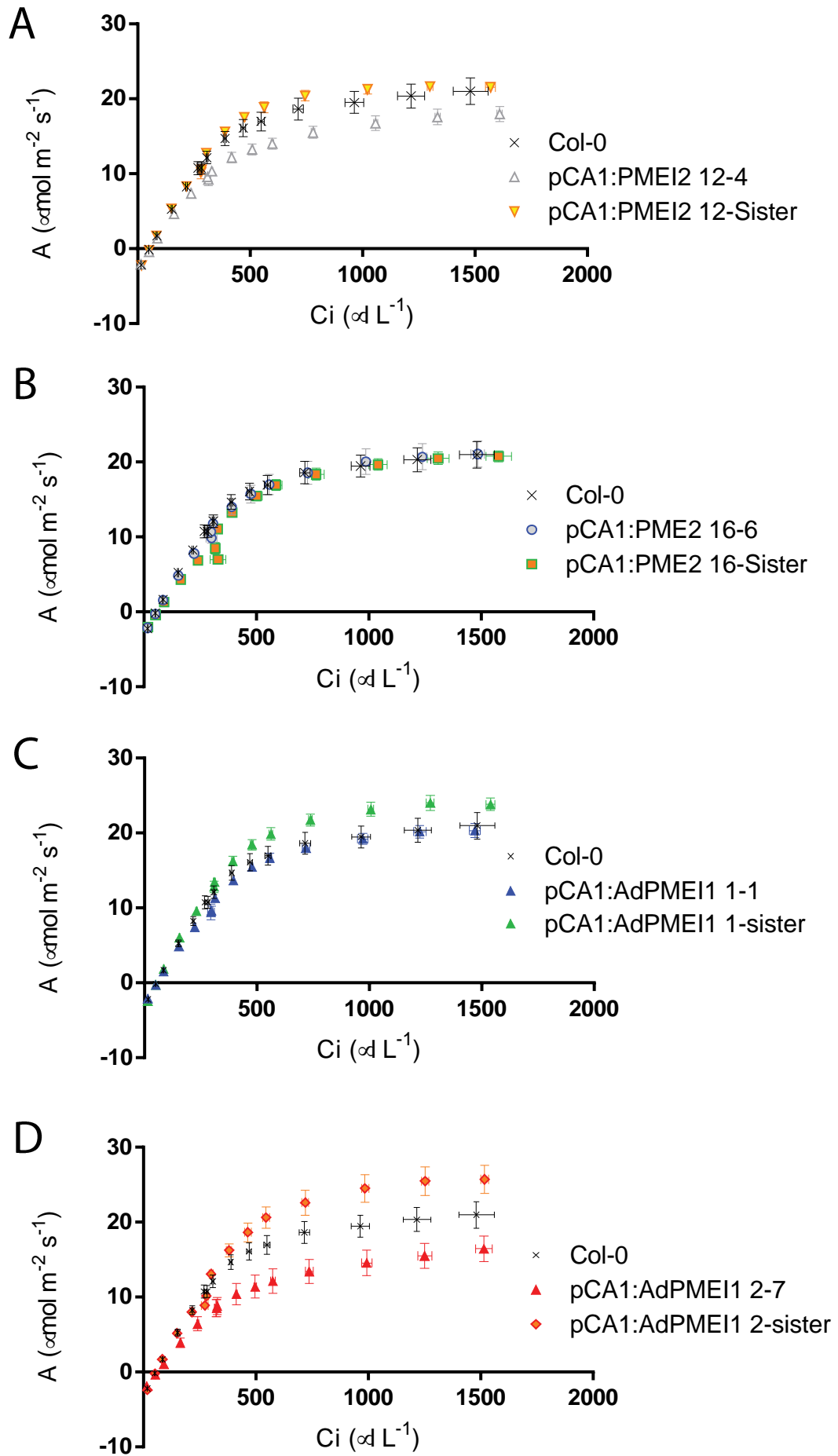


Figure 5.28. Gas exchange analysis of transgenic lines. A-Ci curves measuring assimilation in response to varying CO₂ concentration. A) pCA1:AtPMEI2 12-4 has significantly reduced assimilation at above ambient CO₂ concentrations compared to the sister line and Col-0. (B) No difference is observed between pCA1:AtPMEI2 16-6 and either the sister line or Col-0 (C) No differences are observed between pCA1:AdPMEI1 1-1 and Col-0 however the sister line shows significantly increased assimilation at the higher CO₂ concentrations. (D) pCA1:AdPMEI1 2-7 has significantly reduced assimilation than Col-0 while the sister line had significantly increased assimilation compared to Col-0. Data are means of n=6, error bars represent SEM.

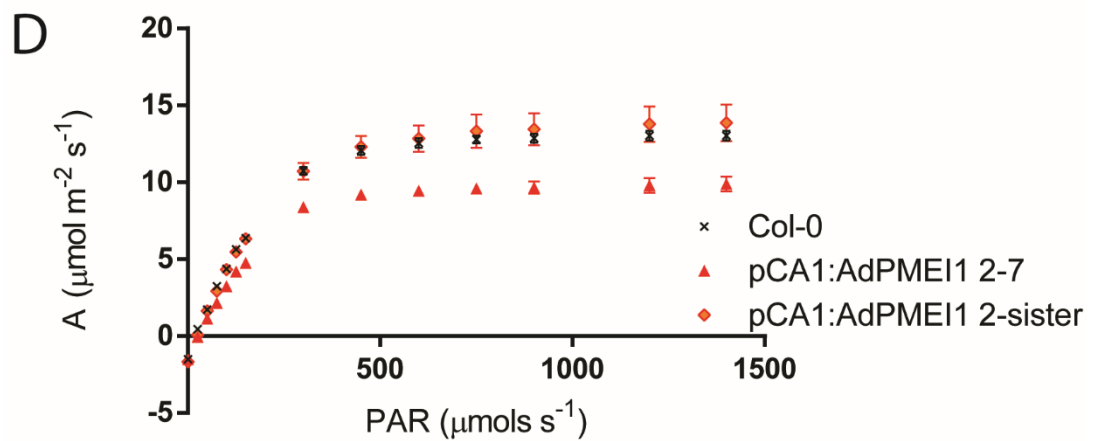
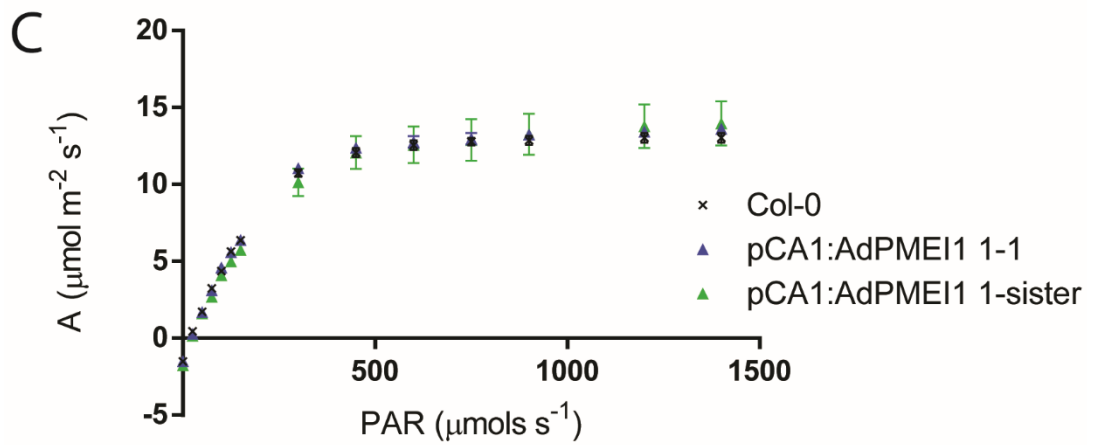
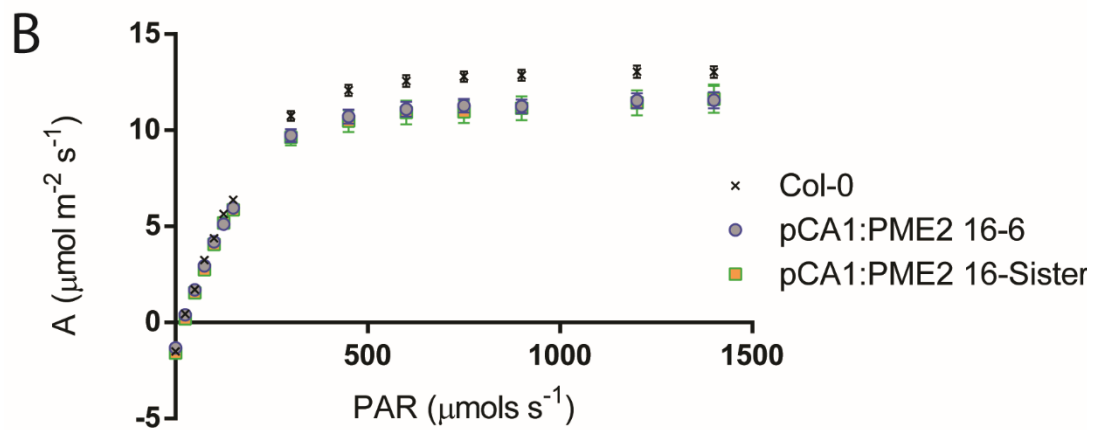
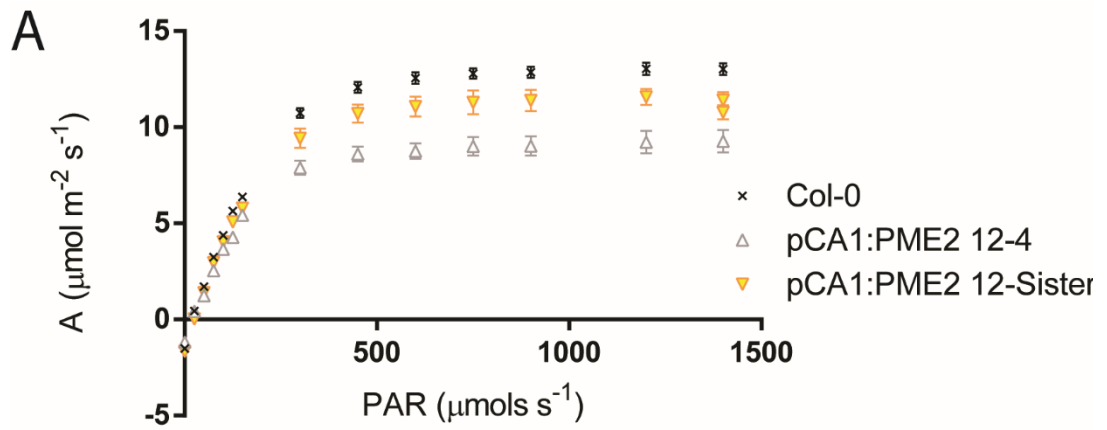


Figure 5.29. Gas exchange analysis of transgenic lines. Light curves measuring assimilation in response to varying PAR levels. A) pCA1:AtPMEI2 12-4 has significantly reduced assimilation at above ambient CO₂ concentrations compared to the sister line and Col-0. (B) No difference is observed between pCA1:AtPMEI2 16-6 and the sister line however both have reduced assimilation compared to Col-0 (C) No differences are observed between pCA1:AdPMEI1 1-1 and Col-0 or the sister line. (D) pCA1:AdPMEI1 2-7 has significantly reduced assimilation than both Col-0 and the sister line. Data are means of n=6, error bars represent SEM.

5.7 Discussion

5.7.1 Cell wall mutants and stomatal function.

The availability of transcriptomic data has allowed the identification of a large number of cell wall related genes which are putatively expressed at a higher level in guard cells than the rest of the leaf. The fact that the majority of these genes are pectin-related underlines the importance of the pectin network to stomatal function. It is unfortunate that a number of the lines ordered from NASC tested negative for the presence of the insertion. Other lines are available from NASC to enable this analysis to continue in the future.

EFP browser data suggests that all of the genes selected for this analysis are expressed only in mature guard cells and not in stomatal lineage cells. This means it is not surprising that no changes to stomatal size or patterning was observed in any of the NASC insertion lines. Growth analysis reveals that there are no major developmental differences between any of the lines and thermal imaging suggests that a similar level of transpiration is occurring at ambient conditions between all of the lines. At5G19730, which is a pectate lyase gene, was the only line to show any growth abnormality. It shows reduced initial growth suggesting that the plants take longer to get established. By 40 days the plants are indistinguishable from Col-0 and the rate of the growth appears very similar to Col-0. The EFP browse suggest that this gene is expressed highly in the seeds and it is possible that this delay in establishment is due to a defect in seed quality rather than an alteration to the stomata. In the future it would be interesting to analyse the seeds of this line to look for abnormalities in seed coat or germination. There was no observed difference in stomatal function in response to CO₂ in this

line, showing that this pectate lyase gene is not required for correct stomatal function.

Contrasting stomatal responses between members of the PME/PMEI family

An especially large number of genes identified as highly expressed in guard cells are from the PME/PMEI family. As discussed in Chapter 4 there is predicted redundancy between the members of this family and it is possible that double or triple mutants will need to be created to detect a phenotype.

Of the 4 PME genes analysed in this chapter, 2 had altered stomatal movement in response to CO₂ while 2 showed no change to Col-0 plants.

This highlights the complexity of studying the PME family and suggest that distinct PME genes have distinct roles in the guard cell wall. At2G26440 has a very similar response to *pme6-1* plants discussed in Chapter 4. No stomatal movement was observed in response to high CO₂ or low CO₂ suggesting that the stomata are non-functional. Further work must be done to assess the stomatal responses to other stimuli, such as ABA and light do determine if the stomata are unable to move or if they are simply insensitive to CO₂. In contrast AT5G19730 has a much subtler phenotype the Col-0. AT5G19730 stomata are more open than Col-0 at ambient conditions despite there being no difference in stomatal size. The stomata are still able to open and close to the same extent suggesting that function is not impaired rather the guard cell aperture at ambient CO₂ has shifted. It is possible that the mechanical advantage that guard cells have over neighbouring epidermal cells has been increased so that stomata are slightly more open under standard conditions. Further testing is needed to confirm this.

The two PMEI genes tested also had differing phenotypes. AT3G62820 was able to open to a greater extent than Col-0 but had a normal stomatal closing

phenotype while AT4G25260 had a normal stomatal opening phenotype but appeared unable to close.

5.7.2 FOCL is required for stomatal function.

The larger stomata observed in *focl* plants combined with a reduction in pavement cell density lead to a significantly increased stomatal index. It has been shown that *focl* is expressed in mature guard cells, not in stomatal precursors or epidermal cells (Hunt et al, unpublished) which means that the difference observed in epidermal patterning is likely a secondary effect, rather than a direct effect on stomatal patterning. It is likely that the plug which covers the majority of the stomata in *focl* plants limits the ability of the plant to assimilate carbon through its stomata. The increase in stomatal size and index may be an attempt to combat this but providing a greater surface area for CO₂ diffusion.

It is likely that this expected reduction in carbon assimilation results in the slower growth observed in *focl* plants. It appears that although *focl* plants take longer to get established and grow at a slower rate than Col-0 plants they eventually reach similar size. In the future a repeat of the growth experiment should be carried out over a longer time period to enable *focl* plant growth to plateau. It is also possible that the reduction of growth is attributable to a reduction in plant transpiration due to the stomatal covering. A reduced transpiration stream can lead to reduced nutrient uptake in the roots and it is possible that this is a factor in the reduced growth rate. *focl* stomata are unable to close their stomata as much as Col-0, so it is likely that to an extent reduced transpiration during the day is counteracted by increased night-time transpiration due to more open stomata. At night time carbon fixation does not occur as the light dependant reactions of photosynthesis are unable to proceed. This suggests that carbon limitation is the most likely explanation for the slow growth rate.

It is not clear if the increased stomatal apertures observed at high CO₂ is due to an inability of the stomata to close or if the increased carbon concentration has a lower impact in *focl* plants as the covering is limiting uptake. Due to its increased size, to reach the same pore width requires a greater shape change in *focl* plants than in Col-0 and it is possible that mechanical limitations prevent this extent of closure. No alterations to cell wall structure were observed in *focl* plants, suggesting that no fundamental structural alterations had occurred to compensate for the change of cell size. Another, simpler explanation is that perhaps the stomatal covering itself is limiting stomatal movement. In transverse sections the covering can be seen to balloon up above the stomata. It is likely that stomatal opening will pull the covering taut and then either the covering must prevent the stomata from opening further or the covering will tear. It is possible that torn coverings due to stomatal movement account for the 10% of stomata which are uncovered in the *focl* line. These uncovered stomata appear to have extended cuticular ledges which is consistent with a torn covering.

Thermal imaging provides a snapshot of plant temperature. When plants are grown in the same conditions then variations in temperature are largely due to differences in transpiration. Small changes in temperature can have large knock on effects on plant processes. *focl* plants were significantly warmer than Col-0 plants. This temperature change is likely due to a limited capacity for transpiration due to the stomatal covering in the *focl* plants. It is important to note that plants were imaged at the same age (45 days post-germination) and that this means that *focl* rosettes are smaller than Col-0. It has been shown that temperature does not vary substantially throughout the latter part of plant development (Sarah Carroll, personal communications) so it is likely that this difference in size does not have an impact. Nevertheless, this experiment should be repeated in the future over a range of ages so that

temperature can be assessed at the same age but also at the same size/developmental stage. This reduction in transpiration is likely to have a number of effects on the plant. As discussed above, nutrient acquisition may be reduced due to a weaker transpiration pull. It seems intuitive to think that *focl* plants would have an advantage under drought conditions. Surprisingly it was shown that excised *focl* leaves lost water at a faster rate than Col-0 leaves (Hunt et al, unpublished), possibly due to the inability of *focl* plants to close their stomata to the same extent as Col-0. A future experiment assessing the response of *focl* plants to drought would be beneficial for understanding how this mutation impacts on the water relations of the plant.

The formation of substomatal air spaces is a relatively unknown process. It is thought that a combination of mesophyll cell separation and mesophyll cell expansion (shizogeny and expansigeny) are responsible for the creation of these cavities. It is not clear whether the formation of a sub-epidermal airspace initiates the formation of a stomata above it or if the formation of a stomata causes an airspace formation below it. These problems are not trivial to decipher and it is possible that mutants such as *focl* can help inform this debate. It is clear from looking at *focl* histology that the presence or absence of the pore covering is strongly impacting on the substomatal airspace. It is possible that intercellular CO₂ diffusion is linked to mesophyll porosity, so intercellular architecture may change to maximise carbon uptake from the available CO₂. It is interesting that *focl* seems to have variable substomatal cavity size depending on whether the stomatal pore is covered or not which suggests that, at least to an extent, stomata are dictating the extent of the substomatal cavity. Further replication of this work is needed, along with a quantification of airspace under uncovered and covered stomata.

Histological analysis of *focl* plants suggest that the stomatal covering is an outgrowth of the cuticular ledge. This finding is purely observational and

further work is needed to confirm this. Hunt et al (unpublished) showed Nile Red, a lipophilic stain, binding in the stomatal covering suggesting that the covering is lipid rich, which is consistent with a cuticular layer. It is not clear if the cuticle is present before stomatal formation and fails to separate or if the cuticular ledges form after stomatal division and grow outwards and join together. Further study, especially histological analysis of young plants containing immature stomata and stomatal precursors, would help shed light on the formation of the stomatal covering. It is likely that the relationship between cuticle and the cell wall is important in the formation of the cuticular ledges. It has been proposed in the past that HGRPs can act as a scaffolding for the correct deposition and anchoring of cell wall components (Cannon et al., 2008). It is hypothesised that *FOCL* plays a role in guiding the formation of the cuticular ledges, along with anchoring the ledges to the guard cell walls (Hunt et al, unpublished).

5.7.3 Creation of transgenic lines

The ability to create transgenic lines in *A. thaliana* is a powerful research tool. In this chapter homozygous lines have been created for 9 constructs as detailed in (Table 5.2). The full set of 9 lines, AtPEMI1 AtPMEI2 and AdPMEI1 expressed either in the mesophyll, epidermis or guard cells should be a useful in further understanding the role of PME and PMEI genes in the maintenance of pectin methylation status in the leaf. Unfortunately, only 2 of these constructs were completed in time for preliminary characterisation, both of which were under control of the mesophyll promoter, meaning that limited conclusions can be drawn from this work as much work is left to be done.

Stomatal patterning has not been altered as stomatal density, size and index are unaffected. Only 2 lines for each of the two constructs were assessed here as part of the preliminary studies however a larger number of lines are

available for future characterisation. The lack of difference in rosette temperature also suggest that stomata are functioning normally, at least under ambient conditions. A priority for future work is the extraction of RNA from leaves to carry out RT-PCR to ensure that the transcripts are present.

As CA1 is a mesophyll promoter it is unsurprising that the immunolabelling did not reveal any differences in guard cell wall composition. The analysis of epitopes under pGC1-D1, the guard cell specific promoter is more likely to reveal guard cell differences. Plant growth was variable between the lines with some lines being smaller and appearing to be lighter in colour (observational, data not shown). At this stage of characterisation, it is possible that these differences are due to position effect of the insertion rather than changes induced by the expression of the genes themselves. Sequencing of the region either side of the insertion should provide information about the location of the gene and if it is likely to have disrupted a native gene.

The immunolabelling revealed what appeared to be abnormal leaf structure in AdPMEI1 1-1 which can be observed in Figure 5.27 in panels A-C, the cell walls surrounding the mesophyll cells appear to be more convoluted (wavy) compared to the straighter cells in Col-0. Further characterisation is necessary to define and confirm this potential phenotype, however changes to cellular shape and circularity can have impacts on carbon diffusion and transport within the leaf so this is an interesting avenue to follow up on. Detailed histological staining and 3D confocal imaging could shed light on any change in sub-epidermal structure. This potential epidermal change does not translate to a change in gas exchange in either the A-Ci curves or the light curves. Mesophyll structure changes could have impacts on carbon assimilation as path length and cell surface area are both important factors in

carbon assimilation. Gas exchange data revealed that pCA1:AtPMEI2 12-4 and pCA1:AdPMEI1 2-7 had a reduction in maximum assimilation in both light curves and A-Ci curves. Confocal microscopy would allow measurement of the mesophyll area to determine if an altered leaf structure is responsible for these differences.

It remains to be seen if the PME genes will be functional in the overexpression lines, PME and PMEI genes are known to function differently under different conditions (Denès et al., 2000) and it is possible that these genes will not be fully functional in the mesophyll, epidermis or guard cells.

In conclusion it appears that a large number of cell wall related genes are expressed at a higher level in the guard cells than in the rest of the leaf, and in particular PME/PMEI genes. Knockout of some of these genes have implications for stomatal function. Combining this approach with a transgenic approach to introduce cell genes that are not usually expressed may reveal new insights into the structure and maintenance of the guard cell walls and the function of the PME/PMEI family. Targeted modulation of the guard cell wall as a way of modifying stomatal function may be made possible by altering the expression of these guard cell wall genes.

Chapter 6. Atomic force microscopy

6.1 Introduction

The Atomic Force Microscope (AFM) is one of a series of scanning probe microscopes (SPMs) developed in the 80s and early 90s by Binnig and Rohrer (Rugar and Hansma, 1990). In contrast to conventional microscopes SPMs do not visualise a sample using light, instead they feel the surface of the sample using a probe. The AFM has the potential to achieve electron microscopy level resolution but there is no need for fixation or pre-treatment of samples, meaning living samples can be imaged. On flat surfaces the AFM has the potential of imaging with atomic resolution. Although this resolution is impossible to achieve on biological samples, it can still achieve sub-molecular resolution for the majority of biopolymers.

In simple terms the AFM (Figure 6.1) consists of a sharp tip (Figure 6.2), which feels the sample, mounted on a cantilever which allows the tip to move up and down. The tip tracks the surface of the sample which is moved in the x and y directions to form a raster image. The tip is usually fabricated from a silicon polymer and the shape and properties of the tip are extremely important in determining the resolution (Butt et al., 2005; Cappella and Dietler, 1999). The sample is mounted onto a piezoelectric transducer capable of moving in the x, y and z directions. In order for the tip to provide any information about the sample there must be a method of tracking the movements of the cantilever. This is most commonly done by an optical detection system, as illustrated in Figure 6.1. A laser beam is focussed on the

cantilever tip and the reflected light sensed by a photodiode. The intensity and positioning of light hitting the photodiode changes as

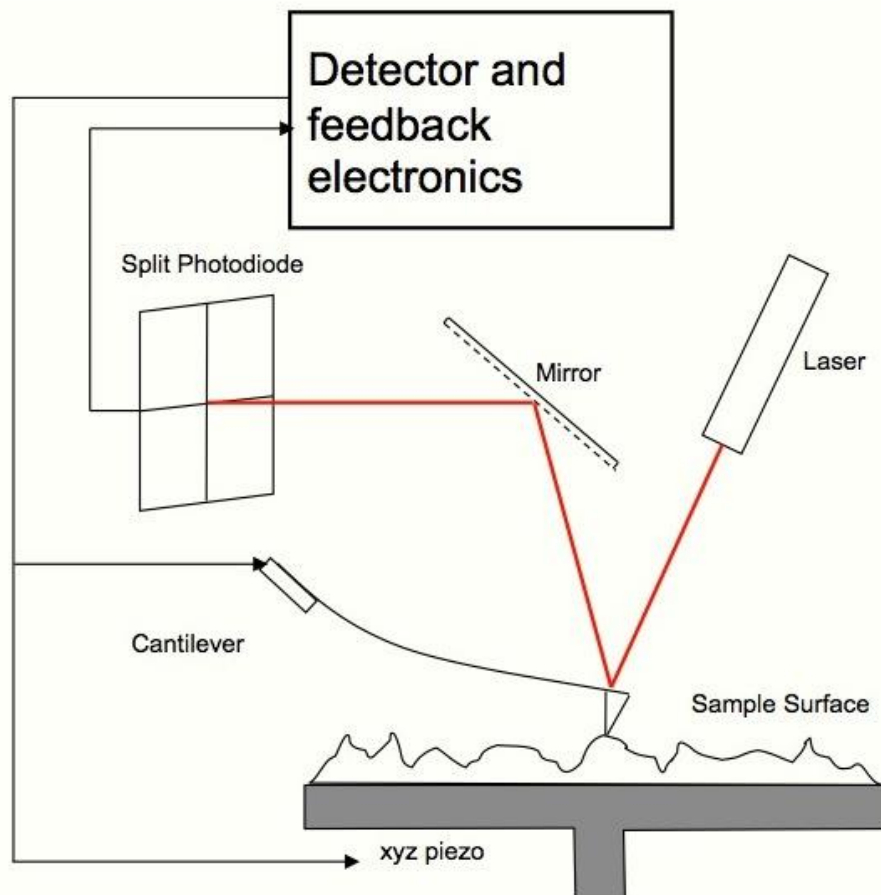


Figure 6.1. Setup for a typical Atomic Force Microscope. The sample is mounted on a piezoelectric stage capable of moving in XYZ. The cantilever has a sharp tip tracking the surface topography of the sample. The movement of the cantilever is detected by laser deflection. The laser is focused on the tip of the cantilever and reflected into the centre of a quadrant split photodiode. The movement of the cantilever causes the deflected laser to move on the split photodiode allowing calculation of the surface topography. Image from Carter et al, unpublished

the tip moves due to the topography of the sample. This is used to construct an image of the surface of the sample. Alternatively, the cantilever can be held at a constant deflection and instead the sample is moved in z , with the movements of the piezoelectric transducer being recorded instead. The individual components of the AFM make a system which allows precise

control of the tip and sample at all times to allow accurate reading (Giessibl, 2003; V. V. Morris et al., 2010; Rugar and Hansma, 1990).

To maintain accuracy and resolution when imaging, it is important to minimise temperature changes in the surrounding environment to prevent thermal expansion of the AFM materials (Cappella and Dietler, 1999). Similarly, background vibrations must be minimised to reduce displacement of the scanning tip if high resolution is to be maintained. AFMs are designed with these factors in mind, materials are chosen with similar thermal expansion coefficients and the design aims to reduce ambient resonance as much as possible (Giessibl, 2003). Despite the ingenuity of design, it is still important to minimise environmental variations and many AFM systems are kept in temperature controlled rooms and suspended on air tables to maintain stability.

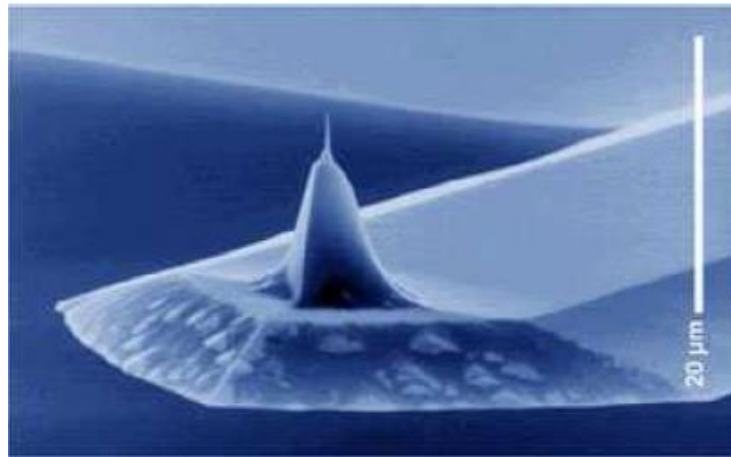


Figure 6.2. AFM cantilever. An SEM image of a silicon cantilever with a 2nm sharpened tip. Image taken from Giessibl, 2003.

Modes of operation

There are many modes of operation for AFMs making it a very versatile tool. The three main modes are contact mode (also known as constant force

mode); tapping mode; and non-contact mode. In contact mode the tip directly touches the sample while it is scanned. The tip is brought into contact with the sample so that it is deflected by a pre-set amount. The piezoelectric scanner moves the sample underneath the tip in a raster fashion. Movements in the z direction maintain the cantilever at a constant deflection and the repulsive forces between the sample and tip are measured (Butt et al., 2005). This mode allows for relatively high contrast but can cause damage to the sample. An important advantage is that this mode allows the use of standard and relatively cheap tips. When viewing samples in air under this mode it is susceptible to capillary force (V. Morris et al., 2010). This is where the tip traps water vapour between it and the sample. When the tip and sample are in close proximity a meniscus force forms which pulls the tip onto sample trapping it. This can damage the sample but imaging the sample under liquid can eliminate this.

Tapping mode uses an electrical oscillator to excite the cantilever so that it taps repeatedly on the surface of the sample. This mode minimises the effects of capillary force and also reduces the shear forces acting upon the sample during a scan. This mode can be used both in air and under liquid.

When using non-contact mode, the tip does not come into contact with the sample at any time. Instead the tip is vibrated above the sample at a known amplitude. Van der Waal forces act between the oscillating tip and the sample. These forces dampen the oscillation of the tip, so as the tip gets closer to the sample the forces get stronger and, thus, the dampening effect gets stronger. The reduction in amplitude of oscillation can be measured to provide information about the topography of the sample. This mode eliminates damage to the sample caused by the tip and allows extremely high contrast. Non-contact mode has relatively slow scan speeds and so is rarely used.

The above modes can all be used to image the topography of a sample at high resolution. This topographical data is relatively easy to interpret although care must be taken to avoid double tip effects where features of the sample are repeated throughout the image. Another useful application for plant biologists is the potential to map mechanical properties of the sample. The tip is lowered into contact with the surface of the sample which it then indents. In hard samples as the tip makes contact with the sample the deflection of the cantilever will increase linearly with a slope of 1. When imaging softer samples, such as biological specimens, the deflection of the cantilever will be more gradual due to the deformation of the sample. This means that in soft samples the deflection of the cantilever is dependent on the viscoelastic properties of the sample. These measurements are known as force measurements and are increasingly being used by biologists looking to understand the mechanical properties of biological samples. Using the AFM in force mode generates data in the form of force-versus distance curves (force curves) (Butt et al., 2005). To calculate the force (F) the deflection of the cantilever (Z_C) is multiplied by the spring constant of the cantilever (K_C) as shown in Equation 6.1 (Butt et al., 2005). To calculate the distance, otherwise known as the tip-sample separation (K_D) then the deflection (Z_C) is added to the position of the piezoelectric scanner (Z_P) (Equation 6.2).

Equation 6.1 Force applied

$$\text{Force } F = K_C \times Z_C$$

Equation 6.2. Distance

$$\text{Distance } D = Z_C + Z_P$$

The sensitivity with which the deflection is measured and the mechanical properties of the cantilever itself are important factors affecting the accuracy of the force measurements taken. These aspects have received considerable

attention in previous reviews (Butt et al., 2005; Cappella and Dietler, 1999). Acquiring force measurements are simpler now as much of the mathematical calculations and calibration can be done through automatic processes included in most AFM processing software. Figure 8 shows an example raw data force curve. The key aspect to note here is that the data starts from the right of the graph where the tip and sample are separated so no forces act between them. The tip and sample are then brought together and the forces measured as the cantilever presses onto the sample; this is called the approach. The tip and sample are then separated, otherwise known as retraction, until no forces act between them again (Butt et al., 2005). Mechanical information about the sample can be extracted from the gradient of the contact region of the curve (between 0.0 and 0.2).

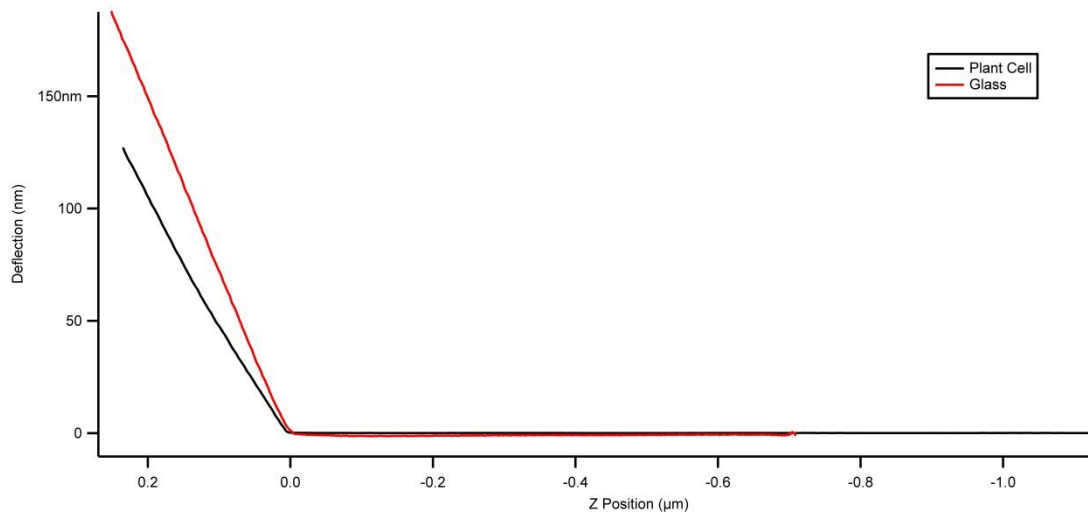


Figure 6.3. A force curve comparing a plant sample and a glass sample. An idealised force curve showing cantilever deflection on glass, which doesn't deform and so shows the innate properties of the cantilever. The plant sample causes less cantilever deflection as the sample itself is deformable.

Analysis of the force curve, specifically the contact section (Figure 6.3), allows determination of sample properties such as elasticity, stiffness and adhesion (Butt et al., 2005). The stiffness of the sample can also be defined as the effective spring constant of the sample, i.e. the force needed to displace

the sample by a specific amount. This is obtained from the gradient of the force curve. Elasticity can be defined in several ways and, for the purpose of this project, elasticity describes the elastic modulus, i.e. the relationship between stress and strain as described by the apparent Young's modulus. A stiffer material has a higher Young's modulus. During this chapter the term stiffness refers to a higher Young's modulus while the term softness refers to a lower Young's modulus.

AFM was first applied to biological samples in the late 80s (Radmacher et al., 1992) and has been conducted on plants material since the early 90s (Kirby et al., 1996). Early work was carried out on cell walls of carrot, apple and water chestnut (Kirby et al., 1996). This work had numerous flaws. Firstly, the samples had been extensively processed in a manner which ruptures the cells allowing internal cellular contents to be washed away. The fact that samples were imaged in air led to problems with the cantilever being pulled to the surface due to meniscus forces. Also the drying of the cell wall fragments meant imaging time was limited to an hour. Despite these limitations the authors were able to see fibrous structures, assumed to be cellulose microfibrils, and were able to measure microfibril thickness.

Analysis of isolated cell wall fragments can provide useful information regarding the properties of individual structural constituents. If we want to achieve a picture of mechanical properties within whole plant structures, then this approach is limited as information about how these constituents interlink and function in a whole plant environment is lost. More recently AFM force data has been used to measure the mechanical properties of plant structures *in vivo*. Force measurements of the *Arabidopsis* shoot apical meristem (SAM) reveals spatial differences in stiffness within the SAM, with faster growing cells at the tip being softer than the slower growing cells at the base and sides of the meristem (Milani et al., 2011). Further work on the

SAM in *Arabidopsis* reveals localised softening precedes organ initiation. The authors suggest that the mechanical changes are driven by changes to the pectin network (Peaucelle et al., 2011) and in further work go on to show that auxin induces a reduction in rigidity which allows organ outgrowth (Braybrook and Peaucelle, 2013). These studies highlight how atomic force microscopy can be used to study live plant tissue to address complex developmental and biological questions.

AFM offers the opportunity to make substantial advances in our understanding of the mechanical properties of cell walls. Combining AFM measurements with other tissue measurements, such as level of pectin methylesterification or cell wall constituents, will allow us to correlate chemical changes in cells with changes in tissue mechanics. Recent work has shown that pectin demethylesterification in the *Arabidopsis* meristem contributes to an increase in tissue elasticity prior to primordia formation (Peaucelle et al., 2011). This demonstrates an observable link between chemical changes and tissue mechanics in the regulation of plant development. Similar insights could provide valuable information about the mechanism of stomatal function and identify what role, if any, the surrounding cells play in supporting and accommodating changes in guard cell shape and size.

This chapter describes the development and testing of an atomic force microscopy technique to analyse *A. thaliana* leaf samples in order to measure the mechanical properties of guard cells and their surrounding epidermal cells in living tissue.

6.2 Development of an AFM method for imaging live leaf samples

6.2.1 Plant growth

The scanning probe microscope, as opposed to the optical microscope, is impacted by the features of the leaf surface. Cuticular waxes are known to be soft and preliminary work was hindered by the tip adhering to the cuticular waxes.

It has been suggested that high humidity grown plants, such as those grown on MS media in culture dishes, have lower levels of cuticular waxes than those grown on soil. Although this has been the subject of some debate within the literature, it remains unclear the extent which humidity impacts on cuticular wax formation. Therefore, we tested material grown on MS media against those grown on soil to determine the quality of images that were possible to obtain for in order to determine which growth protocol to use.

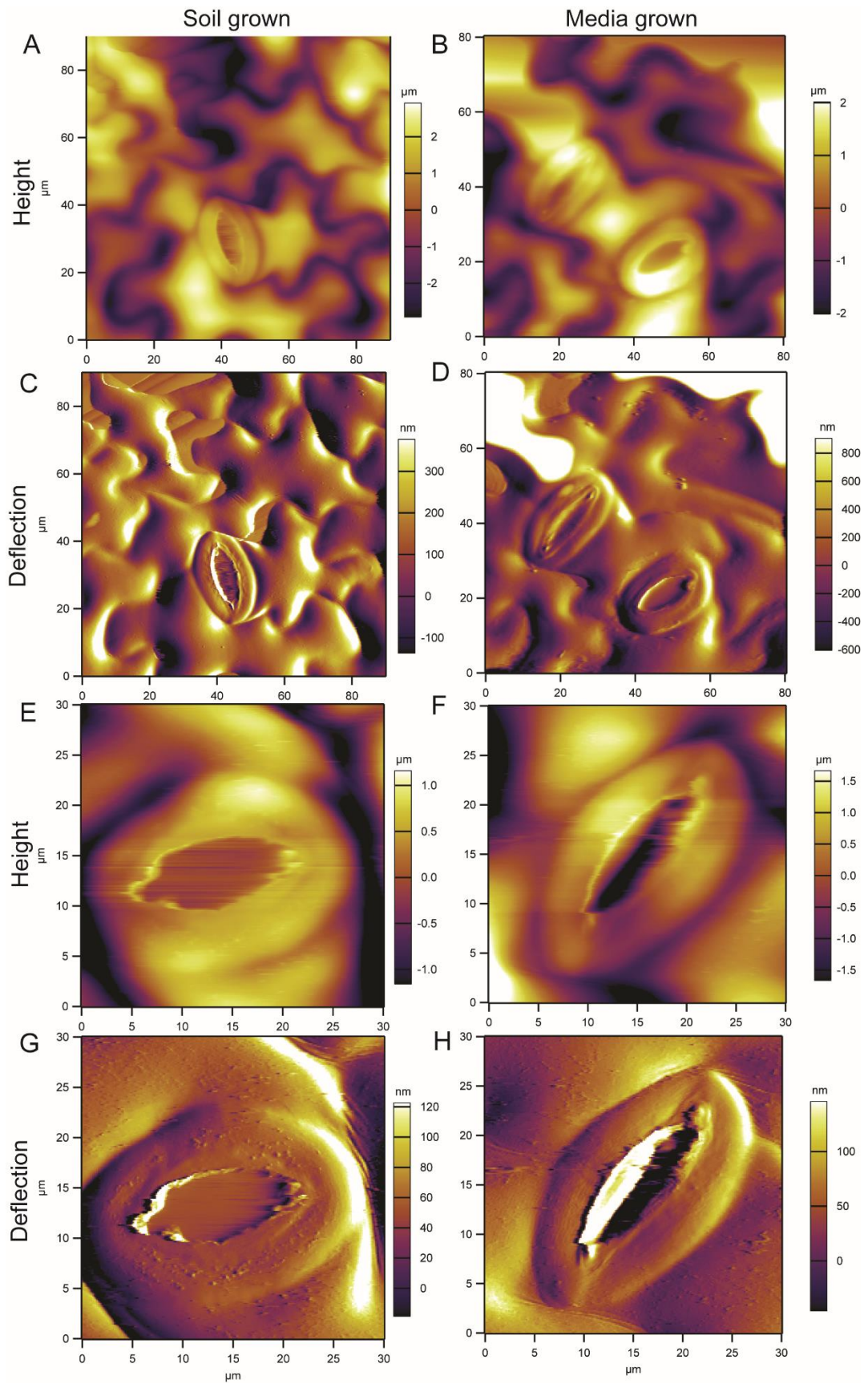


Figure 6.4. Topographical images of stomata from plants grown either on soil (left column) or ½ MS media (right column) no discernible difference in quality was observed between growth conditions (A-D) show zoomed out topography of abaxial surface of the leaf demonstrating the size of scan which is achievable, (A-B) height maps showing outline of stomata and surrounding epidermal cells. (C-D) cantilever deflection maps of the leaf epidermis showing the topography of the leaf including topographical features such as surface waxes (*). (E-H) Close up image of an individual stomata. (E-F) Height maps reveal little difference in image quality between the growth treatments. (G-H) cantilever deflection maps reveal what appears to be cuticular waxes on the surface of the stomata and surrounding cells. These features are present in both growth conditions and soil grown plants do not have appreciably more surface waxes than media grown plants. Images are representative from 8 replicates.

The data in Figure 6.4 show that image quality is comparable between both techniques and the presence of what appear to be cuticular waxes (indicated by * in Figure 6.4.G and H) are visible in both growth treatments to a similar extent.

Our initial data suggest that image quality is not affected by growth conditions but it was noted that after imaging for a long time (more than 1 hour) the image quality decreased and the sample started adhering to the tip. It was hypothesised that this is due to surface structures, such as phenolic waxes on the leaf, adhering to the tip over time combined with a decrease in the sharpness of the tip. Plants grown by both methods were tested to determine the maximum time imaging could be conducted. A stomata was found and centred on during the first 10 minutes of imaging and then the stomata was imaged repeatedly using contact mode to take sequential topographical images. Each scan took 2 minutes to complete and scanning was continuous. Image quality was assessed and the length of time until a subjective quality drop was observed in 3 sequential images was noted for each treatment. The time at which the sample started adhering to the tip was also noted.

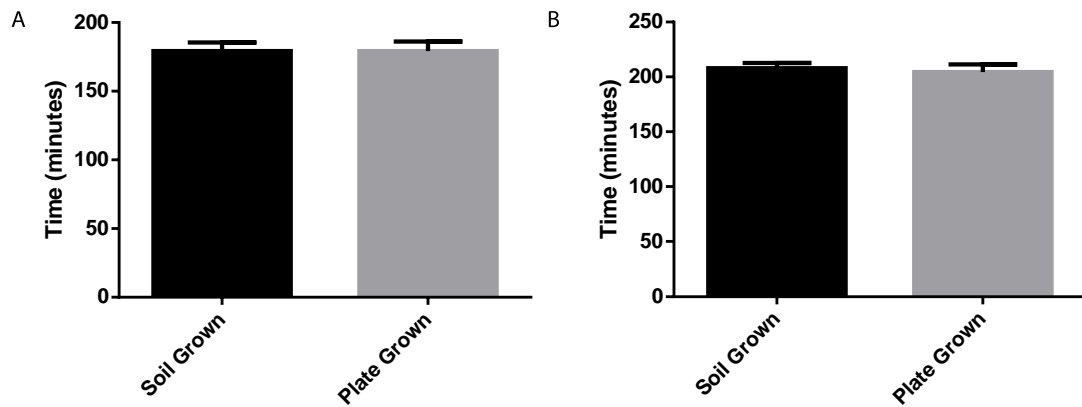


Figure 6.5. Length of time samples can be imaged. (A) The length of time a sample can be continuously imaged for before noise starts appearing on the images resulting in a drop in image quality. (B) The length of time samples can be imaged for before the sample starts adhering to the tip causing severe reduction in image quality and damage to the AFM tip. Error bars=SEM, no statistical differences were observed by students t-test, $p>0.05$, $n=10$

These data in Figure 6.5.A show that imaging can be conducted for the same length of time under either growth condition (soil and MS media). The data also show that the maximum length of time for imaging with the same tip is roughly 4 hours.

Although there is no advantage to either growth technique in terms of AFM image quality, the growth conditions could however impact stomatal function. MS media grown plants experience high humidity and stomatal function has previously been linked to humidity. A stomatal function bioassay was conducted to determine the best growth technique for optimising stomatal function.

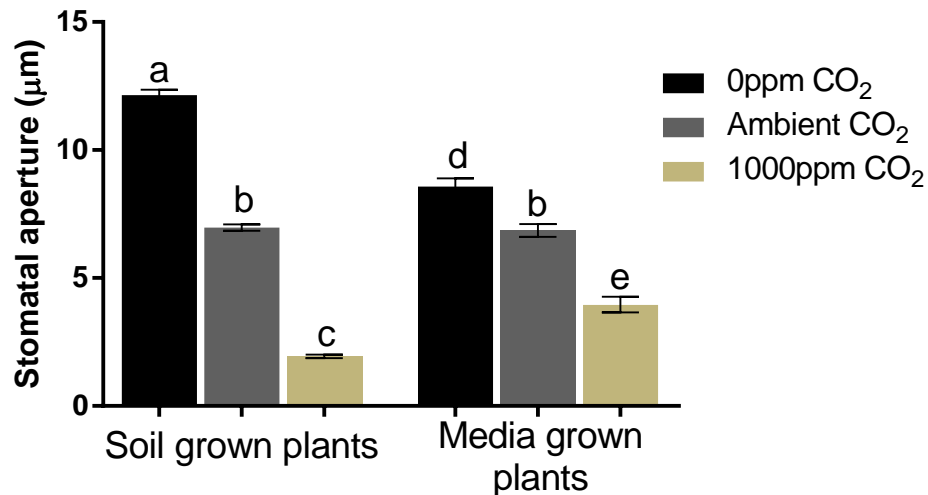


Figure 6.6. Comparison of stomatal responses to CO₂ for plants grown on soil and plants grown on MS media. Soil grown plants have a greater range of stomatal apertures compared to media grown plants. Error bars=SEM, statistical differences determined by anova using multiple comparisons, n=12 plants (20 stomata measured per plant from a single leaf).

The data in Figure 6.6 clearly show that stomata grown on plates have more limited movement compared to those grown on soil. For this reason, all further analysis was carried out on soil grown plants.

6.2.2 Sample preparation

Although AFM can be carried out on live tissue the leaves need to be excised from the plant. The AFM has a limited Z-range of 12µm so leaf selection was crucial to get the flattest leaves. The third true leaf was selected due to the fact that they are old enough to have mature stomata but are still relatively young and so have reduced topography compared to older leaves. Leaf 3 was tested from plants of different ages and imaged using traditional light microscopy to assess the number of mature stomata compared to stomatal precursor cells. This was aimed at finding a sampling age that best represents the compromise between number of mature stomata and leaf topography.

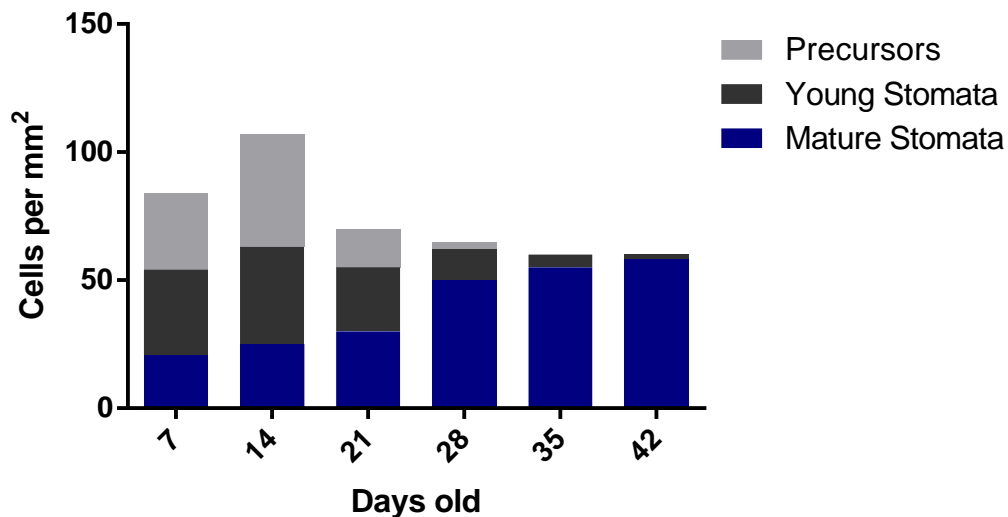


Figure 6.7. Stomatal complement from plants taken at weekly intervals until senescence. Stomata from 28 days old plants appear best for imaging. This is the youngest point at which the majority of stomatal lineage cells are mature stomata.

From these data (Figure 6.7) the third true leaf from 28 day old plants was selected as the optimum for imaging. 28 day old plants have a range of stomatal ages, including precursor cells, allowing assessment of all stages of stomatal development at the same plant developmental stage. Day 28 is the latest age at which all developmental stages of stomata can be imaged.

6.2.3 Mounting the sample

Sample mounting is crucial to obtaining good quality AFM images. Any sample movement during image acquisition would cause the rest of the image to be distorted or introduce noise or double tip effect into the image. Although the need for good sample adherence is important caution is needed to select an adhesive which is not toxic to the plant.

Several mounting methods were tried; microscopy mounting media, dental impression media, glue, double-sided tape. Samples were adhered in petri dishes to facilitate the addition of buffers to the sample during imaging. 8

samples of each type were mounted and submerged in stomatal resting buffer with addition of 10 μ m ABA to promote stomatal closure and 8 samples were submerged in stomatal opening buffer to assess the range of stomatal opening under each type of media.

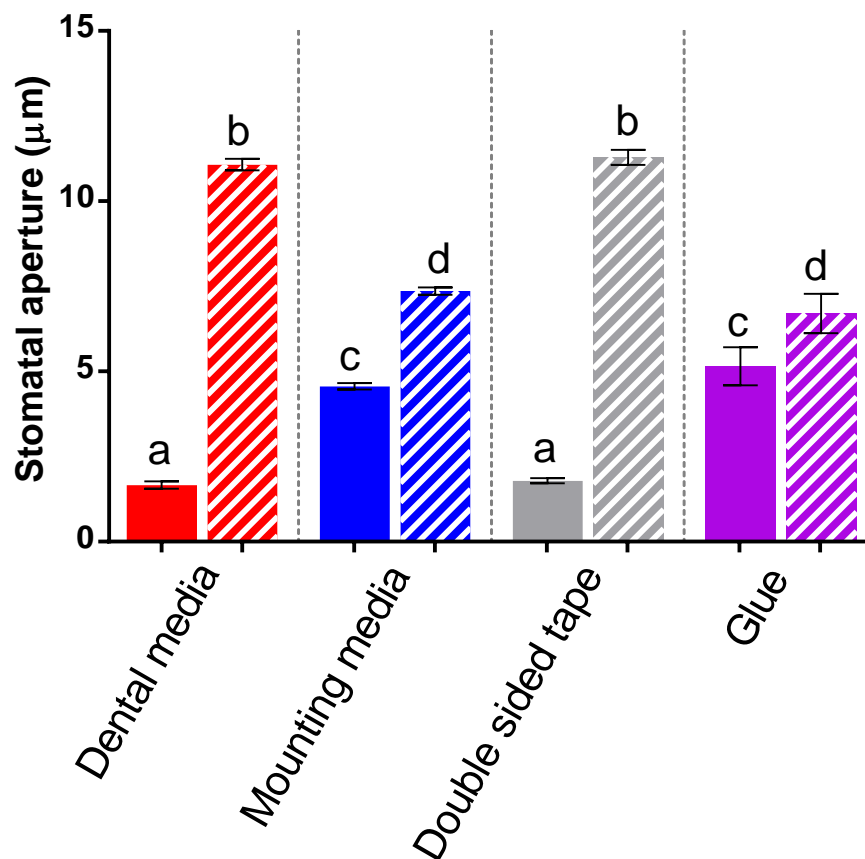


Figure 6.8. Stomatal aperture response to ABA from leaf samples adhered in a range of ways. Solid bars represent samples incubated in resting buffer +10Mm ABA, hatched bars represent samples incubated in opening buffer. Samples adhered with Mounting media and Glue show a reduced range of stomatal opening compared to samples adhered with Dental media or double sided tape. Statistical differences determined by ANOVA, $p < 0.005$, $n = 8$ replicates with 20 stomata measured per plant. Error bars represent SEM

It is clear from Figure 6.8 that the microscopy mounting media and glue are inappropriate methods for adhering leaf sample for AFM as stomatal movement is limited by these methods. Dental media and double sided tape both allowed significant stomatal movement suggesting that function was not being impaired by these methods.

6.2.4 Sample viability

Samples consist of excised leaf tissue and it is important to know that the cells are still alive during and after AFM analysis. To assess this fluorescein diacetate (FDA) was used as a cell viability probe. Non-fluorescent FDA can be converted into the fluorescent compound fluorescein. The production of fluorescein is an indicator that a cell is still living as intercellular esterases are required for the conversion (Jones and Senft, 1985). This can also be used as an indicator of cell membrane integrity as this is required for the intercellular retention of fluorescein.

Tape mounted stomata (Figure 6.9.A) showed green fluorescence indicating that the FDA had been taken up and metabolised to produce fluorescein. This fluorescence was retained within the cell, indicating that the membrane structures of the cell was not disrupted. In contrast, Provil Novo (dental media) mounted stomata (Figure 6.9.B) showed production of fluorescein indicating cell viability, this fluorescein was not retained within the cell, suggesting a breakdown of the membrane structure. It is not clear what could have caused this damage to the membrane structure but it is possible that this is due to compounds given off during the curing process of the dental media.

The data in Figure 6.8 and Figure 6.9 clearly show that doubled sided tape is the most suitable mounting media for the adherence of leaf tissue for AFM analysis and for maintenance of tissue integrity and viability. This method was used for all future experiments

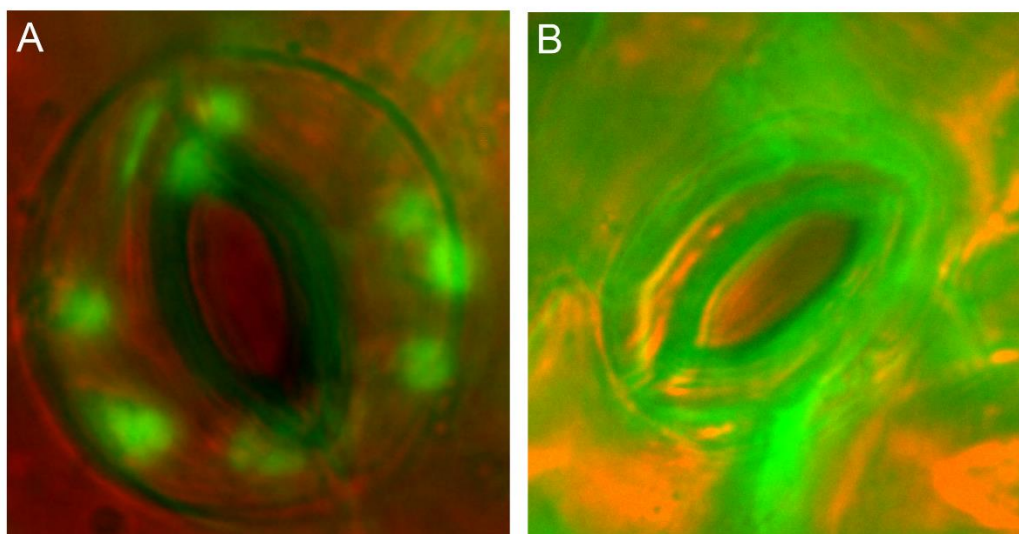


Figure 6.9. Fluorescein diacetate staining of stomata. Samples were mounted as if for AFM and left under resting buffer for 1h to simulate AFM conditions before incubation with FDA. Red channel shows background autofluorescence and green indicates fluorescein. (A) Stomata mounted with double sided tape contain fluorescein which is retained intracellularly indicating viable cells and membrane integrity. (B) Stomata mounted with Provil Novo dental media are viable, indicated by the production of fluorescein, but the membranes have been disrupted as indicated by the lack of cellular retention of fluorescein. Images are representative from 3 independent replicates.

6.3 Analysis of guard cell topography

Topographical data has the potential to provide valuable information about shape, size and surface features of stomata. AFM topography imaging allows 3D reconstruction of topographical images (Figure 6.10). Virtual cross sections can also be taken through topographical data allowing information about the size and shape of the stomatal pore to be recorded.

Topographical data was taken for stomata at a variety of developmental stages from the same age leaf in order to assess what information can be gleaned from this technique and to assess image quality. Height maps and deflection maps are displayed for 4 stages of stomatal development (Figure 6.11). Although deflection maps show greater detail more care must be taken

in their interpretation so comparing the deflection maps with the height maps allows cross-comparison.

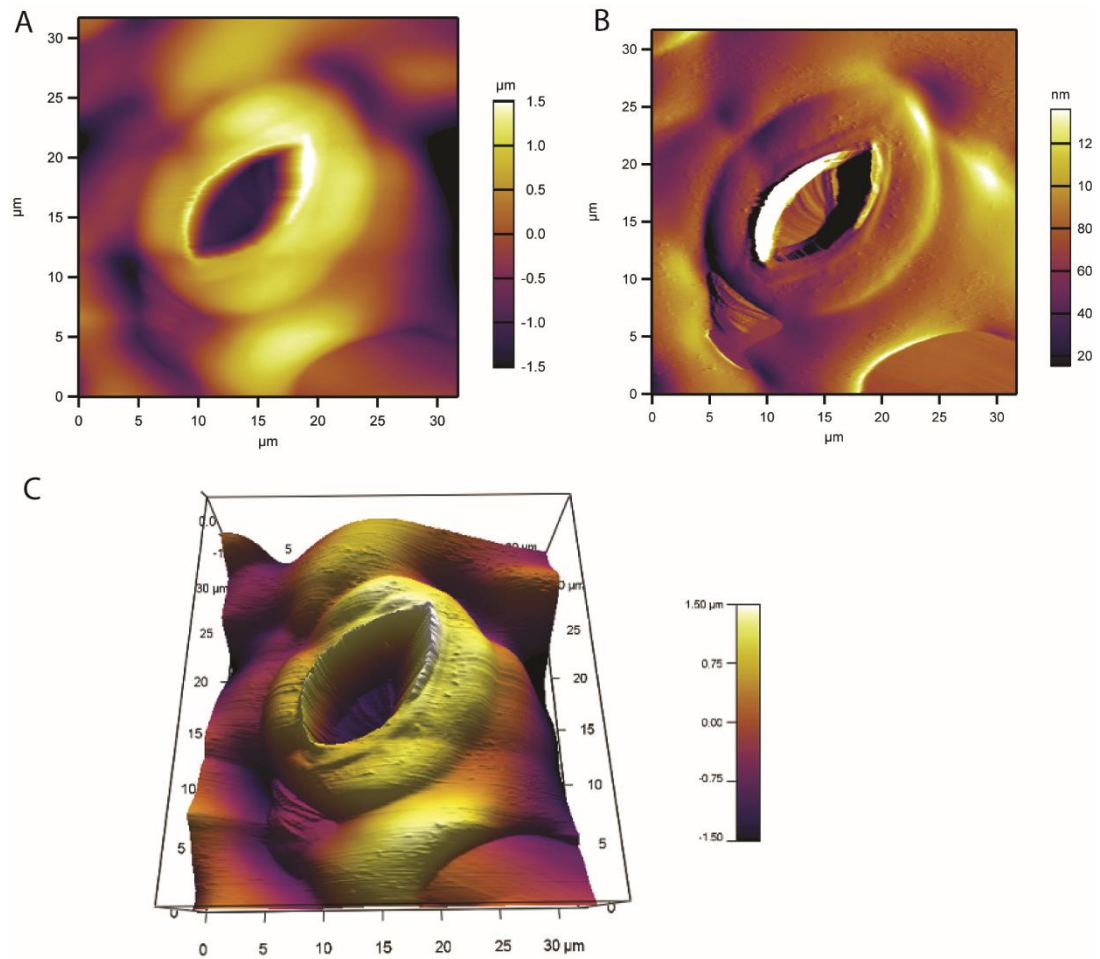


Figure 6.10. AFM data can be represented in multiple ways. 3D rendering of topographical data allows visualisation of stomatal shape (A) Height map of a stomata. (B) Deflection map of a stomata. (C) 3D reconstruction from the height map shown in A.

Figure 6.11. Topography of stomata from early development through to mature stomata. (A-B) A stomata or precursor cell in the early stages of development, the shape of the stomata is not fully oval yet and the pore is not yet developed, both the height map (A) and the deflection map (B) show an area where the pore is in the early stages of developing (marked by arrow). (C-D) Immature stomata. The stomata are now a recognisable stomatal shape and is fully divided, the pore is recognisable in the middle of the complex (*) but the cells have yet to bend apart (E-F) A young mature stomata. This stomata is now fully formed and has opened. The stomata is small and the process of separation has led to a very circular complex with an aspect ratio close to 1. Stomata at this stage are fully functional but the pore is still relatively small. (G-H) A fully mature stomata with a large central pore which is clearly defined and an oval shape with an aspect ratio of between 1.5 and 1.7.

These data (Figure 6.11) show that stomatal topography can be imaged in detail for a variety of stages of stomatal development. Stomata can be identified from their topographical features from before the stage when symmetrical division of a GMC (guard mother cell) is complete. The stomata can be staged in age by a combination of size, pore development and shape with younger stomata being smaller and rounder and having less developed central pores. In Figure 6.11 panels A and B show a stomatal precursor in which the central pore has begun to form (indicated by arrow). C and D show an immature stomate which has recently divided, characterised by its small size and the fact that the pore lips (indicated by arrow) are large showing that the pore has not fully finished forming yet. Panels E and F indicate the earliest stage at which the stomata appear functional; the pore has fully formed and the stomata has opened causing the circular shape often seen in young stomata. G and H show fully mature stomata; the stomata is large compared to previous stages and has a characteristic oval shape caused by anisotropic guard cell growth.

The quality of the topographical images seen in the deflection maps (Figure 6.11. B, D, F and H) is analogous to that of electron microscopy images of stomata but crucially this technique allows the imaging of live samples with no chemical pre-treatment.

The imaging of live samples makes it possible to assess the functionality of individual stomata. It has previously been shown that some stomata seem to close more than others in response to ABA (Mott and Buckley, 2000) and it is not clear why this is the case. Normal methods for assessing stomatal aperture require the measurement of separate populations of stomata, some with ABA and some without, meaning individual stomatal responses are impossible to assess. As shown in Figure 6.12 stomatal aperture of single stomate can be tracked in response to ABA. The height maps show the same

stomate before (Figure 6.12.A) and after 30 minutes in ABA (Figure 6.12.B). After 30 minutes in ABA the pore aperture width reduced by 4 micrometres and the cross-sections (Figure 6.12.C and D) show that the shape of the pore has changed, with the reduction being even more severe further down the Z-axis of pore. Total pore area (Figure 6.12.E) and pore aperture width (Figure 6.12.F) substantially decrease following ABA treatment.

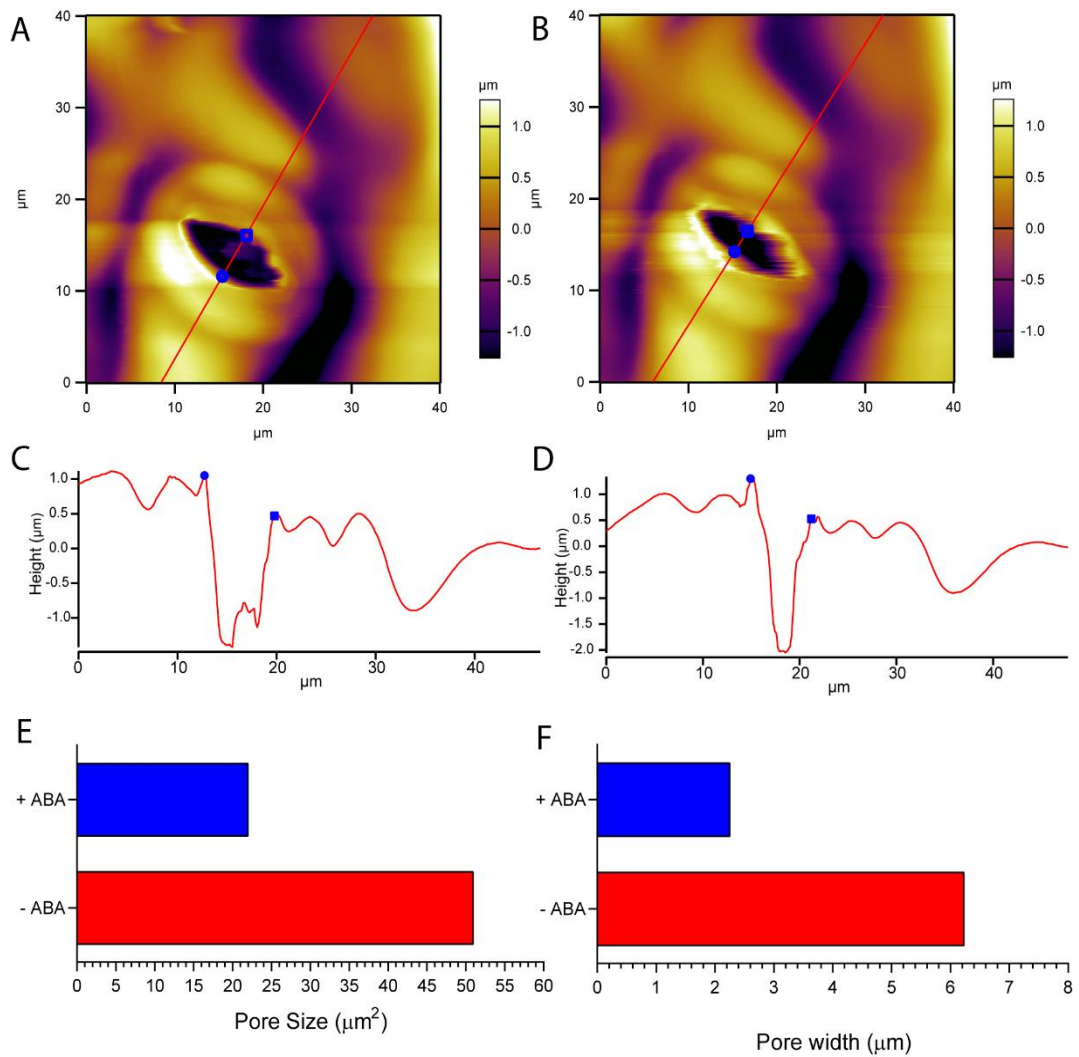


Figure 6.12. The response of a single stomata to ABA. (A) Height map of a stomata imaged in opening buffer prior to the addition of ABA. (B) Height map of the same stomata 30 minutes following addition of ABA to a concentration of 10mM. (C) Cross section of the height map shown in A, the position of this cross section is indicated in A by the red line. This shows a wide pore which is nearly the same width at the top as the bottom. (D) Cross section of the stomata shown in B, the position of the cross section is indicated by the red line in B. The pore is substantially less wide at the top and this difference is even more pronounced at the bottom of the pore. (E) Pore size measured from A (-ABA) and B (+ABA), the addition of ABA has caused a substantial reduction in the pore size. Pore area was measured in ImageJ (F) Pore width measured from A (-ABA) and B (+ABA), the width is measured between the blue markers shown in A-D, the addition of ABA has caused a substantial reduction in the stomatal width. Stomatal width is measured in Igor Pro with Asylum research AFM analysis software add on package using the cross-section tool.

6.3.1 Topographical analysis of *focl* plants

As discussed in Chapter 5 the *focl* mutant has an altered stomatal pore which is covered by a plug of cuticle. As this is a topographical change we used this mutant to test the ability of the AFM technique to detect differences in surface topography. The results of this analysis are shown in Figure 6.13. The topographical changes can be seen clearly, with 3 different types of *focl* stomata detected. Some stomata have a covering which obscures the whole of the pore with no gap at all (Figure 6.13.A). The AFM shows this covering as being slightly submerged below the level of the stomata but it is not clear if this is due to the AFM tip pushing the covering down into the substomatal cavity. Other stomata seem to have a small gap in the middle of the covering (Figure 6.13.B), as if it has ruptured in the middle, while other stomata appear as if they are totally uncovered (Figure 6.13.C) but have a more extensive and less defined cuticular ledge than wild type stomata (Figure 6.13). This is consistent with the finding in 5.3.6 that *focl* plants had approximately 10% of their stomata uncovered.

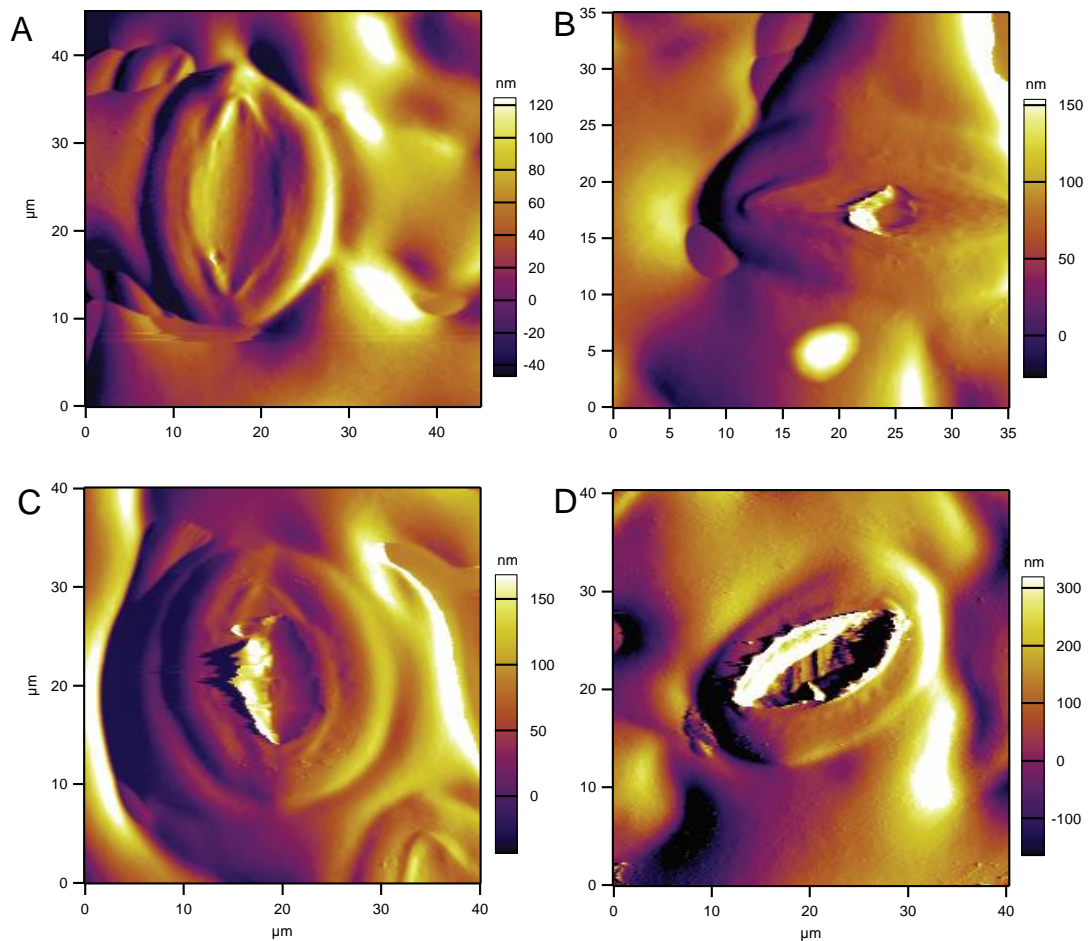


Figure 6.13. *focl* stomatal covering can be observed by AFM. Deflection maps of *focl* and WT stomata (A) Most of the *focl* stomata have a complete covering blocking the entirety of the pore. (B) A small number of covered stomata had a small hole in the centre of the covering revealing the pore below. (C) Some *focl* stomata have no covering over the pore, these stomata have an extended cuticular ledge. (D) A wild type stomata has a defined small cuticular ledge and a large deep pore.

Sequential imaging of *focl* stomata (over a 15-minute period) (Figure 6.14) which had a partial covering showed the pore increasing in size. Figure 6.14.A shows the initial covering with a slight hole in the centre of the stomata. As the stomate is imaged again (Figure 6.14.B) the pore has increased in size. This was due to the AFM tip catching on the edge of the covering and pulling it back.

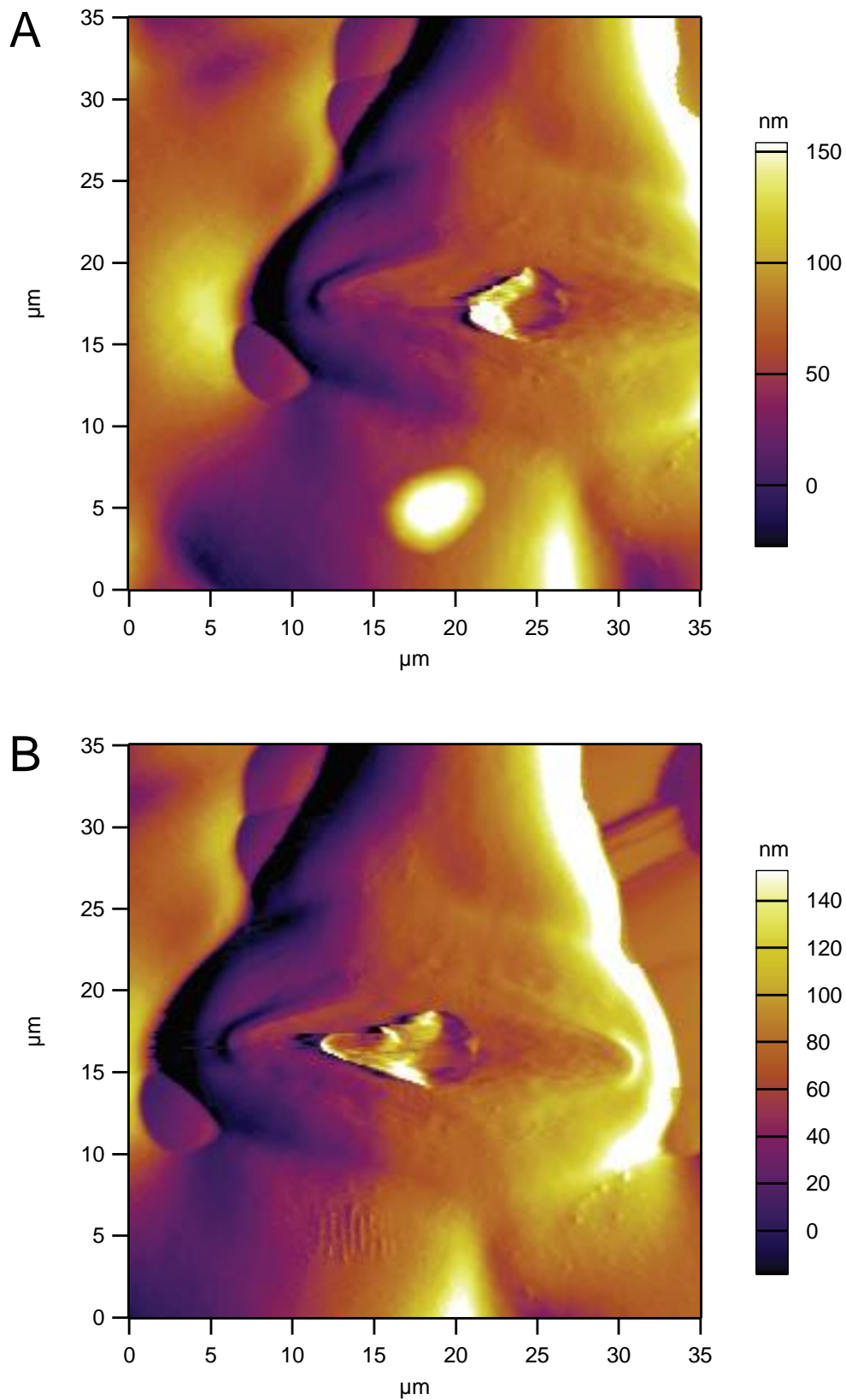


Figure 6.14. Deflection maps of a *focl* stomata imaged sequentially. (A) This first image shows a small central pore in the middle of the pore covering which is typical of *focl* stomata. (B) Imaging the stomata a second time shows that the hole in the centre has increased in size as the pore edge has been caught by the tip and dragged to the left. This suggests that the pore covering is relatively soft and flexible.

These data show that AFM can be used to identify topographical features of the leaf surface in excellent detail. Structural changes which result in altered topography can be identified at a resolution similar to electron microscopy. This offers significant advantages due to the lack of pre-treatment needed and the ability to image live samples.

6.4 Analysis of stomatal elasticity

AFM force measurements were conducted to investigate the mechanical properties of guard cells. Force mapping was carried out to investigate the mechanical properties of a range of guard cells and the relationship between guard cell and supporting cell mechanics. Due to the limited z range on the AFM combined with the highly topographical nature of leaves the scans were kept small to maximise the likelihood of scan success.

The apparent Young's modulus were measured to assess cell wall elasticity in the samples. A higher Young's modulus indicates a stiffer material which deforms less under elastic deformation. Figure 6.15 shows absolute stiffness values for stomata (Figure 6.15.A) and their corresponding supporting cells (Figure 6.15.B). These data show that there is huge variability in stiffness between samples, with each sample being from a different plant. Plotting the stiffness of stomata against the supporting cells (Figure 6.15.C) shows a weak positive correlation between stomatal stiffness and supporting cells stiffness (Spearman's correlation $r=0.6912$ $p=0.0039$). It is possible that the relative difference between stomatal cells and supporting cells is of greater importance than the absolute values.

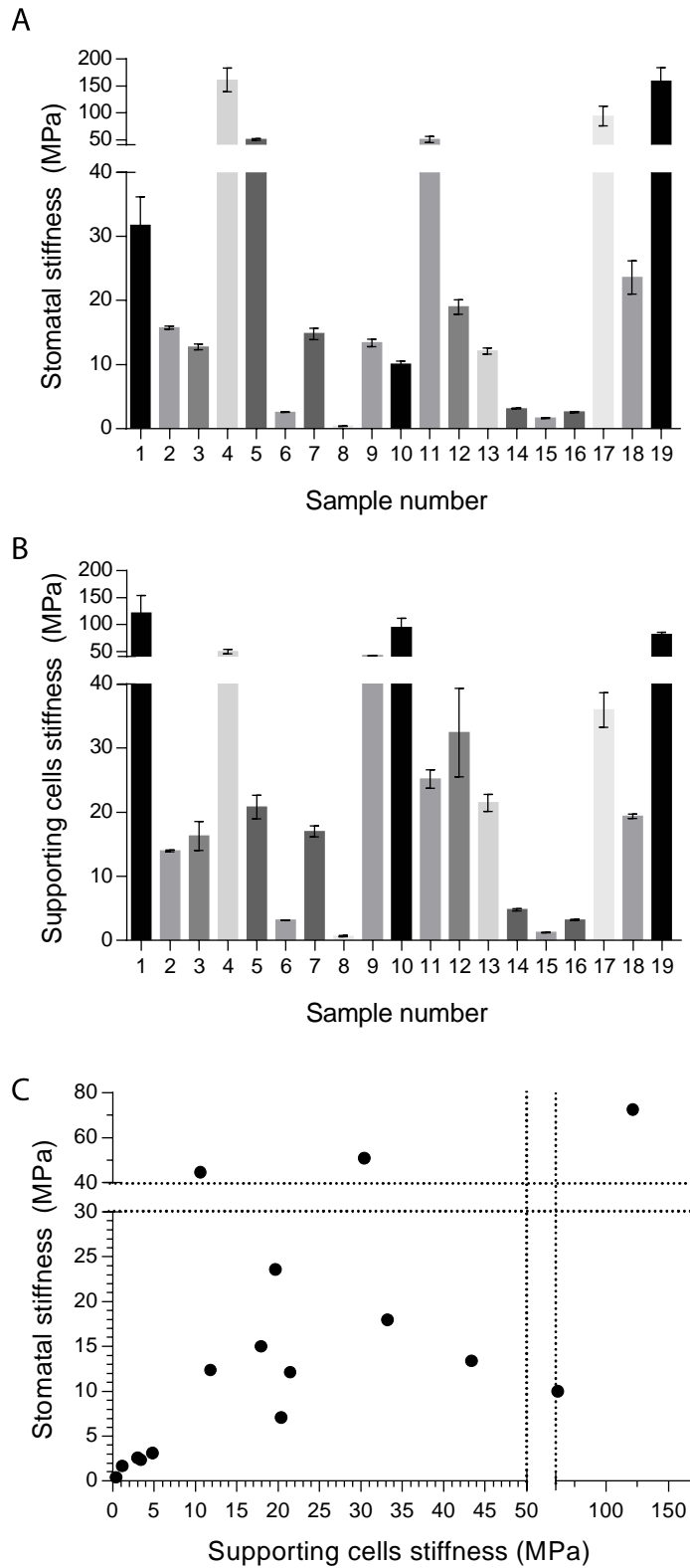


Figure 6.15 Absolute stiffness values show large variability. (A) Stomatal stiffness in MPa shows huge amounts of variability between stomata. The values for the central pore have been excluded from this analysis (B) Stiffness of all non-stomatal cells in scans. The values for the stomata and central pore have been excluded from this analysis. Supporting cells show similar variability in stiffness to stomata. Stiffness is defined by the apparent young's modulus. (C) Stomatal stiffness against supporting cell stiffness. There is a slight trend as stiffer stomata leads to stiffer supporting cells but there is still a large amount of variation.

When analysing stomatal stiffness there are many factors to consider which could account for the variation observed. As very little is known about the mechanical properties of guard cells it is not clear which factors impact, or are impacted by, the stomatal stiffness. Figure 6.17 correlates stiffness values with several known stomatal variables which exhibit variation within and between plants in an attempt to determine the biological features related to stomatal stiffness. The most obvious factor to consider is the size of the stomata. When stomatal stiffness is plotted against stomatal size (Figure 6.17.A) there appears to be a slight trend towards greater stiffness in larger stomata but there is no significant correlation ($r=0.2491$ $p=0.3037$). There is no relationship between the ratio of supporting cell stiffness:stomatal cell stiffness (Figure 6.17.B). Pore size was subtracted from stomatal size calculations to account for stomata at different degrees of opening. These data suggest that as stomatal size increases (which indicates an increase in stomatal maturity) stomatal stiffness tends to increase, but more repetition is needed to confirm this weak trend.

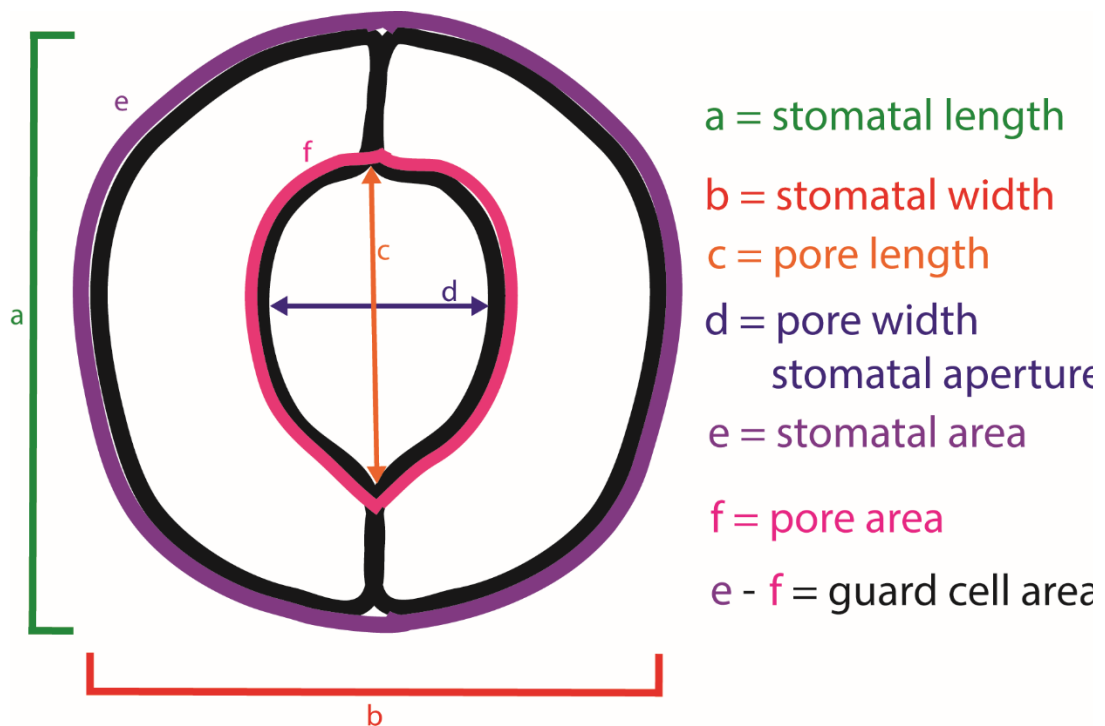


Figure 6.16. Schematic diagram clarifying stomatal dimension. a: stomatal length, defined as the distance between the stomatal poles. b: stomatal width, measured through the centre of the stomate. c: pore length, defined as the height of the pore between the points where the guard cells meet. d: stomatal aperture and pore width are used synonymously, defined as the width of the pore and is measured at the same height as the stomatal width (b). e: stomatal area is defined as the area of the entire complex, including the central pore. f: pore area shows the area of the stomatal pore. Guard cell area is calculated as $e - f$ (stomatal area - pore area).

Pore size is known to vary within stomatal populations. No relationship was observed between pore size and stomatal stiffness (Figure 6.17.C) or stiffness ratio (Figure 6.17.D). As samples were imaged in resting buffer it is likely that not all stomata are fully open, which could have a confounding effect on the data.

Although stomatal size is the most commonly used proxy for age there is also a transition during stomatal maturation from circular to more ellipsoid stomata. This can be defined by the aspect ratio of the stomata, with an aspect ratio of 1 indicating a completely circular stomata.

Equation 6.3: Aspect ratio

$$\textit{Aspect ratio} = \frac{\textit{Stomatal length}}{\textit{Stomatal width}}$$

There was no clear relationship between aspect ratio and stomatal stiffness (Figure 6.17.E). In general, as aspect ratio decreased from 1 the ratio of supporting cells:stomatal stiffness decreases, showing a significant correlation ($r=0.5051$ $p=0.0275$), suggesting that younger, rounder stomata tend to be less stiff than the surrounding epidermal cells. See Appendix 12 for full statistical analysis of Figure 6.17.

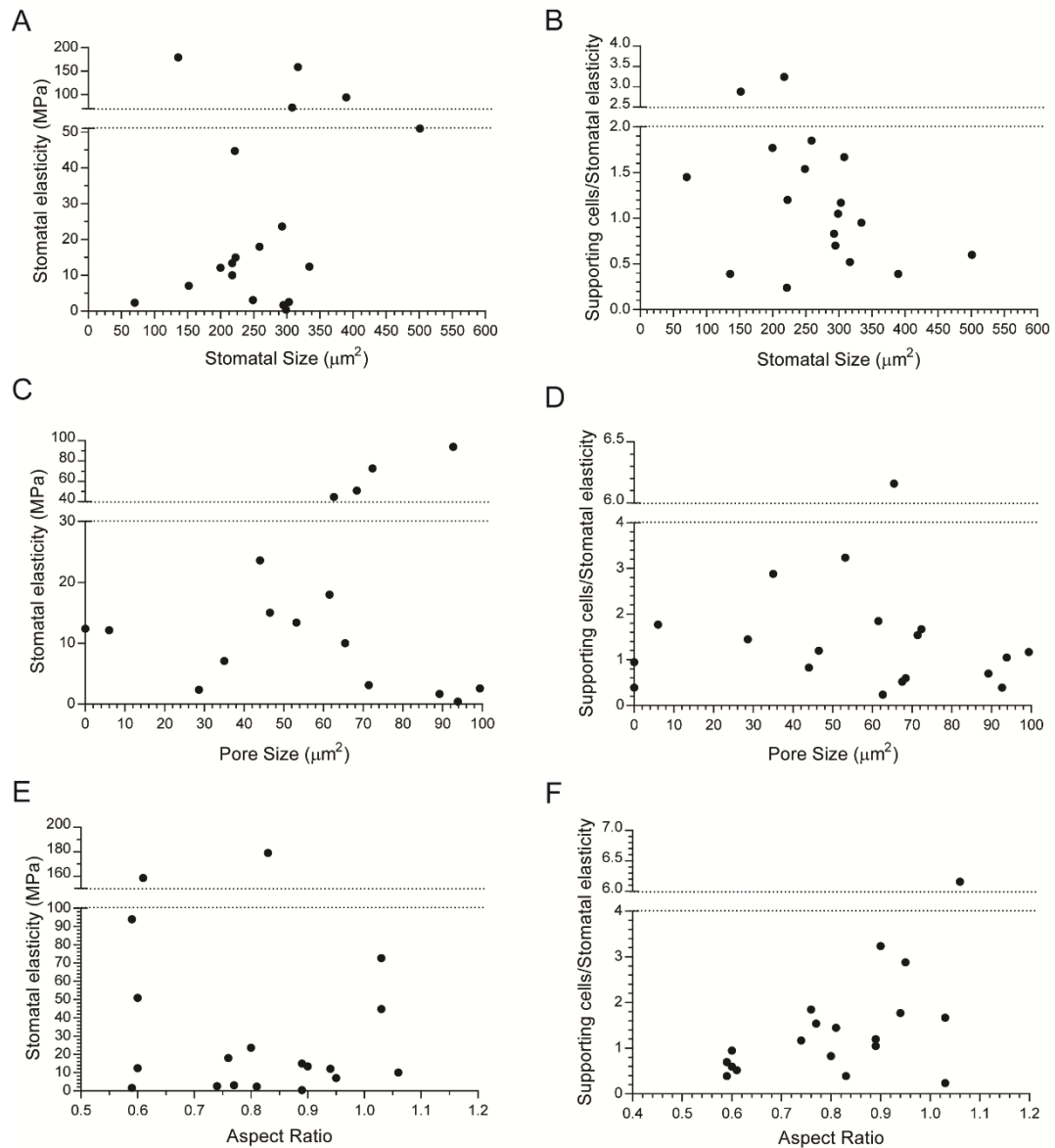


Figure 6.17. Stomatal stiffness does not correlate strongly with size or shape. (A) Stomatal stiffness tends to increase as stomatal size increases but with multiple outliers. (B) The ratio of supporting cell stiffness to stomatal cell stiffness shows no relationship with stomatal size. (C) Stomatal stiffness shows no relationship with pore size (D) The ratio of supporting cell stiffness to stomatal cell stiffness has no relationship to pore size. (E) There is no relationship between stomatal stiffness and the aspect ratio of stomata. As the ratio of supporting cell stiffness to stomatal stiffness increases the aspect ratio tends to increase. This indicates that more circular stomata are less stiff compared to their supporting cells than less circular stomata. Areas were measured on ImageJ. For stomatal size the pore area (as seen in height maps) was excluded so only cellular area was measured. Pore size was measured from height maps and not from the stiffness map. Aspect ratio was calculated as Length/Width. Length was not always the largest dimension but rather was defined as the diameter of the stomata between the poles of the cells where the two guard cells join.

From the force maps it was clear that there is variation within a single guard cell. The stomata were analysed by splitting them into 2 components, the outer stomata and the inner stomata. This was done by isolating the stomate and excluding the pore. The split was made along the centre of the stomate and excluding the pore. The split was made along the centre of the stomate to give two separate sets of values which were then averaged.

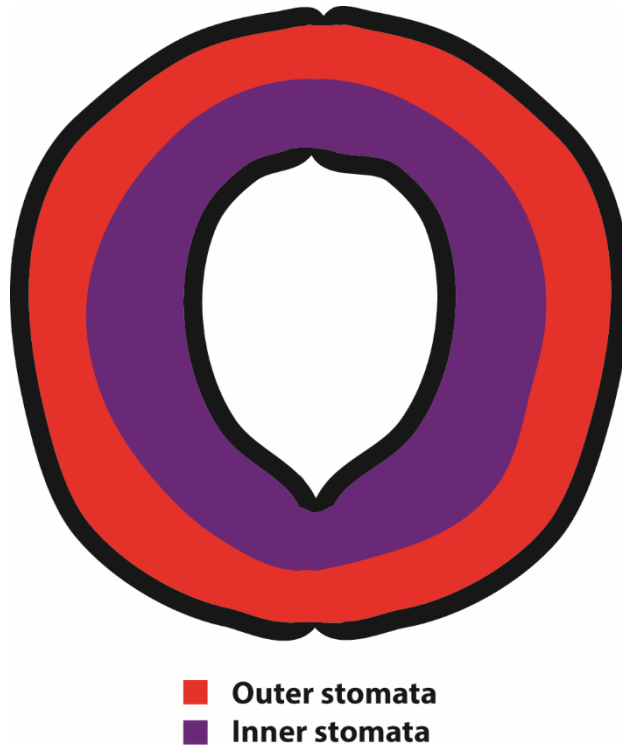


Figure 6.18. Schematic diagram illustrating how the guard cell area is split into inner stomata and outer stomata. The guard cell area is split along the centre of the guard cell width.

Figure 6.19 shows inner stomatal stiffness versus outer stomatal stiffness. As would be expected a positive correlation shows that as inner stomatal elasticity increases outer stomatal elasticity also increases ($r^2=0.4725$ $p=0.0033$). Some stomata seem to have a greater outer stomatal elasticity than inner but other stomata show the reverse. This indicates that the pattern of stiffness within a stomate is not consistent but it is not clear what is causing this variability.

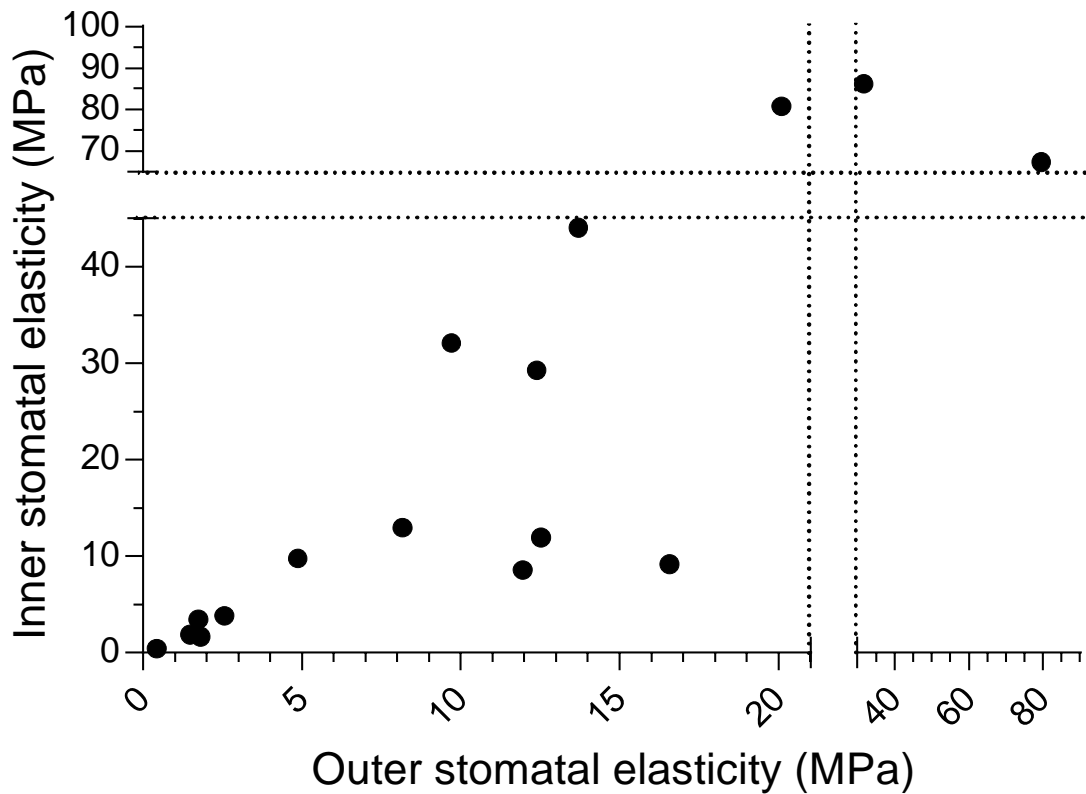


Figure 6.19. Inner stomatal elasticity increases as outer stomatal elasticity increases. Neither value is consistently larger than the other indicating that there is not a consistent pattern of stomatal stiffness across the stomata.

It is clear from the above data that stomatal stiffness is complex and is likely to be affected by multiple aspects of stomatal biology. One of the most likely factors to impact on the mechanical properties of the stomate is its developmental stage. Based upon the height data from the force maps stomata could be grouped into different developmental stages, as shown in Figure 6.20. The stomata were classified into 4 different stages depending on their structural features. Stage 1 stomata have no visible pore in the height map (Figure 6.20.B-C) indicating that a complete division of the guard mother cell has not occurred. In stage 1 stomata a softer region is visible on the force map where the pore will form. Stage 2 stomata (Figure 6.20.D-E) have pores which are visible on both the height map and the force map but the pore is small and sometime poorly defined indicating a recently formed stomate. These stomata tend to be circular, with an aspect ratio close to 1,

and are small compared to mature stomata. Stage 3 stomata (Figure 6.20.F-G) have the characteristic oval shape of *A. thaliana* stomata and have a large well-defined pore. These stomata are slightly bigger than stage 2 stomata. Stage 4 stomata (Figure 6.20.H-I) are fully mature stomata characterised by a large well-defined pore and an aspect ratio in the 1.7-1.8 range. These stomata are larger than any of the previous stages. When plotted as the ratio of stiffness for outer stomata/inner stomata against supporting cells/stomatal cells the different stomatal stages clustered into different quadrants of the graph. In general, the ratio outer/inner stomatal stiffness decreased as stomata matured, with stage 3 and stage 4 being equal. Stage 1 and 4 had stiffer stomata than supporting cells whereas stage 2 and 3 had stiffer supporting cells than stomata. It appears that during guard cell differentiation the central region of the cell becomes softer, as shown in stage one. Following pore formation this softening extends to include the entire guard cell. As guard cells mature to stage 3 and 4 a radial stiffness gradient forms with the inner part of stomata being stiffer than the outer part of the stomata. Stage 2 and 3 stomata are less stiff than their supporting cells, which is likely due to the decrease in stiffness observed in stage 2 carrying over to stage 3. By stage 4 the stomata are stiffer than their supporting cells and have a clear radial patterning where the inner portion of the stomata is stiffer than the outer portion of the stomata. These data show the pattern of stomatal stiffness changes during development and that localised softening precedes the formation of the central pore.

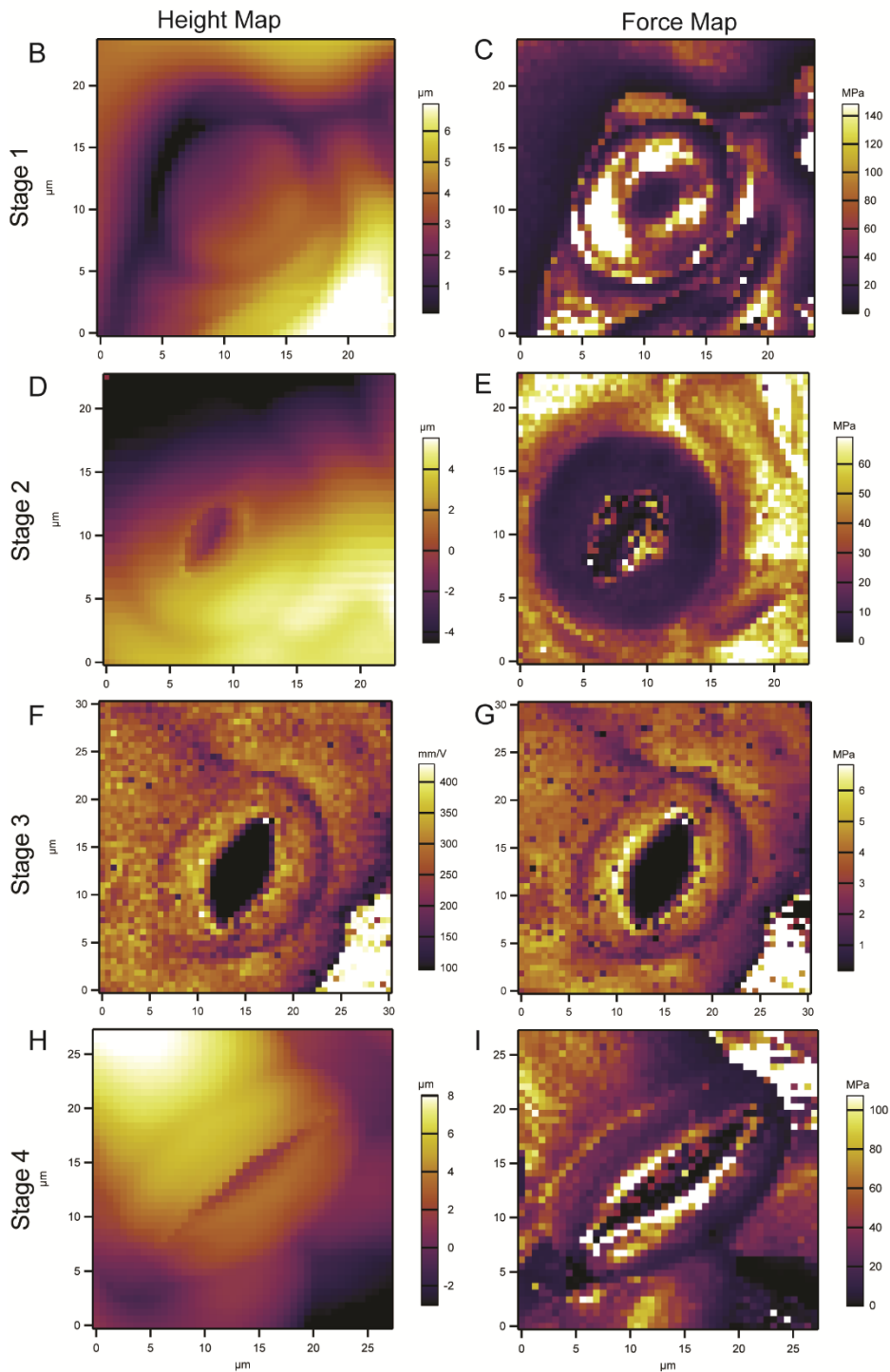
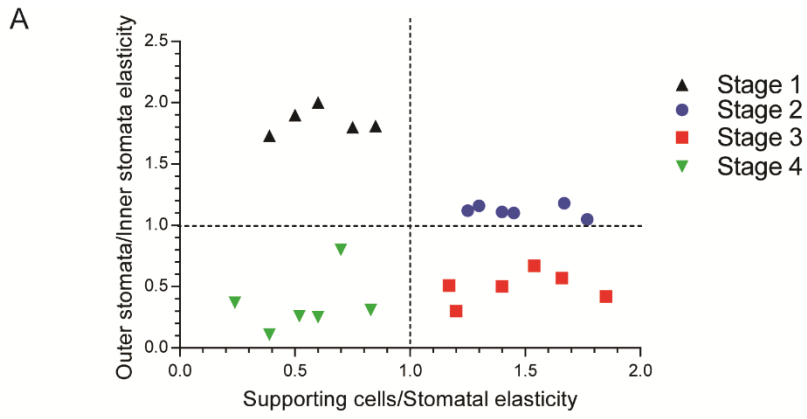


Figure 6.20. Stomatal elasticity properties are dependent on the stage of stomatal development. A) Supporting cells/stomatal cell elasticity vs outer stomata/inner stomata elasticity shows that different stages of stomatal development cluster in different quadrants. Stage one stomata have greater apparent young's modulus in the stomata than in the supporting cells and a greater young's modulus in the outer portion of the stomata than the inner portion. Stage 2 stomata have greater supporting cell young's modulus than stomatal and greater outer stomatal young's modulus than inner although this value is consistently close to 1. Stage 3 stomata have greater supporting cell young's modulus than stomatal cells and have a greater young's modulus in the inner stomata than the outer stomata. The oldest stomata in stage 4 have greater stomatal stiffness than supporting cells and are stiffer on the inner portion of the stomata than the outer. (B-I) representative AFM maps for each stomatal stage. (B-C) Stage 1 stomata are defined by having no visible central pore on the height map (B) but a pore-like region of softer tissue is visible in the centre of the cell on the force map (C), this stage of stomata is very circular. (D-E) Stage 2 stomata are defined by the presence of a visible pore on the height map (D) which is small and this pore is flanked by a region of stiffer tissue on the force map. Stage 3 pores look undefined on the force map (E), these cells are still very circular with an aspect ratio close to 1. (F-G) Stage 3 stomata are characterised by a large pore visible in both the height map (F) and the force map (G) with a region of stiffer tissue surrounding a defined pore area, these stomata are more oval than previous stages. (H-I) Stage 4 stomata are characterised by a large central pore visible and clearly defined on the height map (H) and force map (I), the pore is flanked by a clear region of stiffer tissue and these stomata are highly oval in shape with aspect ratios in the 1.7-1.8 range. Images are representative for 6 stomata per stage (5 for stage 1).

6.5 Discussion

6.5.1 Experimental validation of an AFM method

The application of atomic force microscopy to plant leaves as described in this chapter is a new technique and as such validation was required. The key limiting factor was z-range; the MFP-3D AFM used has only a 12 μ m range and the standard topography of a leaf exceeds this. Most commercial AFMs have a Z-range in the region of 10-15 μ m and so this limitation will often be a consideration when designing AFM experiments. Due to the height issue we did not use intact leaves, instead excising tissue squares of approximately 1cm width. Stomatal function assays show that, when using appropriate mounting techniques, guard cells are still fully functional. This was confirmed by FDA staining which indicated that the guard cells remain viable during imaging.

It is not clear why some mounting media worked better than others, but it is possible that the curing process of the glue and epoxy resins tried released substances toxic to the plant.

The decision to grow plants for AFM analysis on soil provides the opportunity to combine AFM with other measurements such as gas exchange analysis (LI-COR). Image quality was sustained for a similar time when imaging both soil grown plants and media grown plants, this means that the decision to grow the plants on soil did not mean a compromise in the quality of data capture. Using mature plants and growing them as I would for physiological analysis in combination with minimal sample processing allows *in vivo* measurements of plants in as close to normal conditions as possible.

6.5.2 AFM allows high resolution imaging of live tissue

It is clear from the data presented in this chapter that topographical imaging of stomata by AFM allows for high quality imaging of live stomata. The images were of similar quality to some published SEM images. AFM offers significant advantages over other high resolution imaging techniques such as electron microscopy as the samples are alive and have undergone no treatment. This means that by adding chemicals such as ABA, mannitol or enzymes the responses can be tracked in high resolution.

Tracking individual stomata during opening and closing is not a trivial matter using conventional light microscopy techniques due to the need to exchange solutions, e.g. ABA, without disturbing the sample and losing sight of the stomata. The need for a cover slip when using biological objectives and the relatively small working distance of most objectives limits the amount of solution samples can be submerged in. AFM allows tracking of individual stomata, which crucially have been shown to be viable by FDA staining. Imaging under liquid allows the addition of chemicals such as ABA or mannitol to stimulate stomatal movement. Tracking individual stomata is a low throughput technique as it takes approximately 45 minutes per stomata. Using an AFM with a bigger z-range would allow larger scan size, meaning multiple stomata could be imaged at once. It is known that a small portion of stomata do not close in response to common stimuli such as ABA and CO₂ (Chater, personal observation), and it would be interesting to track the opening or closing of individual stomata to determine their functionality and then conduct force mapping to determine if non-functional stomata are characterised by any mechanical differences.

The temptation is to think of stomatal closing in 2D at the leaf surface measurement. The edge of the pore is detected on a conventional light microscope to give an aperture which is then converted into a 2D area.

Figure 6.12 shows that the aperture detected at the surface may not be the minimum aperture since the height section shows that the guard cells are closer together further down the pore. The schematic in Figure 6.21 illustrates this problem. When measuring stomatal aperture line-a is measured however in reality it is likely that the actual pore width is line-b which cannot be measured as easily by traditional methods.

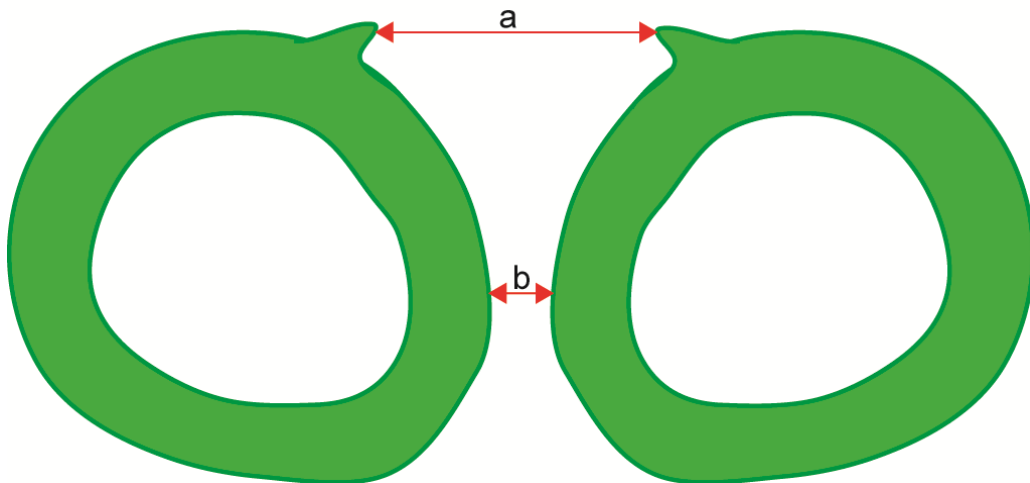


Figure 6.21. Stomatal schematic. Due to the tubular shape of guard cells the aperture measured during stomatal bioassays (a) is between the cuticular ledges. This can be a much greater dimension than further down the stomata, such as in b.

Future work using AFM could provide information about pore size and shape changes during stomatal opening and closing in 3 dimensions, providing much more exact information than current aperture measurements. This can provide useful information about path length for the diffusion of gases which could be useful for modelling leaf photosynthetic properties.

6.5.3 *focl* plants have altered stomatal coverings

focl plants were imaged using the AFM because they had a known change to their topography. Using a known mutant allows us to test the imaging accuracy and quality in order to validate the method. Our data show that AFM can identify the aberrant stomatal coverings observed in sections by

toluidine blue labelling Figure 5.14, indicating that the high resolution topographical data is accurate. 3 different types of *focl* stomata were identified, reflecting the level of detail AFM allows.

The fact that the covering caught on the AFM tip and that this caused the covering to be pulled back suggests that the covering is mechanically soft. The AFM cantilevers are relatively weak and when they get caught on other surface features, such as epidermal cells with a high topography or vasculature, they tend to snap. As the cantilever did not snap it suggests a weak covering. This is consistent with the conclusions from Chapter 5 that the covering of *focl* stomata are cuticular rather than extensions of the cell wall.

6.5.4 Stomatal stiffness changes throughout development.

The AFM data reported here indicate that stomatal and supporting cell stiffness are extremely variable. Stomatal stiffness is shown to be correlated with supporting cell stiffness, suggesting that it may not be the absolute stiffness value which is important but rather the proportional relationship between the two. It seems that stomatal mechanical properties differ between leaves of the same age, the reasons for which are unclear. It was previously shown that mechanical stimulation, such as brushing, alters the mechanical properties of *Arabidopsis* stems (Verhertbruggen et al., 2013). One possibility is that some plants may have been exposed to more air flow in the growth chamber and this agitation causes a change in mechanical properties.

When measuring the stiffness of cells, it is important to consider what we are measuring. There are two main mechanical components to the guard cell. Firstly, the cell wall provides the structural support the cell needs and this is the limiting factor for shape change and expansion. Secondly the turgor

pressure within the guard cell provides an outwards force which limits deformation of the cell wall. As we are only probing the stomata to a depth of 150 nm it is likely that we are measuring the indentation of the cell wall rather than the deformation of the cell wall into the body of the cell (as indicated in Figure 6.22). It is therefore important to consider the fact that turgor pressure could be impacting on the readings. To address this issue, it would be interesting to repeat the measurements reported here on plasmolysed cells to provide a comparison without turgor pressure.

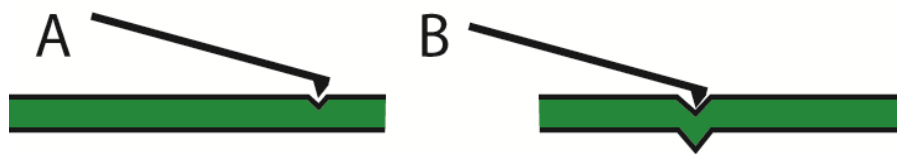


Figure 6.22 Schematic of cell wall deformation and indentation. (A) The cell wall is compressed slightly leading to a localised deformation of the cell wall which is not affected by turgor pressure. (B) Firmer compression leads to an indentation of the entire cell wall which is displaced into the cell, this is impacted by the turgor pressure within the cell.

Although selection of developmentally equivalent leaves is relatively simple, stomata do not all differentiate at the same time, meaning that a range of stomatal ages will be imaged in any one leaf. Variation in stomatal age is likely to explain a large portion of the variation observed. By using well known stomatal development features to categorise the stomata by developmental stage it is possible to get a clearer picture of the mechanical properties (although assigning developmental stages to the guard cells is somewhat arbitrary as in reality stomatal differentiation is a continuum not a series of discrete stages). The earliest stage of stomata that force data was captured for appears to be the guard mother cell (gmc). In all of the gmcs imaged there was no discernible pore, as the cell has not yet divided. Interestingly there is a region of softer tissue at the centre of the cell which is indicative of where the pore will form. This suggests that prior to pore formation cell wall changes are taking place. It is highly unlikely that the

gradient of stiffness observed in gmcs is due to variations in turgor pressure as the measurements are taken from a single cell. Following division and pore formation the central softening seems to extend to cover the whole guard cell. It is likely that this is an extension of the cell wall changes observed in stage 1. It is also possible that stage 2 stomatal softness is due to a transient loss of turgor but it is most likely due to cell wall loosening to facilitate stomatal growth. During stomatal maturation (stages 3 and 4) a pattern of radial stiffness is set up with the inner portion of the stomata being stiffer than the outer portion. This radial stiffness pattern is also observed in plasmolysed cells (Fleming, Unpublished) and so is likely reflective of cell wall changes rather than turgor pressure.

The data in the literature suggests that radial thickening is responsible for stomatal opening, with uneven cell wall expansion causing the cells to bend during stomatal movement (Raschke, 1975). It is logical to suggest that this thickening is at least partially responsible for the radial pattern of stiffness observed in stage 3 and 4. Interestingly stage 2 stomata are still able to open and close (Healicon, unpublished) suggesting that a radial stiffness gradient is not required for stomatal opening and closure.

It is not clear why stage 3 and stage 4 stomata have opposing patterns of guard cell:supporting cell stiffness. It seems likely that the transient cell wall softening observed in stage 2 extends somewhat into stage 3, perhaps as the guard cells are still expanding. As such, stage 3 guard cells are less stiff than the supporting cells, as are stage 2 guard cells. By stage 4 the overall guard cell stiffness is higher, possibly due to the cessation of growth and cell wall remodelling.

Overall these data suggest that prior to stomatal formation cell wall softening is initiated which carries on for the early part of stomatal development.

Young stomata are actively growing cells and previous work has shown that

faster growing cells are softer than slow growing cells (Milani et al., 2011) and this may explain the low elastic modulus in young stomata. Cell wall remodelling causes a stiffening in maturing stomata and leads to a radial stiffness gradient. This is consistent with the fact that numerous cell wall enzymes, such as *PME6*, appear to be expressed only in mature guard cells and not in precursor cells (4.2.1). In Chapter 3 we discuss cell wall components which have differential distribution in the guard cells, in particular feruloylated polymers (indicated by LM12) and xyloglucan (indicated by LM15) are both present in greater abundance in the inner part of the stomata. As previously discussed in chapter 3, feruloylated polymers are known to be involved in the cross-linking of pectins and the presence of xyloglucan tethers are shown to cause an increase in cell wall rigidity (Pena et al., 2007). It is possible that the observed differences in stomatal stiffness between the inside and the outside of the guard cell is due to this spatial regulation of cell wall components.

It is important to understand the limitations of AFM as a technique for measuring *in vivo* plant mechanics. The cell wall is not a homogenous material but rather a complex and heterogeneous structure. Guard cell walls in particular have a high degree of anisotropy and many models of indentation which are used to calculate material properties may be based on invalid assumptions. Care must be taken with the interpretation of force data as cell wall heterogeneity, sample preparation, and tip properties can all impact the data. Young's modulus is an intrinsic property and the calculations of this are reliant on the model of indentation used which requires a number of assumptions.

This chapter demonstrates the potential for the application of AFM to measure plant mechanical properties *in vivo*. The ability to gather high resolution images and mechanical data from the same sample is valuable and

as yet no research is published using AFM on mature plant organs. Although there are a number of limitations to the technique these can be overcome by careful experimental design. Care must be taken to avoid over interpretation of data. This technique provides a valuable tool for the study of stomatal mechanics and in the future the use of cell wall mutants could be used to study the effect of altering cell wall composition on the elasticity of cell wall.

Chapter 7. General Discussion

The research presented in this thesis provides insights into the role that the composition of the guard cell wall has in stomatal function. Initial data from immunolabelling (Chapter 3) provides details on the components of the guard cell wall. Pectins and xyloglucans in particular showed distinct guard cell distributions. Interestingly, unbranched xyloglucan shows asymmetric guard cell distribution, being present only on the inner portion of the guard cell, facing the pore. It is possible that the ratio of xyloglucan to pectin is important in mediating cross links with cellulose (Hayashi et al., 1987), and it is possible that cellulose is cross-linked to a greater extent in the cell walls adjacent to the pore, leading to differences in cell wall extensibility and, therefore, contributing to stomatal opening.

Enzymatic removal of pectin led to an alteration to the binding of some antibodies, illustrating the care that is needed when interpreting antibody binding data. Restriction of antigen access may be the reason that some antibodies do not bind rather than indicating absence of a particular epitope. The overall extent of epitope masking is unclear, both in our work and others, as to date only pectic masking has been demonstrated. Further work is needed in this area.

The study of guard cell wall composition is challenging due to their small size and the fact that they only make up a small proportion of the leaf tissue. Although isolation of guard cells and extraction of cell wall material is possible, this approach provides no spatial information about the distribution of cell wall epitopes within the guard cell or the relationship between the guard cells and neighbouring epidermal cells. The antibody

approach provides spatial information and, to an extent, abundance can be judged by the relative signal intensities within an image.

The abundance of genetic resources associated with *A thaliana* provides additional avenues for guard cell wall research and the identification of a guard cell localised cell wall gene (*PME6*) with a key role in stomatal function has been demonstrated in this research (Chapter 4). Cell wall genes, especially those related to the synthesis and modification of pectin, are often found in large families and it is reasonable to expect a significant amount of genetic redundancy. Although a single PME gene knockout described in this work provided a clear phenotype, other loss of function mutants of putative guard cell wall localised PME and PME1 genes showed no discernible cell wall phenotype, suggesting that some PME genes function redundantly while others do not. Future work exploiting lines overexpressing PME1 genes in the guard cells will hopefully inhibit the action of multiple PMEs, possibly leading to more extreme phenotype.

Manipulating cell walls has an impact on the mechanical properties of the cell wall. Measuring cell wall mechanical properties in intact tissues is challenging but will be key to understanding the role of the guard cell wall in stomatal function (Chapter 6). Altering pectin composition, as in *pme6-1* mutants, can have a number of contrasting effects and can contribute to both increased and decreased cell wall rigidity. Atomic force microscopy allows direct measurements of mechanical properties of guard cells and asymmetric stiffness can be seen within the guard cells. This confirms the hypothesis that asymmetric cell wall structure causes differential stiffness within the guard cell and this is predicted to be important for stomatal function. By combining an immunolabelling approach with genetic techniques and atomic force microscopy, the targeted modulation of cell wall composition can be achieved and the effects of this on cell wall mechanics can be measured

directly. However, care must be taken to avoid over-interpretation of such AFM data as the forces exerted by the guard cell during opening act laterally while the AFM pushes down vertically. In addition, the complex and essentially unknown composition of the cell wall in the area of indentation requires significant assumptions in the calculation of the modulus values. Better knowledge of the guard cell wall composition and how this translates to mechanical properties and, therefore, to stomatal function may allow targeted modulation of the guard cell wall with the aim of manipulating the mechanical properties of guard cells to allow more efficient function in a changing environment. Guard cells also provide a useful system in which to study cell walls as knockouts of guard cell wall genes could have drastic effects on the guard cell wall but still be not be lethal. The study of guard cell walls could provide novel insights into how the cell wall components interact and how they are modified in situ.

7.1.1 Future work

Further work is needed to fully characterise the NASC loss of function lines and PME1 overexpressor lines. Detailed immunolabelling needs to be carried out with sufficient replication to detect any changes in cell wall composition. A full range of stomatal function assays should also be carried out to see if the stomatal movement phenotypes observed in Figure 5.12 are observed in response to a number of different stimuli.

Further genetic work is needed to better understand the importance of the different cell wall components in the guard cells. It is not known at what developmental stage guard cell pectin is demethylesterified and the creation of inducible RNAi lines to knockdown PME6 activity could provide insights into this. In addition, cell wall components other than pectin, such as

xyloglucan could be studied by the same approach, Appendix 7 shows that some xyloglucan synthesis genes appear highly expressed in guard cells. As pectins have been implicated in cellulose deposition and changes to mechanical stresses are known to cause cellulose re-orientation, it would be interesting to look at *pme6-1* mutants with fluorescently tagged microtubules to determine if the distinct radial pattern of microtubules associated with stomata was disrupted.

This thesis describes the development of an AFM technique to measure mechanical properties of stomata but to date this has only been used on wild type plants. A full set of experiments needs to be conducted to assess the mechanical properties of a range of stomatal developmental stages, as shown in Figure 6.20 but with greater replication. It is not fully clear whether the current technique measures cell wall properties, turgor pressure or both and testing both turgid and plasmolysed tissue would elucidate this. The next step is to use the AFM to assess the mechanical properties of stomata in mutant lines, such as *pme6-1*, to determine what impact the alteration in pectin composition has on stomatal mechanics. Additionally, exogenous enzyme treatments can be applied to remove structural cell wall components and to assess the impact this has on guard cell mechanics.

Finally, there is a limit to the use of microarray data in the identification of guard cell specific gene expression, and mRNA abundance does not always correlate with protein abundance. The use of laser dissection microscopy in combination with tandem mass spectrometry (MS/MS) would allow the characterisation of the stomatal proteome to allow greater insight into the construction and modification of the guard cell wall. To date stomatal proteomics have only been carried out on protoplasts which makes the study of proteins at the cell wall impossible (Zhao et al., 2008).

In conclusion this study has furthered the knowledge of guard cell wall composition and has provided new information on the genetic control of guard cell wall composition. The development of an AFM technique could provide valuable information on guard cell wall mechanics and dynamics, allowing the further development of this field.

Bibliography

- Ache, P., Becker, D., Ivashikina, N., Dietrich, P., Roelfsema, M.R.G., Hedrich, R., 2000. GORK , a delayed outward rectifier expressed in guard cells of *Arabidopsis thaliana* , is a K^+ -selective , K^+ -sensing ion channel. *FEBS Lett.* 486, 93–98.
- Ahmed, A.E., Labavitch, J.M., 1980. Cell wall metabolism in ripening fruit. *Plant Physiol.* 65, 1014–6.
- Albersheim, P., Darvill, A.G., Roberts, K., Sederoff, R., Staehelin, R., 2011. *Plant Cell Walls*, 1st ed. Garland Science, New York.
- Alonso, A.P., Piasecki, R.J., Wang, Y., LaClair, R.W., Shachar-Hill, Y., 2010. Quantifying the Labeling and the Levels of Plant Cell Wall Precursors Using Ion Chromatography Tandem Mass Spectrometry. *Plant Physiol.* 153, 915–924.
- Amsbury, S., Hunt, L., Elhaddad, N., Baillie, A., Lundgren, M., Verhertbruggen, Y., Scheller, H. V., Knox, J.P., Fleming, A.J., Gray, J.E., 2016. Stomatal function requires pectin de-methyl-esterification of the guard cell wall. *Curr. Biol.* 26, 2899–2906.
- Andersson-Gunneras, S., Mellerowicz, E.J., Love, J., Segerman, B., Ohmiya, Y., Coutinho, P.M., Nilsson, P., Henrissat, B., Moritz, T., Sundberg, B., 2006. Biosynthesis of cellulose-enriched tension wood in *Populus*: global analysis of transcripts and metabolites identifies biochemical and developmental regulators in secondary wall biosynthesis. *Plant J.* 45, 144–65.
- Apostolakos, P., Livanos, P., Nikolakopoulou, T.L., Galatis, B., 2010. Callose

- implication in stomatal opening and closure in the fern *Asplenium nidus*. *New Phytol.* 186, 623–635.
- Assmann, S.M., Shimazaki, K., 1999. The Multisensory Guard Cell. Stomatal Responses to Blue Light and Abscisic Acid. *Plant Physiol.* 119, 809–816.
- Assmann, S.M., Snyder, J.A., Lee, Y.J., 2000. Mutants of *Arabidopsis* have a wild-type stomatal response to humidity. *Plant, Cell Environ.* 23, 387–395.
- Aylor, D.E., Parlange, J.-Y., Krikorian, A.D., 1973. Stomatal mechanics. *Am. J. Bot.* 60, 163–171.
- Baskin, T.I., 2005. Anisotropic expansion of the plant cell wall. *Annu. Rev. Cell Dev. Biol.* 21, 203–22.
- Bergmann, D.C., Lukowitz, W., Somerville, C.R., 2004. Stomatal development and pattern controlled by a MAPKK kinase. *Science* (80-.). 304, 1494–7.
- Bergmann, D.C., Sack, F.D., 2007. Stomatal development. *Annu. Rev. Plant Biol.* 58, 163–181.
- Bhave, N.S., Velez, K.M., Nadeau, J. a, Lucas, J.R., Bhave, S.L., Sack, F.D., 2009. TOO MANY MOUTHS promotes cell fate progression in stomatal development of *Arabidopsis* stems. *Planta* 229, 357–67.
- Boddiger, D., 2007. Boosting biofuel crops could threaten food security The USA and Europe have made plans to substantially increase their use of biofuels over the The printed journal includes an image merely for illustration. *Lancet* 370, 923–924.
- Boerjan, W., Ralph, J., Baucher, M., 2003. Lignin biosynthesis. *Annu. Rev. Plant Biol.* 54, 519–46.
- Bonawitz, N.D., Chapple, C., 2010. The genetics of lignin biosynthesis:

- connecting genotype to phenotype. *Annu. Rev. Genet.* 44, 337–63.
- Bouton, S., Leboeuf, E., Mouille, G., Leydecker, M.-T., Talbotec, J., Granier, F., Lahaye, M., Höfte, H., Truong, H.-N., 2002. QUASIMODO1 encodes a putative membrane-bound glycosyltransferase required for normal pectin synthesis and cell adhesion in *Arabidopsis*. *Plant Cell* 14, 2577–2590.
- Braybrook, S.A., Jönsson, H., 2016. Shifting foundations: The mechanical cell wall and development. *Curr. Opin. Plant Biol.* 29, 115–120.
- Braybrook, S.A., Peaucelle, A., 2013. Mechano-chemical aspects of organ formation in *Arabidopsis thaliana*: the relationship between auxin and pectin. *PLoS One* 8, e57813.
- Braybrook, S., Hofte, H., Peaucelle, A., 2012. Probing the mechanical contributions of the pectin matrix. *Plant Signal. Behav.* 7, 1037–1041.
- Bruce, R.J., West, C. a, 1989. Elicitation of lignin biosynthesis and isoperoxidase activity by pectic fragments in suspension cultures of castor bean. *Plant Physiol.* 91, 889–897.
- Brummell, D. a, Harpster, M.H., 2001. Cell wall metabolism in fruit softening and quality and its manipulation in transgenic plants. *Plant Mol. Biol.* 47, 311–40.
- Buapet, P., Rasmusson, L.M., Gullström, M., Björk, M., 2013. Photorespiration and carbon limitation determine productivity in temperate seagrasses. *PLoS One* 8, 1–9.
- Burgert, I., 2006. Exploring the micromechanical design of plant cell walls. *Am. J. Bot.* 93, 1391–401.
- Butt, H.-J., Cappella, B., Kappl, M., 2005. Force measurements with the atomic force microscope: Technique, interpretation and applications.

- Surf. Sci. Rep. 59, 1–152.
- Caffall, K., Mohnen, D., 2009. The structure, function, and biosynthesis of plant cell wall pectic polysaccharides. *Carbohydr. Res.* 344, 1879–900.
- Cannon, M.C., Terneus, K., Hall, Q., Tan, L., Wang, Y., Wegenhart, B.L., Chen, L., Lamport, D.T.A., Chen, Y., Kieliszewski, M.J., 2008. Self-assembly of the plant cell wall requires an extensin scaffold. *Proc. Natl. Acad. Sci.* 105, 2226–31.
- Cappella, B., Dietler, G., 1999. Force-distance curves by atomic force microscopy. *Surf. Sci. Rep.* 34, 1–104.
- Catoire, L., Pierron, M., Morvan, C., du Penhoat, C.H., Goldberg, R., 1998a. Investigation of the action patterns of pectinmethylesterase isoforms through kinetic analyses and NMR spectroscopy. Implications In cell wall expansion. *J. Biol. Chem.* 273, 33150–6.
- Catoire, L., Pierron, M., Morvan, C., du Penhoat, C.H., Goldberg, R., 1998b. Investigation of the action patterns of pectinmethylesterase isoforms through kinetic analyses and NMR spectroscopy: Implications in cell wall expansion. *J. Biol. Chem.* 273, 33150–33156.
- Chen, C., Xiao, Y.-G., Li, X., Ni, M., 2012. Light-regulated stomatal aperture in *Arabidopsis*. *Mol. Plant* 5, 566–72.
- Clough, S.J., Bent, A.F., 1998. Floral dip: A simplified method for *Agrobacterium*-mediated transformation of *Arabidopsis thaliana*. *Plant J.* 16, 735–743.
- Corson, F., Hamant, O., Bohn, S., Traas, J., Boudaoud, A., Couder, Y., 2009. Turning a plant tissue into a living cell froth through isotropic growth. *Proc. Natl. Acad. Sci.* 106, 8453–8458.
- Cosgrove, D.J., 2005. Growth of the plant cell wall. *Nat. Rev. Mol. Cell Biol.* 6,

850–61.

- Cosgrove, D.J., 2014. Re-constructing our models of cellulose and primary cell wall assembly. *Curr. Opin. Plant Biol.* 22, 122–131.
- COSGROVE, D.J., 1993. Wall extensibility: its nature, measurement and relationship to plant cell growth. *New Phytol.* 124, 1–23.
- Cosgrove, D.J., Volkenburgh, E., Cleland, R.E., 1984. Stress relaxation of cell walls and the yield threshold for growth. *Planta* 162, 46–54.
- Davies, W.J., Zhang, J., 1991. Root Signals and the Regulation of Growth and Development of Plants in Drying Soil. *Annu. Rev. Plant Physiol. Plant Mol. Biol.* 42, 55–76.
- DeMichele, D.W., Sharpe, P.J.H., 1973. An analysis of the mechanics of guard cell motion. *J. Theor. Biol.* 41, 77–96.
- Denès, J.M., Baron, A., Renard, C.M.G.C., Péan, C., Drilleau, J.F., 2000. Different action patterns for apple pectin methylesterase at pH 7.0 and 4.5. *Carbohydr. Res.* 327, 385–393.
- Derbyshire, P., McCann, M.C., Roberts, K., 2007. Restricted cell elongation in *Arabidopsis* hypocotyls is associated with a reduced average pectin esterification level. *BMC Plant Biol.* 7, 31.
- Dick-Pérez, M., Zhang, Y., Hayes, J., Salazar, A., Zabortina, O.A., Hong, M., 2011. Structure and interactions of plant cell-wall polysaccharides by two- and three-dimensional magic-angle-spinning solid-state NMR. *Biochemistry* 50, 989–1000.
- Doheny-Adams, T., Hunt, L., Franks, P.J., Beerling, D.J., Gray, J.E., 2012. Genetic manipulation of stomatal density influences stomatal size, plant growth and tolerance to restricted water supply across a growth carbon dioxide gradient. *Philos. Trans. R. Soc. Lond. B. Biol. Sci.* 367, 547–55.

- Dong, J., Bergmann, D.C., 2010. Stomatal patterning and development. *Curr. Top. Dev. Biol.* 91, 267–97.
- Drake, P.L., Froend, R.H., Franks, P.J., 2013. Smaller, faster stomata: scaling of stomatal size, rate of response, and stomatal conductance. *J. Exp. Bot.* 64, 495–505.
- Duvetter, T., Fraeye, I., Sila, D.N., Verlent, I., Smout, C., Hendrickx, M., Van Loey, A., 2006. Mode of de-esterification of alkaline and acidic pectin methyl esterases at different pH conditions. *J. Agric. Food Chem.* 54, 7825–7831.
- Easlon, H.M., Bloom, A.J., 2014. Easy Leaf Area: Automated digital image analysis for rapid and accurate measurement of leaf area. *Appl. Plant Sci.* 2, 1400033.
- Eriksson, E.M., Bovy, A., Manning, K., Harrison, L., Andrews, J., De Silva, J., Tucker, G.A., Seymour, G.B., 2004. Effect of the Colorless non-ripening mutation on cell wall biochemistry and gene expression during tomato fruit development and ripening. *Plant Physiol.* 136, 4184–97.
- Fargione, J., Hill, J., Tilman, D., Polasky, S., Hawthorne, P., 2008. Land clearing and the biofuel carbon debt. *Science* (80-.). 319, 1235–8.
- Franks, P., Farquhar, G., 2007. The mechanical diversity of stomata and its significance in gas-exchange control. *Plant Physiol.* 143, 78–87.
- Franks, P.J., Buckley, T.N., Shope, J.C., Mott, K. a, 2001. Guard cell volume and pressure measured concurrently by confocal microscopy and the cell pressure probe. *Plant Physiol.* 125, 1577–84.
- Franks, P.J., Cowan, 1, 2 I. R., Farquhar, G.D., 1998. A study of stomatal mechanics using the cell pressure probe. *Plant, Cell Environ.* 21, 94–100.
- Franks, P.J.P., Farquhar, G.D.G., 2007. The mechanical diversity of stomata

- and its significance in gas-exchange control. *Plant Physiol.* 143, 78–87.
- Geitmann, A., 2010. Mechanical modeling and structural analysis of the primary plant cell wall. *Curr. Opin. Plant Biol.* 13, 693–9.
- Geitmann, A., Ortega, J.K.E., 2009. Mechanics and modeling of plant cell growth. *Trends Plant Sci.* 14, 467–478.
- Giessibl, F.J., 2003. Advances in atomic force microscopy. *Rev. Mod. Phys.* 75, 949–983.
- Groll, U. Von, Berger, D., Altmann, T., 2002. The subtilisin-like serine protease SDD1 mediates cell-to-cell signaling during Arabidopsis stomatal development. *Plant Cell* 14, 1527–1539.
- Gross, K.C., Wallner, S.J., 1979. Degradation of cell wall polysaccharides during tomato fruit ripening. *Plant Physiol.* 63, 117–120.
- Hamant, O., Heisler, M.G., Jönsson, H., Krupinski, P., Uyttewaal, M., Bokov, P., Corson, F., Sahlin, P., Boudaoud, A., Meyerowitz, E.M., Couder, Y., Traas, J., 2008. Developmental patterning by mechanical signals in Arabidopsis. *Science* (80-.). 322, 1650–5.
- Hara, K., Kajita, R., Torii, K.U., Bergmann, D.C., Kakimoto, T., 2007. The secretory peptide gene EPF1 enforces the stomatal one-cell-spacing rule. *Genes Dev.* 21, 1720–5.
- Harholt, J., Suttangkakul, A., Vibe Scheller, H., 2010. Biosynthesis of pectin. *Plant Physiol.* 153, 384–395.
- Harris, P.J., Northcote, D.H., 1971. Polysaccharide formation in plant golgi bodies. *Biochim. Biophys. Acta* 237, 56–64.
- Hayashi, T., Marsden, M.P.F., Delmer, D.P., 1987. Pea xyloglucan and cellulose : xyloglucan-cellulose interactions in vitro and in vivo. *Plant*

Physiol. 83, 384–389.

- Hongo, S., Sato, K., Yokoyama, R., Nishitani, K., 2012. Demethylesterification of the primary wall by PECTIN METHYLESTERASE35 provides mechanical support to the Arabidopsis stem. *Plant Cell* 24, 2624–34.
- Hosy, E., Vavasseur, A., Mouline, K., Dreyer, I., Gaymard, F., Poree, F., Boucherez, J., Lebaudy, A., Bouchez, D., Very, A.-A., Simonneau, T., Thibaud, J.-B., Sentenac, H., 2003. The Arabidopsis outward K⁺ channel GORK is involved in regulation of stomatal movements and plant transpiration. *Proc. Natl. Acad. Sci.* 100, 5549–5554.
- Hothorn, M., Wolf, S., Aloy, P., Greiner, S., Scheffzek, K., 2004. Structural insights into the target specificity of plant invertase and pectin methylesterase inhibitory proteins. *Plant Cell* 16, 3437–3447.
- Hunt, L., Bailey, K.J., Gray, J.E., 2010. The signalling peptide EPFL9 is a positive regulator of stomatal development. *New Phytol.* 186, 609–614.
- Hunt, L., Gray, J.E., 2009. The signaling peptide EPF2 controls asymmetric cell divisions during stomatal development. *Curr. Biol.* 19, 864–869.
- Jennings, A.V., Hall, K.M., 1891. Notes on the Structure of *Tmesipteris*. *Proc. R. Irish Acad.* 2, 1–15.
- Jones, H.G., Archer, N., Rotenberg, E., Casa, R., 2003. Radiation measurement for plant ecophysiology. *J. Exp. Bot.* 54, 879–889.
- Jones, K.H., Senft, J. a, 1985. An improved method to determine cell viability by simultaneous staining with fluorescein diacetate-propidium iodide. *J. Histochem. Cytochem.* 33, 77–79.
- Jones, L., Milne, J.L., Ashford, D., McCann, M.C., McQueen-Mason, S.J., 2005. A conserved functional role of pectic polymers in stomatal guard cells from a range of plant species. *Planta* 221, 255–64.

- Jones, L., Milne, J.L., Ashford, D., McQueen-Mason, S.J., 2003. Cell wall arabinan is essential for guard cell function. *Proc. Natl. Acad. Sci.* 100, 11783–11788.
- Jones, L., Seymour, G.B., Knox, J.P., 1997. Localization of pectic galactan in tomato cell walls using a monoclonal antibody specific to (1-4)- β -D-Galactan. *Plant Physiol.* 113, 1405–1412.
- Juge, N., 2006. Plant protein inhibitors of cell wall degrading enzymes. *Trends Plant Sci.* 11, 359–367.
- Karabourniotis, G., 2001. Epicuticular phenolics over guard cells: Exploitation for in situ stomatal counting by fluorescence microscopy and combined image analysis. *Ann. Bot.* 87, 631–639.
- Kars, I., Krooshof, G.H., Wagemakers, L., Joosten, R., Benen, J.A.E., Van Kan, J.A.L., 2005. Necrotizing activity of five *Botrytis cinerea* endopolygalacturonases produced in *Pichia pastoris*. *Plant J.* 43, 213–225.
- Kieliszewski, M.J., Lamport, D.T.A., 1994. Extensin: Repetitive motifs, functional sites, post-translational codes, and phylogeny. *Plant J.*
- Kim, T.-H., Böhmer, M., Hu, H., Nishimura, N., Schroeder, J.I., 2010. Guard cell signal transduction network: advances in understanding abscisic acid, CO₂, and Ca²⁺ signaling. *Annu. Rev. Plant Biol.* 61, 561–591.
- Kirby, A.R., Gunning, A.P., Waldron, K.W., Morris, V.J., Ng, A., 1996. Visualization of plant cell walls by atomic force microscopy. *Biophys. J.* 70, 1138–43.
- Knox, J.P., 1992. Cell adhesion, cell separation and plant morphogenesis. *Plant J.* 2, 137–141.
- Knox, J.P., 2008. Revealing the structural and functional diversity of plant cell

- walls. *Curr. Opin. Plant Biol.* 11, 308–313.
- Kumar, M., Campbell, L., Turner, S., 2016. Secondary cell walls: Biosynthesis and manipulation. *J. Exp. Bot.* 67, 515–531.
- Lampard, G.R., Macalister, C.A., Bergmann, D.C., 2008. Arabidopsis stomatal initiation is controlled by MAPK-mediated regulation of the bHLH SPEECHLESS. *Science* (80-.). 322, 1113–6.
- Lebaudy, A., Pascaud, F., Very, A.A., Alcon, C., Dreyer, I., Thibaud, J.B., Lacombe, B., 2010. Preferential KAT1-KAT2 heteromerization determines inward K⁺ current properties in Arabidopsis guard cells. *J. Biol. Chem.* 285, 6265–6274.
- Levesque-tremblay, G., Müller, K., Mans, S.D., Haughn, G.W., 2015. HIGHLY METHYL ESTERIFIED SEEDS is a pectin methyl esterase involved in embryo development. *Plant Physiol.* 167, 725–737.
- Li, Y., Beisson, F., Koo, A.J.K., Molina, I., Pollard, M., Ohlrogge, J., 2007. Identification of acyltransferases required for cutin biosynthesis and production of cutin with suberin-like monomers. *Proc. Natl. Acad. Sci.* 104, 18339–18344.
- Limberg, G., Körner, R., Buchholt, H.C., Christensen, T.M.I.E., Roepstorff, P., Mikkelsen, J.D., 2000. Analysis of different de-esterification mechanisms for pectin by enzymatic fingerprinting using endopectin lyase and endopolygalacturonase II from *A. Niger*. *Carbohydr. Res.* 327, 293–307.
- Lionetti, V., Cervone, F., Bellincampi, D., 2012. Methyl esterification of pectin plays a role during plant–pathogen interactions and affects plant resistance to diseases. *J. Plant Physiol.* 169, 1623–1630.
- Liu, T., Ohashi-Ito, K., Bergmann, D.C., 2009. Orthologs of Arabidopsis thaliana stomatal bHLH genes and regulation of stomatal development

in grasses. *Development* 136, 2265–2276.

Long, S.P., Ainsworth, E.A., Rogers, A., Ort, D.R., 2004. Rising atmospheric carbon dioxide: Plants FACE the Future. *Annu. Rev. Plant Biol.* 55, 591–628.

Lu, P., Outlaw Jr, W.H., Smith, B.G., Freed, G.A., 1997. A New Mechanism for the Regulation of Stomatal Aperture Size in Intact Leaves (Accumulation of Mesophyll-Derived Sucrose in the Guard-Cell Wall of *Vicia faba*). *Plant Physiol.* 114, 109–118.

Macgregor, D.R., Deak, K.I., Ingram, P. a, Malamy, J.E., 2008. Root system architecture in *Arabidopsis* grown in culture is regulated by sucrose uptake in the aerial tissues. *Plant Cell* 20, 2643–2660.

Majewska-Sawka, A., Münster, A., Rodríguez-García, M.I., 2002. Guard cell wall: immunocytochemical detection of polysaccharide components. *J. Exp. Bot.* 53, 1067–79.

Marcus, a I., Moore, R.C., Cyr, R.J., 2001. The role of microtubules in guard cell function. *Plant Physiol.* 125, 387–95.

Marcus, S.E., Blake, A.W., Benians, T.A.S., Lee, K.J.D., Poyser, C., Donaldson, L., Leroux, O., Rogowski, A., Petersen, H.L., Boraston, A., Gilbert, H.J., Willats, W.G.T., Knox, J.P., 2010. Restricted access of proteins to mannan polysaccharides in intact plant cell walls. *Plant J.* 64, 191–203.

Marcus, S.E., Verhertbruggen, Y., Hervé, C., Ordaz-Ortiz, J.J., Farkas, V., Pedersen, H.L., Willats, W.G.T., Knox, J.P., 2008. Pectic homogalacturonan masks abundant sets of xyloglucan epitopes in plant cell walls. *BMC Plant Biol.* 8, 60.

Markovič, O., Janeček, Š., 2004. Pectin methylesterases: Sequence-structural features and phylogenetic relationships. *Carbohydr. Res.* 339, 2281–2295.

- Markovič, O., Kohn, R., 1984. Mode of pectin deesterification by *Trichoderma reesei* pectinesterase. *Experientia* 40, 842–843.
- Marry, M., Roberts, K., Jopson, S.J., Huxham, I.M., Jarvis, M.C., Corsar, J., Robertson, E., McCann, M.C., 2006. Cell-cell adhesion in fresh sugar-beet root parenchyma requires both pectin esters and calcium cross-links. *Physiol. Plant.* 126, 243–256.
- Masle, J., Gilmore, S.R., Farquhar, G.D., 2005. The *ERECTA* gene regulates plant transpiration efficiency in *Arabidopsis*. *Nature* 436, 866–70.
- McCartney, L., Marcus, S.E., Knox, J.P., 2005. Monoclonal antibodies to plant cell wall xylans and arabinoxylans. *J. Histochem. Cytochem.* 53, 543–6.
- McFarlane, H.E., Döring, A., Persson, S., 2014. The cell biology of cellulose synthesis. *Annu. Rev. Plant Biol.* 65, 69–94.
- McQueen-Mason, S., Durachko, D.M., Cosgrove, D.J., 1992. Two endogenous proteins that induce cell wall extension in plants. *Plant Cell* 4, 1425–1433.
- Melotto, M., Underwood, W., Koczan, J., Nomura, K., He, S.Y., 2006. Plant stomata function in innate immunity against bacterial invasion. *Cell* 126, 969–80.
- Micheli, F., 2001. Pectin methylesterases: cell wall enzymes with important roles in plant physiology. *Trends Plant Sci.* 6, 414–9.
- Miedes, E., Vanholme, R., Boerjan, W., Molina, A., 2014. The role of the secondary cell wall in plant resistance to pathogens. *Front. Plant Sci.* 5, 358.
- Milani, P., Gholamirad, M., Traas, J., Arnéodo, A., Boudaoud, A., Argoul, F., Hamant, O., 2011. In vivo analysis of local wall stiffness at the shoot apical meristem in *Arabidopsis* using atomic force microscopy. *Plant J.* 67, 1116–1123.

- Mohnen, D., 2008. Pectin structure and biosynthesis. *Curr. Opin. Plant Biol.* 11, 266–277.
- Moller, I., Marcus, S.E., Haeger, A., Verhertbruggen, Y., Verhoef, R., Schols, H., Ulvskov, P., Mikkelsen, J.D., Knox, J.P., Willats, W., 2008. High-throughput screening of monoclonal antibodies against plant cell wall glycans by hierarchical clustering of their carbohydrate microarray binding profiles. *Glycoconj. J.* 25, 37–48.
- Morris, V., Kirby, A., Gunning, A., 2010. Atomic force microscopy for biologists, Second Edi. ed. Imperial College Press, London.
- Morris, V.V., Kirby, A.A.A., Gunning, A.P.A., 2010. Atomic force microscopy for biologists, Second Edi. ed. Imperial College Press, London.
- Mott, K.A., Franks, P.J., 2001. The role of epidermal turgor in stomatal interactions following a local perturbation in humidity. *Plant, Cell Environ.* 24, 657–662.
- Mott, K. a, Buckley, T.N., 2000. Patchy stomatal conductance: emergent collective behaviour of stomata. *Trends Plant Sci.* 5, 258–62.
- Mustilli, A.-C., Merlot, S., Vavasseur, A., Fenzi, F., Giraudat, J., 2002. Arabidopsis OST1 protein kinase mediates the regulation of stomatal aperture by abscisic acid and acts upstream of reactive oxygen species production. *Plant Cell* 14, 3089–99.
- Newman, R.H., Hill, S.J., Harris, P.J., 2013. Wide-angle x-ray scattering and solid-state nuclear magnetic resonance data combined to test models for cellulose microfibrils in mung bean cell walls. *Plant Physiol.* 163, 1558–67.
- Northcote, D.H., Pickett-Heaps, J.D., 1966. A function of the Golgi apparatus in polysaccharide synthesis and transport in the root-cap cells of wheat.

Biochem. J. 98, 159–167.

Novák, V., Vidovič, J., 2003. Transpiration and nutrient uptake dynamics in maize (*Zea mays* L.). *Ecol. Modell.* 166, 99–107.

Ohashi-Ito, K., Bergmann, D.C., 2006. Arabidopsis FAMA controls the final proliferation/differentiation switch during stomatal development. *Plant Cell* 18, 2493–505.

Orfila, C., Sørensen, S.O., Harholt, J., Geshi, N., Crombie, H., Truong, H.N., Reid, J.S.G., Knox, J.P., Scheller, H.V., 2005. QUASIMODO1 is expressed in vascular tissue of Arabidopsis thaliana inflorescence stems, and affects homogalacturonan and xylan biosynthesis. *Planta* 222, 613–622.

Ortega, J.K.E., Zehr, E.G., Keanini, R.G., 1989. In vivo creep and stress relaxation experiments to determine the wall extensibility and yield threshold for the sporangiophores of phycomyces. *Biophys. J.* 56, 465–475.

Palevitz, B.A., Heple, P.K., 1976. Cellulose microfibril orientation and cell shaping in developing guard cells of *Allium*: The role of microtubules and ion accumulation. *Planta* 132, 71–93.

Palin, R., Geitmann, A., 2012. The role of pectin in plant morphogenesis. *Biosystems.* 109, 397–402.

Pandey, S., Wang, R.-S., Wilson, L., Li, S., Zhao, Z., Gookin, T.E., Assmann, S.M., Albert, R., 2010. Boolean modeling of transcriptome data reveals novel modes of heterotrimeric G-protein action. *Mol. Syst. Biol.* 6, 1–17.

Pandey, S., Zhang, W., Assmann, S.M., 2007. Roles of ion channels and transporters in guard cell signal transduction. *FEBS Lett.* 581, 2325–2336.

Park, Y.B., Cosgrove, D.J., 2012. Changes in cell wall biomechanical properties in the xyloglucan-deficient xxt1/xtt2 mutant of Arabidopsis.

Plant Physiol. 158, 465–475.

Parry, M., Rosenzweig, C., Iglesias, a, Livermore, M., Fischer, G., 2004.

Effects of climate change on global food production under SRES emissions and socio-economic scenarios. Glob. Environ. Chang. 14, 53–67.

Pauly, M., Keegstra, K., 2010. Plant cell wall polymers as precursors for biofuels. Curr. Opin. Plant Biol. 13, 304–311.

Paynel, F., Leroux, C., Surcouf, O., Schaumann, A., Pelloux, J., Driouich, A., Mollet, J.C., Lerouge, P., Lehner, A., Mareck, A., 2014. Kiwi fruit PME1 inhibits PME activity, modulates root elongation and induces pollen tube burst in *Arabidopsis thaliana*. Plant Growth Regul. 285–297.

Peaucelle, A., Braybrook, S.A., Le Guillou, L., Bron, E., Kuhlemeier, C., Höfte, H., 2011. Pectin-induced changes in cell wall mechanics underlie organ initiation in *Arabidopsis*. Curr. Biol. 21, 1720–6.

Peaucelle, A., Braybrook, S., Höfte, H., 2012. Cell wall mechanics and growth control in plants: the role of pectins revisited. Front. Plant Sci. 3, 1–6.

Peaucelle, A., Louvet, R., Johansen, J.N., Höfte, H., Laufs, P., Pelloux, J., Mouille, G., 2008. *Arabidopsis* phyllotaxis is controlled by the methylesterification status of cell-wall pectins. Curr. Biol. 18, 1943–8.

Pedersen, H.L., Fangel, J.U., McCleary, B., Ruzanski, C., Rydahl, M.G., Ralet, M.C., Farkas, V., Von Schantz, L., Marcus, S.E., Andersen, M.C.F., Field, R., Ohlin, M., Knox, J.P., Clausen, M.H., Willats, W.G.T., 2012. Versatile high resolution oligosaccharide microarrays for plant glycobiology and cell wall research. J. Biol. Chem. 287, 39429–39438.

Pelloux, J., Rustérucci, C., Mellerowicz, E.J., 2007. New insights into pectin methylesterase structure and function. Trends Plant Sci. 12, 267–77.

- Pena, M., Zhong, R., Zhou, G., Richardson, E., O'Neill, M., Darvill, A., York, W., Ye, Z., 2007. Arabidopsis irregular xylem8 and irregular xylem9: implications for the complexity of glucuronoxylan biosynthesis. *Plant Cell* 19, 549–63.
- Peterson, R.L., Firminger, M.S., Dobrindt, A.L., 1975. Nature of the guard cell wall in leaf stomata of three *Ophioglossum* species. *Can. J. Bot. Can. Bot.* 53, 1698–1711.
- Pickett-Heaps, J.D., 1968. Further ultrastructural observations on polysaccharide localization in plant cells. *J. Cell Sci.* 3, 55–64.
- Pillitteri, L.J., Peterson, K.M., Horst, R.J., Torii, K.U., 2011. Molecular profiling of stomatal meristemoids reveals new component of asymmetric cell division and commonalities among stem cell populations in *Arabidopsis*. *Plant Cell* 23, 3260–75.
- Pingali, P.L.P., 2012. Green Revolution: Impacts, limits, and the path ahead. *Proc. Natl. Acad. ...* 109, 12302–12308.
- Radmacher, M., Tillmann, R., Fritz, M., Gaub, H., 1992. From molecules to cells: imaging soft samples with the atomic force microscope. *Science* (80-.). 257, 1900–1905.
- Rao-Naik, C., Delacruz, W., Laplaza, J.M., Tan, S., Callis, J., Fisher, A.J., 1998. The Rub Family of Ubiquitin-like Proteins. *J. Biol. Chem.* 273, 34976–34982.
- Raschke, K., 1975. Stomatal action. *Annu. Rev. Plant Physiol.* 26, 309–340.
- Ray, J., Knapp, J., Grierson, D., Bird, C., Schuch, W., 1988. Identification and sequence determination of a cDNA clone for tomato tectin esterase. *Eur J Biochem* 174, 119–124.
- Ridley, B.L., O'Neill, M.A., Mohnen, D., Neill, M.A.O., Mohnen, D., 2001.

- Pectins: structure, biosynthesis, and oligogalacturonide-related signaling. *Phytochemistry* 57, 929–967.
- Rowe, M.H., Bergmann, D.C., 2010. Complex signals for simple cells: the expanding ranks of signals and receptors guiding stomatal development. *Curr. Opin. Plant Biol.* 13, 548–555.
- Rugar, D., Hansma, P., 1990. Atomic force microscopy. *Phys. Today* 43, 23.
- Rui, Y., Anderson, C.T., 2016. Functional analysis of cellulose and xyloglucan in the walls of stomatal guard cells of *Arabidopsis thaliana*. *Plant Physiol.* 170, pp.01066.2015.
- Sack, F., Paolillo, D.J., 1983. Structure and Development of Walls in *Funaria* Stomata. *Am. J. Bot.* 70, 1019–1030.
- Scheller, H.V., Ulvskov, P., 2010. Hemicelluloses. *Annu. Rev. Plant Biol.* 61, 263–289.
- Scholl, R.L., May, S.T., Ware, D.H., 2000. Seed and molecular resources for *Arabidopsis*. *Plant Physiol.* 124, 1477–1480.
- Schols, H.A., Bakx, E.J., Schipper, D., Voragen, A.G.J., 1995. A xylogalacturonan subunit present in the modified hairy regions of apple pectin. *Carbohydr. Res.* 279, 265–279.
- Schroeder, J., Allen, G., 2001. Guard cell signal transduction. *Annu. Rev. Plant Physiol.* 52, 627–58.
- Somerville, C., 2006. Cellulose synthesis in higher plants. *Annu. Rev. Cell Dev. Biol.* 22, 53–78.
- Somerville, C., Youngs, H., Taylor, C., Davis, S., Long, S., 2010. Feedstocks for lignocellulosic biofuels. *Science* (80-.). 329, 790–2.
- Southworth, J., Randolph, J.C., Habeck, M., Doering, O.C., Pfeifer, R. a., Rao,

- D.G., Johnston, J.J., 2000. Consequences of future climate change and changing climate variability on maize yields in the midwestern United States. *Agric. Ecosyst. Environ.* 82, 139–158.
- Srivastava, L.M., Singh, A.P., 1972. Stomatal structure in corn leaves. *J. Ultrastructure Res.* 39, 345–363.
- Sterling, J.D., Atmodjo, M. a, Inwood, S.E., Kumar Kolli, V.S., Quigley, H.F., Hahn, M.G., Mohnen, D., 2006. Functional identification of an *Arabidopsis* pectin biosynthetic homogalacturonan galacturonosyltransferase. *Proc. Natl. Acad. Sci.* 103, 5236–5241.
- Sterling, J.D., Quigley, H.F., Orellana, A., Mohnen, D., 2001. The catalytic site of the pectin biosynthetic enzyme α -1,4-galacturonosyltransferase is located in the lumen of the Golgi. *Plant Physiol.* 127, 360–71.
- Stolle-Smits, T., Beekhuizen, J.G., Kok, M.T.C., Pijnenburg, M., Recourt, K., Derksen, J., Voragen, A.G.J., 1999. Changes in cell wall polysaccharides of green bean pods during development. *Plant Physiol.* 121, 363–372.
- Sugano, S.S., Shimada, T., Imai, Y., Okawa, K., Tamai, A., Mori, M., Hara-Nishimura, I., 2010. Stomagen positively regulates stomatal density in *Arabidopsis*. *Nature* 463, 241–4.
- Tallman, G., 2004. Are diurnal patterns of stomatal movement the result of alternating metabolism of endogenous guard cell ABA and accumulation of ABA delivered to the apoplast around guard cells by transpiration? *J. Exp. Bot.* 55, 1963–1976.
- Thompson, A.J., Tor, M., Barry, C.S., Vrebalov, J., Orfila, C., Jarvis, M.C., Giovannoni, J.J., Grierson, D., Seymour, G.B., 1999. Molecular and genetic characterization of a novel pleiotropic tomato-ripening mutant. *Plant Physiol.* 120, 383–389.

- Tieman, D.M., Handa, A.K., 1994. Reduction in pectin methylesterase activity modifies tissue integrity and cation levels in ripening tomato (*Lycopersicon esculentum* Mill.) fruits. *Plant Physiol.* 106, 429–436.
- United Nations Department of Economic and Social Affairs/Population Division, Nationen, V., 2011. *World Population Prospects The 2010 Revision*.
- Vahisalu, T., Kollist, H., Wang, Y.-F., Nishimura, N., Chan, W.-Y., Valerio, G., Lamminmäki, A., Brosché, M., Moldau, H., Desikan, R., Schroeder, J.I., Kangasjärvi, J., 2008. SLAC1 is required for plant guard cell S-type anion channel function in stomatal signalling. *Nature* 452, 487–91.
- Vanholme, R., Demedts, B., Morreel, K., Ralph, J., Boerjan, W., 2010. Lignin biosynthesis and structure. *Plant Physiol.* 153, 895–905.
- Vatén, A., Bergmann, D.C., 2012. Mechanisms of stomatal development: an evolutionary view. *Evodevo* 3, 11.
- Verhertbruggen, Y., Marcus, S.E., Chen, J., Knox, J.P., 2013. Cell wall pectic arabinans influence the mechanical properties of *arabidopsis thaliana* inflorescence stems and their response to mechanical stress. *Plant Cell Physiol.* 54, 1278–1288.
- Verhertbruggen, Y., Marcus, S.E., Haeger, A., Ordaz-Ortiz, J.J., Knox, J.P., 2009a. An extended set of monoclonal antibodies to pectic homogalacturonan. *Carbohydr. Res.* 344, 1858–62.
- Verhertbruggen, Y., Marcus, S.E., Haeger, A., Verhoef, R., Schols, H.A., McCleary, B. V., McKee, L., Gilbert, H.J., Knox, J.P., 2009b. Developmental complexity of arabinan polysaccharides and their processing in plant cell walls. *Plant J.* 59, 413–425.
- Vincken, J.P., de Keizer, A., Beldman, G., Voragen, A., 1995. Fractionation of

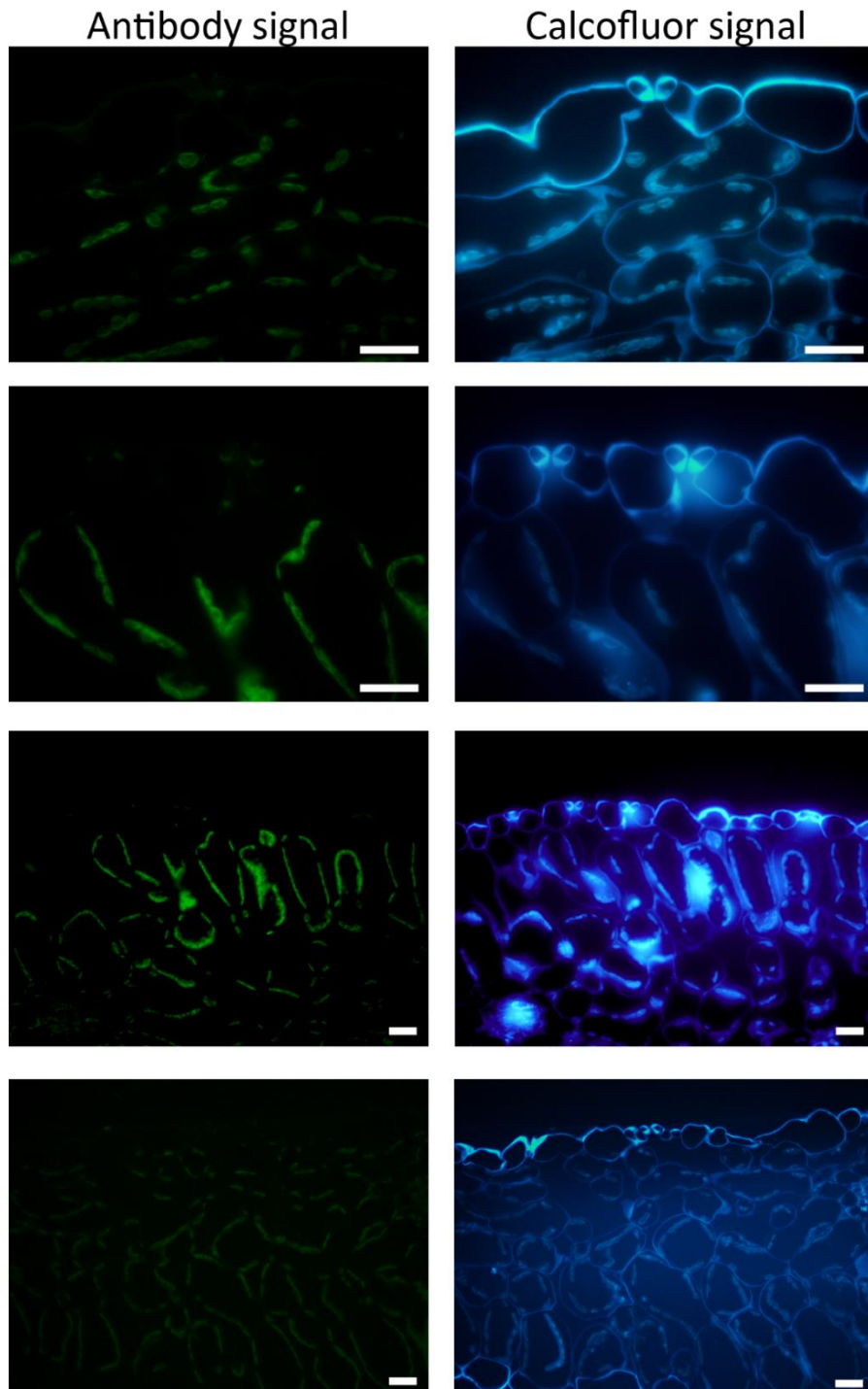
- xyloglucan fragments and their interaction with cellulose. *Plant Physiol.* 108, 1579–1585.
- Wang, H., Ngwenyama, N., Liu, Y., Walker, J.C., Zhang, S., 2007. Stomatal development and patterning are regulated by environmentally responsive mitogen-activated protein kinases in *Arabidopsis*. *Plant Cell* 19, 63–73.
- Wang, L., Wang, W., Wang, Y.-Q., Liu, Y.-Y., Wang, J.-X., Zhang, X.-Q., Ye, D., Chen, L.-Q., 2013. *Arabidopsis* galacturonosyltransferase (GAUT) 13 and GAUT14 have redundant functions in pollen tube growth. *Mol. Plant* 6, 1131–48.
- Wang, M., Yuan, D., Gao, W., Li, Y., Tan, J., Zhang, X., 2013. A Comparative Genome Analysis of PME and PME1 Families Reveals the Evolution of Pectin Metabolism in Plant Cell Walls. *PLoS One* 8, e72082.
- Wang, T., Zabolina, O., Hong, M., 2012. Pectin-cellulose interactions in the *Arabidopsis* primary cell wall from two-dimensional magic-angle-spinning solid-state nuclear magnetic resonance. *Biochemistry* 51, 9846–9856.
- Wei, H., Xu, Q., Taylor, L.E., Baker, J.O., Tucker, M.P., Ding, S.-Y., 2009. Natural paradigms of plant cell wall degradation. *Curr. Opin. Biotechnol.* 20, 330–338.
- Wen, F., Zhu, Y., Hawes, M.C., 1999. Effect of pectin methylesterase gene expression on pea root development. *Plant Cell* 11, 1129–40.
- Willats, W.G., McCartney, L., Mackie, W., Knox, J.P., 2001. Pectin: cell biology and prospects for functional analysis. *Plant Mol. Biol.* 47, 9–27.
- Willats, W.G.T., Orfila, C., Limberg, G., Buchholt, H.C., Van Alebeek, G.J.W.M., Voragen, A.G.J., Marcus, S.E., Christensen, T.M.I.E.,

- Mikkelsen, J.D., Murray, B.S., Knox, J.P., 2001. Modulation of the degree and pattern of methyl-esterification of pectic homogalacturonan in plant cell walls: Implications for pectin methyl esterase action, matrix properties, and cell adhesion. *J. Biol. Chem.* 276, 19404–19413.
- Williamson, R., 1990. Alignment of Cortical Microtubules by Anisotropic Wall Stresses. *Aust. J. Plant Physiol.* 17, 601.
- Winter, D., Vinegar, B., Nahal, H., Ammar, R., Wilson, G. V., Provar, N.J., 2007. An “electronic fluorescent pictograph” Browser for exploring and analyzing large-scale biological data sets. *PLoS One* 2, 1–12.
- Wolf, S., Greiner, S., 2012. Growth control by cell wall pectins. *Protoplasma* 249 Suppl, S169-75.
- Wolf, S., Hématy, K., Höfte, H., 2012. Growth control and cell wall signaling in plants. *Annu. Rev. Plant Biol.* 63, 381–407.
- Wolf, S., Mouille, G., Pelloux, J., 2009. Homogalacturonan methyl-esterification and plant development. *Mol. Plant* 2, 851–60.
- Yang, M., Sack, F.D., 1995. The too many mouths and four lips mutations affect stomatal production in *Arabidopsis*. *Plant Cell* 7, 2227–39.
- Yang, Y., Costa, A., Leonhardt, N., Siegel, R.S., Schroeder, J.I., 2008. Isolation of a strong *Arabidopsis* guard cell promoter and its potential as a research tool. *Plant Methods* 4, 6.
- Yates, E.A., Knox, J.P., 1994. Investigations into the occurrence of plant cell surface epitopes in exudate gums. *Carbohydr. Polym.* 24, 281–286.
- Yoneda, A., Ito, T., Higaki, T., Kutsuna, N., Saito, T., Ishimizu, T., Osada, H., Hasezawa, S., Matsui, M., Demura, T., 2010. Cobtorin target analysis reveals that pectin functions in the deposition of cellulose microfibrils in parallel with cortical microtubules. *Plant J.* 64, 657–667.

- Zablackis, E., Huang, J., Muller, B., Darvill, a G., Albersheim, P., 1995. Characterization of the cell-wall polysaccharides of *Arabidopsis thaliana* leaves. *Plant Physiol.* 107, 1129–1138.
- Zeng, W., Melotto, M., He, S.Y., 2010. Plant stomata: A checkpoint of host immunity and pathogen virulence. *Curr. Opin. Biotechnol.* 21, 599–603.
- Zhang, G.F., Staehelin, L.A., 1992. Functional compartmentation of the Golgi apparatus of plant cells : immunocytochemical analysis of high-pressure frozen- and freeze-substituted sycamore maple suspension culture cells. *Plant Physiol.* 99, 1070–83.
- Zhao, L., Sack, F.D., 1999. Ultrastructure of stomatal development in *Arabidopsis* (Brassicaceae) leaves. *Am. J. Bot.* 86, 929–939.
- Zhao, Z., Zhang, W., Stanley, B. a, Assmann, S.M., 2008. Functional proteomics of *Arabidopsis thaliana* guard cells uncovers new stomatal signaling pathways. *Plant Cell* 20, 3210–3226.
- Zhong, R., Ye, Z.-H., 2015. Secondary cell walls: Biosynthesis, patterned deposition and transcriptional regulation. *Plant Cell Physiol.* 56, 195–214.
- Zimmermann, P., Hennig, L., Gruissem, W., 2005. Gene-expression analysis and network discovery using Genevestigator. *Trends Plant Sci.* 10, 407–409.
- Zykwinska, A.W., Ralet, M.J., Garnier, C.D., Thibault, J.-F.J., 2005. Evidence for in vitro binding of pectin side chains to cellulose. *Plant Physiol.* 139, 397–407.

Appendices

Appendix 1: A selection of control samples incubated with secondary antibody in the absence of primary antibody.



Appendix 2: Antibody binding summary

Antibody	Any binding	Guard cells	Epidermal binding	Guard cell junctions	Cuticle binding	Enzymatic pretreatment
LM1						No change
LM2						
LM5						No change
LM6						Increased
LM7						
LM8						Increased
LM9						
LM10						
LM11						No change
LM12						
LM13						Increased
LM14						Increased
LM15						
LM16						No change
LM17						
LM18						
LM19						Reduced
LM20						Reduced
LM21						Increased
LM22						
LM23						
LM24						No change
LM25						Increased
JIM4						
JIM5						
JIM7						Reduced
JIM8						
JIM11						
JIM12						
JIM23						
JIM14						
JIM15						
JIM16						No change
JIM19						
JIM20						
2F4						
PTD5						
PAM1						No change

Binds
Doesn't bind
Not tested

Appendix 3: Summary of antibodies tested for binding in leaves treated with ABA

The following table shows antibodies which showed no difference in their binding patterns or intensity in samples which had been treated with ABA prior to treatment. Full details of all antibodies are available from Plant Probes (Leeds, UK).

Antibody	Cell wall epitope	References
Hemicelluloses		
LM15	Xyloglucan (XXXG)	Marcus et al. (2008) BMC Plant Biology 8:60
LM24	Xyloglucan	Pedersen et al. (2012) J. Biol Chem. 47, 39429–39438
LM25	Xyloglucan	
LM21	Mannan	Marcus et al. (2010) Plant Journal 64, 191-203
Pectins		
JIM7	Partially/completely de-esterified homogalacturonan	Verhertbruggen et al. (2009) Carbohydr. Res. 344, 1858-1862
2F4	Calcium-crosslinked pectins	Liners F, Van Cutsem P (1992) Protoplasma 170, 10-21
LM19	unesterified homogalacturonan	Verhertbruggen et al. (2009) Carbohydr. Res. 344, 1858-1862
LM20	highly esterified homogalacturonan	
LM13	Linearised-(1->5)- α -L-arabinan	Moller et al. (2007) Glycoconjugate J. 25, 37-48
Other glycans		
LM12	Feruloylated polymers	Pedersen et al. (2012) J. Biol Chem. 47, 39429–39438
AGP'S		
LM14	AGP glycan	Moller et al. (2007) Glycoconjugate J. 25, 37-48
JIM8	AGP glycan	Pennell RI et al. (1991) Plant Cell 3:1317-1326.

Appendix 4: Information on plant lines used in this project

Chapter 3	Col-0 plants were used for all experiments in chapter 3
Chapter 4	<p><i>L.er</i> was used as WT for all experiments in chapter 4.</p> <p><i>PME6</i> knockout line (<i>pme6-1</i>): NASC ID: SGT6342 had insertion in <i>PME6</i> in the <i>L.er</i> background.</p> <p>The <i>PME6</i> GUS reporter line and complemented line was kindly donated by Dr Lee Hunt and are described in Amsbury et al., 2016 in the supplemental methods.</p>
Chapter 5	<p>Col-0 was used as WT for all experiments in this chapter.</p> <p>Loss of function mutants were obtained from NASC and are summarised below. All NASC lines are in the Col-0 background.</p> <p>The loss of function mutant <i>focl</i> was donated by Lee Hunt (NASC ID: WiscDsLoxHs053_08G).</p> <p>Gain of function mutants were created by agrobacterium mediated transformation and are summarised below.</p>
Chapter 6	Col-0 was used for all AFM experiments except where the <i>focl</i> line was used as described above.

Summary of PME1 overexpression lines used during this project

Line Name	Gene of interest	Promoter
pGC1:AtPMEI1	AtPMEI1	pGC1-D1
pGC1:AtPMEI2		
pGC1:AdPMEI1		
pCA1:AtPMEI1	AtPMEI2	pCA1
pCA1:AtPMEI2		
pCA1:AdPMEI1		
pATML:AtPMEI1	AtPMEI2	pATML
pATML:AtPMEI2		
pATML:AdPMEI1		

Summary of loss of function mutant lines obtained from NASC. Lines highlighted in yellow were taken forwards for further observation while other lines were discarded due to not being homozygous.

AT3G24670	Pectate lyase	SALK_109494
AT4G25260	Plant invertase/Pectin methylesterase (PME)	SALK_033203
AT3G62820	Plant invertase/Pectin methylesterase inhibitor (PMEI)	SALK_027168
AT5G19730	Pectin methylesterase (PME)	SALK_136556
AT2G26440	Plant invertase/Pectin methylesterase (PME)	SALK_117817
AT4G25260	Pectin methylesterase inhibitor (PMEI)	SALK_036325
AT2G47340	Pectin methylesterase (PME)	SALK_079711
AT3G62820	Pectin methylesterase (PME)	SALK_027168
AT1G11580	Pectin methylesterase (PME)	SALK_076974
AT1G01390	Glycosyltransferase	SALK_083984
AT3G60730	Pectin methylesterase (PME)	SALK_074653
AT3G43270	Pectin methylesterase (PME)	SALK_013629
AT4G38420	Pectin methylesterase (PME)	SALK_011162
AT5G19730	Pectin methylesterase (PME)	SALK_117724

Appendix 5: Primers used during the project

PME6 primers:

Primer name	Sequence
<i>PME6</i> Fwd	TCTGAGTCGTGTAAACGAGCC
<i>PME6</i> Rev	CCTCTTCGTATTCAAAGTATTTC
<i>PME6</i> Fwd RT-PCR	GGAAGATTCCAAAACACTACGGC
<i>PME6</i> Rev RT-PCR	GCCGTCCTAAATAAGTTTC
DS5-1	ACGGTCGGGAAACTAGCTCTAC
RUB1 Fwd	GCGAACTTCGTCTTCACAA
RUB1 Rev	GGAAAAAGGTCTGACCGACA

Primers used during creation of PME1 overexpression lines:

Primer name	Sequence
AtPMEI1 Fwd	CACCATGGCTGCGAATCTAAGG
AtPMEI1 Rev	TTAATTACGTGGTAACATGTTAGAGATAAC
AtPMEI2 Fwd	CACCATGGCAGCATACTG
AtPMEI2 Rev	TCACATCATGTTTGAGATGACAAGTAC
AdPMEI1 Fwd	CACCATGGCCTTTCC
AdPMEI1 Rev	CTATTTTGATCCAGGCAAAAG
ATML1_BamHI	CCGTTTAAACCGATGCATAGTTTCTAAAATGTGC
ATML1_PmeI	GGCGGATCCAAATGGAGGATAGTTAACGA
CA1_BamHI	CCGTTTAAACAAGGACTCACCAGGACAGGA
CA1_PmeI	GGCGGATCCTACTCACACCCTTGCTTAAT
GC1-D1_BamHI	GAGCGGATCCATTTCTTGAGTAGTGATTTTGAAG
GC1-D1_PmeI	TCCGGTTTAAACATGGTTGCAACAGAGAGGATGA
M13_Fwd	GTAAAACGACGGCCAGT

Primers for genotyping of NASC lines:

Primer name	Sequence
SALK_109494 Fwd	CCTAGCTCAATGAAGCCAATG
SALK_109494 Rev	GAGTCTCTCTGATGCCACTGG
SALK_033203 Fwd	CTTACCAGCCTCTTGCAGATG
SALK_033203 Rev	GGCATTAGAGGTCCTTTTCCTG
SALK_027168 Fwd	CTCCGACACCTACAAATGGAC
SALK_027168 Rev	CCGACTTCTTCTCACGTTTTG
SALK_136556 Fwd	AAAGAAAGGAGAGTTGACCGC
SALK_136556 Rev	GCCATTGATTCTCTCCCTCTC
SALK_117817 Fwd	ATGAGTAACGACAGGGTGCTG
SALK_117817 Rev	CTGTTGCCGTGAAGTTAAAGG
SALK_036325 Fwd	CAAGTCATGGCAGAGGAGAAG
SALK_036325 Rev	TTGGTATTCACATTGCAGCAC
SALK_079711 Fwd	CAGAGATTCAGCTTCCATTCTG
SALK_079711 Rev	AATCCTTCCATTCCGAATTTG
SALK_076974 Fwd	TTTTTACCGCGTGTTTATTGTC
SALK_076974 Rev	TGGAAAGAAGTGGTTGGTTTG
SALK_083984 Fwd	CGAAGTTGATCACAATTTGGG
SALK_083984 Rev	ACCAAACATATCGACGACGAG
SALK_074653 Fwd	CATGGACCATCAAGACCAAAC
SALK_074653 Rev	TGGTTTCCAATTCGATTTCTG
SALK_013629 Fwd	CTGCCCTTTTAAGGGAAGATG
SALK_013629 Rev	TGTTTTGGAAGGTGATATCGC
SALK_011162 Fwd	AAACGCAGTCTCAGCCTACAG
SALK_011162 Rev	GCAGCATAGCACAAACCTAAGG
SALK_117724 Fwd	TTGTCCCTACCACAAAGCAAC
SALK_117724 Rev	ATGTTGTTAGATGCGGTCGAG
LB 1.3	ATTTTGCCGATTTTCGGAAC

Appendix 6: Antibodies tested against pme6-1 samples which are not shown in Chapter 4.

All antibodies listed below are available from Plant Probes (Leeds, UK) and showed no differences in binding pattern between *L.er* plants and *pme6-1* plants.

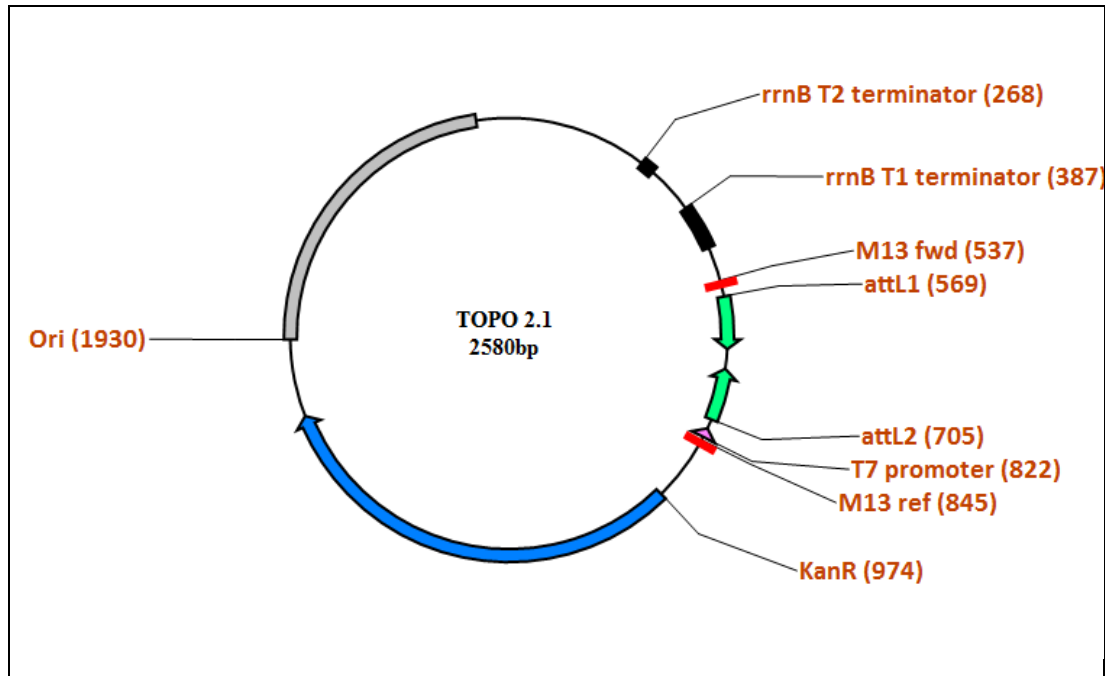
Antibody	Cell wall epitope	References
Hemicelluloses		
LM15	Xyloglucan (XXXG)	Marcus et al. (2008) BMC Plant Biology 8:60
LM24	Xyloglucan (XLLG)	Pedersen et al. (2012) J. Biol Chem. 47, 39429–39438
LM25	Xyloglucan	
LM21	Mannan	Marcus et al. (2010) Plant Journal 64, 191-203
Pectins		
2F4	Calcium-crosslinked pectins	Liners F, Van Cutsem P (1992) Protoplasma 170, 10-21
LM13	Linearised-(1->5)- α -L-arabinan	Moller et al. (2007) Glycoconjugate J. 25, 37-48
Other glycans		
LM12	Feruloylated polymers	Pedersen et al. (2012) J. Biol Chem. 47, 39429–39438
AGP'S		
LM14	AGP glycan	Moller et al. (2007) Glycoconjugate J. 25, 37-48
JIM8	AGP glycan	Pennell RI et al. (1991) Plant Cell 3:1317-1326.

Appendix 7: Putative cell wall genes with high guard cell expression.

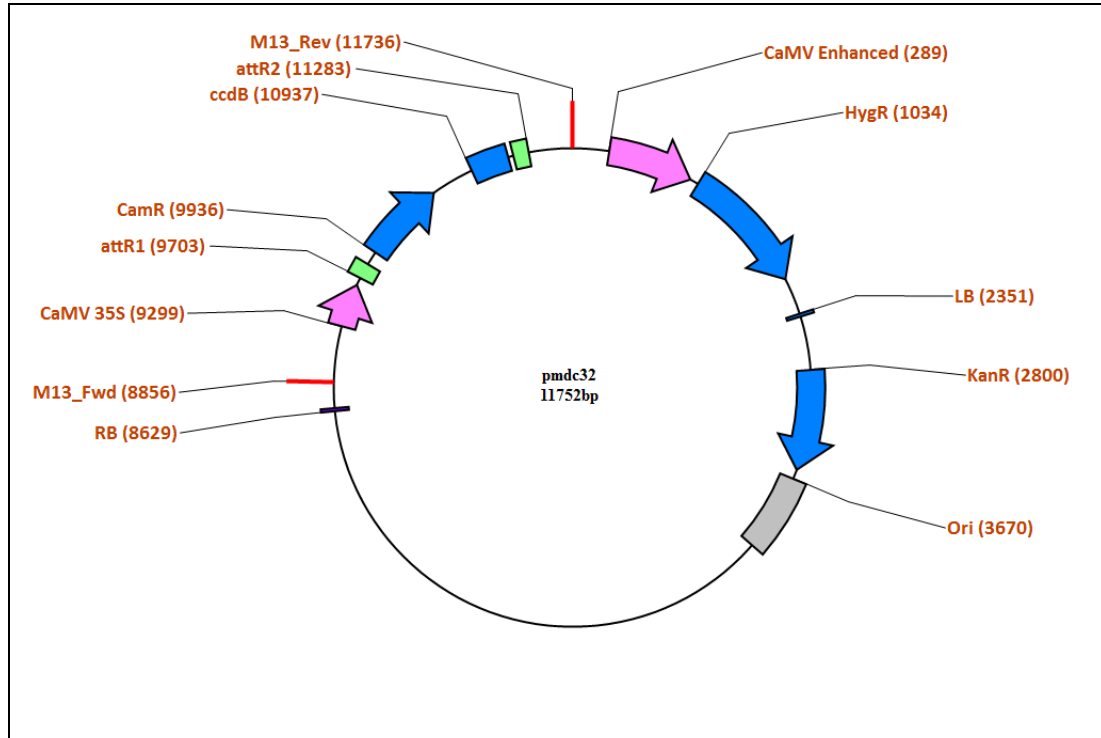
Accession number	Putative function	Expression: GC/WL
At2g18570	putative flavonol 3-O-glucosyltransferase	2.226583408
At1g05680	putative indole-3-acetate beta-glucosyltransferase	2.021341463
At1g80050	adenine phosphoribosyltransferase	2.292642692
At1g62900	O-methyltransferase 1, putative	2.70212766
At1g01390	flavonol 3-o-glucosyltransferase, putative	3.616402116
At2g47280	putative glucosyltransferase	2.040816327
At3g03680	putative phosphoribosylanthranilate transferase	2.198675497
At4g37580	probable N-acetyltransferase hookless 1	9.854545455
At5g05880	glucuronosyl transferase-like protein	2.148148148
At5g48060	phosphoribosylanthranilate transferase-like protein	2.961165049
At5g14860	glucosyltransferase -like protein	3.612244898
At5g20830	sucrose-UDP glucosyltransferase	2.250900901
At5g04370	S-adenosyl-L-methionine:salicylic acid carboxyl methyltransferase-like protein	6.357142857
At1g23200	putative pectinesterase	3.042694497
At1g05310	putative pectin methylesterase	2.604743083
At2g47280	putative pectinesterase	2.219081272
At3g10720	putative pectinesterase	1.727988195
At4g38420	putative pectinesterase	8.290187891
At3g43270	pectinesterase -like protein	3.517110266
At3g60730	pectinesterase - like protein	4.694444444
At5g47500	pectin methylesterase-like	2.420492349
At5g64640	pectin methylesterase-like protein	2.502688172
At5g19730	pectin methylesterase-like protein	2.601382488
At1g02810	Plant invertase/pectin methylesterase inhibitor superfamily	2.392523364
At1g11580	pme	3.406553398
At1g23205	Plant invertase/pectin methylesterase inhibitor superfamily	2.07892204
At2g47340	Plant invertase/pectin methylesterase inhibitor superfamily	4.582278481
At3g17130	Plant invertase/pectin methylesterase inhibitor superfamily	1.734910277
At3g49220	Plant invertase/pectin methylesterase inhibitor superfamily	1.722832601

At3g62820	Plant invertase/pectin methylesterase inhibitor superfamily	5.123302553
At4g00080	pmei?	2.859813084
At4g25260	Plant invertase/pectin methylesterase inhibitor superfamily	1.730844794
At5g09760	Plant invertase/pectin methylesterase inhibitor superfamily	2.483856894
At5g20740	Plant invertase/pectin methylesterase inhibitor superfamily	2.200421941
At5g62360	pme	1.970680628
At2g02380	putative glutathione S-transferase	1.773869347
At3g21800	putative UDP-glucose glucosyltransferase	1.75
At4g01130	putative acetyltransferase	1.827757125
At5g54060	flavonol 3-O-glucosyltransferase-like	1.81655481
At4g36770	glucosyltransferase-like protein	1.782608696
At2g46630	putative extensin	5.689990282
At1g17150	putative polygalacturonase	2.751724138
At1g78400	similar to exopolygalacturonase precursor sp Q00293 PGLX_ASPTU	1.743494424
At1g70500	putative polygalacturonase	2.4
At5g44830	polygalacturonase-like protein	1.72
At2g26620	putative polygalacturonase	6.954545455
At3g19620	beta-xylosidase, putative	2.679012346
At5g66460	mannan endo-1,4-beta-mannosidase	1.971760797
At1g02730	cellulose synthase catalytic subunit, putative	3.045380875
At4g13390	extensin-like protein	2.038461538
At4g13210	pectate lyase like protein	1.805991441
At3g55500	expansin-like protein	2.103194103
At1g56680	endochitinase, putative	2.069620253

Appendix 8: Plasmid map showing locations of key features of the TOPO 2.1 vector



Appendix 9: Plasmid map showing locations of key features of the PMDC32 vector



Appendix 10: DNA sequences for PME1 genes overexpressed in *A. thaliana*.

AtPMEI1

ATGGCTGCGAATCTAAGGAACAATGCGTTCCTTGTCTTCTCTCATGTTTCTTCT
CTTGATCGGTTTCATCATAACGCAATCACAAGTTCAGAAATGAGCACAATCTGT
GACAAAACCTTAAATCCATCTTTCTGTCTTAAGTTCCTCAATACGAAATTCG
CATCGCCTAATCTTCAAGCCTTGGCAAAAACCACTTGATTCTACACAAGC
GAGAGCTACACAAACGTTAAAGAACTCCAATCTATTATCGATGGAGGAGT
CGACCCTCGATCTAAGTTAGCTTACAGGTCATGCGTAGATGAATACGAGAG
CGCGATTGGAAACCTCGAGGAAGCTTTTGAGCATTAGCTTACAGGAGATGGT
ATGGGGATGAACATGAAAGTTTCTGCTGCATTGGATGGAGCTGATACATGTT
TAGATGATGTGAAGAGATTGAGATCAGTAGATTCTTCGGTTGTGAATAACAG
TAAAACAATTAAGAATCTTTGTGGTATTGCTCTTGTTATCTCTAACATGTTAC
CACGTAATTAA

AtPMEI2

ATGGCAGCATACTGACGAACAGAGTTTTAATGTCTTCTCTGATGTTTTTGT
AATGACTGGTTCTTTGAACGCACAAGTGGCAGACATAAAAGCGATATGTGG
AAAAGCGAAAAACCAATCCTTCTGTACGAGCTACATGAAATCCAACCCAAA
GACCTCAGGTGCTGATCTTCAAACGCTTGCAAATATCACATTTGGTTCTGCA
CAAACAAGTGCATCAGAAGGTTTCAGGAAAATTCAATCTCTAGTCAAGACA
GCAACCAACCCCACTATGAAGAAAGCATAACCTCATGTGTACAACATTAT
AAGAGTGCAATAAGCAGTCTCAATGATGCTAAGCAGAGCCTGGCGTCAGGC
GATGGCAAAGGGTTGAACATTAAGGTTTCAGCAGCTATGGAAGGACCTTCA
ACATGTGAACAAGACATGGCGGATTTCAAAGTTGATCCTTCAGCTGTGAAG
AACAGTGGTGATTTTCAGAATATTTGTGGCATTGTACTTGTCTCATCTCAAACAT
GATGTGA

AdPMEI1

CACCATGGCCTTTTCCTATTGTAGCTCTTCCTTGTTTGTTTCTCTTTTAC
TTGTCATTCTATTCATTAGCCCATTGTCCCAAAGGCCGAGCGTAAAAG
CAGAAAACCATTTGATTAGCGAAATCTGTCCCAAACCTCGCAATCCT
TCTCTGTGCCTGCAGGCTTTAGAATCCGATCCTCGCTCAGCTAGTAAA
GATCTTAAAGGCCTTGGCCAGTTCTCTATCGACATAGCTCAGGCCAGT
GCTAAACAAACCTCCAAAATCATTGCCTCGCTTACAAACCAAGCAAC
TGACCCTAAACTCAAAGGTCGATACGAGACTTGCTCAGAAAATTATG
CTGATGCGATCGATAGCCTTGGACAAGCCAAGCAGTTTTTGGACATCC
GGAGACTATAATAGCCTAAACATTTACGCTTCCGCTGCCTTTGATGGG
GCTGGAACCTTGTGAAGATAGTTTTGAAGGACCACCGAATATACCAAC
TCAACTCCACCAAGCAGATCTGAAGTTGGAAGACCTTTGTGATATCG
TTCTGGTTATATCTAATCTTTTGCCTGGATCAAATAG

Appendix 11. DNA sequences for tissue specific promoters.

pATML1

CGATGCATAGTTTCTAAAATGTGCTAAAATTCAGAACTGAAACATGATTCATTGTC
TGAAACTTTGTTTCAAATTACTGAAAATAATCATTCACTGGACCAAACAAATAAAT
AAAATAAAATCGAATTTCTGAATTTGGAAATTGGTTTTTGGTTTTTAATTTAAACAA
AACAAAAACGAAATTTGAAGGCAATAAATGAGTTAGTTGGTAGGCAGAAGTCACTC
GTTCCCACTAGCTATTATTATTAGAAGAAACGTCCCCACAACCTCCAAGGCGTTTCAG
TTCCTTTAATTTACTGAATTACCCTCCTCATATCTATAAAAAATCACCTCTTGTACCA
ATGCCCCATTTACACATCCTGTCGTTTATTTCTAGACTAAGTGGACTACATGTCGGTT
ATTTGATTCGCACCATGCGTATTTGGATTATCGCTAACACACCCCTTCAAACAATACG
CTTAACCTCGTATTACAAAATTTCAAGTGATGAATTATCTATGTATAAGATATAGATA
GGAACAATAAGCATCGAGAAATTTGTATATAAATCAACTAGACTTATATATATTTTC
GATACAGAATTTATACGTATTATATCAAATTAATTAGTAATTGTTTCCTCTACGTGAG
TTTAATTAACAATGATAAGCTACATTGAGTGTATCAGTTCTAAAACCTTTATAGTATGC
TACAATCAATTTTTCTAAGTAACAACCTTCAAGCAAGGAATCACACACACACAGTGGT
ACATAATAAACTTGATTTTAATATCATATGATCAGCATCATTAAACGGAATAAGTTAA
GTAATTCGTCATCCATACTACTAAGTCATATTAATAATCATAATCAAACCTTAAAAGCC
GATTAGAAAGAGAGCAAATATATCTAAAAATTCACGAGGAAGACGACAAATGCAA
GGAAACACAGCTAGTATTATTAACCTTAATAGATATTGGATGAATGACTGCATAATA
TATATCACATTAATAAGTGGACATAAATTTGCATATGTGTAATGTACCTCTCCACAATT
AATCGCGGACCATTTATTTTACTATTACAAGTCAAGTAACTTTATATTGTTGATCCAT
AATTCTTTTCGAACATAAAATCATATACTTAGGCCATTTTCAACTGTCAAAACTCGAA
TCCGAGAACCAAATTTACCATTTTCCAAAAATGATGAGTGTGACCAAATGGGGTA
CTACTGTCTAATCAGGAACTTGTGAACAAATTTCAACCTTTTCAAATAAGACGAG
TGTC AACCAACTTTTTCCAACCAAGAGATATTGGGTTGCTACACAAATACTTAATAG
CCATTGCATATTTATGCATATGCAAATGCAGGGTCGTGGCGTCAGAAAGAAACATA
GGACCCTCAACATATTTAATATTTTGGGAGCTATATTTGACTATTTTCATATTAGAAAA
TAATAATAAAAAAGTGTGGTTTTATATCAAATTGTAATTTACGAAAACTTATGCTT
TTGCGCAATGATTTTTGTAAAGTATCTACTATGTTTAGTGTTTACATTGATTAGTAGGC

TGCCGTTTTTTTTCTTGTGTATTATGTACTATATATGAATATGAACATTTGTAAAAGTG
AATCTTGTCATTTTCTTGTGAAAACATATATAGTATGTGCAAACAAAGCATAGGTTA
ATCCAATACCACACAAATAACACGTCAGGTAAATCCAATAATAAATCGTATGTGCA
TGTATGTGTATTTCATGTATGTTACATGAATGTCTGAATCAGTCAGTGTACGTATATGA
TGTAGGIGATGTAAATCTTAATGTATGAGCTGTTTCTTGGACCATGGTCCACAATGGA
TATTGCTCCCCAACTACATTAGTCAATCGACTGGCCAATTTTAAATTAAGATAATTAA
TCCAAACTACCATTAAATATAACTTTGACCTTTTTTCTATTCATTTTTAGATATTATTG
GAACTTACGTAGTTTACATGCATCTCATCCCTTCTTTTCTCCTTGAAAGTGGGTCCA
ATCACAAAAAATGATCTTATATTTTGTATTTTGTATTTTAAAACTCATAATTATATA
GGTTCAAAAATTTAATTAACATCAGTGTATACTATAATTACTACTCTAGCCAACAAG
ATAAATTCATTTTGACATCAGCCAAAAGATAAAAATTTGGTTAAAACTATTGGATT
AGCTTTTAGTATTTAATATTTTATGTACTGATTAATAACGAATTTAGAAATCTAGGAT
ATAAGTGAGGGTGTATAATAAGGGAGGGGTGGACCATTAATAGCGATGTGCAATTA
AAAATTATGATTAAGAATCTAGGAAATTTGTAGATTGCTTAGTTATTTTTATGGCGAT
CGTCGTGTCAATGTCATGGATTTTGAAACTTTAAATTAATCTCTTAAATTAGCACCTA
CCTTTGAATTTTATAGAATCTTTTTATTTTATATGTTTAAATTTATAGAATCTAACTAGC
TTATTTTGAGATTA AATTGTTTACTTTTATAACAGTATAAATGTATAATGAGGA
CCTAAGAATGTAGTCTGTAATGTTCTTGCTATTCTACTTAATCTCATCACCAATCAA
CCATCAAAAAGAAGCTAGTACTAATAAACCTGCAGGTATTCGAATAATAATTAAGC
TCAAACACTATACTAATTTATGGAGGATTATATATTC AATGAATTAGGAACCTCATG
ATGGACATTATTGACTGATATAATGTGTATACTAATTGTGAGTATTTAAAAACCATA
CAAAGCATTATATGTCCACATATATTGGACACACATGCAATCAATGTTCAATATGC
TCCACACACAGAAATAAAAATACTCTTTCTGATCATATGATACATCATACTATACT
AAAAAATCTAAAATGAACTATAACCACAAGCATATATAATAACAATGAAATGGTA
ATGTTTCTTCATTTTTATTTGTTCAAATCTTATTCGGTTGTTTTTCTTACCCTACGAG
AATCCGTGAGGTCAAAGGGAAACAGTGATTTTTTTTTTGTATTTTGTTTTTAAATTGA
TGAAGTGTAAAACCTCTCTCTCTAGAAAAATATATAAGTAGTAGTATGAATTTTCTCTC
ACTAAAAGCATTAAATGGACCTTTCGATAATCATAAATGCAATGCACCCTCTCTATGC
ATTTTCGCAATAACTCCTTTTCTTCTGCCACATCCTCTTCTCACCTCTTCTCTTCTC
CCTTCTCCTAAGTTCCTCCTCCACCAAATCTCCATTTATTCGTTAACTATCCTCCA
TTT

pCA1

AAGGACTCACCAGGACAGGAGTATTGCATCTATGTTTTTATTTCGAATATTTCTCGTTA
CACAATAGAAAAACAAAACAAATCCACGGAAAGGATAATGAGCTTATACGTGGAC
AATATTGAGACTATATTTCTATGGTTGAAATCATGTGAATTTATGAGAGCTGTACTTA
CTCACTAAAACAAACAAAAAACTAAAACAAACAAAAAACTGAAACAAACAAAAT
CCTCCATAAAAAGATGAATCGAACATTTTCTTTTTGTTCATGATACATATATATATA
TATATATATATATATATGTATATGTATATATATATATATATGTATATATATATACAC
ACACACACACACATATATATATATATATATATATATATGTATGTATGTATATATGTATAT
ATATATGTGTGTGTGTGTGAATATGTTGCATATATATTGAGAAATGGAAATTAAGT
ACAATAATATTCTCTACATAGAGGCGTTAATGCGTCAATTTTGTGTGTTAAAGACAT
AATCTAATAACAACATTGAAGATTTTCTATGAATTTGGAAAGTATGTATACACAAAAA
TTATGTAAGAGATAAAAAGACTTGTGTGGAAATCAAATACCTATAAAAATAATTGCAAT
TGTTACGAAAGATGATTTGTTTATTTATGTATTAACTTTTTACATAAAAATACCTACTA
AGTTTGATTTTTAAAATAAAAATTACTCTTAAATTTTAGCAGAATAACCAGGTAAACTC
ATAAACACATGGTACTGACTTTTACACTCACCCATTAGCTAAGTGTGTTTGTGATACA
ACCCTATTTTCGTATTATGTATAAACTCACAAATCTAGTTGTATGCATTAGGTGTGAG
ATAGCCCCAGAAAGTTTTATGAGAGGGTTGTATGTCCAAAACTTTATGATCATATA
GGTTTTGTTTTTTTTGTTTTTTTTGTTTTTTTTGTTTTTTTTGTTTTTTTTGTTTTTT
TGTTTTGTTTTTTTTGTTTTTTTTGTTTTTTTTGTTTTTTTTGTTTTTTTTGTTTTTT
TTTTGCGTGTGCGTGTATGAGAGCTAGTGAGGGTACCACCGATAAAAATGCCACTGA
AATCGATATTGAATATAACGACCTTTGCAAGAAGAGAATTAAGTATTTATGAGTACA
TACTTTTGAAGGCTTTCTCGTATTTAATCTTTTCGCAGGTTTAAAAATATTAATTATATA
TTACACCCCAATGCTTTTAAATCTTTACAACCTAATCCTTATAATTTTTCATTTTCAAC
TTTGATCCCATATACTTTTTTATATTTTATAAAAATTTTTATCTTACTTTTCAGTCTAAAT
TTTACGAGTTAACAAGCGGCAACGTGCGCGTGTGGCTTCAATGTTTCTACGCATATTT
TTCCATTTGACGGCCCCGTCACAACGCACAAGTCATAGATAGACCTAGCTATTATTTT
TTTTAATAATATTTTACGTTTGTTCATGGGTGATTCAACGTTTTTATGCATAATTTTCAT
GTTGATTTATTTATTTTTGTTGTACTTTATAATGCGAGTATTTCCGGTGTTAATGATGG
ATGATGTTAAATGACATCGTTTTAATACTAATTGTTTTTTAATTTACAAAACCTCTCAA
CAAATGATTAGTTGGGTTAGTTATTCATAGGAAAGCGGACGAGCATGTCGTTATAAT
TAAAAAATATCAAAAAGAGTAAACAAAAAAGGAAAAAGACTAATTATTTAGATAA
TAATAATATCCACAAAATATTCGAATTCTTCAATCCTGAGTTTGCTCTGTGGATGAG

TTTCTGTATCATTGATACTTGATACCTGTAATTCACACACCTCATATCTCATACTTCAT
CTATAAATACCCAATTCATTTTGCTCAAAGTCTCAACACTGAGCATACCCAATATTC
AGGTGATCTAATTTAACGTTTGCATGAGTATTTTCTTAATAAAAATTTATGTTGGGTTTA
CAGTATCTATTGGGTGGATTCTTAAACGGATTGTGGTTTGATTAATAAAAAATCTTA
ATGAGAAGTTTGTGATAATATGCTGAAATGGGTTGTTTTTGTGTTAATTTTCAGGGTT
GGAGGGGAATTAAGTATTAAGCAAGGGTGTGAGTA

pGC1-D1

TTTTATATAAAACTTTGGACGTGTAGGACAACTTGTCAACATAAGAAACAAAATGG
TTGCAACAGAGAGGATGAATTTATAAGTTTTCAACACCGCTTTTCTTATTAGACGGA
CAACAATCTATAGTGGAGTAAATTTTTATTTTGGTAAAATGGTTAGTGAATCAAAT
ATCTAAATTTTGTGACTACTAACATTAACAAATATGCATAAGACATAAAAAAAG
AAAGAATAATTCTTATGAAACAAGAAAAAAACCTATAACAATCAATCTTTAGGAAT
TGACGATGTAGAATTGTAGATGATAAATTTTCTCAAATATAGATGGGCCTAATGAAG
GGTGCCGCTTATTGGATCTGACCCATTTGAGGACATTAATATTTTCATTGGTTATAA
GCCTTTTAATCAAATTTGTCATTAATTTGATGTCTCCCTCTCGGGTCATTTTCCTTTCT
CCCTCACAATTAATGTAGACTTTAGCAATTTGCACGCTGTGCTTTGTCTTTATATTTAG
TAACACAAACATTTTGACTTGTCTTGTAGAGTTTTTCTCTTTTATTTTTCTATCCAATAT
GAAAACATAAAAGTGTCTCGTATACATATATTTAAAATTAAGAAACCTATGAAAAC
ACCAATACAAATGCGATATTGTTTTCAGTTCGACGTTTCATGTTTGTTAGAAAATTTT
TAATGACGTTTGTATAAAATAGACAATTAACGCCAAACACTACATCTGTGTTTTCG
AACAATATTGCGTCTGCGTTTCCTTCATCTATCTCTCAGTGTACAATGTCTGAACT
AAGAGACAGCTGTAACTATCATTAAAGACATAAACTACCAAAGTATCAAGCTAATG
TAAAATTAATCTCATTTCACGTAACAAATTGAGTTAGCTTAAGATATTAGTGAAA
CTAGGTTTGAATTTTCTTCTTCTTCCATGCATCCTCCGAAAAAAGGGAACCAATC
AAAACGTTTGCATATCAAACCTCCAACACTTTACAGCAAATGCAATCTATAATCTGT
GATTTATCCAATAAAAACCTGTGATTTATGTTTGGCTCCAGCGATGAAAGTCTATGC
ATGTGATCTCTATCCAACATGAGTAATTGTTTCAGAAAATAAAAAGTAGCTGAAATGT
ATCTATATAAAGAATCATCCACAAGTACTATTTTCACACACTACTTCAAATCACTA
CTCAAGAAATATG

Appendix 12. Correlation analysis of AFM force data

Correlation analysis of stomatal stiffness traits. All data sets were tested for normality using D'Agostino-Pearson K^2 test. Correlation analysis was then carried out using Spearman's nonparametric correlation for data that was not normal and Pearson's correlation calculation for normally distributed data.

	Is the data normal		Test used	r value	r ² value	P value
Stomata vs Supporting cells elasticity	No	p=0.0050	Spearman's	0.6912	N/A	0.0039
Stomatal elasticity vs stomatal size	No	p=0.0009	Spearman's	0.2491	N/A	0.3037
Supporting/stomata elasticity vs stomatal size	Yes	p=0.07	Pearson's	-0.944	0.1555	P=0.1
Stomatal elasticity vs pore size	No	p=0.0051	Spearman's	-0.6373	N/A	0.8094
Supporting/stomata elasticity vs pore size	No	p<0.0001	Spearman's	0.1488	N/A	0.5423
Stomatal elasticity vs aspect ratio	No	p=0.0009	Spearman's	-0.0519	N/A	0.8331
Supporting/stomata elasticity vs aspect ratio	No	p<0.0001	Spearman	0.5051	N/A	0.0275
Inner stomata vs outer stomatal elasticity	Yes	p=0.0938	Pearson's	0.6874	0.4725	0.0033

Appendix 13: Publications arising from this thesis

Amsbury, S., Hunt, L., Elhaddad, N., Knox, J.P., Fleming, A.J., Gray, J.E.,
Stomatal Function Requires Pectin De-methyl- esterification of the
Guard Cell Wall. *Current Biology*. 2016.

Lee Hunt, Samuel Amsbury, Alice L Baillie, Mahsa Movahedi, Alice Mitchell,
Mana Afsharinafar, Kamal Swarup, Thomas Denyer, Jamie Hobbs,
Ranjan Swarup, Andrew J. Fleming and Julie E Gray. Formation of
the Stomatal Outer Cuticular Ledge Requires a Guard Cell Wall
Proline-Rich Protein. *Plant Physiology*. 2017